RESEARCH INTO INNOVATIVE TECHNOLOGIES FOR GAS DRAINAGE IN UNDERGROUND THICK SEAM LIGNITE OPERATIONS

Jerneja Sedlar

Doctoral Dissertation
Jožef Stefan International Postgraduate School
Ljubljana, Slovenia, July 2015

Evaluation Board:

Prof. Dr. Milena Horvat, Chairman, Jožef Stefan Institute, Ljubljana, Slovenia

Prof. Dr. Nives Ogrinc, Member, Jožef Stefan Institute, Ljubljana, Slovenia

Prof. Dr. Anna Korre, Member, Imperial College London, United Kingdom

MEDNARODNA PODIPLOMSKA ŠOLA JOŽEFA STEFANA
JOŽEF STEFAN INTERNATIONAL POSTGRADUATE SCHOOL



Jerneja Sedlar

RESEARCH INTO INNOVATIVE TECHNOLOGIES FOR GAS DRAINAGE IN UNDERGROUND THICK SEAM LIGNITE OPERATIONS

Doctoral Dissertation

RAZISKAVE INOVATIVNIH METOD RAZPLINJEVANJA DEBELE PLASTI LIGNITNEGA SLOJA

Doktorska disertacija

Supervisor: Prof. dr. Sevket Durucan

Co-supervisor: Dr. Simon Zavšek

Ljubljana, Slovenia, July 2015

Abstract

Coal seam gas (CSG) emission in coal mines can create unsafe working conditions, where occurrences of coal and gas outbursts are responsible for many mining accidents resulting in injury and death. High CSG emissions also cause economic losses due to production stoppages and increases the costs associated with mine ventilation. Mining at the Velenje Coal Mine is made difficult, not just because of the depth of the seam (500 m), but because of the high CSG emissions. The lignite coal seam is also heterogeneous which comprises of different porosities and fracture systems that act as gas reservoirs in which CSG can be trapped under high pressure, creating an ever-present risk of coal and gas outbursts.

Coal seam gas drainage methods are one of the main tools for minimizing CSG emissions in mines and many different drainage techniques have been developed in coal mines around the world. At present, methods for draining CSG can be divided into pre-drainage and post-drainage with in-seam goaf drainage. Here at the Velenje Coal Mine the CSG composition is predominately CO_2 and CH_4 and because of the high gas emission (up to maximum 10 m^2/t of extracted coal), the the mine implemented the first pre-drainage test in 2013, to minimize the CSG emission at the longwall face.

The research work reported herein focuses on the numerical modelling of CSG gas flow around a drainage borehole with the aim of simulating gas drainage from a borehole and CSG migration in the lignite seam. The absence of gas drainage models in the literature describing thick lignite seams highlights the need for a study such as this in order to better understand the mechanism of CSG migration before and during CSG drainage. In the first stage of this research the emphasis was on understanding the geomechanical characteristics of the lignite and geochemical characteristics of the CSG. This included CSG composition monitoring, making CSG borehole pressure measurements, and performing CSG carbon isotope analysis. The highest CSG pressures (up to 2.5 MPa) were found in the first mining level under fresh overburden. The stable carbon isotope composition of CH_4 and CO_2 indicate that methane was generated *via* acetate fermentation and the reduction of CO_2 ($\delta^{13}C_{CH4}$ from -70.4 to -50.0 ‰), which was confirmed by the $\alpha^{13}C_{CO2\text{-}CH4}$ fractionation factor. The higher values of $\delta^{13}C_{CH4}$ also indicate that thermogenic methane ($\delta^{13}C_{CH4}$ values from -50.0 to -18.8 ‰) migrated from deeper layers in the basin. $\delta^{2}H_{CH4}$ at the longwall faces varied from -358.5 to -291.4 ‰. The different Velenje lignite lithotype groups, which consist of xylite and detrite, are also discussed in detail since their geomechanical characteristics greatly influence gas adsorption capacity, geomechanical strength and gas flow characteristics of the seam.

Active seismic tomography was also conducted across two 100 m sections of two longwall panels: K.-130/B and K.-50/C. At the longwall panel K.-130/B the P-wave velocities decreased by up to 600 m/s as the face moved closer to the tomography zone at longwall panel K.-130/B and by up to 250 m/s in the case of longwall panel K.-50/C. An increase in the S-wave velocity to 400 m/s was measured as the K.-130/B longwall face advanced. The data obtained from active tomography monitoring is used for numerical modelling set-up.

State-of-the-art computer numerical modelling software is used to construct a gas flow model to simulate gas migration and drainage in the coal seam during excavation.

Geomechanical modelling was performed using FLAC^{3D} software for different lithotypes: 100% xylite, 100% fine detrite and a 50% of xylite and 50% of fine detrite mixed lithotype. Maximum vertical stresses vary depending on lithotype and were the highest for the detrite lithotype (23 MPa) during horizontal excavation. The distance to the longwall face, where these maximum values occur, varied from 6.7 m for detrite to 7.9 m for xylite and 6.8 m for mixed lithotype coal. The Top Coal Caving models produced maximum vertical stresses at 22 m in front of the longwall panel. The maximum vertical stresses were 24 MPa in detrite, 26 MPa in xylite and 30 MPa in mixed lithotype respectively. The CSG flow modelling was also performed using TREACT version of TOUGH2 software with ECO2N equation-of-state (EOS). The most efficient gas drainage occurs, when the borehole is between 40 m and 20 m to the longwall in all lithotype groups. When the borehole < 20 m to the longwall face, the pressure drops to almost the atmospheric pressure, but gas still flows. Closer to the longwall face (5 m) gas flow is reduced to the level that drainage is no longer possible.

Combining the data from these geomechanical and gas flow models revealed the complex relationship between stress, permeability and gas migration through the lignite. These results will be vital in the future design of an efficient drainage system for the Velenje Coal Mine and for thick or steep coal seams in general.

Povzetek

Emisije premogovnih plinov v premogovnikih povzročajo nevarne pogoje za delo, saj so izbruhi premoga in plina odgovorni za številne rudarske nesreče s poškodbami ali tudi s smrtjo. Velike količine emisij premogovnih plinov lahko povzročajo tudi ekonomske izgube, saj se zaradi večkratnih zaustavitev proizvodnje in povečanega stroška prezračevanja jamskih prostorov stroški proizvodnje večajo. Rudarjenje v Premogovniku Velenje je poleg globine premogovnega sloja (do 500 m) oteženo tudi zaradi velikih količin emisij premogovnih plinov. Velenjski lignitni sloj je zelo heterogen in je sestavljen iz različnih sistemov poroznosti in različnih prelomov, ki delujejo kot plinski rezervoar, ter predstavlja vedno prisotno nevarnost za izbruhe plina in premoga. Izbruhi plina lahko nastanejo ob napredovanju izgradnje rudarskih prog preko lokacije z visoko vsebnostjo premogovnega plina, ki je shranjen v premogu pod visokim pritiskom.

Metode razplinjevanja premogovnega plina so eno izmed učinkovitih orodij za zmanjšanje emisij premogovnih plinov. Na svetu obstaja veliko različnih metod razplinjevanj, ki so prilagojene posameznim razmeram, in sicer razplinjevanje pred odkopne plošče pred odkopavanjem, razplinjevanje po odkopavanju z razplinjevanjem zarušenega dela odkopne plošče. V Premogovniku Velenje pa premogovni plin v splošnem sestavljata pretežno CO_2 in CH_4 v razmerju 2:1.Z namenom zmanjšati emisije na odkopu se je v letu 2013 izvedel prvi testni poskus razplinjevanja odkopne plošče.

V prvem delu raziskovalnega dela je bil podroben poudarek na poznavanju geomehanskih lastnosti lignita in geokemičnih lastnosti premogovnega plina. Te meritve so bile meritve sestave premogovnih plinov, meritve tlaka premogovnega plina v vrtinah ter analize izotopske sestave premogovnega plina. Najvišje vrednosti tlaka plina (do 2.5 MPa) so bile izmerjene na prvih odkopnih ploščah, odkopane pod svežo krovnino. Meritve izotopske sestave ogljika v metanu in v CO_2 so pokazale, da je metan nastal kot rezultat acetatne fermentacije ter redukcije CO_2 ($\delta^{13}C_{CH4}$ from -70.4 to -50.0 ‰), kar je bilo potrjeno z rezultati $\alpha^{13}C_{CO2-CH4}$ frakcionacije. Visoke vrednosti $\delta^{13}C_{CH}$ nakazujejo tudi na termogen izvor plina ($\delta^{13}C_{CH4}$ values from -50.0 to -18.8 ‰), ki bi potencialno lahko migriral skozi sloje iz globjih magmatskih plasti. Rezultati $\delta^{2}H_{CH4}$ v odvzetih vzorcih varirajo med -358.5 to -291.4 ‰. V doktorskem delu so predstavljene različne litotipne skupine lignita, ki predstavljajo lignit z različnimi geomehanskimi in geokemičnimi lastnostmi, ki zelo vplivajo na zmogljivost adsorpcije plina, na trdnostne lastnosti in na sposobnosti pretoka premogovnega plina.

Poleg *in-situ* meritev se je izvajala tudi aktivna seizmična tomografija, ki je bila izvedena na dveh 100 m dolgih odsekih na dveh odkopnih ploščah K.-50/C in K.-130/B. Rezultatio so pokazali močno zmanjšanje hitrosti P valov na odkopni plošči K.-130/B do 600 m/s v času, ko se odkop približuje opazovani lokaciji. Medtem ko se P valovi na odkopni plošči K.-50/C zmanjšali za do 250 m/s. Opažen je bil porast histrosti S valov do 400 m/s v času napredovanja odkopnega čela proti opazovalni lokaciji. Analizirani rezultati so zelo uporabne informacije za postavitev numeričnega modela.

Raziskovalno delo je bilo osredotočeno na numerično modeliranje pretoka premogovnega plina okoli razplinjevalne vrtine z namenom simulirati razplinjevanje in

pretokov premogovnih plinov v lignitnem sloju. V literaturi ni bilo objavljenih veliko rezultatov razplinjevanj v debelih lignitnih slojih, zato se je pokazala potreba po razumevanju mehanizma migracij premogovnih plinov, kar je bil glavni vzrok za to raziskovalno delo.

Uporabljeni sta bili najnovejši dosegljivi programski opremi za numerično modeliranje, s katerima sta bila sestavljena geomehanski in plinski model, ki posnemata obnašanje premoga pri odkopavanju ter obnašanje premogovnega plina pri odkopavanju ter razplinjevanju. Geomehanski numerični modeli so bili izvedeni s programsko opremo FLAC^{3D} za različne litotipne skupine: 100 % ksilita, 100 % drobnega detrita in 50 % ksilita in 50 % drobnega detrita. Maksimalne vertikalne napetosti so bile odvisne od litotipne sestave in so bile najvišje dosežene v detritu (23 MPa) v primeru horizontalnega odkopavanja na razdalji od odkopa 6.7 m (v ksilitu 7.9 m in v mešani zgradi 6.8 m). V primeru nadkopnega pridobivanja so se maksimalne vertikalne napetosti razvile na oddaljenosti od odkopa 22 m. Vrednosti vertikalnih napetosti pa so dosegle 24 MPa v detritu, 26 MPa v ksilitu in 30 MPa v mešani strukturi. Numerično modeliranje pretokov premogovnih plinov je bilo opravljeno z uporabo TREACT različice programske opreme TOUGH2 z ECO2N skupino. Rezultati so pokazali, da je najučinkovitejšo razplinjevanje možno na oddaljenosti od odkopa med 40 m in 20 m v vseh litotipnih skupinah. S približevanjem odkopa proti razplinjevalni vrtini (manj kot 20 m), se tlak plina zniža na skoraj atmosferski tlak, vendar pretok plina je še vedno vzpostavljen. Ko pa se odkop približa na manj kot 5 m, razplinjevanje ni več mogoče, zaradi previsokih vsebnosti kisika v plinski mešanici.

Geomehanski numerični model in numerični model pretoka plina skupaj prikazujejo prepleten odnos med napetostmi, prepustnostjo in posledično migracijo premogovnih plinov skozi premog. Rezultati lahko pomagajo v prihodnosti pri dimenzioniranju razplinjevalnega sistema v Premogovniku Velenje ter tudi v drugih debelih in strmih slojih premoga v premogovnikih po svetu.

Acknowledgements

This Doctoral Dissertation was conducted in the company Velenje Coal Mine, d.d with the cooperation of the Imperial College London and the Jožef Stefan International Postgraduate School.

I would like to thank my husband Matej and my parents Tatjana and Marjan for the constant support during the entire studying process.

I would like to express my special gratitude to my supervisor, Professor Dr. Sevket Durucan for all the advice, effort and experience he has devoted to me.

A very special thanks goes out to my supervisor from the industry Dr. Simon Zavšek for all the time, suggestions, and scientific approach and for helping me understand how diverse the coal system is.

My sincere thanks go to Sergej Jamnikar for his technical and professional help during my research work. I will also like to thank to Gregor Uranjek for all of his encouraging words he gave me throughout the whole period.

I would like to express special gratitude to Dr. Tjaša Kanduč for helping me prepare a scientific paper, because without her expertise it would be much more difficult.

I would like to thank the entire Department of Earth Science and Engineering at Imperial College London, Royal School of Mines, especially to Professor Dr. Anna Korre, Guangyao Si, Dr. Ji-Quan Shi and Dr. Giacomo Bacci for their expertise and extensive contribution to my research work.

I would also like to thank the whole company Velenje Coal Mine, d.d. with its managements for enabling my studies and for all the support and flexibility for my needs of work through the whole study.

I also want to thank the Jožef Stefan International Postgraduate School for all the suggestions and help through the process. I would like to thank the Dean Professor Dr. Aleksandra Kornhauser-Frazer for many encouraging words and support.

A special thanks goes to Dr. Emil Rojc, without whom the era of my research work would not have started.

I would also like to thank my committee members Professor Dr. Milena Horvat, Professor Dr. Nives Ogrinc, and Professor Dr. Anna Korre for their interest in my work.

I would like to express special gratitude to Dr. David Heath for precise corrections of the English language of my doctoral thesis.

In conclusion, I recognize that this research would not have been possible without the Agency SPIRIT Slovenia – Public Agency of the Republic of Slovenia for the Promotion and Entrepreneurship, Innovation, Development, Investment and Tourism, due to their financial assistance of my postgraduate study within the project of Young researchers from the Industry MR-2010.

This work was also supported by the Slovenian Research Agency (L2-4066 and L1-5451).

Table of Contents

Abstract ..... **V**

Povzetek ..... **VII**

Acknowledgements ..... **IX**

List of Figures ..... **XIII**

List of Tables ..... **XIX**

Abbreviations ..... **XXI**

1 Introduction and Objectives **1**
1.1 Background 1
1.2 Motivation 4
1.3 Objectives and Methodology 6

2 Review of Current Knowledge on Gas Retention and Flow in Coal Seams **9**
2.1 Introduction 9
2.2 Review of Coal Seam Gas Migration 10
2.3 Review of the Effects of Stress Distribution around a Longwall Face on Permeability 13
2.4 Review of Active Seismic Tomography of the Longwall Face 16
2.5 Review of Current Knowledge on Coal Seam Gas Drainage 19
2.6 Review of Numerical Modelling Used in Mining 22

3 Velenje Lignite **27**
3.1 Introduction 27
3.2 Geology of the Velenje Basin 27
3.3 Velenje Mining Method 28
3.4 Structural Properties of the Lignite 31
3.4.1 Lithotype Classification 32
3.4.1 Geomechanical Properties of the Velenje Lignite 34
3.4.1.1 *In-situ* stress measurements around the longwall panel 35
3.4.2 Geochemical Properties of the Velenje Lignite 37

4 Field Measurement Campaigns to Characterise the Coal Seam Behaviour around LTCC Faces **39**
4.1 Geomechanical Properties of Lignite and Studies Related to Coal Seam Gas 39
4.2 Active Seismic Tomography of the Longwall Panel 39
4.2.1 P Wave Seismic Tomography Measurements at Longwall Panel K.-50/C 41

4.2.2 P Wave Seismic Tomography Measurements at Longwall Panel K.-130/B 43
4.2.3 S Wave Seismic Tomography Measurements at the Longwall Panel K.-130/B..46
4.2.4 Conclusions from the Seismic Tomography Measurements.....46
4.3 Coal Seam Gas Pressure Measurements.....47
4.3.1 Coal Seam Gas Pressure Data Interpretation 49
4.4 Geochemical Properties of the Coal Seam Gas 53
4.4.1 Coal Seam Gas Concentration and Stable Isotopic Composition Results 56
4.5 Coal Seam Gas Drainage Trial Test 71
4.5.1 Design of the Drainage System.....71
4.5.2 Trial Test Procedure.....74
4.5.3 Summary of the Drainage Analysis 74
4.6 Conclusions.....79

5 Development of Geomechanical Model of Advanced Longwall Face using FLAC^{3D} 81
5.1 Introduction.....81
5.2 Grid Generation 82
5.3 Boundary and Initial Conditions.....82
5.4 Constitutive Models.....83
5.4.1 The Null Model.....83
5.4.2 The Mohr-Coulomb Model.....83
5.4.3 The Strain-Hardening/Softening Mohr-Coulomb Model.....84
5.4.4 The Hoek-Brown Model 85
5.5 Geomechanical Model of Longwall Panel K.-65/F in the Pesje Mine District 86
5.6 Results and Discussion 89
5.7 Conclusions.....92

6 Development of a Coal Seam Gas Flow Model 93
6.1 Model Development in TOUGH2 93
6.1.1 ECO2N EOS Module.....94
6.1.2 Data Collection and Input 96
6.1.3 Boundary and Initial Conditions 97
6.1.4 Sinks and Sources 98
6.1.5 Output from TOUGH2 and Visualisation of the Results with TECPLOT360 98
6.2 Gas Flow Model Development under Dynamic Influence of Longwall Face Advance 99
6.2.1 Geometry and Material Properties of the Models.....99
6.3 Results and Discussion 100
6.3.1 100 % Xylite Flow Model.....101
6.3.2 100 % Detrite Flow Model.....103
6.3.3 50 % Xylite and 50 % Detrite Flow Model.....105
6.4 Conclusions.....106

7 Conclusions 109

8 References.....113

Appendix 123

List of Figures

Figure 1: *Trend in CO_2 (in Gt) emissions from fossil fuel combustion from 1870 to 2010* (IEA, 2013).....1
Figure 2: *Outburst risk matrix* (Black et al., 2009). 2
Figure 3: *Fatalities in coal mines from methane gas explosion or outbursts in the year 2008-2010* (Black, 2011). 3
Figure 4: *Rock bursts at the Velenje Coal Mine from 1961 to 2014, the number of longwall faces working per year and coal production in tonnes.* 5
Figure 5: *Formation of Explosive Mixtures* (UN, 2010). 9
Figure 6: *Fracture system in coal* (modified after Shi and Durucan, 2003).....10
Figure 7: *Gas transport in the coal between micro pores and cleats* (Guo et al., 2003).....11
Figure 8: *Relationship between depth and gas content in the Surat Basin, Australia* (Scott et al., 2007, Moore, 2012).....12
Figure 9: *Relationship between permeability and coal seam depth a) in the Upper Silesian Coal Basin, Poland* (McCants et al., 2001, Moore, 2012), *b) in the Permian aged Bowen Basin, Australia, where two geological domains (geographic areas of similar geology and gas relationship) have been identified* (Esterle et al., 2006, Moore, 2012).....13
Figure 10: *Schematic of strata response to longwall mining* (Singh and Kendorski, 1981; and Karacan et. al, 2007b).....14
Figure 11: *Longitudinal section of an advancing longwall face: strata and stress behaviour around the longwall face* (Durucan et al., 2014). 15
Figure 12: *S-wave velocity tomogram across a longwall coal panel in the Velenje Coal Mine* (Zavšek et al., 2008). 18
Figure 13: *Typical gas drainage methods* (Lunarzewski, 2001). 19
Figure 14: *Coal seam gas pre-drainage and gob drainage Scheme* (Sharma, 2008).....20
Figure 15: *Gas drainage techniques and their applicable conditions* (Wang & Xue, 2008).....21
Figure 16: *Different borehole patterns for horizontal methane drainage of a longwall panel* (Karacan et al., 2007 a). 22
Figure 17: *Geological map of the Velenje Basin area* (Brezigar et al., 1987). 28
Figure 18: *Geologic profile Šoštanj – Tičnica*.....29
Figure 19: *Schematic geological cross-section of the Velenje Basin (*Brezigar et al., 1987).....30
Figure 20: *Excavation scheme of the Velenje Mining Method.* 31

Figure 21: *Lithotype components of the Velenje lignite visible in a horizontally drilled borehole-core:* ***a)*** *and* ***b) Detrite (D)*** *forms fine-detrital lignite. It is typically crushed (a) and cracked due to desiccation (b),* ***(c)*** *and* ***d) Xylo-detrite (xD)*** *composed of xylitic pieces smaller than half of the core diameter, and* ***detro-xylite (dX)*** *composed of xylitic pieces bigger than half of the core diameter, both within fine-detrital matrix.* ***e)*** *and* ***f) Xylite (X)*** *as xylitic pieces bigger than the core diameter (e), and extending over the entire core dimensions (f). Note also the scale-bar of 64 mm, which corresponds to the core diameter* (Markič & Sachsenhofer, 2010). 33

Figure 22: *Gelified lithotype components of the Velenje lignite.* ***a)*** *Gelo-detrite (gD) with a developed cleat system; below is mineral-rich detrite (mD) with calcite inclusions.* ***b)*** *Detro-gelite (dG) with very high developed cleat system.* ***c)*** *Gelo-xylite (gX)* (Markič, 2009). 34

Figure 23: *Cross section of the stress monitoring borehole installed with Glőtzl cells* (Jeromel et al., 2010). 35

Figure 24: *The size of the normalized stress in overburden strata excavation under several panels using a mechanized excavation method* (adapted from Kočar et al., 1989). 36

Figure 25: *Increments of the normalized stress in the overburden strata, when excavation takes place under fresh intact overburden* (adapted from Kočar et al., 1989). 36

Figure 26: *Increments of the normalized stress in the coal seam in front of the longwall face* (adapted from Kočar et al., 1989). 37

Figure 27: *Location of longwall panel K.-50/C and longwall panel K.-130/B.* 40

Figure 28: *Location of seismic tomography measurement area at longwall panel K.-50/C.* 40

Figure 29: *Location of seismic tomography measurements on the longwall panel K.-130/B.* 41

Figure 30: *Longwall K.-50/C P-wave velocity tomograms in Y-component for the (a) 1st tomography campaign during 21-22 May 2011 and (b) 2nd tomography campaign during 18-19 June 2011.* 42

Figure 31: P_y *velocity tomogram, difference between* 2^{nd} *and* 1^{st} *measurement in longwall panel K.-50/C.* 43

Figure 32: P_y *velocity tomogram,* 1^{st} *measurement at longwall panel K.-130/B.* 44

Figure 33: P_y *velocity tomogram,* 2^{nd} *measurement at longwall panel K.-130/B.* 45

Figure 34: P_y *velocity tomogram, difference between* 2^{nd} *and* 1^{st} *measurement at longwall panel K.-130/B.* 45

Figure 35: S_z *velocity tomogram, difference between* 2^{nd} *and* 1^{st} *measurement at longwall panel K.-130/B.* 46

Figure 36: *Location of the CSG pressure boreholes at Mine Pesje.* 48

Figure 37: *A pressure sensor probe, pressure gauge and temperature probe installed in the CSG pressure borehole in the mine.* 48

Figure 38: *Gas pressure measurements in borehole JPK 59 +10°/12 at longwall panel K.-65/F.* 49

Figure 39: *Gas pressure measurements in borehole JPK 60 +10°/12 at longwall panel K.-65/F.* 50

Figure 40: *Gas pressure measurements in borehole JPK 61 +10°/12 at longwall panel K.-65/F.* 50
Figure 41: *Pressure measurements in the borehole JPK 69 (+10°)/13 at longwall panel K.-65/E.* 51
Figure 42: *Comparison of the pressure build up results at borehole JV E1 (+20°)/13.* 52
Figure 43: *Comparison of the pressure build up results at borehole JV E2 (+10°)/13.* 52
Figure 44: *Comparison of the pressure build up results at borehole JV E2 (+20°)/13.* 53
Figure 45: *Figure of the sampling borehole* (Jamnikar, 2015)..... 53
Figure 46: *Location of sampling boreholes in the active parts of the Velenje Coal Mine (Pesje, South Preloge and North Preloge mining districts).* 55
Figure 47: *Distribution of gas concentration as the longwall face advances at longwall G2/C in North Preloge mining district.* 65
Figure 48: *Distribution of gas concentration as the longwall face advances at longwall K.-130/A in South Preloge mining district.* 65
Figure 49: *Distribution of gas concentration as the longwall face advances at longwall K.-50/C in Pesje mining district.* 66
Figure 50: *Distribution of gas concentration as the longwall face advances at longwall K. -5/A in Pesje mining district.* 66
Figure 51: *Distribution of gas concentration as the longwall face advances at longwall K.-65/F in North Preloge mining district.* 67
Figure 52: *Interpretation of the origin of CO_2 from the analysed coalbed gas samples from the Velenje Basin using the $\delta^{13}C_{CO2}$ versus CDMI index in the lignite seam ahead of the working face at the longwall face G2/C in the North Preloge mining district.* 69
Figure 53: *Interpretation of the origin of CO_2 from the analysed coalbed gas samples from the Velenje Basin using the $\delta^{13}C_{CO2}$ versus CDMI index in the lignite seam ahead of the working face at the longwall face K.-130/A in the South Preloge mining district.* 69
Figure 54: *Interpretation of the origin of CO_2 from the analysed coalbed gas samples from the Velenje Basin using the $\delta^{13}C_{CO2}$ versus CDMI index in the lignite seam ahead of the working face at the longwall face K.-50/C in the Pesje mining district.* 70
Figure 55: *Interpretation of the origin of CO_2 from the analysed coalbed gas samples from the Velenje Basin using the $\delta^{13}C_{CO2}$ versus CDMI index in the lignite seam ahead of the working face at K.-5/A in the Pesje mining district.* 70
Figure 56: *Interpretation of the origin of CO_2 from the analysed coalbed gas samples from the Velenje Basin using the $\delta^{13}C_{CO2}$ versus CDMI index in the lignite seam ahead of the working face at K.-65/F in the North Preloge mining district.* 71
Figure 57: *Trial drainage system location at the longwall panel K.65/F in the Pesje Mine District.* 72
Figure 58: *The Nash 2BE1 203 drainage pump showing all elements* (Jamnikar, 2015)..... 73

Figure 59: *Drained gas concentration sensors (from left: CO_2 (0 – 100 %), CH_4 (0 – 100 %), CO (0 – 200 ppm*)). (Jamnikar, 2015) 73
Figure 60: *Drained gas pressure and temperature monitoring (from left: pressure sensor (-1 – 1 bar), pressure gauge (-1 – 5 bar), temperature sensor (0 - 100 ℃)* (Jamnikar, 2015)..... 74
Figure 61: *The distribution of vertical stress around the longwall face* (Likar et. al, 2006). 81
Figure 62: *Flac^{3D} modelling steps flowchart* (modified after Board & Peirce, 2009). 82
Figure 63: *Mohr-Coulomb Failure Criteria* (Burke, 2003). 84
Figure 64: *Variation of cohesion (a) and friction angle (b) with plastic* strain (modified from Itasca, 2005). 85
Figure 65: *Approximation by linear segments* (modified by Itasca, 2005). 85
Figure 66: *Cross section of the longwall panel K.-65/F.* 86
Figure 67: *Geomechanical model with represented block groups.* 87
Figure 68: *Geological profile of the model at longwall panel K.-65/F.* 88
Figure 69: *Schematic illustration of observation points' position in the z-direction.* 90
Figure 70: *Vertical stresses at the longwall face during horizontal excavation for different lithotypes.* 91
Figure 71: *Vertical stresses at the longwall face during top coal caving for different lithotypes.* 91
Figure 72: *Modular architecture of TOUGH2 (Pruess, et al., 2012).* 93
Figure 73: *TOUGH2 input formats* (Pruess et al., 1999). 95
Figure 74: *TOUGH2 input formats (continued)* (Pruess et al., 1999). 96
Figure 75: *Schematic geometry used in TOUGH2 flow models in the top coal caving model.* 99
Figure 76: *2D model equilibrium situation.* 101
Figure 77: *Left) Simulation results of drainage at 100 m to the longwall face in xylite; Right) Simulation results of drainage at 60 m to the longwall face in xylite.* 102
Figure 78: *Left) Simulation results of drainage at 40 m to the longwall face in xylite. Right) Simulation results of drainage at 20 m to the longwall face in xylite.* 103
Figure 79: *Left) Simulation results of drainage at 10 m to the longwall face in xylite. Right) Simulation results of drainage at 5 m to the longwall face in xylite* . 103
Figure 80: *Left) Simulation results of drainage at 100 m to the longwall face in detrite. Right) Simulation results of drainage at 60 m to the longwall face in detrite.* 104
Figure 81: *Left) Simulation results of drainage at 40 m to the longwall face in detrite. Right) Simulation results of drainage at 20 m to the longwall face in detrite.* 104
Figure 82: *Left) Simulation results of drainage at 10 m to the longwall face in detrite. Right) Simulation results of drainage at 5 m to the longwall face in detrite.* 104

Figure 83: *Simulation results of drainage Left) 100 m in front of the longwall face for a mixed lithotype and Right) 60 m in front of the longwall face for a mixed lithotype.* 105
Figure 84: *Left) Simulation results of drainage at 40 m in front of the longwall face for a mixed lithotype. Right) Simulation results of drainage at 20 m in front of the longwall face for a mixed lithotype.* 106
Figure 85*: Left) Simulation results of drainage 10 m in front of the longwall face for a mixed lithotype. Right) Simulation results of drainage at 5 m in front of the longwall face for a mixed lithotype.* 106

List of Tables

Table 1: *Langmuir Pressure and Langmuir Volume results, measured at Imperial College London* (Durucan et al., 2012). 34
Table 2: *Methane and carbon dioxide concentrations and their stable carbon isotope composition in coalbed seam gases at G2/C (North Preloge).* 58
Table 3: *Methane and carbon dioxide concentrations and their stable carbon isotope composition in CSG at K.-50/C (Pesje).* 59
Table 4: *Methane and carbon dioxide concentrations and their stable carbon isotope composition in CSG at K.-50/C (Pesje) - continued.* 60
Table 5: *Methane and carbon dioxide concentrations and their stable carbon isotope composition in CSG at K.-130/A (South Preloge).* 61
Table 6: *Methane and carbon dioxide concentrations and their stable carbon isotope composition in CSG at K.-5A (Pesje).* 62
Table 7: *Methane and carbon dioxide concentrations and their stable carbon isotope composition in CSG at K.-65/F (Pesje).* 63
Table 8: *Results of stable carbon and hydrogen isotope composition of methane*... 64
Table 9: *Drainage borehole parameters.* 72
Table 10: *Drainage results from borehole R3* (Jamnikar, 2015). 76
Table 11: *Drainage results from the borehole R4* (Jamnikar 2015)..... 77
Table 12: *Result of gas drainage from borehole R5* (Jamnikar, 2015). 78
Table 13: *Material properties used in a geomechanical model of the longwall panel K. 65/F in the 100 % xylite model.* 88
Table 14: *Material properties used in a geomechanical model of the longwall panel K. 65/F in the 100 % fine detrite model.* 89
Table 15: *Material properties used in a geomechanical model of the longwall panel K. 65/F in the 50 % of xylite and 50 % of fine detrite model.* 89
Table 16: *TOUGH2 input data blocks* (Pruess et al., 1999). 97
Table 17: *Material properties used in the 100% xylite model.* 100
Table 18: *Material properties used in the 100% detrite model.* 100
Table 19: *Material properties used in the 50% xylite and 50% detrite model.* 100

Abbreviations

^{2}H/H	=	ratio between deuterium and hydrogen
a	=	constant representing the goaf`s deformation modulus
ASCII	=	American Standard Code for Information Interchange
ATEX	=	Appareils destinés à être utilisés en ATmosphères EXplosibles (directive to protect employees from explosion risk in areas with an explosive atmosphere)
b	=	limiting vertical strain
c	=	cohesion
C	=	constant
$C_{\phi\sigma}$	=	compressibility parameter
CDMI	=	carbon dioxide-methane index
CoGasOUT	=	project Development of Novel Technologies for Predicting and Combating Gas Outbursts and Uncontrolled Emission in Thick Seam Coal Mining
CSG	=	coal seam gas
D	=	detrite
D	=	diffusion coefficient
D	=	disturbance factor
dG	=	detro-gelite
dX	=	detro-xylite
EOS	=	equation-of-state
f	=	yield function
FLAC	=	Fast Lagrangian Analysis of Continua software by Itasca
g	=	gravity
gD	=	gelo-detrite
gX	=	gelo-xylite
GSI	=	geological strength index
IEA	=	International Energy Agency
ICCP	=	International Committee for Coal and Organic Petrology
k	=	permeability
K_i	=	constant
k	=	permeability
k_0	=	initial permeability
LTCC	=	longwall top coal caving
m	=	mass flow rate
m_b	=	parameter analogous to the frictional strength of the rock
m_i	=	material constant of the intact rock
mD	=	mineral-rich detrite
q	=	flow rate
P	=	pore pressure
P	=	pressure
P_L	=	Langmuir pressure
P-wave	=	longitudinal seismic wave

P_y	=	longitudinal seismic wave in y-direction
RFCS	=	Research Fund for Coal and Steel
RZ2D	=	one-dimensional radially symmetric mesh
RZ2DL	=	two-dimensional radially symmetric mesh
s	=	factor of how fractured the rock is
S-wave	=	shear seismic wave
S_z	=	shear seismic wave in z-direction
T	=	tension
T	=	temperature
T_0	=	limit tension
THM	=	thermal-hydrologic-mechanical analysis
THMC	=	thermal-hydrologic-mechanical-chemical analysis
X	=	xylite
X3	=	CO_2 mass fraction in the aqueous phase, or in the gas phase, in the three-component system water-salt-CO_2
xD	=	xylo-detrite
X_{sm}	=	salt mass fraction X_s in a two component water-salt system, or solid saturation S_s+10;
XYZ	=	two or three dimensional Cartesian mesh
v	=	velocity vector
V_L	=	Langmuir volume
UN	=	United Nations
VELGASPREVENT	=	project Model for preventive recognition of the geodynamic phenomena in coal mines based on geophysics borehole measurements
VPDB	=	Vienna Pee Dee Belemnite
v_p/v_s	=	ratio between longitudinal seismic velocity and shear seismic velocity
α	=	Biot`s coefficient
$\alpha^{13}C_{CO2\text{-}CH4}$	=	carbon isotope fractionation factor between methane and carbon dioxide
σ	=	total stress
$\sigma_1, \sigma_2, \sigma_3$	=	principal stresses
σ_0^e	=	initial effective stress
σ_{ci}	=	uniaxial compressive strength
$\sigma_{i\,j}^N$	=	stress within a zone with *i* and *j* coordinate
σ_{xx}^e	=	effective stress component in x-direction
σ_{yy}^e	=	effective stress component in y-direction
σ_{zz}^e	=	effective stress component in z-direction
σ_n	=	generalized stress component from *i=1* to *i=n*
σ_v	=	vertical stress
$\delta^{13}C_{CH4}$	=	isotopic composition of carbon (13) in methane
$\delta^{13}C_{CO2}$	=	isotopic composition of carbon (13) in carbon dioxide
ΔC	=	concentration gradient
$\Delta\varepsilon^{ps}$	=	shear parameter
ΔP	=	pressure gradient
ϕ	=	angle of internal friction
Φ	=	cleat porosity
Φ_0	=	initial cleat porosity
ρ_f	=	fluid density
τ_{max}	=	maximum tension

μ_f	=	fluid viscosity

1 Introduction and Objectives

1.1 Background

The release of Coal seam gas (CSG) during underground coal mining creates unsafe working conditions in many mines around the world. Coal seam gas outbursts and explosions are responsible for thousands of mine injuries and fatalities each year (United Nations, 2010). Coal seam gases include mostly methane (CH_4), carbon dioxide (CO_2), nitrous oxide (N_2O), water vapour (H_2O) and in small quantities fluorinated greenhouse gases.

Due to regulation requirements on minimising greenhouse gas emissions, new technologies are being developed to reduce CSG emissions, which have led to the development of coal gas drainage and utilisation systems and improvement in many coal mines. According to the International Energy Agency (IEA, 2013), global emissions of CO_2 from fossil fuel combustion increased from 20.7 billion tonnes (Gt) in 1990 to 31 Gt in 2011 (Figure 1). Coal mines are a significant source of methane emissions accounting for 6 % of global anthropogenic methane emissions are released from coal mines, or about 400 million tonnes of CO_2 equivalent ($MtCO_2e$) per year (United Nations, 2010).

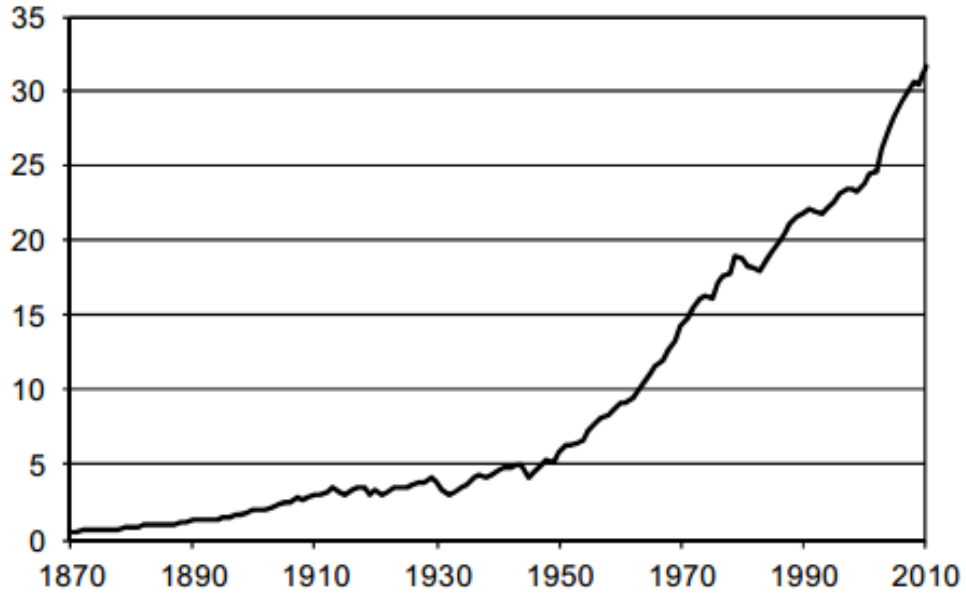


Figure 1: *Trend in CO_2 (in Gt) emissions from fossil fuel combustion from 1870 to 2010* (IEA, 2013).

Gases trapped in coal seams means that there is the ever-present threat of coal and gas outbursts. A coal outburst is an event where coal is ejected from the advancing development roads of the longwall face, while a gas outburst is an event where both coal and/or CSG is released in the working area of the mine. The factors that influence the risk of an outburst are gas content and permeability (Figure 2) i.e., the risk of an outburst increases if the coal seam has low permeability, low strength and a high gas content and high gas saturation. When all these criteria are present the mine should have in place adequate outburst

prevention measures including a suitable gas drainage scheme.

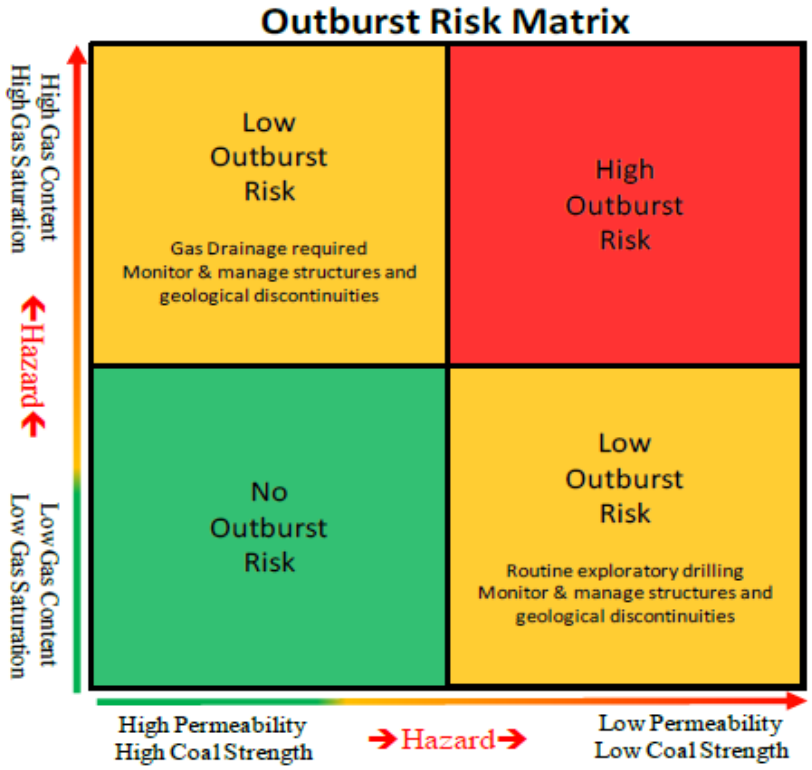


Figure 2: *Outburst risk matrix* (Black et al., 2009).

Outbursts of CO_2 have been experienced in Europe, Australia, Poland, Canada, Czech Republic and France. The largest outburst occurred at the Gagarin Colliery in the Donetsk coalfield (Russia) where 14,500 tonnes of coal were ejected together with 60,000 m^3 of methane (Lama and Saghafi, 2002). Numerous factors have been stated to influence the occurrence of outbursts, including the properties of coal, geology (e.g., joints, folds, and faults), mining induced stresses, strong sandstone beds in the roof, pillar size and shape, mining technique and mining rate (Westman, et al., 2001). Usually outbursts occur in coal mines with high rank coal (bituminous, anthracite or semi-anthracite), due to its greater gas adsorption capacity, higher internal surface area, lower permeability and lower porosity.

Coal seams also contain natural fractures or cleats, which act as a major flow network for gas inside the seam. Gas outbursts occur at areas where a high amount of gas is concentrated under high pressure in pockets of isolated coal when disturbed by mine workings or drilling. Coal seam gas emissions can also affect coal production. In the case of high CSG emissions into the area along the longwall face or in the return gate road, coal production must be halted until the level of CSG in the mine air is sufficiently diluted to an acceptable level. Mine ventilation systems are designed to satisfy mining safety regulations concerning the minimum volume of air flow required to maintain CSG emission under permissible limits.

From 2008 to 2010, more than 561 lives were lost in coal mines worldwide as a direct result of methane gas explosions and outbursts (Figure 3) (Black, 2011). Threshold values for levels of CSG for outburst prone areas vary from one coal mine to another, especially in coal mines with mixed CSG composition. In Australian and German coal mines the threshold values are 9 m^3/t for methane and 5 m^3/t for carbon dioxide (Beamish, 1984; Beamish & Crosdale; 1998).

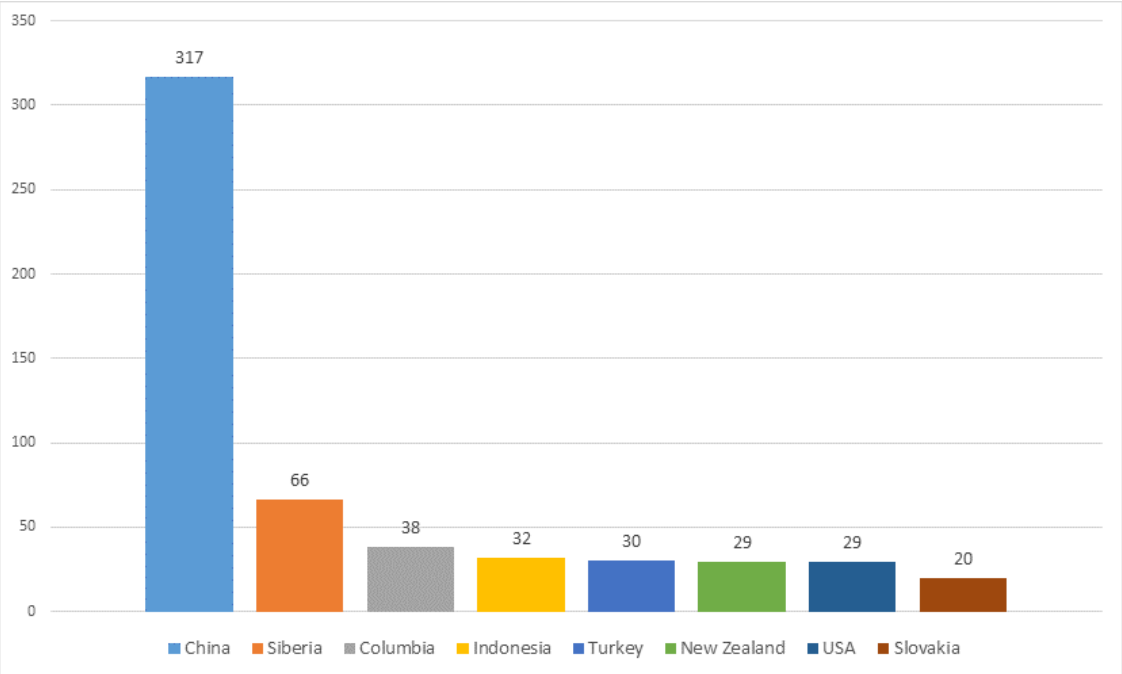


Figure 3: *Fatalities in coal mines from methane gas explosion or outbursts in the year 2008-2010* (Black, 2011).

Mining activities change the stress and pore pressure distribution around the longwall panel releasing gas into roadways and longwall faces. The most important factors that influence the occurrence of outbursts are the:

- gassiness of the coal seam;
- geological structures;
- properties of the coal and rock; and
- vertical and lateral stresses acting on the seam and/or rock as part of the coal seam (Lama & Bodziony, 1998).

Coal is a relatively soft rock compared with other geological materials, where the amount of stored strain energy is limited to the maximum coal strength. When an outburst occurs, this stored strain energy is usually not sufficient to cause an outburst and requires an additional source of energy which comes from gas adsorbed within the coal matrix in the micro pores and gas compressed in cleats and fractures. Outbursts involving CO_2 are typically more violent, more difficult to control and more dangerous because of the greater sorption capacity of coal for CO_2 (Lama & Saghafi, 2002). For example, in Polish coals and in the Velenje coal seam, the volume of CO_2 adsorbed at a given pressure is approximately twice that of methane (Ceglarska-Stefańska, et. al, 2008; Durucan et al., 2012).

The accumulation of methane and carbon dioxide in the mine has the potential to exceed the diluting capacity of the mine's ventilation and gas drainage systems, and the maximum permissible gas concentration limits (Black, 2011). Current practice in controlling the emission of CSG underground is mainly based on drainage from the source seams before the gas reaches the workings (Durucan & Edwards, 1986). For example, in gassy outburst prone coal i.e., the Bulli seam in Australia, coal mines typically drill in the order of 100, 000 m of inseam boreholes annually for the purpose of CSG drainage (Black, 2011). In the Pocahontas No.3 coalbed in USA, a drainage system comprising horizontal boreholes found that six months of longwall panel gas drainage reduced the ventilation air volume at the longwall face from 3,400 m^3/min to 720 m^3/min (Aul & Ray, 1991; Karacan et al.,

2007a, b). The low permeability of the Velenje lignite means that gas drainage is possible only when the coal mass is disturbed during active mining so that permeability is increased and a gas flow can be established. Gas drainage is also possible from the goaf area where the permeability of the coal is higher than in the unmined areas.

1.2 Motivation

Although lignite is a low rank coal the Velenje Coal Mine is still prone to uncontrolled gas emissions or gas outbursts and the mine loses on average 5 working days' worth of production per year, (equivalent to approximately 35 000 tonnes of coal) per stoppage and costing the mine 1 million Euro annually. The Velenje Coal Mine uses the mining method of longwall top coal caving (LTCC) of its ultra-thick coal seam because it represents high production and high efficiency mining. The patented Velenje Mining Method VMM, extracts lignite from the roof by taking advantage of natural breakage and crushing of the coal above the hydraulic shield supports. The lignite seam in the Velenje basin is up to 160 m thick and 200 to 500 m below ground level and is one of the thickest in the world. The impermeable clay overburden protects the coal seam from water inflow and prevents the CSG from escaping so that the seam acts as one huge gas reservoir.

Historically, all recorded gas outbursts at the Velenje Coal Mine have occurred at production faces, whereas coal and gas outbursts occur mainly at development headings when advancing into virgin areas. Figure 4 shows the number of rock bursts at the mine for the years 1961 to 2014. The highest number of rock bursts occurred between 1975 and 1985, which coincided with the highest number of longwall panels excavated and peak coal production. In 1985, 55 rock bursts were recorded with 47 of them in the Pesje mining district. The highest number of rock bursts was 99 events in 1992, of which 82 of them were also in the Pesje mining district. The mine experienced a major rock burst in 1994 at the longwall face K.+40/D, where one miner died and two were injured and again in 2003 this time killing two miners. From 2012 onwards, there have been an increasing number of rock and gas outbursts, possibly due to mining of the remaining and highly stressed coal block, which represents the main gas outburst or rock burst risk.

Potentially, the mine is facing an increased number of rock bursts, therefore, the number of longwall faces in the mine has fallen to an average of 6 per year. This is due to the mining of the remaining coal pillars, where the stable transportation gate roads are located. The mine is now developing a new longwall panel in the central pillar, which had previously been left unmined, and this has led to many coal outbursts during gate road development.

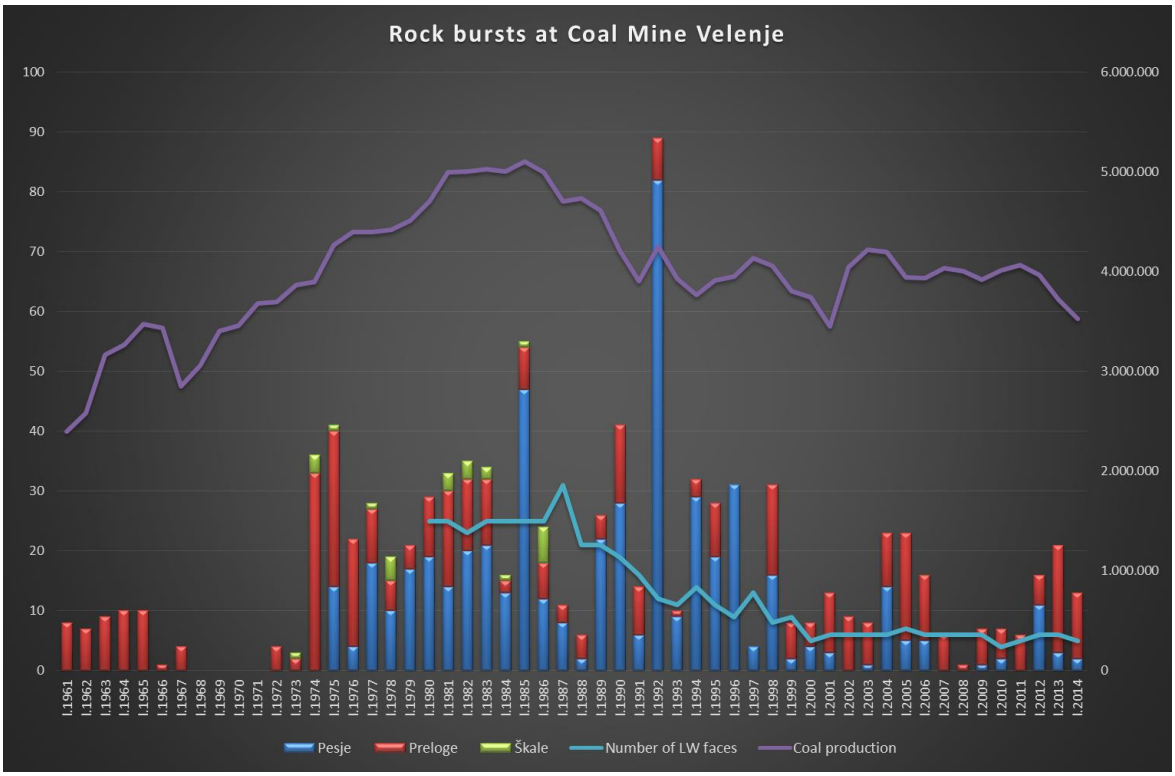


Figure 4: *Rock bursts at the Velenje Coal Mine from 1961 to 2014, the number of longwall faces working per year and coal production in tonnes.*

The Velenje mine has been researching into coal seam gases for the past 15 years and has found that CSG in the Velenje basin consists of a mixture of carbon dioxide (CO_2) and methane (CH_4) with nitrogen and other hydrocarbons as minority gases. The average gas mixture is approximately CO_2:$CH_4 \geq 2$:1 (Zavšek, 2004), where a high proportion of the carbon dioxide is adsorbed in the coal structure. Under normal burial conditions, CH_4 remains trapped and is dispersed through the coal as a free gas (Cervik, 1969).

Lignite in the Velenje seam is composed of different lithotypes, from fine detrite to the xylite and gelite. Previous studies at the mine found that outbursts are most common in areas of fine-detrital gelified lignite whereas, xylite-rich lignite is more stable and is less prone to outbursts. Also, xylitic lignite has higher mechanical strength and a low permeability, and can act as a gas barrier preventing gas from migrating. The critical zones for outbursts are where the fine detrital lignite is isolated by xylite-rich lignite and, when this layer is disturbed by mining activities the CSG is released rapidly as an outburst (Zavšek, 2004). Outbursts also occur in the vicinity of geological faults and shear zones.

To understand the physical and chemical characteristics of CSG at the Velenje mine a number of different investigations have been carried out in order to investigate the potential of installing a gas drainage system. These investigations included drilling long boreholes into the longwall panels from the gate roads to measure *in-situ* gas composition, coal seam gas pressure, gas isotopic composition and the stresses in the rock. Coal seam gas composition monitoring was performed on several longwall panels to collect data on the CSG composition of intact coal and to observe the influence of the longwall face on the migration of CSG. Active seismic tomography has also been performed with the aim of understand the kind of stress changes that occur in a panel, when the longwall face is at various distances to the seismic tomography section.

In 2013 the first pilot drainage experiments at the longwall panel K.-65/F were successfully performed. The pilot test was conducted under the RFCS funded project CoGasOUT, which confirmed the permeability of the Velenje coal seam and that, without

the presence of de-stressed rock material around the borehole, gas drainage is inefficient at a distance of >30 m out from the longwall face. Closer to the longwall face (< 30 m), the coal is crushed due to the induced stress from the advancing longwall face, which increases permeability allowing the CSG to flow. Following these early pilot experiments it was decided to proceed with more detailed testing of a gas drainage system at the mine.

The main reasons for establishing a CSG drainage scheme at Velenje Coal Mine are as follows:

- **Safety**: a pre-drainage system will reduce CSG emissions, especially of methane, and the risk of a gas outburst, which will result in safer working conditions for the miners.
- **Technical actions**: Reduced emissions of CSG in the gate roads and at the longwall faces will reduce deadlocks (stoppages) and increase coal production. Lower concentrations of CSG will also reduce the amount of ventilated air required in the mine and help to reduce dust levels.
- **Better working environment:** Lower velocities of ventilated air, due to lower CGS emission, is preferred for better working environment
- **Economy**: A CSG pre-drainage system and gas utilisation will reduce greenhouse gas emissions from the main ventilation airshaft, which will also reduce the cost of ventilation.

1.3 Objectives and Methodology

This research investigated the dynamic properties of coal seams during longwall production and aimed at establishing an understanding of the relationship between coal gas content, migration and gas emissions. Since the lignite seam in the Velenje basin is heterogeneous, many different CSG mixtures can be found in the mine. In addition, different petrographic properties of the lignite in different parts of the mine affect gas composition and emission rates. This heterogeneity in gas composition is one of the parameters that have been investigated. The flow and emission characteristics of gases in the Velenje Coal Mine has never been modelled using state-of-the-art computer numerical modelling software and the purpose of this doctoral work was to apply numerical modelling using *in-situ* measurements to construct a new gas migration model. This model will be a vital tool for drainage system design and for predicting gas emission at new longwall panels, as well in similar coal mines from around the world which are faced with the problem of high coal seam gas emissions. The main objectives of this research were:

- To provide a detailed review of the literature regarding CSG migration, numerical modelling and gas drainage.
- To provide an improved understanding of the characteristics of the geochemical behaviour of CSG in the Velenje lignite seam.
- To collate and analyse existing geomechanical and geochemical data.
- To develop a geomechanical model of longwall top coal caving processes for a representative longwall panel.
- To develop and validate a numerical model for gas flow and drainage with actual data obtained from pilot drainage studies, ventilation data and CSG compositional data.

Numerical modelling is widely used in coal mining to understand the behaviour of coal under dynamic stresses. Besides the field monitoring of gas pressure and composition around LTCC faces at the Velenje Coal Mine, this research used numerical modelling to establish the knowledge necessary for the design of a drainage system at the mine. Simple numerical models of the longwall panel K.-65/F were created to observe vertical and

horizontal stresses. In this research, the software package FLAC^{3D} was used for geomechanical modelling. FLAC^{3D} is a three-dimensional explicit finite-difference program designed for engineering mechanics computation. Materials are represented by polyhedral elements within a three-dimensional grid that can be adjusted by the user to form the shape of the object to be modelled (Itasca, 2005).

Geomechanical modelling was performed for the two main representative types of lithotypes and their mixtures:

- 100 % xylite;
- 100 % fine detrite
- And mixture of 50 % xylite and 50 % fine detrite.

The objective of the geomechanical modelling was to represent the different stress states at different distances from the longwall face, to generate the basic stress – permeability data that could then be used to model gas flow using the TOUGH2 software. TOUGH2 is a numerical simulator used for non-isothermal flows of multicomponent and multiphase fluids in one, two, and three-dimensional porous and fractured media (Pruess et. al, 1999). The objective of using TOUGH2 was to model gas drainage from a single borehole. The software takes into account different lithotype mixtures and varying distances of the borehole to the longwall face to determine the optimal distance of the borehole and the amounts of coal seam gas that can be drained from the seam. The data obtained from the numerical modelling can then compared with the actual drainage pilot test results, and be recalibrated, leading to drainage efficiency at the Velenje Coal Mine.

2 Review of Current Knowledge on Gas Retention and Flow in Coal Seams

2.1 Introduction

For any simulation, a thorough understanding of the basic principles is required. It is essential, for determining how CSG will behave around the active longwall face. This chapter presents a review of the geochemical properties of CSG, and its migration through coal into mine gate roads and longwall faces. It also describes the effect that mining has on coal permeability, the use of active seismic tomography and the different CSG drainage methods used in mines from around the world. A review of the use of numerical modelling in coal mining is also presented.

Coal seam gas is comprised mainly of methane and carbon dioxide. Methane is a colourless, odourless gas with a molar mass of 16.04 g mol^{-1}, and has a density of 0.656 kg/m^3 at 25 °C and 1 Atm (101.325 kPa), and 0.716 kg/m^3 at 0°C and 1 atm. Methane has low mass and because it can diffuse 1.6 times faster than air this allows it to easily pass through porous materials (Ediz, 1991). The presence of methane in a mine is a major hazard because it is highly explosive when in a concentration in air of between 5 - 15 vol. %. Figure 5 shows the different explosive methane/air mixtures where the explosive zone (red) is from 12 vol. % oxygen and 5 vol. % methane to 18 to 20 vol. % oxygen and 5 to 15 vol. % methane.

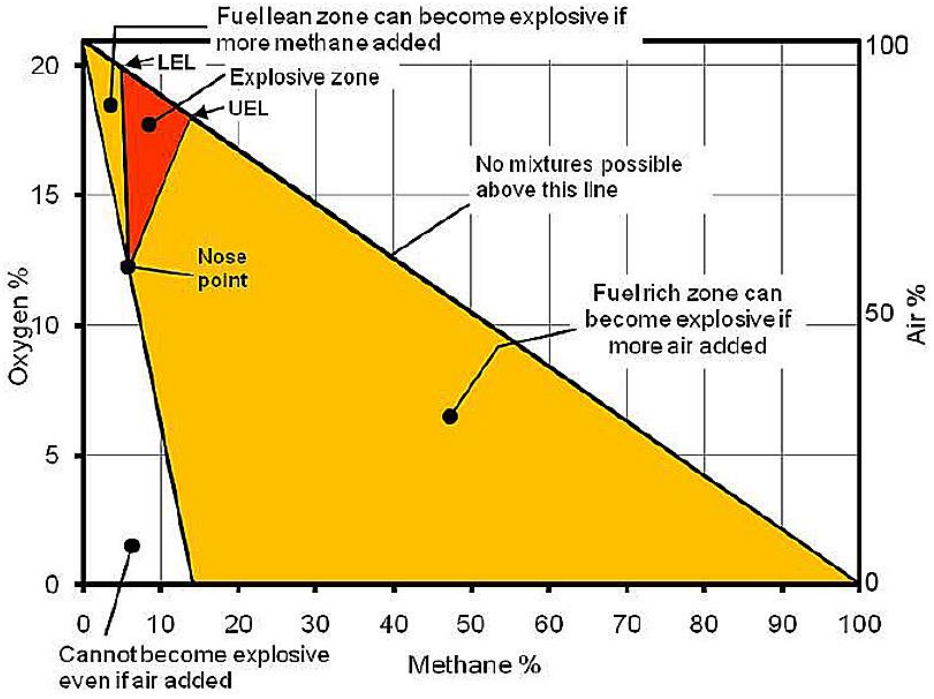


Figure 5: *Formation of Explosive Mixtures* (UN, 2010).

Carbon dioxide is naturally present in the atmosphere as part of the Earth`s carbon cycle and it is the most important greenhouse gas. It is also a colourless and odourless gas at low concentrations and has a molar mass of 44.01 g mol^{-1}. In high concentrations (> 2 vol. %) it has a sharp, acid odour. It is heavier than air (1.977 kg/m^3 at 0°C and 1 Atm) and is toxic at a concentration > 5 vol. %, while physiological effects can be experienced at concentrations as low as 1 vol. % (UN, 2010).

2.2 Review of Coal Seam Gas Migration

Coal deposits act as self-sourced natural gas reservoirs wherein the three crucial elements of the petroleum system, which are the source rock, reservoir and trap, are located together in a single geologic unit (Karimi, 2005).

Coal seam gas is typically stored in coal in four separate ways (Curl, 1978; Osisanya and Schaffitzel, 1996; Mastalerz et al., 2004 and Black, 2011):

1) adsorbed on the internal surfaces (micro pores);
2) absorbed into the molecular structure of the coal;
3) as free gas within voids, cleats and fractures;
4) as a solute in groundwater present within the coal seam.

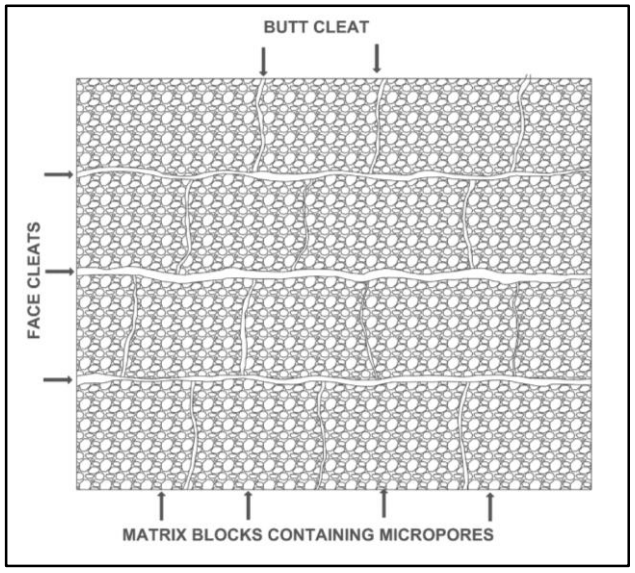


Figure 6: *Fracture system in coal* (modified after Shi and Durucan, 2003).

Coal seams are characterised by two distinctive porosity systems: a well-defined and almost uniformly distributed network of natural fractures (cleats) and a coal matrix containing a highly heterogeneous porous structure between the cleats (Shi and Durucan, 2003). The coal matrix permeability represents the gas flow in the pores that are ≤2 nm in size, while fracture permeability can occur in flow paths > 50 nm (Adeboye, 2011). Coal cleats are extension (opening-mode) fractures that form as a result of the stress generated by volume contraction or shrinkage of the coal matrix due to dehydration during maturation (Nelson, 2000). Cleats are made up of butt and face cleats, which are oriented perpendicular to each other (Figure 6). They represent < 2 % of the coal seam bulk volume, but are important in coal bed reservoirs because reservoir permeability derives mainly from the presence of these cleat networks (Karimi, 2005). Guo et al. (2003) describes the characteristics of coal reservoirs in two ways: 1) the coal matrix micro pores represent low permeability and high storage and are the primary porosity system and 2) the cleat macro

pores represent high permeability and low storage and are referred to as the secondary porosity system. The opening and closing of the cleats is particularly sensitive to horizontal stresses, because the cleat system is oriented normal to the bedding plane (Karimi, 2005).

In virgin coal, the pressure in the fracture system and the concentration of CSG in the micro pore structure are in equilibrium (Cervik, 1969). Migration occurs when the pressure around the coal mass is reduced and then stops again when a new equilibrium is reached. The release of CSG and its flow through the strata towards the working areas of the mine is also governed by the permeability of the surrounding coal (Durucan and Edwards, 1986). Permeability is controlled by the physical properties of the fractures, specifically their orientation, spacing, compressibility and effective porosity (Karimi, 2005). Modern coal mining methods with their high production rates create dynamic stresses in the coal, which in turn affects the permeability of the strata.

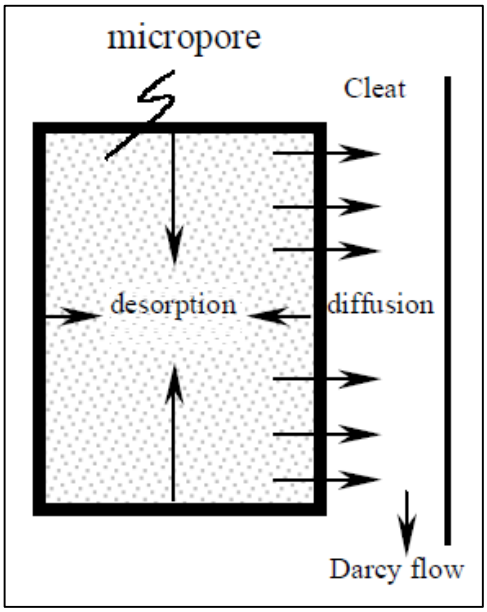


Figure 7: *Gas transport in the coal between micro pores and cleats* (Guo et al., 2003).

Two processes cause gas to flow in coal: 1) diffusion, where gas is desorbed from the coal matrix into the fracture network (Fick`s diffusion law), and 2) a pressure difference that drives gas flow through the fracture network as described by Darcy`s law (Williams and Weissman, 1995). Fick`s diffusion law is defined as:

$$m = -D\Delta C \tag{1}$$

Where m is the mass flow rate, D is the diffusion coefficient and ΔC is the concentration gradient. Darcy`s law is defined as:

$$v = -\frac{k}{\mu_f}(\Delta P - \rho_f g) \tag{2}$$

Where v is the velocity vector, k is the permeability tensor, μ_f is the fluid viscosity, ΔP is the pressure gradient, ρ_f is fluid density and g is acceleration due to gravity. Gas transport in the coal between the micro pores and cleats is shown in Figure 7. The mass of the desorbed gas from the micro pores and the mass of the diffused gas should represent the total mass of free gas. The porosity of the cleat system is related to permeability using the following equation:

$$k = k_0 \left(\frac{\phi}{\phi_0}\right)^3 \quad (3)$$

Where k is the permeability, k_0 is the initial permeability, ϕ is the cleat porosity and ϕ_0 is the initial cleat porosity (Connell, 2009). Permeability depends on the effective stresses in the coal.

Owili-Eger and Ramani (1974) found that the volume of CSG released into the mine air from fissures is generally a result of diffusion. Coal seam gas emissions in the mines are influenced mainly by the gas content, thickness of the coal seam, the depth of the seam, the pressure inside the coal seam, the mining method used and the rate of coal production (Vutukuri and Lama, 1986; Ediz, 1991). As the rank of a coal increases, its maximum capacity to adsorb gas also increases (Moore, 2012). The depth of the coal seam also influences the CSG content. For example, the gas content of the coal-bearing sequences in the Czech part of the Upper Silesian Coal Basin is between 2 m^3/t and 10 m^3/t and shows an overall drop in gas content with increasing depth (Hemza et al., 2009, Weniger et al., 2012). However, as Figure 8 shows clearly, in the Australian Surat Basin gas content increases with depth (Scott et al., 2007, Moore, 2012). The depth of the coal seam also influences permeability i.e., the deeper the coal seam the lower the permeability. This was shown to be the case for several coal basins (Figure 9) including the Carboniferous in the Upper Silesian Coal Basin in Poland, and the Bowen Basin and the Permian Coal Basin in Australia (Moore, 2012).

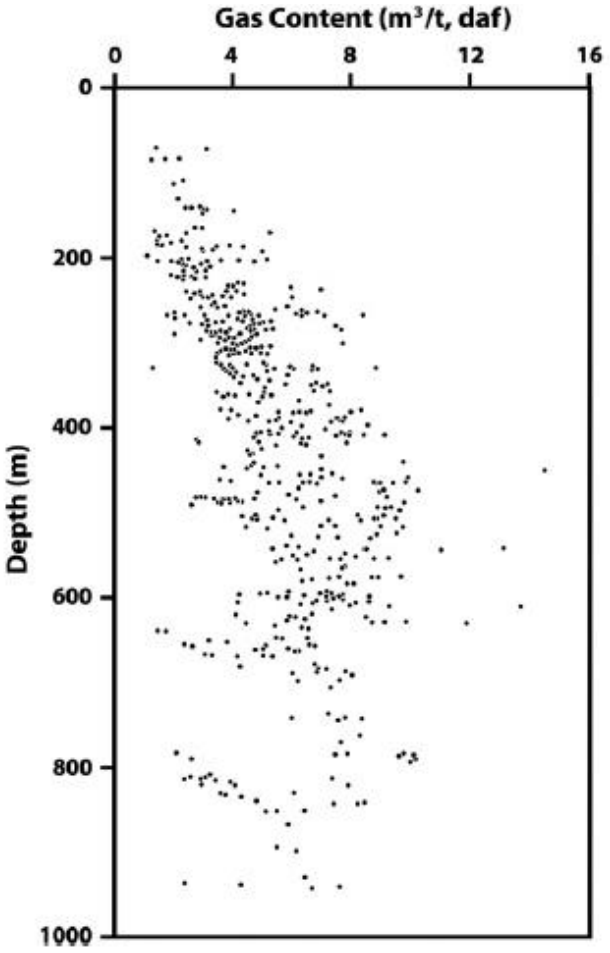


Figure 8: *Relationship between depth and gas content in the Surat Basin, Australia* (Scott et al., 2007, Moore, 2012).

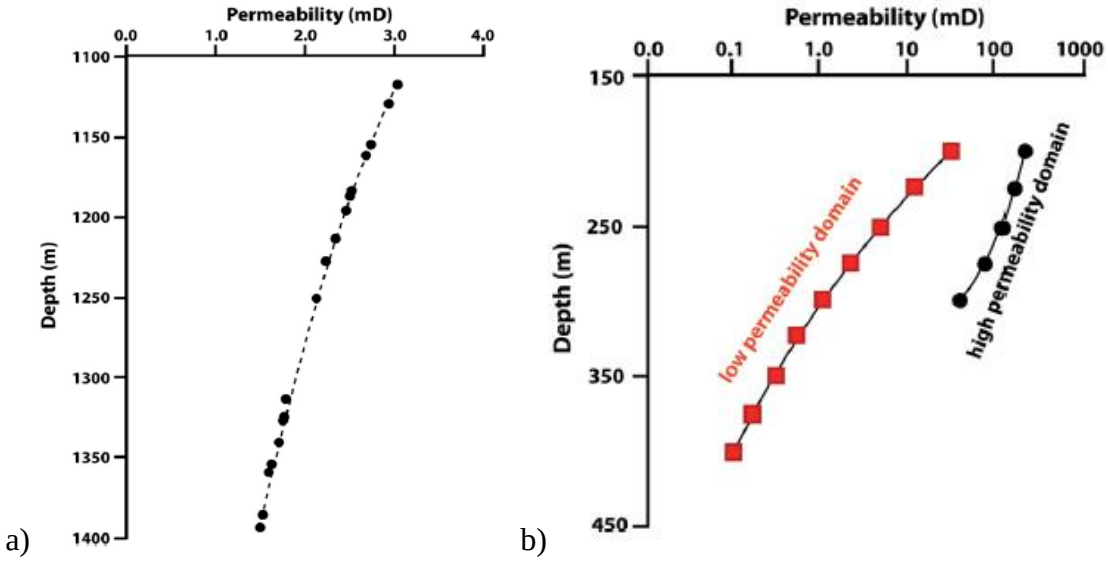


Figure 9: *Relationship between permeability and coal seam depth a) in the Upper Silesian Coal Basin, Poland* (McCants et al., 2001, Moore, 2012), *b) in the Permian aged Bowen Basin, Australia, where two geological domains (geographic areas of similar geology and gas relationship) have been identified* (Esterle et al., 2006, Moore, 2012).

Understanding the origins of CSG is essential when attempting to understand gas migration. A portion of the CSG may be sources from deep seated activities, and migrates either through the natural fault systems or as a result of thermal migration due to volcanic activities. Human activities can also cause CSG to migrate, such as mining and gate road development. Stable carbon isotope analysis of the CSG can define the different origins of the CSG at the same location in the mine resulting from mining activites. It can aid in inputting the correct parameters into a flow model and to calibrate the results from the flow model using actual mine gas data. Stable carbon isotope analysis of CSG is discussed in detail in Chapter 4. For instance, Moore (2012) writes that the gas content of coals of biogenic origin is lower than in thermogenic coal. Gas of biogenic origin is rarely found in concentrations above 4 to 6 m^3/t, while high rank coals can store up to 20 m^3/t of CSG. In addition, the chemical processes occurring in the coal structure, such as diffusion and adsorption/desorption, are essential factors in CSG migration and must be accounted for when modelling CSG emissions and uncontrolled gas outbursts.

2.3 Review of the Effects of Stress Distribution around a Longwall Face on Permeability

Coal seam gas can represent a major hazard during mining involving large rock mass disturbances. The dynamic influence that mining has on the surrounding coal can influence CSG migration through the coal seam. Different porosity systems, and consequently permeability, influence how CSG will migrate. The changes in the stress state of the strata surrounding an advancing (conventional) longwall face have been extensively studied (Whittaker, 1974). For instance, Whittaker (1974) describes the changing dynamic stresses and the formation of stress abutment in the worked seam ahead of an advancing longwall face (Figure 10). When the excavation of the coal is performed, three zones are visible in the overburden according to the degree of rock deformation and fracturing, these are the caved zone, fractured zone and the continuous deformation zone (Figure 10). At the Velenje Coal Mine, the caved zone is three times larger than the extraction thickness.

In the Velenje Mining Method, the coal face is divided into the footwall section and the

hanging wall section. The footwall section or so-called lower excavation section is 4 to 5 m in height and exploitation is performed by cutting of the coal face. The hanging wall, or upper excavation section, measuring from 5 - 17 m in height is exposed to dynamic stress conditions, which causes the coal to cave in. In the caved zone crushed fragments of coal are irregular in shape giving this zone a relatively high void ratio and permeability. By advancing the coal face, the caved zone becomes more compressed due to the height of the overburden. Here permeability is expected to be high after the consolidation process is complete. The second zone is the fractured zone that occurs above and around the caved zone. The fractured zone can extend out to a distance of 30 to 60 times that of the thickness of extraction height (Esterhuizen and Karacan, 2005). The permeability in this region continues to increase. The third zone is the bending zone and contains either only small or no fractures.

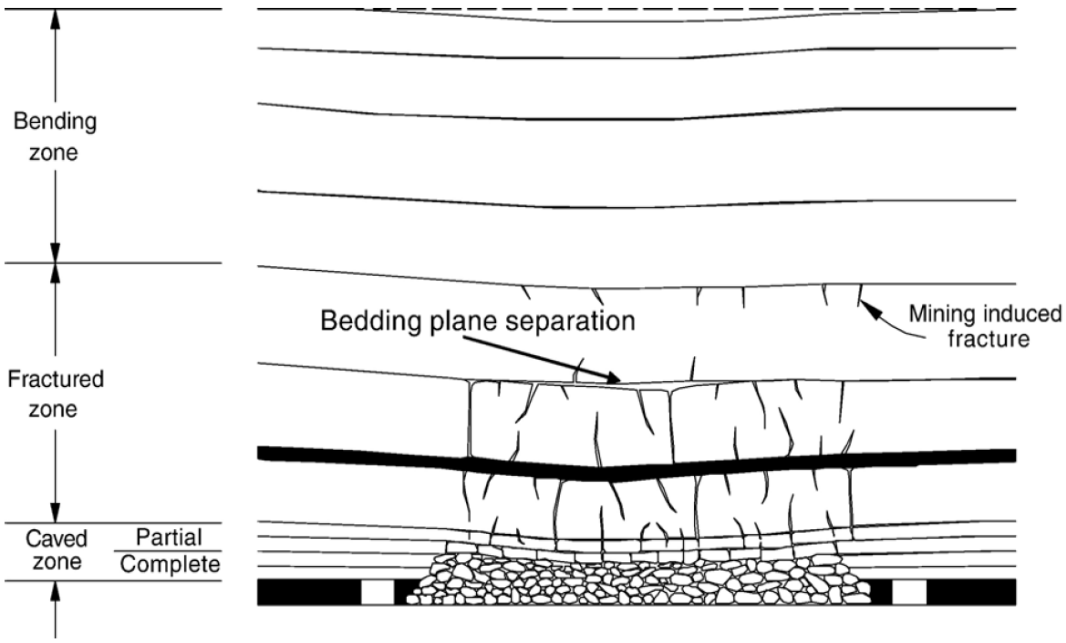


Figure 10: *Schematic of strata response to longwall mining* (Singh and Kendorski, 1981; and Karacan et. al, 2007b).

Recognising the impact of stress on coal permeability, McPherson (1975) was the first to consider the dynamic changes in the permeability of a worked seam in response to longwall coal extraction (Figure 11) (Durucan et al., 2014). This high-pressure zone is called the pressure abutment zone.

Stress distribution has a major influence on the bulk volume permeability of the fractured and disturbed zone (Whittles et al., 2006). The opening and closing of cleats is particularly sensitive to effective horizontal stresses, and the permeability of the cleat system is primarily controlled by changes in the effective horizontal stresses (Karimi, 2005). Mine workings, containing air at near atmospheric pressure create a “pressure sink” into which CSG flows from the zone of gas emission surrounding the mine workings (Dunmore, 1975; Harpalani and McPherson, 1998; Ediz, 1991).

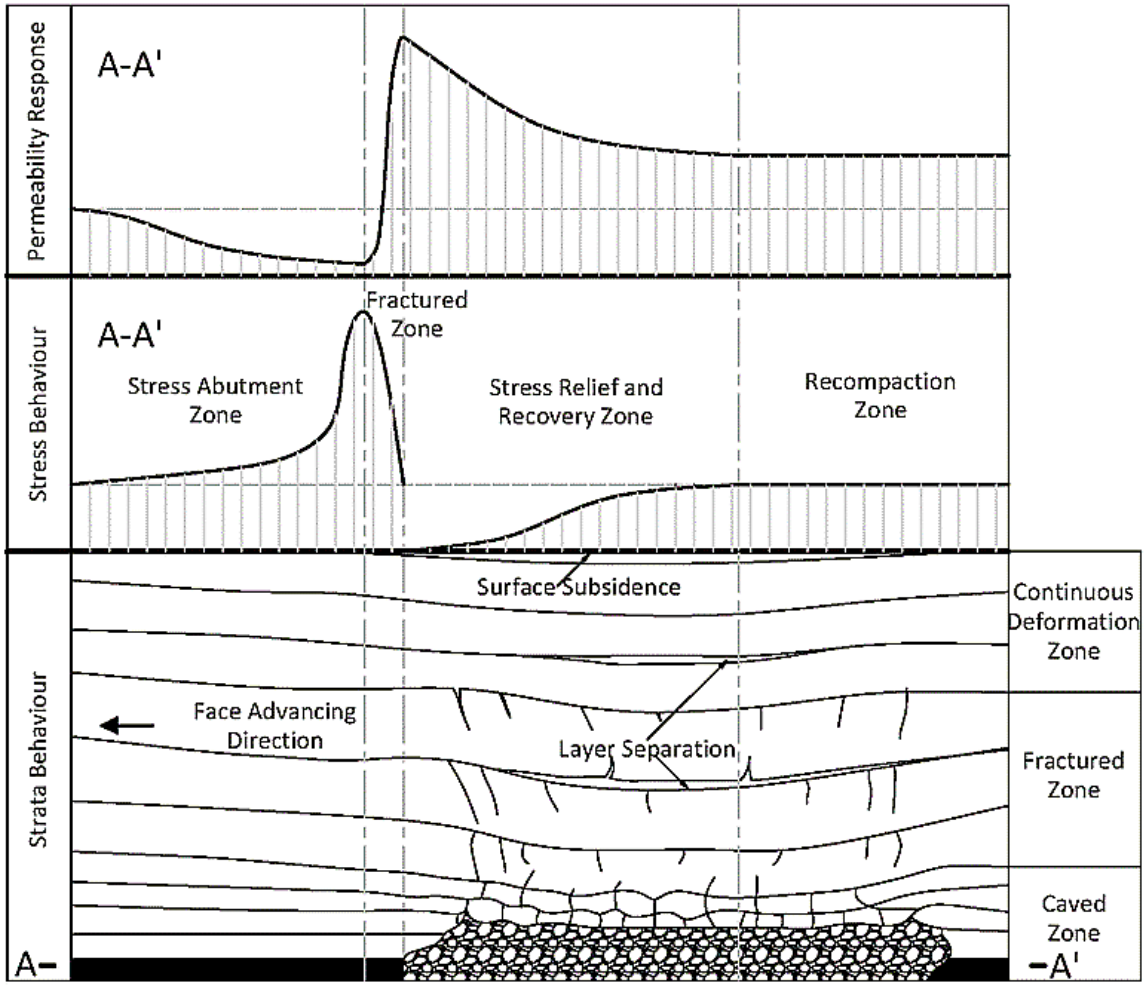


Figure 11: *Longitudinal section of an advancing longwall face: strata and stress behaviour around the longwall face* (Durucan et al., 2014).

Effective stresses can be linked to pressure and strain and then to permeability by the following:

$$k = k_0 e^{-3C_{\phi\sigma}(\sigma^e - \sigma_0^e)} \quad (4)$$

where $C_{\phi\sigma}$ is a compressibility parameter referred to as the cleat volume compressibility, σ_0^e is the initial effective stress with $\sigma_e = \sigma - \alpha P$ where σ is the total stress, positive in compression, α is Biot`s coefficient and P is the pore pressure (associated with the macro porosity in the dual-porosity framework) (Seidle et al., 1992; Connel, 2009). Combined numerical modelling and laboratory investigations into the stress-permeability relationship of coals and detailed numerical modelling of the permeability distribution and associated gas flow around an advancing longwall coal face were performed by Durucan (1981). Later Durucan & Edwards (1986) developed an exponential equation, which provides a best fit to the stress – permeability correlation (Equation 5):

$$K = (1{,}12 - 0{,}03\sigma_3) K_i e^{-(1{,}12 - 0{,}03\sigma_3) C \sigma_3} \quad (5)$$

where K_i and C are constants, σ_3 is the radial stress applied (σ_1=2.7 σ_3) and K is the permeability at stress σ,. Constant C, which represents the compressibility of coal i.e. the degree of reduction in permeability under stress, is the behaviour of the micro-structure of coal under stress and is determined individually for each seam. Constant K_i defines the relative incidence of existing fissures and fractures in the coal (Durucan & Edwards, 1986).

This means that the coal with a higher value of K_i will have higher permeability. Also, Shi & Durucan (2004) introduced a physical relationship for each normal effective stress component (Equation 6):

$$\sigma_{xx}^{e} = E\left[\frac{1}{1+\nu}\overline{\varepsilon}_{xx} + \frac{\nu}{(1+\nu)(1-2\nu)}\overline{\varepsilon} + \frac{1}{3(1-2\nu)}\right]\overline{\varepsilon}^{S}$$
$$\sigma_{yy}^{e} = E\left[\frac{1}{1+\nu}\overline{\varepsilon}_{yy} + \frac{\nu}{(1+\nu)(1-2\nu)}\overline{\varepsilon} + \frac{1}{3(1-2\nu)}\right]\overline{\varepsilon}^{S} \quad (6)$$
$$\sigma_{zz}^{e} = E\left[\frac{1}{1+\nu}\overline{\varepsilon}_{zz} + \frac{\nu}{(1+\nu)(1-2\nu)}\overline{\varepsilon} + \frac{1}{3(1-2\nu)}\right]\overline{\varepsilon}^{S}$$

where the overpressure represents the "increment", E is the Young modulus, ν is the Poisson ratio, volumetric strain is defined as $\varepsilon = \varepsilon_{xx} + \varepsilon_{yy} + \varepsilon_{zz}$ and ε^{S} is the volumetric adsorption strain (Connel, 2009). The absolute permeability of coalbeds has been shown to vary exponentially with horizontal stresses sustained by the coalbed reservoir (Durucan & Edwards, 1986; McKee et al., 1988; Seidle et al., 1992, Syed, 2011).

Obtaining accurate permeability measurements in lignite samples is made difficult by the development of new fissures and fractures, as the coal loses its moisture after the samples are brought to the surface. In addition, the lignite heterogeneity is one of the factors that make it impossible to define uniform coal seam permeability in the 160 m thick coal seam in the Velenje Basin. Until now, only an approximation of the permeability of the Velenje Lignite has been used.

2.4 Review of Active Seismic Tomography of the Longwall Face

In the mining industry tomography measurements are used to image geological characteristics, such as major faults and joint systems, and mining induced features. Seismic velocity tomography is a non-invasive technology for studying the internal properties of a coal panel by observing the actions of pressure waves in the panel. Seismic tomography uses mathematical modelling of P and S wave travel times to map velocity interference in the interior of the coal. The ray paths of seismic waves are bent by the changes in the velocity structure of the medium. Two-dimensional travel time inversions can be performed to define the velocity of the waves at any point. The distribution of the wave velocities is presented as tomograms.

Active seismic tomography is a special seismic method, whereby the transmitters and the receivers of the seismic waves are placed on opposite sides of the panel. The primary energy sources used are seismic waves generated by explosives for P-waves and by a shear wave vibrator for S waves. More recently, to generate controlled S-waves a new high-energy borehole S-wave vibrator has been developed the prototypes of which were built and designed in the workshop of the K-UTEC AG Salt Technologies in Sondershausen, Germany. Active seismic tomography has been used to help understand the stress distribution in coal seams during mining activities. The tomography method has also been adapted to image stress concentrations ahead of a longwall face by a unique method of using the longwall mining equipment as the seismic source.

Seismic tomography techniques have been applied more often in oil and gas exploration and in earthquake studies than in the coal mining industry where it was originally employed in coal mines to detect voids, image structures and/or old workings typically from a single location in the mine e.g., face areas of mines and gate roads developments, well ahead of the planned developments (Hanson et al., 2002). Tomograms typically show P-wave velocities but can also reveal the seismic attenuation of a particular geologic structure (Glazer & Lurka, 2007; Furniss, 2009). Previous measurements have focused on P-waves but nowadays P-waves and S-waves are measured since their both types of wave velocities

provide more information, since how they vary, given in response to the many parameters, differs.

The velocity-stress relationship during laboratory testing of rocks indicates that the P-wave velocity slightly increases with initial axial stress. Prior to peak stress the elastic wave velocity begins to decrease rapidly as micro cracks propagate (Paterson & Wong, 1978). An increase in velocity is indicative of an increase in stress, but a decrease in velocity is not necessarily indicative of failure but may be a pre-failure indicator. The described changes in P-wave velocity result largely from changes in the fracture zones and porosity (Thill, 1973). It is vital that the velocity-stress relationship is carefully considered when using velocity tomograms to make inferences about the relative stress in the coal seam (Durucan et al., 2011). Other factors also affect P-wave velocity, including fluid saturation, which can increase the wave speed (Thoksoz et al., 1976) and the preferred orientation of the cracks, which can give rise to velocity anisotropy.

Westman (1996) describes a case study where the stress distribution in a segment of a coal mine was imaged using both compression and shear wave tomography. In the study, two sets of measurements were conducted around a 215 m wide coal panel. The first set was performed when the longwall face was 25 m away from the survey area and the second when the longwall face was within 8 m of the observation area. Seismic sources were place on one side of the panel and a series of receivers at 6 m intervals on the other side (Durucan et al., 2011). The results of the study revealed the following:

- A good correlation between *in-situ* shear wave velocity distributions with stress measurements with conventional mining instrumentation taken at the survey location.
- In the *in-situ* shear wave velocity tomogram the distribution of stresses are clearly seen.
- The *in-situ* P-wave velocity tomogram does not correlate with the distribution of stresses.

A literature search found few large-scale seismic tomography mine studies. Friedel et al. (1997) used active sources to span drifts and image areas of high velocity in the longwall faces, while Kormendi et al. (1986) described an early study of imaging the velocities through a longwall panel, which resulted in high velocity areas in advance of the longwall face.

Tomographic imaging of the excavation of a longwall panel section has been described by Westman (2001), where roof bolt mounted receivers were used in combination with a longwall shearer. The tomography results were then correlated with shield pressure data measurements on the longwall shields at the face. The results show a clear correlation between the tomograms and the seismically active areas. Westman's study also shows that tomography can be used for imaging the stress conditions around a longwall face without disrupting production.

Zheng et al. (1991) measured ultrasonic velocities on relatively "undisturbed" coal samples using triaxial and hydrostatic compression. The coal used in their study was surface mined and degassed. The effects of water saturation on the coal static-dynamic behaviour were also examined. Their results show how P-wave velocity increases, while S-wave velocity decreases as the level of saturation increases. It is hypothesized that this is an effect of the cleat/fracture system in the coal, arguing that pore fluid dampens S-wave propagation by reducing the solid-solid contact area (Zheng et al., 1991).

Yu et al. (1993) found from laboratory measurements of P- and S-waves on Permian coals from Wollongong, New South Wales, Australia, that water saturation has a strong influence on P-wave velocities, while it has only a minor effect on S-wave velocities. This behaviour is attributed to the presence of thin cracks.

Xue (Xue, 2005) using coal samples from the Kushiro coal mine, Northeast Hokkaido, Japan carried out laboratory experiments on coal matrix swelling strain and noted that P-wave velocity changes during CO_2 injection. In a fractured sample coal matrix swelling caused the P-wave velocity to increase by 12.7%. This increase was greater than the 9.4% increase observed when the sample was subjected to a hydrostatic pressure of 2.5 MPa (Xue, 2005). This result suggests that the swelling of the coal matrix during CO_2 injection caused cleat closure and a reduction in the coal's permeability.

The relationship between induced stress and velocity is very diverse (Westman, et al. 2008). The different lithologies in the coal influence seismic velocity distribution. At the Velenje mine, seismic methods have been previously applied to study outburst prone lithotypes in the lignite as part of the Eureka Project VELGASPREVENT in cooperation with K-UTEC (Zavšek et al., 2008). Their aim was to develop, test and take geophysical measurement procedures using long, horizontal research boreholes with the overall goal to identify the various lignite lithotypes related to coal and gas outbursts. Seismic P-wave velocities were measured on core samples taken from different parts of the coal seam (Zavšek et al., 2008). During the project an S-wave vibrator was developed and tested. Figure 12 shows the S-wave velocity distribution across a longwall panel analysed under the VELGASPREVENT project. The S-wave velocities correlated well with laboratory tomography measurements. But, the shear-wave vibrator used in the VELGASPREVENT project was limited in its capacity for making successful measurements under the actual strata conditions that prevail in the mine (Zavšek et al., 2008).

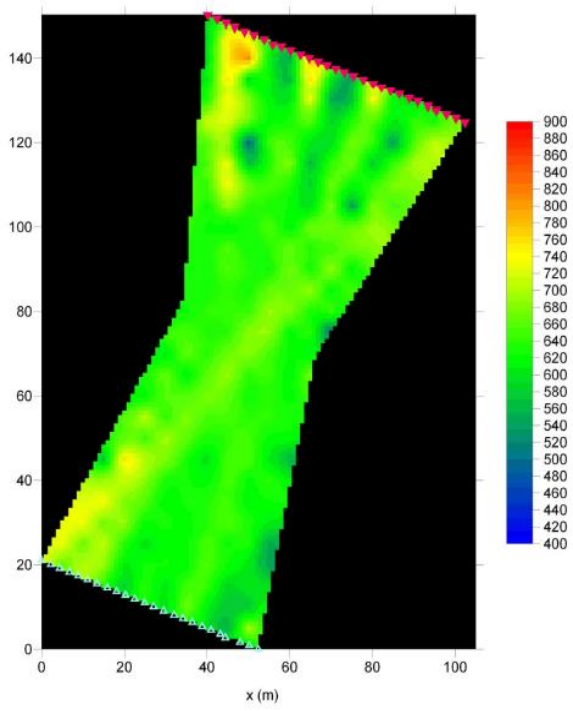


Figure 12: *S-wave velocity tomogram across a longwall coal panel in the Velenje Coal Mine* (Zavšek et al., 2008).

Active seismic tomography can help to understand the dynamic influence that the advancing longwall face has on the coal, either in front of or in the surroundings of the longwall face. This knowledge is useful for use in geomechanical models and for gas flow modelling. The tomographic data obtained reveal areas that are more disturbed by active mining, which are essential for predicting the flow paths of CSG. It also reveals the influence of the longwall face advance and the size of the zones of disturbed coal and how they are evolving.

2.5 Review of Current Knowledge on Coal Seam Gas Drainage

Coal seam gas drainage is not new. The first recorded methane drainage utilisation was recorded at Salton Colliery in Northwest England. The methane was drained and brought to the surface through a square wooden pipe where it was used to heat specially constructed furnaces (Hendriks & de Jager, 2001). In the first half of the 20th century more modern drainage systems were developed in Europe. Systematic and effective gas drainage methods were being used throughout Europe by the 1950s although full-scale pre- and post-drainage of gas only began in Australia in 1980 at the West Cliff and Appin Collieries (Lunarzewski, 2001). Coal seam gas may be liberated into a mine from a number of sources including the following (Black, 2011):

- Exposed mine roadways;
- During coal cutting in both development gate roads and longwall panels;
- Into the longwall goaf from adjacent gas bearing coal seams and strata;
- From the longwall goaf into connecting airways; and
- From coal being transported from mine via the coal transportation system.

At present several CSG drainage systems exist, from pre-drainage to post-drainage to in-seam goaf drainage (Figure 13 and Figure 14). Selection of the most appropriate gas drainage method depends mainly on site specific geological and mining conditions, such as coal seam permeability, seam gas content, seam hardness, and cost (Wang and Xue, 2008). The classification of gas drainage methods is based on the phase during which degasification is performed in relation to coal extraction (Lunarzewski, 2001). They are classified as the following:

- Pre-drainage by vertical or directional boreholes drilled from the surface;
- Pre-drainage by horizontal long boreholes drilled from development gate roads;
- Pre-drainage by inseam headings;
- Post-drainage of relaxed strata using cross-measure boreholes drilled into the overlying and underlying gas sources;
- Post-drainage by boreholes drilled from the surface;
- Post-drainage of old or active goaf areas from underground.

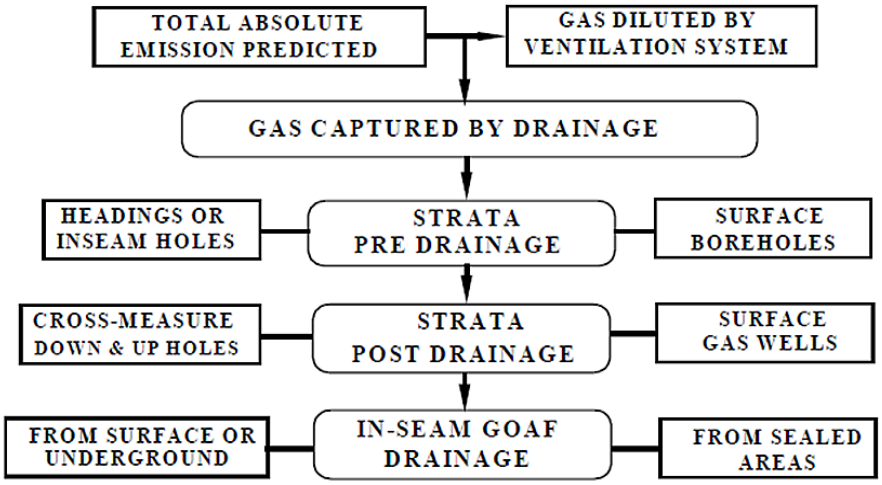


Figure 13: *Typical gas drainage methods* (Lunarzewski, 2001).

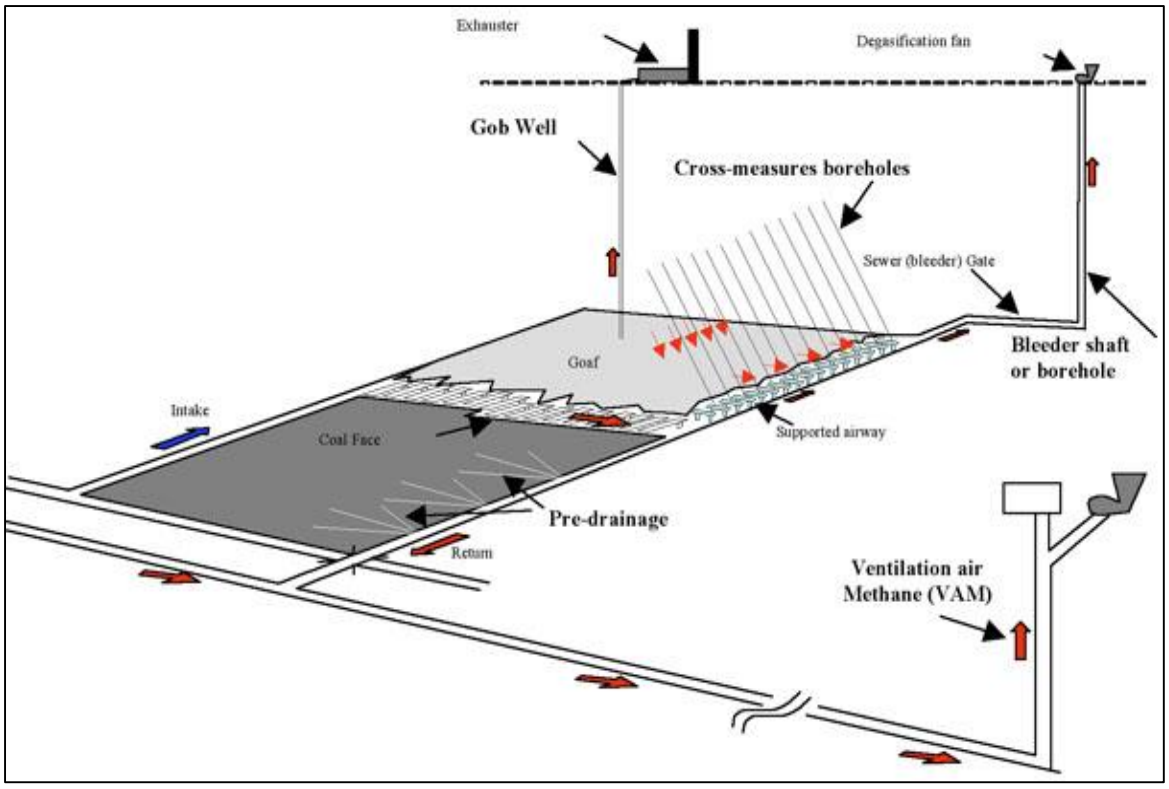


Figure 14: *Coal seam gas pre-drainage and gob drainage Scheme* (Sharma, 2008).

In China, the largest coal producing country in the world, gas drainage technology is divided into drainage of the working seam, the adjacent seam and the goaf (Wang & Xue, 2008). Where the coal seam is gassy or outburst prone then the mostly widely used method involves pre-drainage of the working seam. When the coal seams are thin and they do not have thick protective seams in the middle, drainage is possible using a single system. Wang & Xue (2008) also describe how it is possible to adopt the techniques of gas drainage while developing gate roads but only in mines that have high gas content and small gate road development advance. Adjacent coal seam drainage is possible if CSG is emitted from an adjacent coal seam and causes problems during the ventilation of the gate roads. Adjacent seam drainage is most effectiveness if the coal seams are located in the de-stressed fractured zones. During mining a significant amount of CSG can be trapped in the goaf, and in coal mines with high gas content in the goaf. In such cases drainage of the goaf is proposed. Different techniques of placing drainage pipes into the goaf areas can be found in the literature. Figure 15 shows the different CSG drainage techniques and their applicable conditions after Wang & Xue (2008).

Technique of gas drainage				Applicable conditions
Working seam drainage	Drainage without de-stressing	Pre-drainage of seam roadway development	Cross-measure boreholes drilled from rock roadway Inseam boreholes ahead of inseam roadway development	Outburst prone seam Gassy seam
		Pre-drainage of working face	Inseam boreholes	Outburst prone seam Gassy seam
			Cross-measure seam boreholes drilled from cross measure roadway, rock roadway or roadway in adjacent seams	Drainable seam Outburst prone seam
			Surface boreholes	Gassy and easily drainable seam Relatively shallow seam
	Drainage with de-stressing	Drainage while developing seam roadway	Boreholes ahead of development headings	Outburst prone seam Gassy seam
		Drainage while face retreating /advancing	Boreholes ahead of mining face	Outburst prone seam Gassy seam
			Cross-measure or inseam boreholes drilled from rock roadway ahead of mining face	Outburst prone seam Gassy seam
		Inter-crossing pre-drainage (measures taken to increase seam permeability)	Inseam boreholes Boreholes drilled from rock roadway or surface	Gassy and hardly drainable seam
Adjacent seam drainage	Drainage with de-stressing	Drainage of overlying and underlying seams	Cross-measure boreholes to adjacent seam	High gas emission from adjacent seam.
			Tunnel in adjacent seam for gas drainage	High gas emission from adjacent seam and normal boreholes can not cope with gas emission
			Surface boreholes	When surface borehole is considered to be a better option than underground borehole.
Goaf drainage			Pipes placed in goaf	No sponcom risk seam Sponcom risk seam where measures taken to mitigate sponcom risk
			Boreholes into goaf	
			Surface boreholes	

Figure 15: *Gas drainage techniques and their applicable conditions* (Wang & Xue, 2008).

Low permeability coal seams, like those in the Velenje Basin, are suitable targets for developing new technologies for drainage systems. The basic principle is that the lower permeability of the coal the greater the number of drainage boreholes that are needed to successfully drain off the CSG. Coal mines usually use either hydraulic fracturing of the coal seam by high pressure water injection in the boreholes, or long borehole blasting to increase the permeability. Post-mining drainage involves intercepting the methane released by mining before it can enter a mine airway (United Nations, 2010). In West Cliff Colliery in Australia, drainage was found to be difficult because of the low permeability resulting from high water saturation (Black, 2011). The data from the mine clearly shows how the degree of water saturation has a significant impact on CSG drainage and that a conventional underground-to-seam drainage method was not possible. Black (2011) proposed a new method for CSG production in low permeability seams using cyclic injection of inert gas, such as nitrogen or air. With this method a net increase in the effective permeability is

achieved. The method included repeated cycles of gas injection and release after a specific period of time with the purpose of enhancing gas desorption.

Different in-seam borehole patterns were studied in the Pittsburgh Coalbed in Greene County, Pennsylvania (Karacan et al., 2007 a). Figure 16 shows a schematic demonstration of five studied drainage patterns. The total lengths of the simulated boreholes were 5610 m, 8480 m, 1160 m, 2320 m and 1840 m for patterns A, B, C, D and E, respectively. The authors concluded that the most effective drainage pattern in pre-mining and during active mining is the trilateral configuration (B).

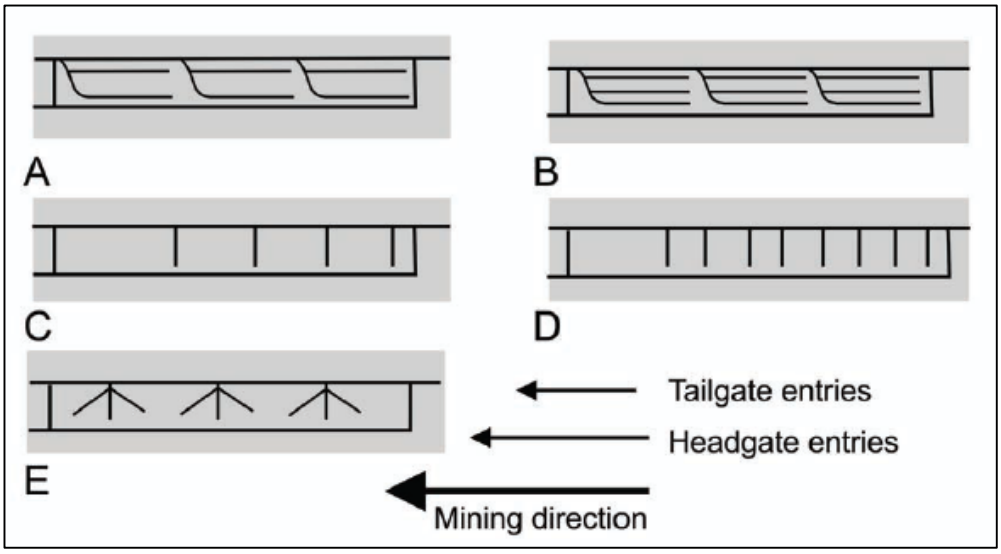


Figure 16: *Different borehole patterns for horizontal methane drainage of a longwall panel* (Karacan et al., 2007 a).

In 2012, the Velenje Coal Mine began to plan its first drainage pilot test at the longwall panel K.-65/F in the North Preloge Mining district. Due to the different drainage methods available, the first stage of planning was to determine the number and design of boreholes and their length and inclinations. The different geological and geomechanical conditions in comparison with other coal basins and knowledge of drilling were key elements in planning and designing the pilot test (Chapter 4.5).

2.6 Review of Numerical Modelling Used in Mining

During the development stage of a coal mining operation, a good understanding of strata behaviour under existing conditions is essential to achieve an efficient production goal. Until recently, analytical physical models were used to estimate the behaviour of the geological formations under different stress conditions in advance of the gate roads and longwall panels. These methods were based on laboratory data and in-situ measurements and were time-consuming. Nowadays, computers have high capacitive storage and high-speed performance allowing computer simulations to be widely used in coal mining.

Kidybinski & Babcock (1973) used a finite element method to study stress redistribution and fracturing within the roof of a longwall face, while Karacan (2008) reported the development of an artificial neural network-based methodology to predict gas emissions in ventilation airflow from longwall mines. In the UK, researchers at the University of Nottingham conducted numerical modelling studies on gas emissions during longwall mining (Keen, 1977; O'Shaughnessy, 1980; Ediz, 1991). Ren & Edwards (2000) developed a three-dimensional methane flow model based on computational fluid dynamics, with permeability values from 10^{-14} to 10^{-8} m^2 assigned to the different regions in the low model,

estimated from an understanding of the longwall geomechanics and an empirical stress-permeability relationship obtained from laboratory tests by Durucan (1981).

Numerical modelling of longwall panels using the computer software package FLAC^{3D} (Itasca, 2005) has developed over the last decade and numerical simulations have been published regarding Turkish (Yasitli & Unver, 2005), North American (Esterhuizen & Karacan, 2005; Zipf, 2006) and Chinese mines (Liu et al, 2011). Three dimensional (3D) mine-scale inelastic numerical modelling is now used routinely in hard rock mines, but their use in the coal industry has been limited, usually used only for conducting research and not for operational design (Vakili et al., 2010). Three-dimensional geomechanical numerical analysis is capable of modelling the behaviour of rock masses (stresses and displacements) around longwall panels. FLAC^{3D} is now widely used numerical software for stress and deformation analysis of surface and subsurface structures built from both soil and rock (Yasitli & Unver, 2005). In FLAC^{3D}, materials are represented by polyhedral elements within a three-dimensional grid that can be adjusted to fit the shape of the object to be modelled (Itasca, 2005).

One of the main difficulties in longwall modelling is the modelling of cave and goaf behaviour (Vakili et al., 2010). The goaf behaviour is based on a compaction model given by Salamon (1991), who explains how during compaction of the material behind the longwall face the vertical stress σ_v increases exponentially with increasing vertical strain ε_v, according to:

$$\sigma_v = \frac{a\varepsilon_v}{b-\varepsilon_v} \tag{7}$$

Where *a* is a constant representing the goaf`s deformation modulus and *b* is the limiting vertical strain (Ozbay & Rozgonyi, 2003).

Whittles et al. (2006) presented a method to derive the dynamic changes in the permeability of coal measures using data obtained from geomechanical modelling of a longwall face for fluid flow simulation. Esterhuizen & Karacan (2005) studied numerical models to investigate changes in permeability and gas emission around the longwall mining panel. Their paper describes the application of a geomechanical simulator to simulate the continuous advance of a longwall face, where results give the dynamic permeability for gas emission modelling in a reservoir simulation. The advance of a longwall face was modelled as a moving boundary problem, and restart models were run sequentially to represent the different mining steps and corresponding strata responses. Based on this approach, the performance of in-seam degasification boreholes and goaf gas drainage boreholes were evaluated by the same authors (Karacan et al., 2007a; 2007b). When mining thick seams using the longwall top coal caving (LTCC) method, stress changes in both the worked seam and the surrounding strata are expected to differ from those induced by conventional longwall mining. Although extensive research has been carried out on gas emissions from longwall panels in thin seams (Karacan, 2011; Lunarzewski, 1998; Noack, 1998), few studies into gas emission issues relating to the mining of thick and ultra-thick coal seams have been published.

Increasing amounts of research on drainage feasibilities and CSG behaviour in coal mines is being performed using computational numerical modelling. The advanced numerical models present an opportunity to simulate the response of the rock mass to longwall operations as well as the associated CSG liberation and flow in the fractured rock mass (Esterhuizen & Karacan, 2005). Numerical modelling is widely used in the coal mining industry to understand the behaviour of coal under dynamic stresses in correlation with CSG (Owuku-Eger & Ramani, 1974; O'Shaughnessy, 1980; Ediz, 1991; Gou et. al, 2003; Ozbay and Rozgonyi, 2003; Esterhuizen & Karacan, 2005; Yasitli & Unver, 2005; Likar et. al, 2006; Zipf, 2006; Vakili et. al, 2010; Liu et. al, 2011). Numerical modelling of

longwall mining has been performed mostly on brown and black coals with little research on lignite. Yasitli & Unver (2005) have published numerical modelling of underground structures, where finite–difference model FLAC^{3D} was used to simulate the dynamic behaviour of the rock strata around the longwall panel in the Tuncbilek District of Turkey. Their results show that numerical modelling could provide an understanding of strata behaviour around longwall faces when the material properties were derived from laboratory data using the Hoek-Brown failure criterion. The complexity of underground mining in thick coal seams requires the use of 3D modelling while 2D modelling cannot properly model together both the longwall panel and its surroundings (Yasitli & Unver, 2005).

Esterhuizen & Karacan (2005) have studied the recent application of geomechanical and reservoir modelling techniques to show the effects that longwall mining on the permeability and CSG flow in the surrounding strata in working areas of US coal mines. Two stages were used to construct both the geomechanical model and a methane emission flow model. The geomechanical model was constructed using the FLAC^{2D} finite difference code and 3D composition reservoir simulator (GEM) for permeability distribution (Esterhuizen & Karacan, 2005). The data from the FLAC^{3D} simulations was then used to calculate changes in permeability, based on empirical relationships developed by Durucan (1981). The study was successful in matching actual goaf gas production and in evaluating sources of methane and flow patterns in the overburden (Esterhuizen & Karacan, 2005). This paper shows that numerical modelling can aid in understanding and predicting CSG flow, and to evaluate the potential of coal seam drainage.

In recent years, there has been interest in developing geomechanical, fluid and heat flow coupling simulators and coupled models such as TOUGH-FLAC. A number of simulators have also been used for oil and gas reservoir engineering, such as VISAGE (Koutsabeloulis, 1998), STARS (CMG, 2003), and a number of academic codes (Rutqvist, 2011). A few of the most important geoscientific applications of the flow-geomechanical simulator include nuclear waste disposal in geological media, deep underground injection of hazardous waste, geothermal energy extraction, enhanced oil and gas recovery, and for underground carbon capture (Rutqvist et al., 2002).

Gas flow numerical modelling is usually based on the principles of gas flow under Darcy`s law. Many parameters are important in gas flow modelling including the:

- porosity of the material,
- viscosity of the media,
- pressure distribution in the model, and
- permeability of the material.

Amongst these parameters, permeability is considered to be most critical in terms of reliability of the results (Ediz, 1991). Permeability distribution together with hydrogeological parameters are obtained using the multi–dimensional fluid and heat flow numerical simulator - TOUGH2, developed by Pruess et al. (1999) to solve mass and energy balance equations describing fluid and heat flow in general multiphase and multicomponent systems.

TOUGH-FLAC numerical simulations are often used to solve different geomechanical-geochemical problems. Rutqvist et al. (2002) for example describes the thermal-hydrologic-mechanical (THM) analysis of multiphase fluid flow, heat transfer and deformation in fractured and porous rock. Until this article, there was no simplified one single computer code for modelling THMC (including chemical processes) in geological media. Rutqvist and co-workers joined two established codes TOUGH2 and FLAC^{3D} using sequential execution and data transfer using coupling functions for modelling three-dimensional problems. Two examples were presented: sequestration of CO_2 in brine aquifers and a high temperature nuclear waste repository in unsaturated rock (Rutqvist et

al., 2002). Both examples showed that complex problems can be solved with coupled THMC simulation.

Walsh et al. (2012) used TOUGH-FLAC simulation to create a simplified one-dimensional hydromechanical model. TOUGH2, in this case, modelled the changes in mechanical loading over a large area, such as occurs during continental glaciation or laterally extensive erosion/deposition events. Their results revealed that one dimensional flow modelling is limited due to its simple design in uni-axial strain. They also found that the presence of partial gas saturations in a formation can affect the hydromechanical behaviour of the system. In layered systems with variable properties, the effects of partial gas saturation are contradictory (Walsh et al., 2012).

Javeri and Baltes (2008) studied the coupled thermo-hydrologic-geomechanical processes of gas and nuclide transport in a two-phase flow through porous medium using both TOUGH2 and $FLAC^{3D}$ computational software while investigating nuclear waste disposal in rock salt. Their results were dependent on hydrological properties, such as porosity, permeability and capillary pressure, which in turn depend on volumetric strain, effective stress or on minimum compressive principal stress.

Reference to TOUGH2 simulations in relation to coal mines is found only in cases of numerical modelling of CO_2 storage in abandoned coal mines (Malolepszy, 2003; Loschetter et al., 2012). Malolepszy (2003) described two-dimensional TOUGH2 heat-exchange models in abandoned underground workings in the Nowa Ruda coal mine in Poland. These abandoned flooded workings acts as large volume open spaces with high permeability and geothermal gradients that could be considered as man-made reservoirs of warm mine water. Their results revealed the amount of time required, in case of pumping warm water to the surface, for natural thermal conditions to return in the rock in 10 years.

Simulation of CO_2 storage in coal seams is the subject of Loschetter et al. (2012)'s work who investigated coupled flow and the mechanical processes around the injection point at the bottom of the Montsacro mine in Asturias, Spain. TOUGH2 was used to model CO_2 storage in addition with the solver for the geomechanics CODE ASTER. The authors used this tool were the first to verify and validate *in-situ* data gained from CO_2 injection at the mine. There are no scientific papers describing the use of TOUGH2 to model the flow of CSG migration in coal mines.

3 Velenje Lignite

3.1 Introduction

At 2.5 million years old the Velenje lignite is considered geologically young when compared to other coal fields. In order to better understand CSG behaviour, the basic geology of the Velenje Basin and structural properties of the Velenje lignite, i.e., lithotype characterisation, geomechanical and geochemical properties are presented. The Velenje Mining method is also explained which has a significant effect on both the surrounding coal and CSG.

3.2 Geology of the Velenje Basin

The Velenje coal seam is located in the northern territory of Slovenia near the town of Velenje. The Velenje Basin (Figure 17) dates from the Pliocene to Pleistocene and formed by polyphase dextral strike-slip faulting at the junction of three tectonic units: the Central Karavanke Mountains, the Southern Karavanke Mountains and the Gorenje-Šoštanj block (Brezigar et al., 1987). The Velenje Basin is filled with Plio-Pleistocene sediments of terrestrial coarse-grained basalt beds with fine-grained marshy sediments more than 1000 m thick. The lignite seam lies in the middle of the Plio-Pleistocene succession. Along the Smrekovec fault at the southern edge of the Basin andesite bodies lie at the bottom of the Basin while on the northern parts of the Velenje Basin in the footwall can be found Triassic dolomites and limestone close to the Velenje fault (Brezigar et al., 1987).

Under the lignite seam the Pliocene strata is up to 50 m thick, and consists of shales, clay, coal and lignite. Above the Pliocene strata lie up to 250 m thick green sandy silts. The lignite seam, whose thickness can reach up to 165 m, lies above the footwall. Above the coal seam, a thin layer of marls with lacustrine molluscs is present followed by up to 350 m thick lacustrine strata consisting of clays, marls, and silts. These strata are overlain with a 90 m thick sand-silt formation, while the upper most part of the Basin consists of terrestrial silts, overlain by recent fluvial sediments (Brezigar et al., 1987) (Figure 18).

Many geological processes, such as magmatic activity, strike-slip reverse faulting and erosion, helped form the Velenje Basin. Studies suggest that heat flows were elevated in the Velenje area during Oligocene times as a result of Smrekovec volcanism (Brezigar et al., 1987). With the hypothesis that the andesite tuffs, identified in logged cores from boreholes drilled deep beneath the coal seam, lie at the same altitude as the external tuffs, then it can be concluded that the northern wing of the Šoštanj fault has dropped by at least 1500 m in depth relative to the southern part of the fault (Seher, 1995). The rise in the northern part of the Velenje fault means that the coal seam is situated on the triad layers.

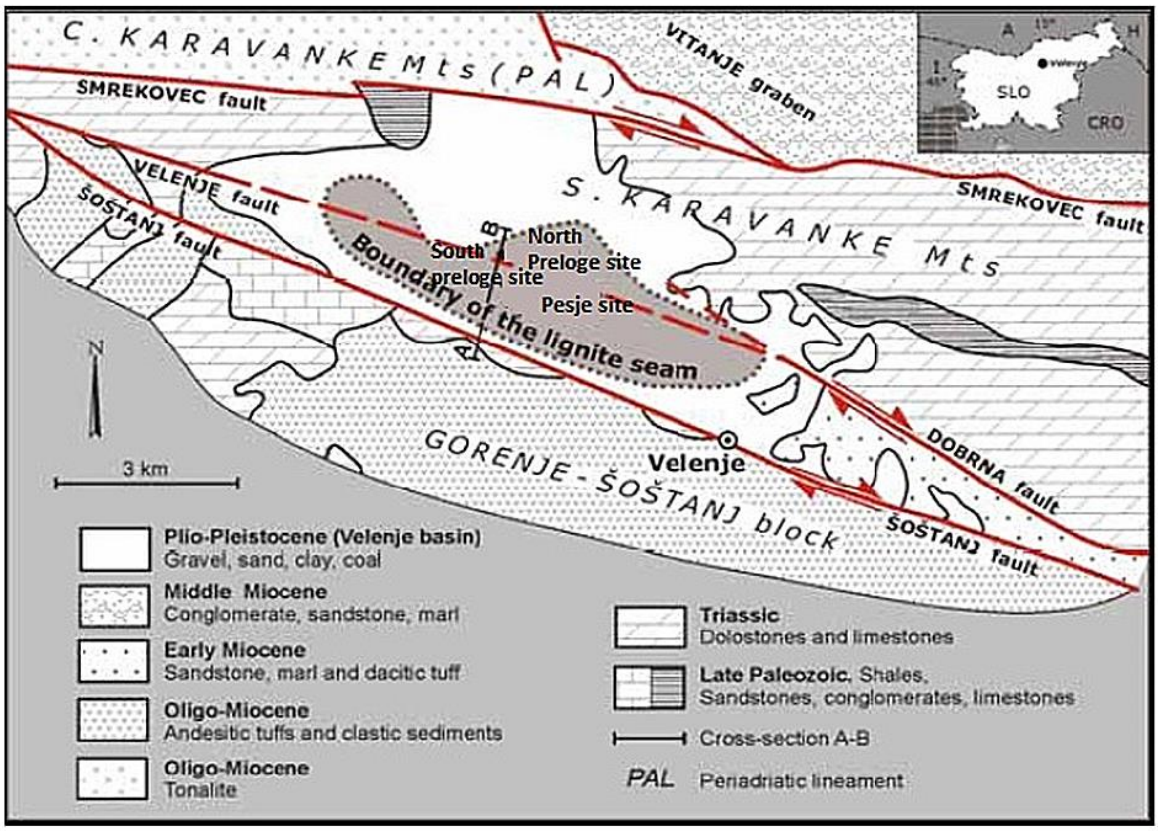


Figure 17: *Geological map of the Velenje Basin area* (Brezigar et al., 1987).

Hydrogeological systems in the Velenje coal mine can be distinguished by the following: 1) PlioQuarternary and Pliocene aquifers, and 2) Carbonate aquifers (Figure 19). The geochemical characteristics of groundwater in the Triassic aquifer and groundwater in the PlioQuarternary and Pliocene aquifers, mixing between groundwaters and surface waters, the origin of and the biogeochemical processes occurring in surface waters and groundwaters were described by Kanduč et al. (2014).

3.3 Velenje Mining Method

The Velenje Mining Method was developed to achieve the highest rate of extraction possible. The entire process is based on the consideration of natural characteristics, provision of adequate safety and the prediction of impacts on the environment (Medved and Golob, 2013). Extraction of coal is carried out from the hanging wall at the top of the seam downwards to the footwall (Figure 20). The natural characteristics of the coal and the roof strata help in its exploitation, which includes braking and crushing of the seam. The allowed face heights depend on the thickness of the insulating clay in the hanging wall, which in turn allows coal production in the first place by protecting the coal face from water and sand inrush.

The Velenje Mining Method is based on a lower number of wider and longer longwall faces. Present annual production of lignite is stabilized at 4 million tons, which has been achieved with an average of two to three active faces. The majority of the lignite produced is consumed by the nearby 755 MW Šoštanj power plant (Markič, 2009).

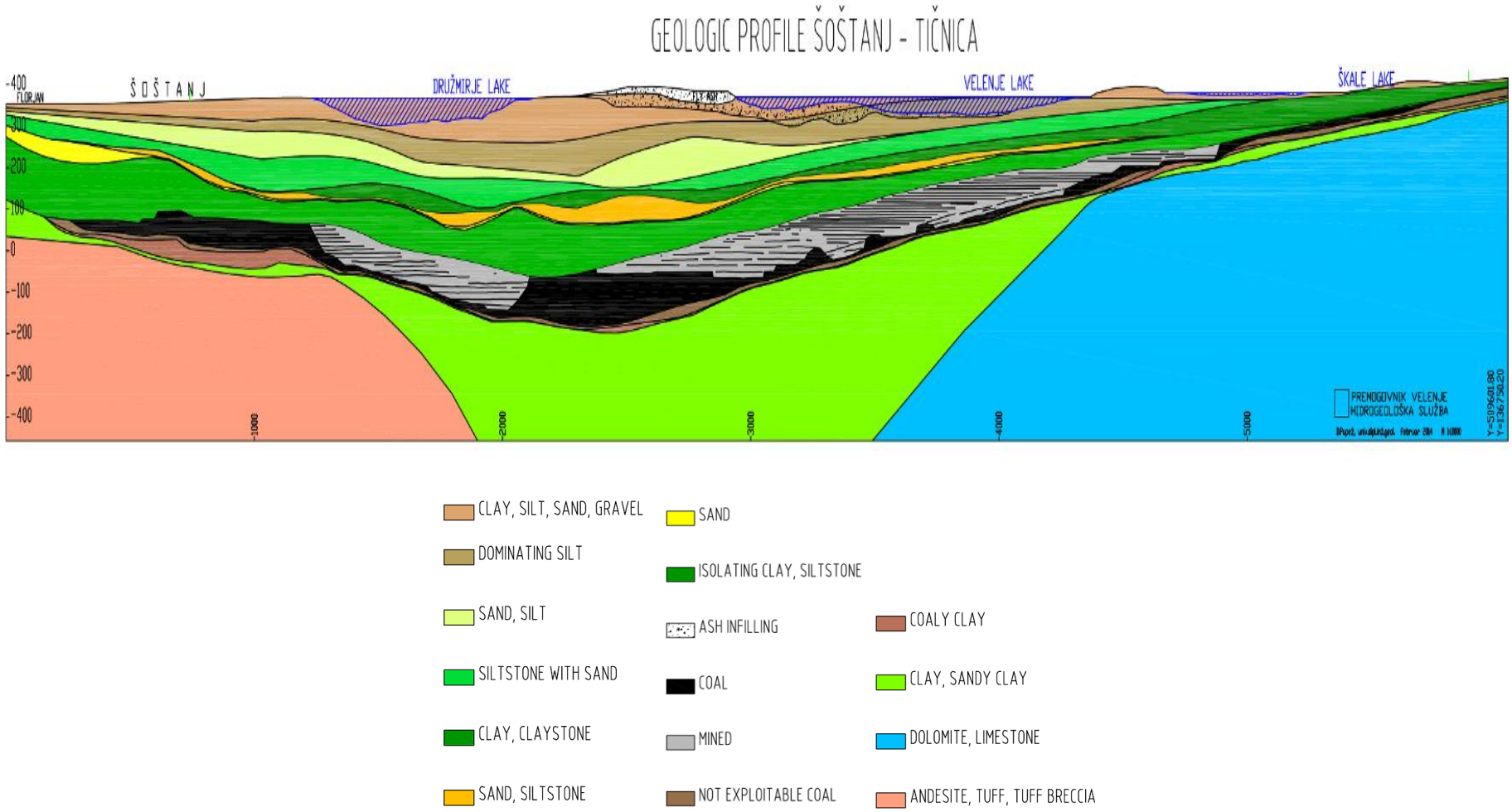


Figure 18: *Geologic profile Šoštanj – Tičnica*.

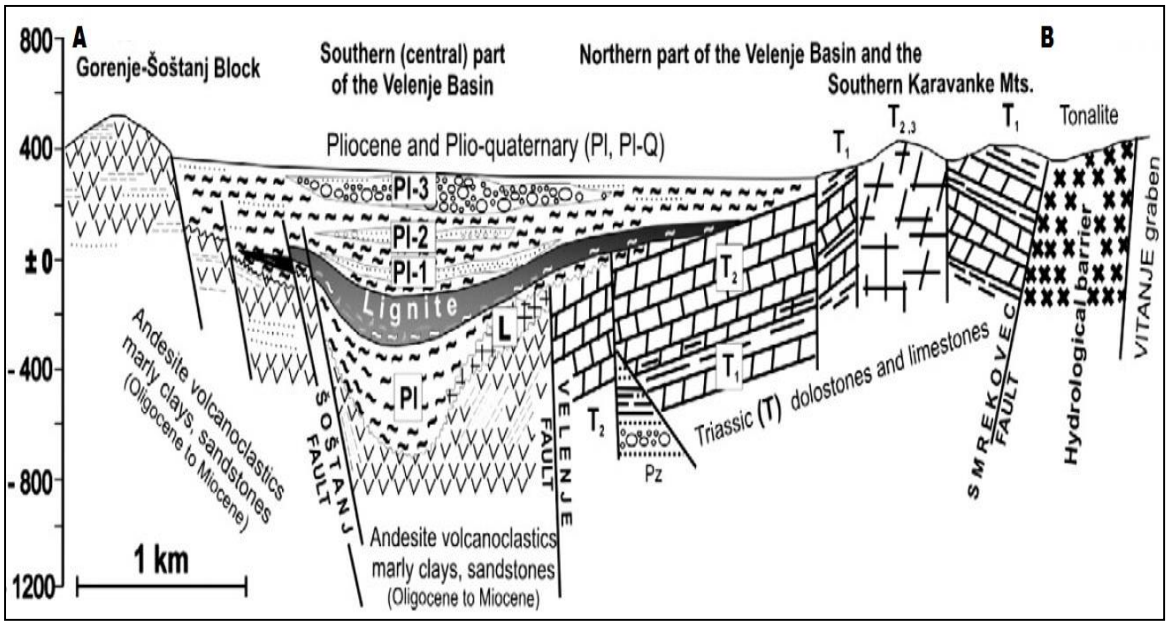


Figure 19: *Schematic geological cross-section of the Velenje Basin (*Brezigar et al., 1987).

During the excavation of the coal, secondary fissures are generated and the release of coal seam gases occurs. It is known that coal seam gases are trapped in the porous structure of the coal reservoir and are generated by the redistribution of the primary stress state. This process occurs during the longwall method of excavation; as the neighbouring strata collapses gas is released. The amounts of coal seam gases, which are released due to excavation, are therefore dependent on the method of excavation and the amount of coal lying inside the collapsed structure (Beamish & Crosdale, 1998).

A complex pattern of stress distribution is generated during excavation of the lignite, where a dynamic wave is produced whose shape and size is dependent on the parameters of excavation and the geotechnical conditions in the excavation column, also dynamic stresses are much greater than primary stresses. The higher the rate of advancement of the longwall face, the closer is the stress wave to the excavation site (Zavšek, 2004). In the Velenje coal Basin the longwall method of excavation has been used since 1960 (Zavšek, 2004). Due its high productivity, it has proven to be the most appropriate method for excavating thick coalbed strata.

Once the main and return gate roads have been constructed and the longwall shield supports installed, excavation proceeds by retreating the excavation to the excavation boundary in panels 400-800 m in length and from 3 to 15 m in height. From experience coal seam gas outbursts are generated in the upper parts of the lignite strata below the so-called "fresh hanging wall", where no mining activities have been performed and therefore no geomechanical stress was attained (Zavšek, 2004). The hanging wall is typically composed of clay, rarely sands, and silts. All these sediments are problematical for accumulation of gases, especially clays, which represent barriers to the migration of gases in the upper parts of the strata, while porous sands allow migration of gases.

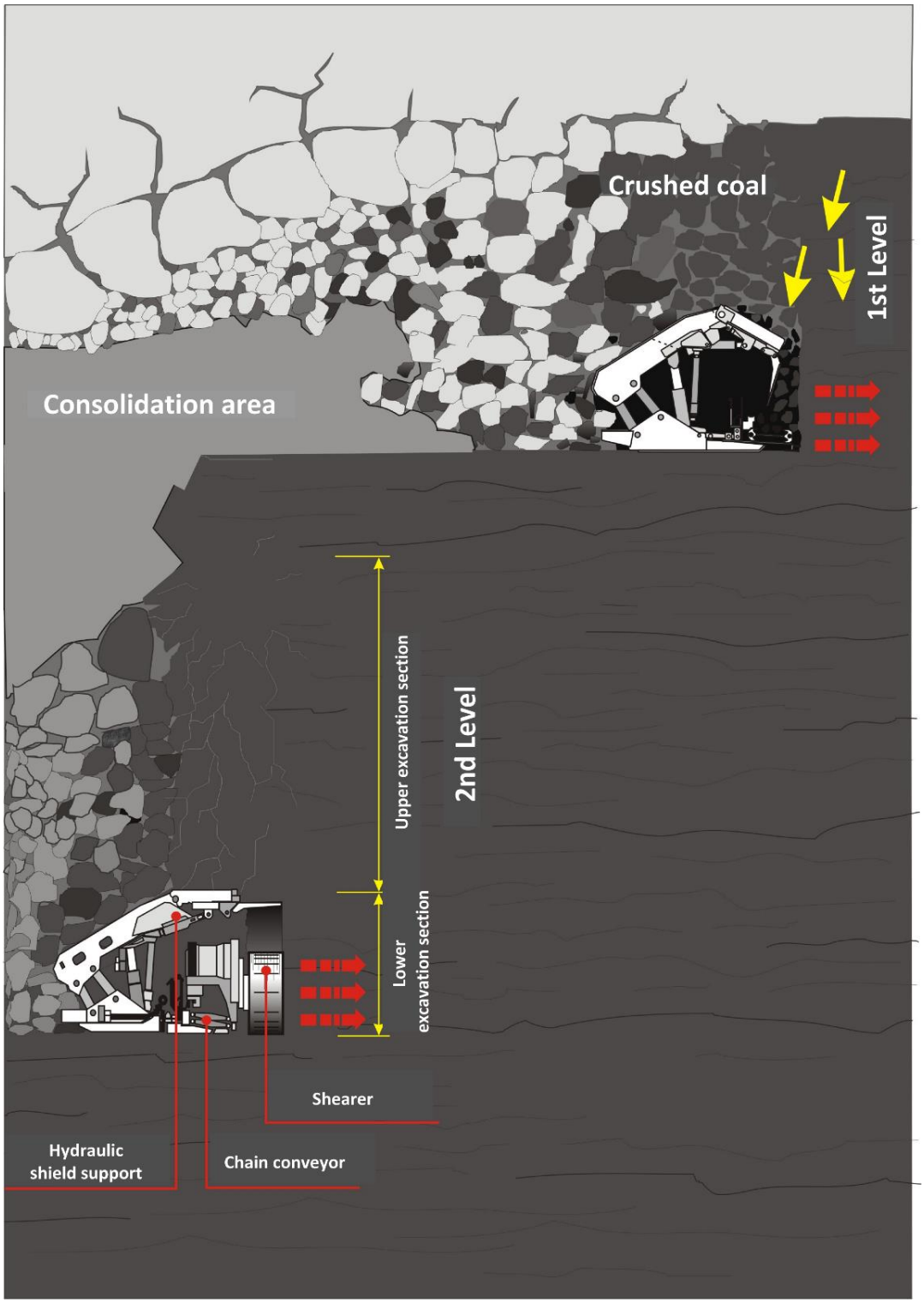


Figure 20: *Excavation scheme of the Velenje Mining Method.*

3.4 Structural Properties of the Lignite

The Velenje lignite is a humic type of lignite, more or less rich in xylite and fusinite fragments and mineral matter (Zavšek, 2013) and is very heterogenic with a fine detrital matrix. Structural properties such as porosity, the distribution of pores in the lignite, specific surface area, adsorption and desorption properties of the lignite, all have an effect on its permeability. The concentrations of coal gases in the fractures and mircroporous

structures of the lignite seam is likely related to tectonic events before and at the time of formation of the Velenje basin (Kanduč & Pezdič, 2005). Studies show that the specific pore surface of the lignite varies from 40 to 180 m^2/g (Zavšek, 2004). In the following chapters, lithotype classification, geomechanical properties and geochemical properties of the Velenje lignite and CSG will be presented.

3.4.1 Lithotype Classification

In 1992 Markič (Markič, 2009), performed a detailed petrological characterization of the Velenje lignite. In total, 285 m of lignite core in the four structural boreholes in addition to the many underground boreholes were macropetrographically logged (Markič, 2009). Underground mine working including road development heads and longwalls were also logged. The International Committee for Coal and Organic Petrology (ICCP) lithotype classification for soft brown coals was not suitable for the Velenje lignite and the concept of fragmental lithotype components was introduced using terms such as: detrite (D), xylo-detrite (xD), detro-xylite (dX), xylite (X) and fusinite (Figure 21).

Different lithotypes create the Velenje lignite, from detrite to xylite. Detrite (D) is characterised by the fine-detrital homogeneous plant material that represents the matrix between the larger fragmented inclusions and is dark brown to black (Markič, 2009). Xylite consists of large brown pieces of wood lying within a fine-detrital matrix (Zavšek, 2013). The heterogeneity of the lithotype composition of the lignite is evidenced by the different geomechanical properties, sorption capacities, gas contents and permeability. From a geomechanical perspective the lignite has much greater strength characteristics than the materials in the hanging wall and in the footwall of the basin.

Xylite (X) is a synonym for the large brown pieces of wood found amongst the fine-detrital matrix. It has a smaller specific surface area than the fine detrite. For example, the specific surface of the pores of homogenous fine-detrital lignite is greater than 180 m^2/g, whereas for xylite it is about 35 m^2/g (Markič, 2009). In addition, the difference between these two lithotypes is shown in their compressive strength. Previous tests have shown that the unconfined compressive strength of detrite is smaller (approx. from 6 to 9 MPa) than of xylite (9-14 MPa). Xylo-detrite (xD) and detro-xylite (dX) are lithotype components composed of different percentages of xylitic fragments in a fine detrital matrix.

Lignite can be gelified, mostly it is the fine detrital matrix, and mostly in the upper part of the seam, nevertheless in the lower part of the seam gelification of xylite occurs. Gelification is the result of biochemical processes during the earliest stage of coal diagenesis (Markič, 2009). Lignite, which is gelified, is usually black, hard and brittle (Figure 22). Gelified lignite has a more developed cleat system, where the face and butt cleats can be easily distinguished.

Studies of Velenje lignite show that fine-detrital varieties are more prone to gas outbursts than the xylite rich lignite. The accumulation of strain energy is also smaller in fine detrite lignite than it is in xylite. Fine detrite has the highest specific pore surface of all the lithotypes and the highest adsorption capacity; therefore, it has the highest potential for being a gas reservoir (Zavšek, 2004). The adsorption capacity of coal samples from two different mining districts of the Velenje basin have been analysed at Imperial College London. The coal samples were taken from Pesje and South Preloge mining districts. The sample from Pesje was a xylitic type while the coal from South Preloge was composed of fine detrite. A general observation is that, in both locations, the volume of CO_2 adsorbed at a given pressure is approximately twice the volume of methane. Table 1 gives the calculated Langmuir Pressure and Langmuir Volume for the Velenje coal (Durucan et al., 2012).

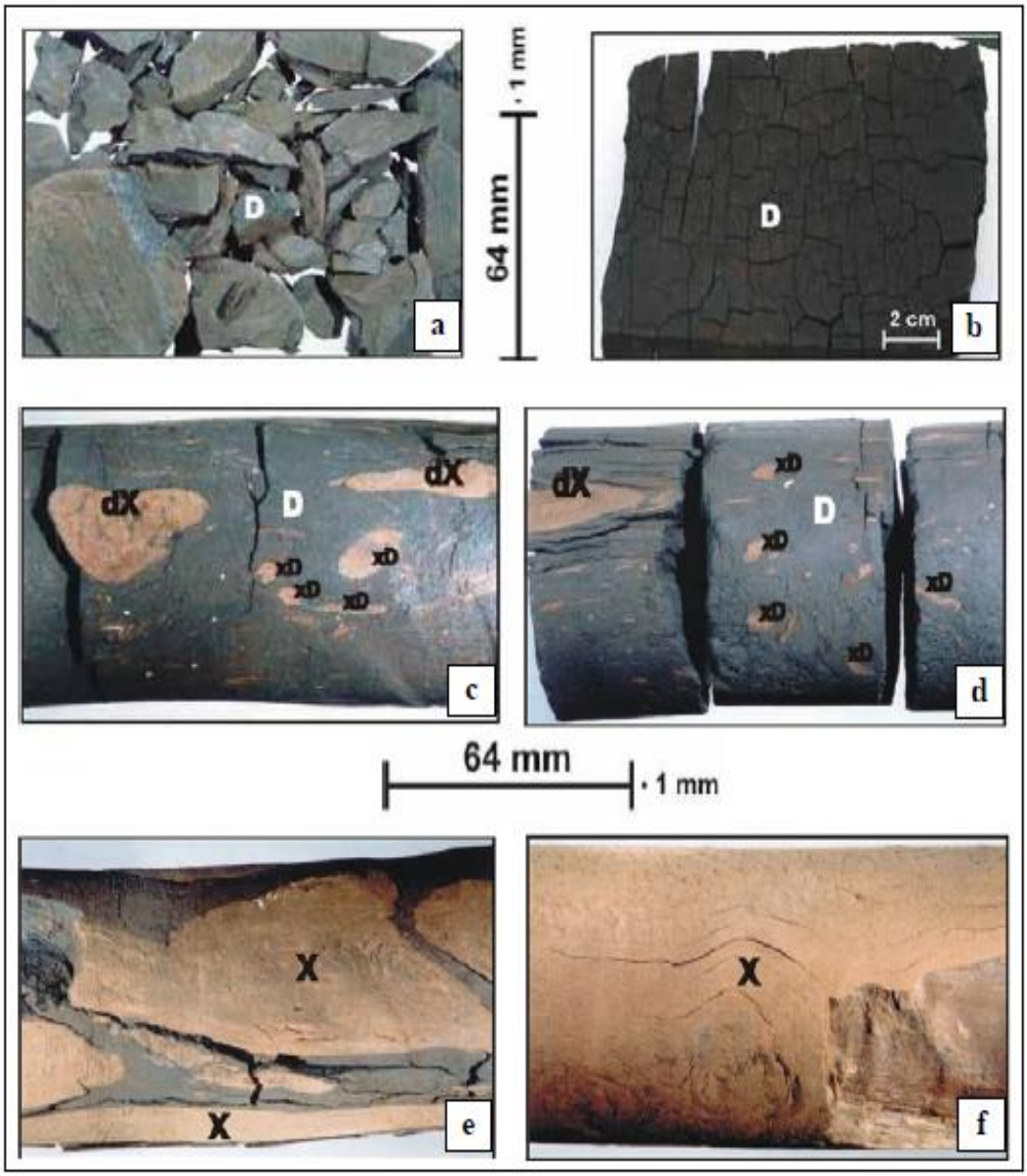


Figure 21: *Lithotype components of the Velenje lignite visible in a horizontally drilled borehole-core:* ***a)*** *and* ***b) Detrite (D)*** *forms fine-detrital lignite. It is typically crushed (a) and cracked due to desiccation (b),* ***(c)*** *and* ***d) Xylo-detrite (xD)*** *composed of xylitic pieces smaller than half of the core diameter, and* ***detro-xylite (dX)*** *composed of xylitic pieces bigger than half of the core diameter, both within fine-detrital matrix.* ***e)*** *and* ***f) Xylite (X)*** *as xylitic pieces bigger than the core diameter (e), and extending over the entire core dimensions (f). Note also the scale-bar of 64 mm, which corresponds to the core diameter* (Markič & Sachsenhofer, 2010).

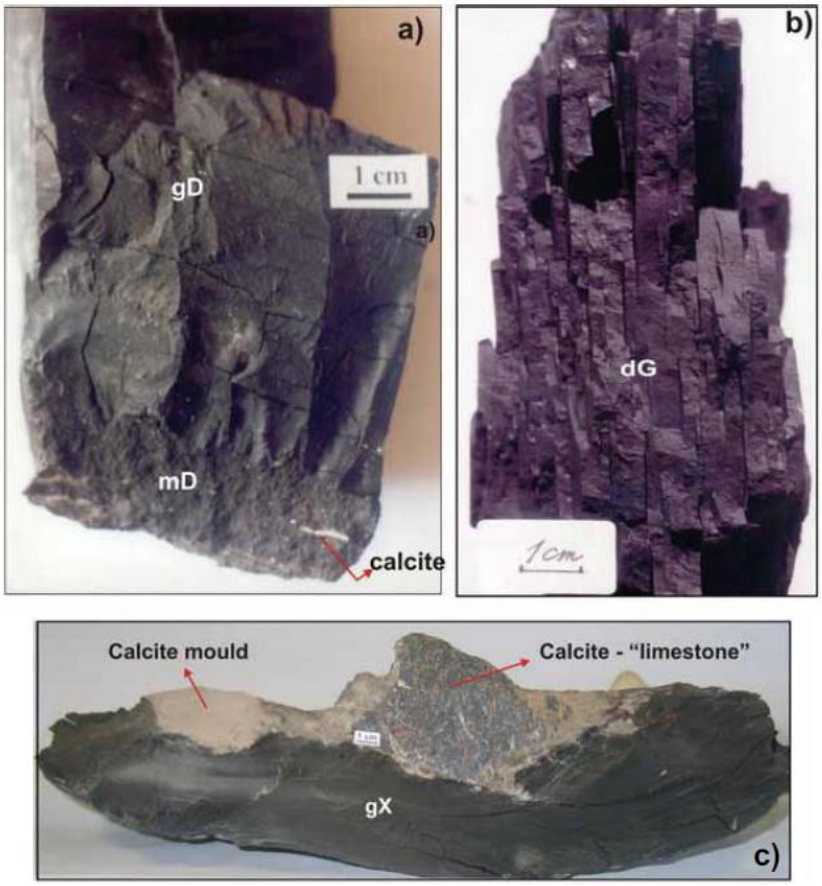


Figure 22: *Gelified lithotype components of the Velenje lignite.* ***a)*** *Gelo-detrite (gD) with a developed cleat system; below is mineral-rich detrite (mD) with calcite inclusions.* ***b)*** *Detro-gelite (dG) with very high developed cleat system.* ***c)*** *Gelo-xylite (gX)* (Markič, 2009).

Table 1: *Langmuir Pressure and Langmuir Volume results, measured at Imperial College London* (Durucan et al., 2012).

Coal Type	P_L(MPa)	V_L(m^3/t)
Pesje – Methane	3.50	9.40
Pesje – CO_2	3.35	28.65
Preloge – Methane	5.93	9.77
Preloge – CO_2	6.46	48.66

3.4.1 Geomechanical Properties of the Velenje Lignite

The geomechanical properties of lignite have been the subject of investigations at the Velenje Coal Mine for many years. This has included many *in-situ* measurements and laboratory analyses of coal samples. Laboratory measurements were performed in the mine's own geotechnical laboratory and the behaviour of the coal strata under the advancing longwall face were reported in a study entitled "Study to solve the problem of the safe extraction and determination of criteria for the design and excavation of coal under the aquifer layers in the Velenje Coal Mine" (Kočar et al., 1989).

3.4.1.1 *In-situ* stress measurements around the longwall panel

In addition to CSG pressure and CSG composition measurements in boreholes, rock stress behaviour has also been monitored at the mine. Rock stress measurements were taken using Glötzl hydraulic stress cells, which are the most suitable instruments for measuring stress in lignite coal. The stress cells were placed in a borehole at two different depths (20 m and 30 m) such that the cells are perpendicular to each other with an orientation of 0° and 90°. The boreholes were then filled with a mixture of fly ash and cement in a ratio to simulate the strength of the adjacent lignite. Figure 23 shows a cross section of the stress measurement borehole. The Glötzl cells were used to measure the secondary stress state and deformations. The principle of the measurements is based on the hydraulic system. By increasing the pressure in the neighbouring rock a membrane in a cell is activated, which reduces the pressure in a pressure conduit as soon as the pressure in the cell equalizes. This gives a measure of the actual pressure acting on the measuring cell. (Jeromel, 2010).

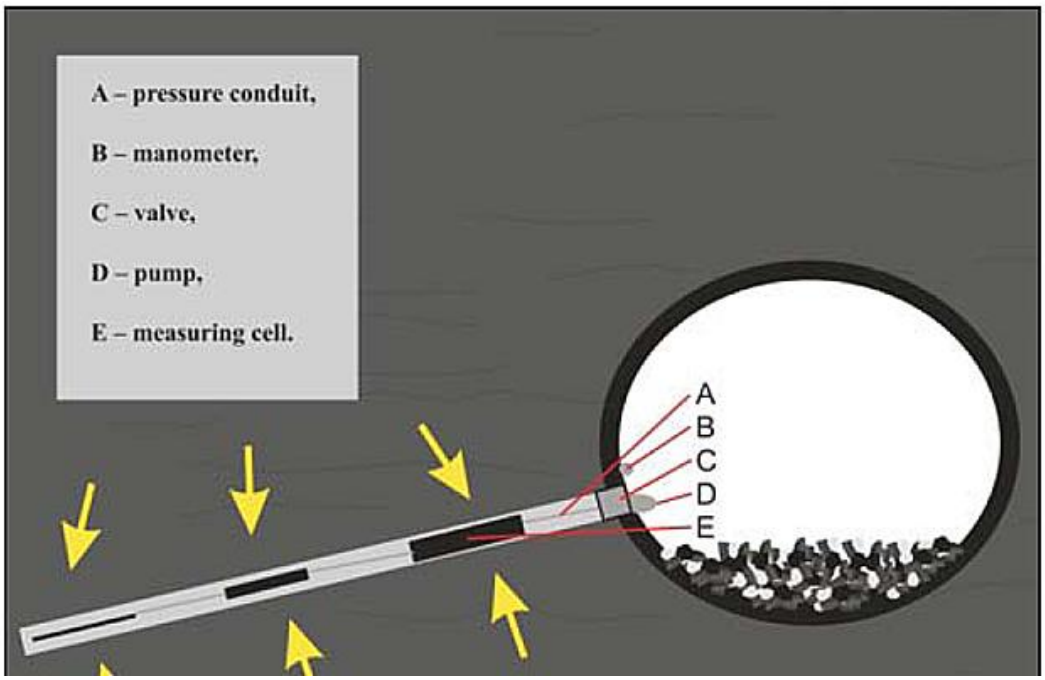


Figure 23: *Cross section of the stress monitoring borehole installed with Glőtzl cells* (Jeromel et al., 2010).

In a study by Kočar et al. (1989) vertical stress is represented as the ratio between the secondary and primary stress state. Figure 24, 25, and 26 reveal the changes in the stress state in the stress cells at different locations in the mine.

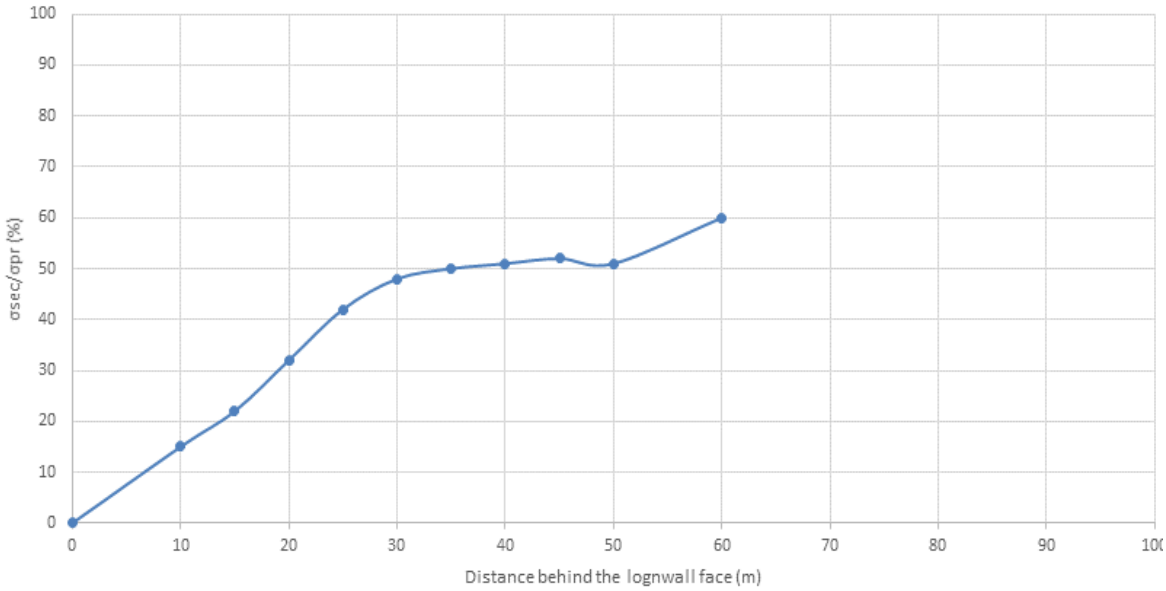


Figure 24: *The size of the normalized stress in overburden strata excavation under several panels using a mechanized excavation method* (adapted from Kočar et al., 1989).

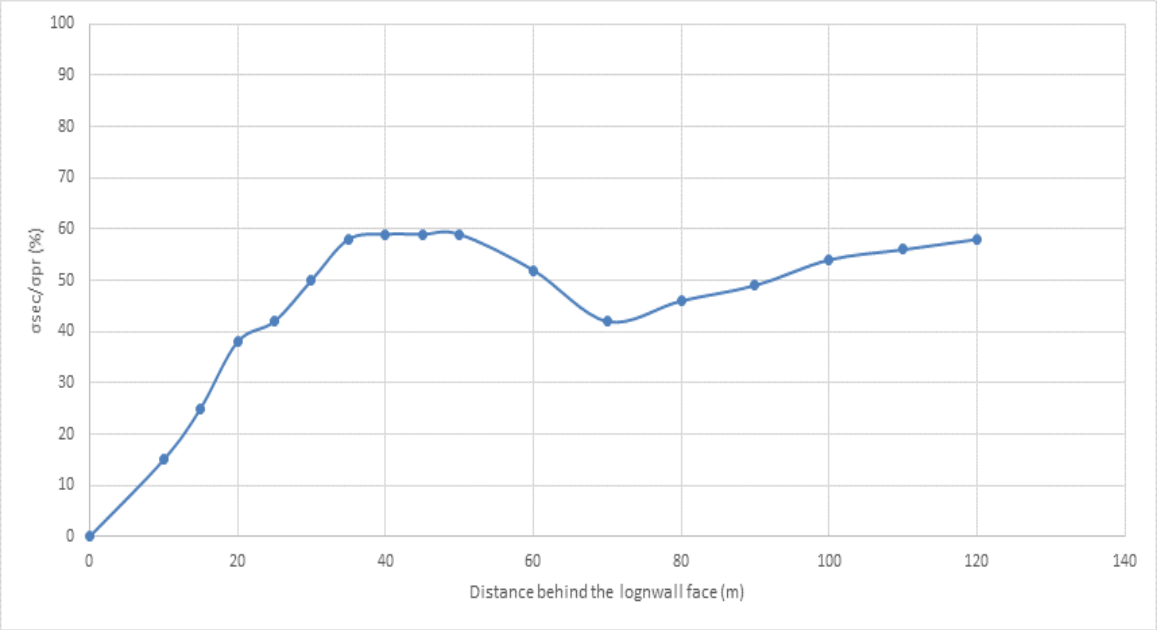


Figure 25: *Increments of the normalized stress in the overburden strata, when excavation takes place under fresh intact overburden* (adapted from Kočar et al., 1989).

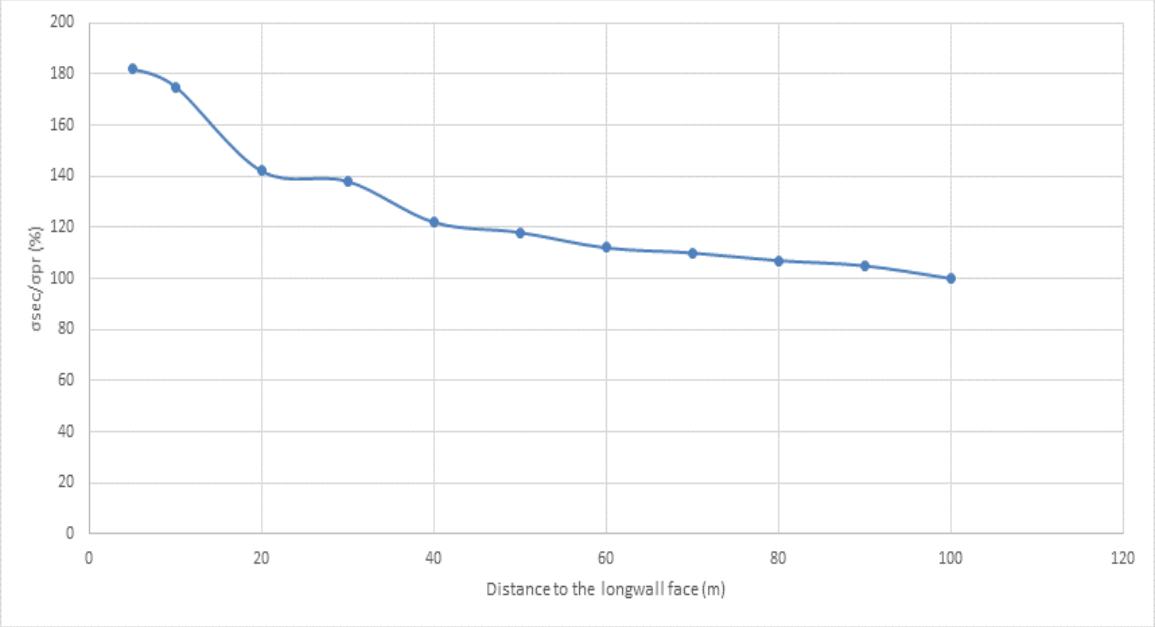


Figure 26: *Increments of the normalized stress in the coal seam in front of the longwall face* (adapted from Kočar et al., 1989).

3.4.2 Geochemical Properties of the Velenje Lignite

An improved understanding of the geochemical processes that control the occurrence and composition of coalbed gas provides an important contribution to the mine's knowledge not only about the mitigation of potential environmental or mining hazards, but also for exploration and development strategies for utilizing coalbed gas as an energy resource (Clayton, 1998). The stable carbon isotopes of coalbed methane are usually applied to identify its genesis (Gouyi et al, 2007). Over the past 15 years there have been several studies performed in the Velenje mine in an attempt to understand the geochemical properties of the CSG. More recently the CSG composition has been upgraded with isotopic composition measurements (Kanduč, & Pezdič, 2005; Kanduč, et al., 2011; Kanduč, et al., 2012; Sedlar, et al., 2014), and a programme of monitoring the geochemical parameters was set up to help understand the behaviour of the CSG distribution in advance of the working face using mass spectrometric methods to study both its molecular and isotopic compositions and origin (Sedlar, et al., 2014)..

The isotopic composition of CO_2 in conjunction with the CDMI index (Equation 8) is often used to infer the origin of the CO_2 in coal gas (Kotarba, 2001; Kotarba & Rice, 2001; Smith & Pallasser, 1996). This index was used to decipher the origin of CO_2 in the Velenje Basin, as in the Bowen and Sydney Basins in Australia (Smith & Gould, 1980; Faiz et al., 2007).

$$CDMI = \left[\frac{CO_2}{(CO_2+CH_4)}\right] 100\ (\%) \qquad (8)$$

There are three main sources of hydrocarbon gases and CO_2 in sedimentary basins: abiogenic, microbial and thermogenic (Rice, 1993). In general, thermogenic gases are typically associated with high rank coals, whereas microbial gases are connected with low rank coals. The thermal generation of hydrocarbon gases in sedimentary systems such as the Western Canadian sedimentary basin show that low temperature thermal generation of non-methane hydrocarbons occurs at temperatures below 62°C and possibly as low as 20°C (Rowe & Muehlenbachs, 1999).

As already stated, CO_2 is the predominant gas in the Velenje lignite. It is generated during thermogenic processes while nitrogen generally forms during thermal transformation of organic matter and from NH_4-rich illites of clayey facies of the Lower Palaeozoic strata. In spite of losses due to reactions and dissolution during migration and entrapment, the $\delta^{13}C$ values of pyrolysis CO_2 are within the same range as for CO_2 present in natural gases. Abiogenic sources of gas are typically found in deep subsurfaces (Sherwood Lollar et al., 2006) where carbonate rock, clastic rock, the coal seam and magmatic rock are the main CO_2 reservoirs; solubility trapping by the formation of water sinks is the dominant forms of CO_2 in the rock layer (Gillfilan et al., 2009). Natural analogue studies of CO_2 occurring in the subsurface have the potential to yield insights into the mechanisms of CO_2 storage over geological time scales. The sources and distribution of gases in the lignite therefore represent the basis for understanding coalbed gas behaviour. Most of the CO_2 in the seam is adsorbed on the surface of the microporous coal matrix.

The distribution of CSG in relation to high CO_2 concentrations in the Velenje Basin is related to the spatial position of the mining field and to whether or not the longwall panel is either under fresh overburden or under a pre-mined area (Sedlar et al., 2014). During active lignite mining, CH_4 migrates faster than CO_2 and accumulates in the upper part of the coal seam, while CO_2 is adsorbed in the lignite in the pre-mined excavation fields.

The lignite in the Velenje Basin, in comparison with other coal seams, is geologically young and it is one of the few examples of lignite having a high CO_2 content. It is important to understand the different properties of the lithotype because without this knowledge it is impossible to construct robust geomechanical and flow models. The different structural properties of the Velenje lignite, requires a diverse geomechanical and flow model, which is described in this thesis. The most important factors used to develop such a model are the changes in strength, porosity and adsorption/desorption capacity, which will be discussed in the following chapters.

4 Field Measurement Campaigns to Characterise the Coal Seam Behaviour around LTCC Faces

4.1 Geomechanical Properties of Lignite and Studies Related to Coal Seam Gas

Geomechanical characterisation of lignite has been the subject of many studies at the Velenje Coal Mine. In this Chapter, the methods used in active seismic tomography measurements, coal seam gas composition and pressure monitoring are described. The methodology behind the CSG drainage trial system is also presented.

4.2 Active Seismic Tomography of the Longwall Panel

Two longwall panels were selected for seismic tomography studies as part of the RFCS funded project CoGasOUT. Figure 27 shows both longwall panels where active seismic tomography was completed. The first was the longwall panel K.-50/C located in the Pesje mining district. At this longwall panel, the NW half of the panel was located directly under solid (virgin) coal and intact roof strata, whereas the SE part was located under pre-mined coal and deformed roof strata (Durucan, et al, 2014). The second longwall panel was K.-130/B located in the Southern Preloge mining district and situated under the pre-mined mining district.

The first series of P-wave seismic tomography measurements were performed on the longwall panel K.-50/C (Figure 28) as part of two measurement campaigns: 21st-22nd May 2011 and 18th-19th June 2011. Seismic sources (vibrators) were located in the return air gate road and the receivers (geophones) were located in the intake air gate road. A 100 m long section of the longwall panel was studied. The longwall panel K.-50/C was 684 m long and 144 m wide. During the 1st campaign the nearest receiver to the longwall face was positioned at a distance of 95 m from the face, while during the 2nd set of measurements this was reduced to 47 m. Both source and receiver were placed 2.8 m apart. In total, 39 source points were recorded using 120 receivers located at 40 receiver points.

The second series of measurements was performed in 2012 on the longwall panel K.-130/B in the Southern part of the Preloge mining district (Figure 29), where the 1st set of measurement was made using 40 source- and 40 receiver points, each equipped with three-dimensional receiver components. The distance from the longwall face was 87 m. A second set of measurements was made at -1.5 m from the longwall face. The positioning of the mining equipment being next to the longwall face meant that the last receiver was placed at the source point number 36. The last possible explosive charge position was located at the source point number 38. The distance between the last receiver and the longwall face exceeded 8.5 m and the distance from the last explosive charge to the longwall face was 2.6 m.

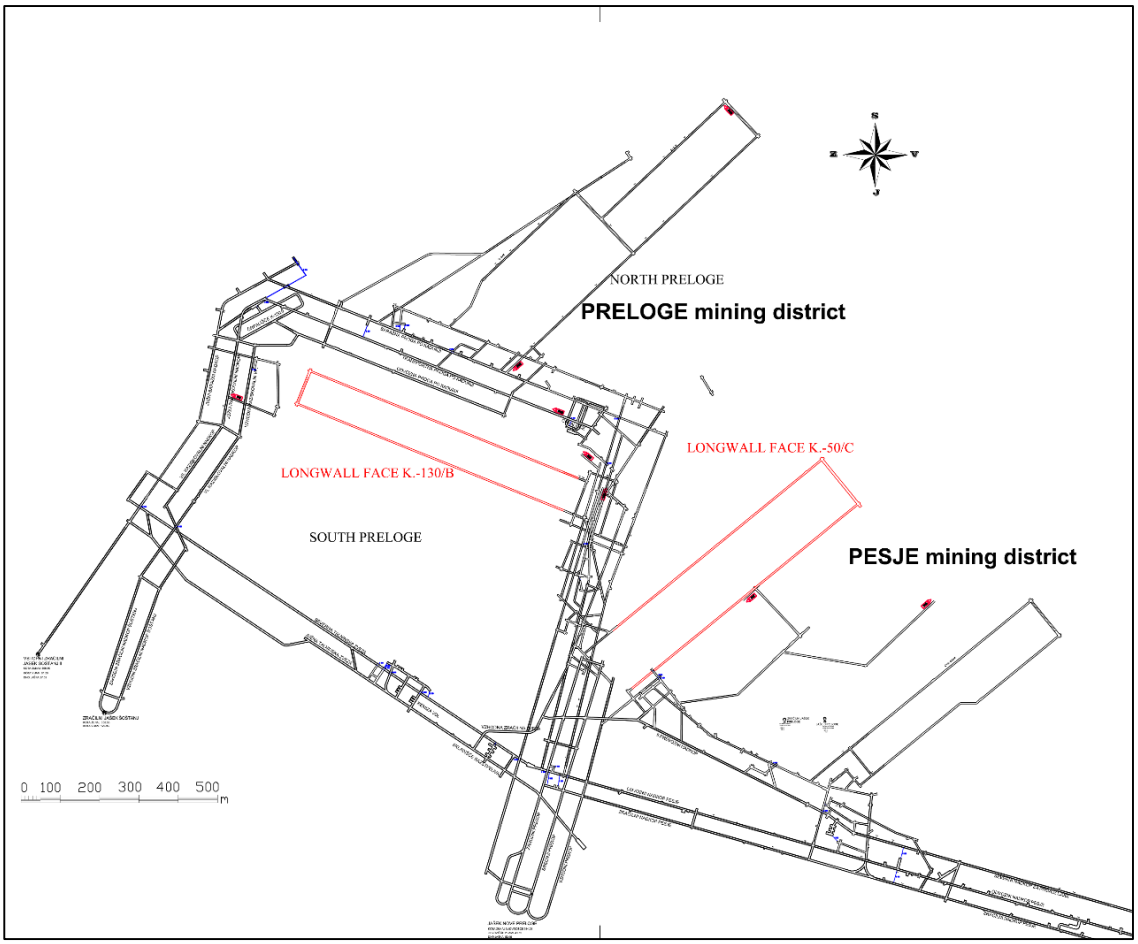


Figure 27: *Location of longwall panel K.-50/C and longwall panel K.-130/B.*

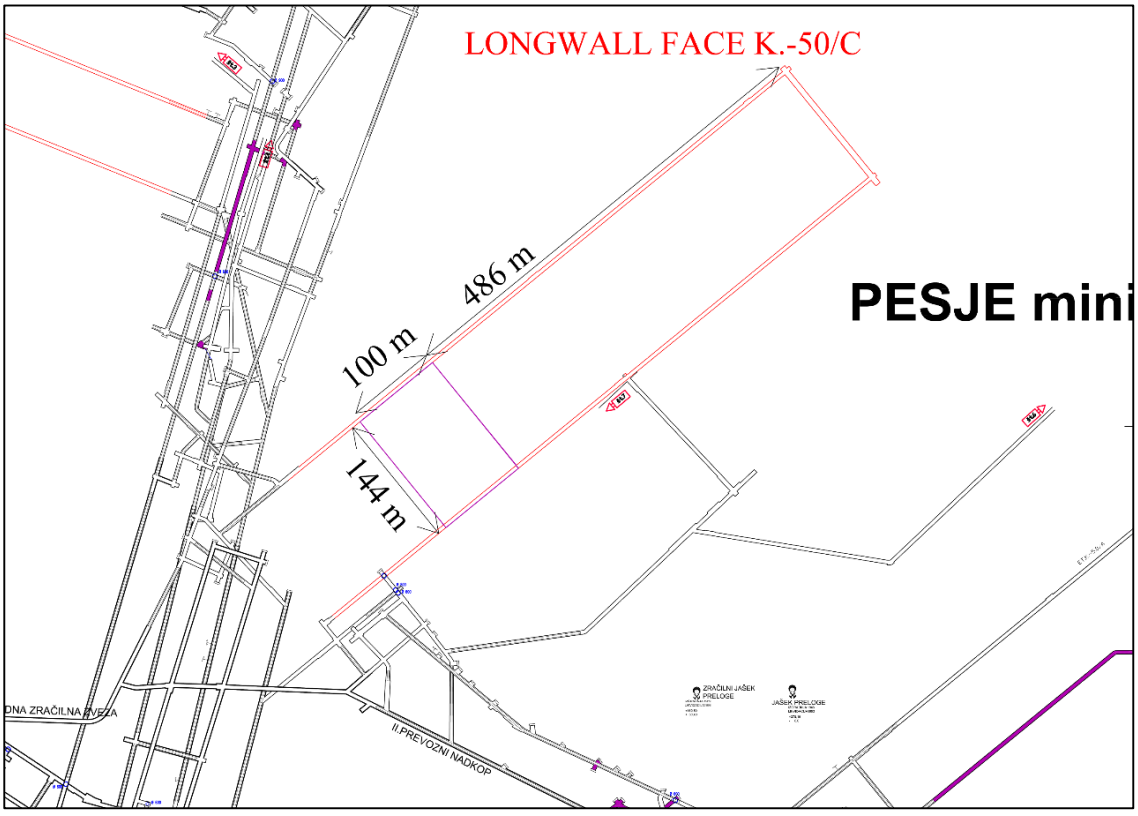


Figure 28: *Location of seismic tomography measurement area at longwall panel K.-50/C.*

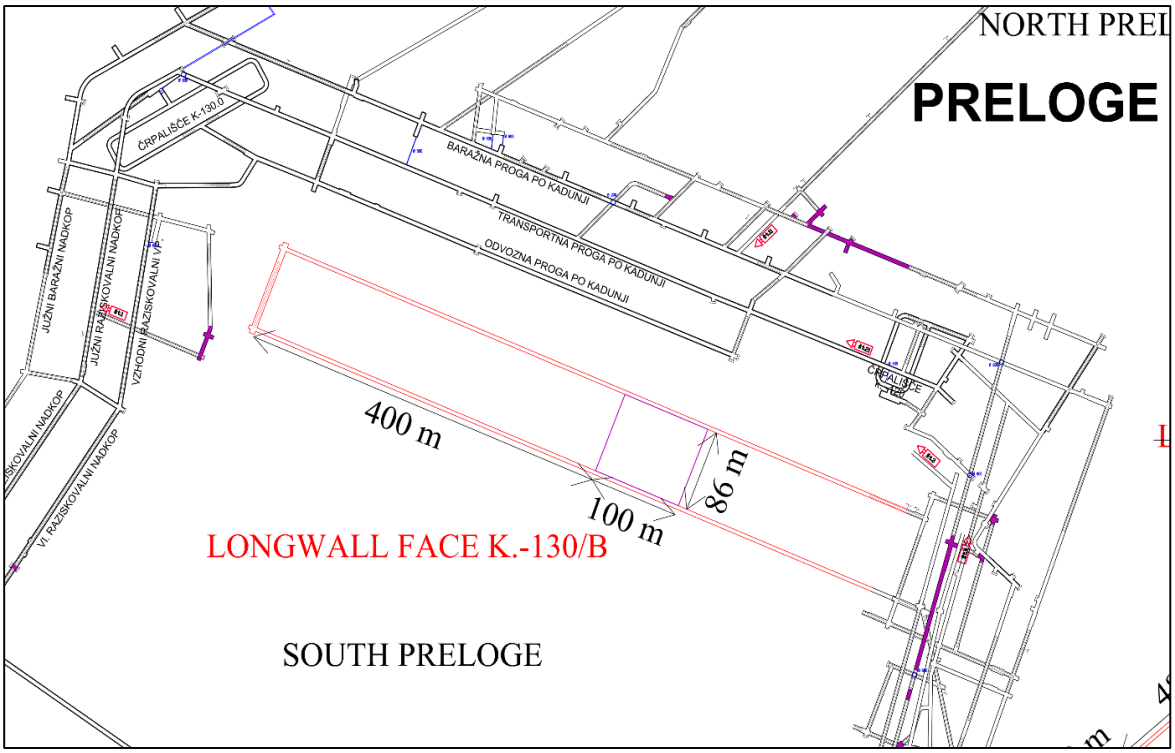
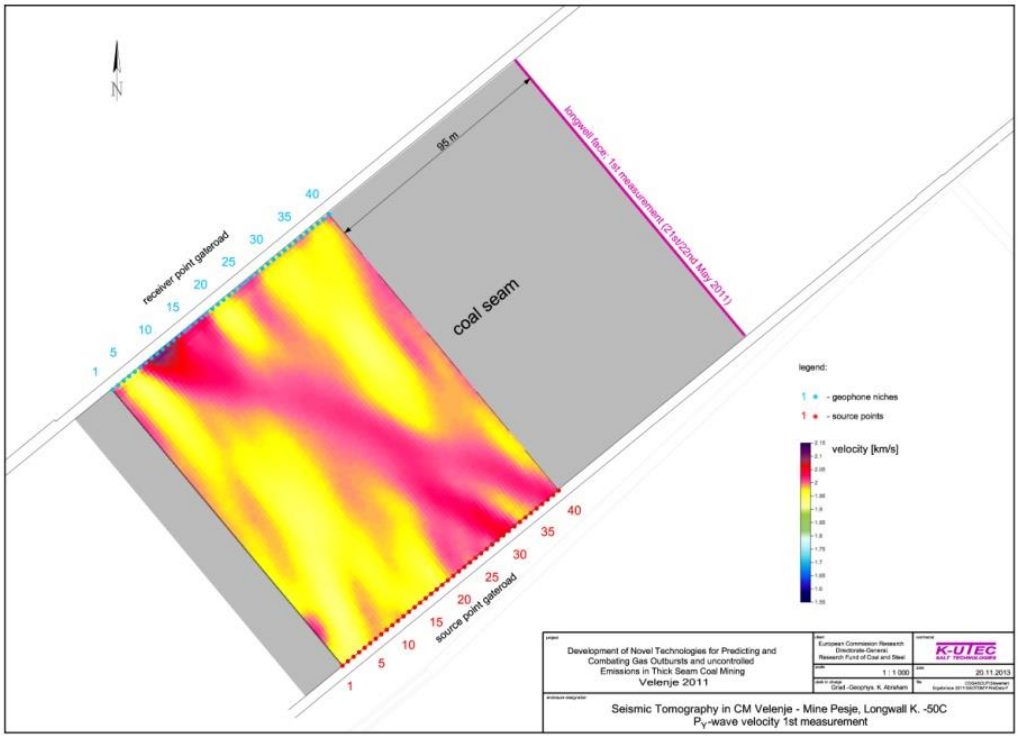


Figure 29: *Location of seismic tomography measurements on the longwall panel K.-130/B.*

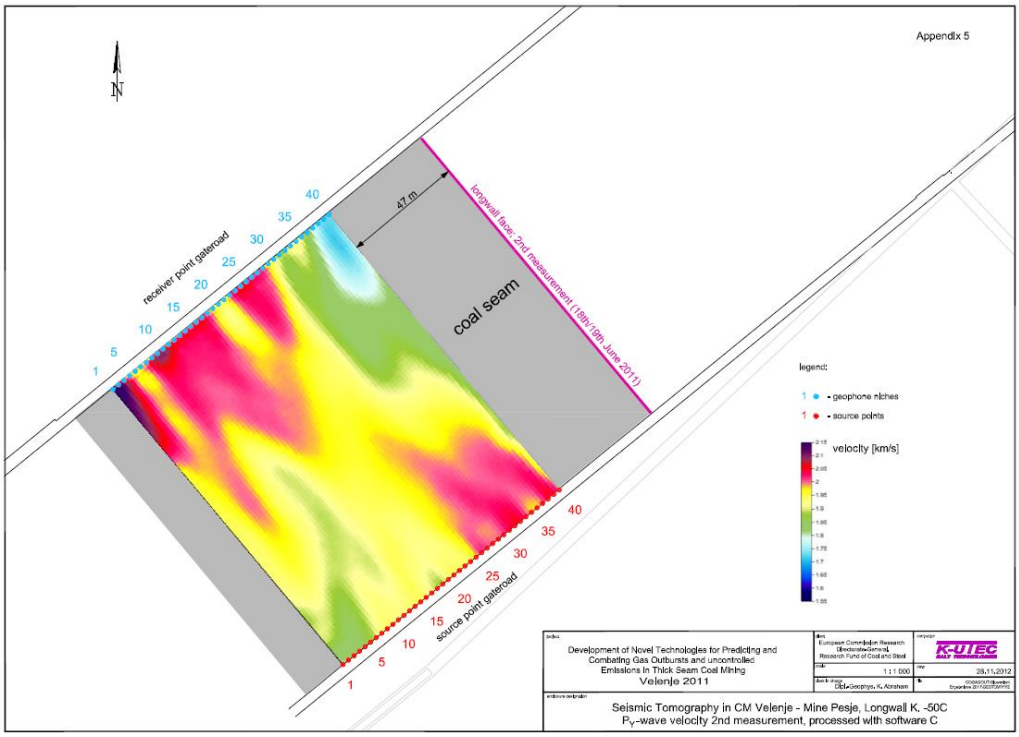
4.2.1 P Wave Seismic Tomography Measurements at Longwall Panel K.-50/C

Figure 30 shows a P_y – velocity tomograms of the 1st and 2nd measurements campaingns, where the longwall face was 95 m and 47 m from the tomography zone respectively. In the 1st tomography, the red zone, which is an area of high velocity, expands diagonally from one side to the other side of the panel, and can be explained by the type of lignite and its ability to take on additional stress (xylite, composite lignite type).

Figure 31 shows the Y-component velocity difference tomogram (P_{y2} - P_{y1}), calculated as the difference between the 2nd and 1st campaigns. Significant changes in velocity are observed as the longwall face approaches the tomography zone. At 47 m from the tomography zone, the area nearest to the approaching face in the NW half of the panel has the lowest P-wave velocities i.e., a decrease of 250 m/s, suggesting that fracturing of the coal under extreme abutment stresses under solid coal roof has occurred. The slightly higher velocity behind this area can be attributed to the initial stages of fracture formation, while the zone of high velocity beyond these results from the compaction of coal under the increased abutment stresses.



(a)



(b)

Figure 30: *Longwall K.-50/C P-wave velocity tomograms in Y-component for the (a) 1st tomography campaign during 21-22 May 2011 and (b) 2nd tomography campaign during 18-19 June 2011.*

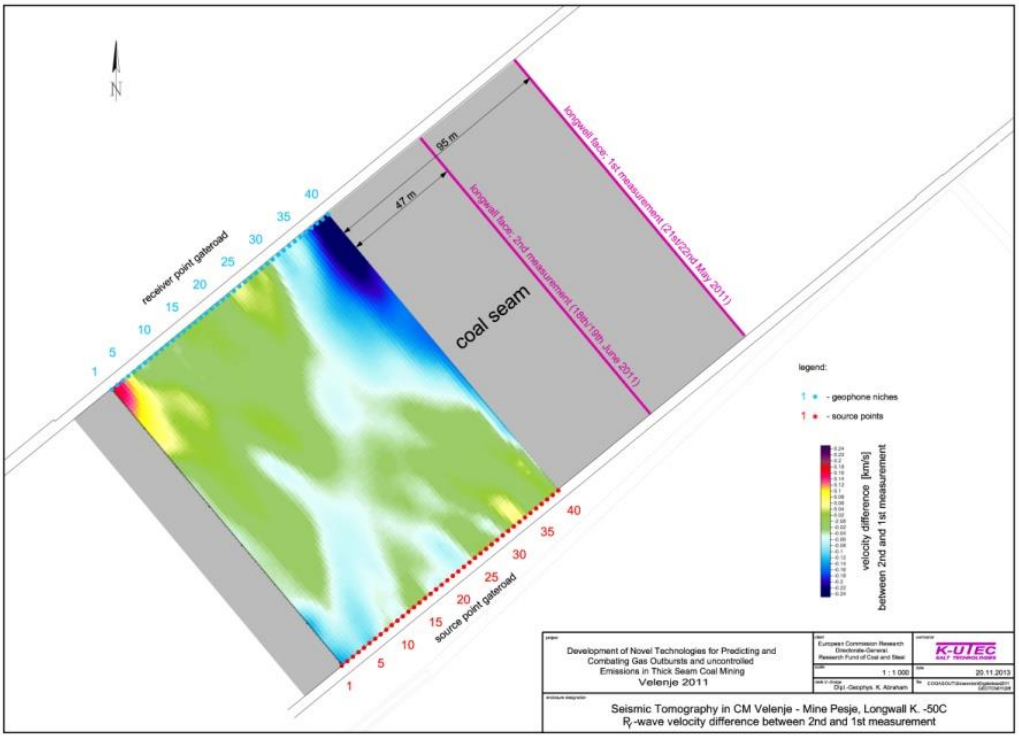


Figure 31: *P_y velocity tomogram, difference between 2nd and 1st measurement in longwall panel K.-50/C.*

The SE half of the tomogram suggests that the seam, under a relatively thin slice of coal and caved roof, only experiences a mild abutment stress sufficient to compact the coal seam (but not fracture) leading to high P-wave velocities at the front and lower P-wave velocities beyond this area due to a slight decrease in stress. Accumulation of either additional energy or stresses is possible where the material is ductile and sufficiently hard to withstand such changes and the accumulation of additional energy is greater below the fresh-undisturbed roof (hanging wall). The ductile material in the Velenje seam is xylite, which is capable of storing a significant amount of energy.

4.2.2 P Wave Seismic Tomography Measurements at Longwall Panel K.-130/B

Compared with the seismic tomography campaign performed at longwall panel K.-50/C, there were two significant differences in the K.-130/B panel's measurement area. First, a geological fault crosses the panel and second, previously mined panels fully cover the measurement area.

Inside the measurement area, next to the receiver gate road (South), a mine monitoring station was installed. This had included gas sampling boreholes and a pressure borehole, which were filled with cement. This had the effect of creating high velocity gradient coefficients that are visible in the tomograms. The crushed coal, fractured by mounting the instruments, creates lower P-wave velocities whereas the xylitic coal, which is dense and uncrushed, produced higher P-wave velocities.

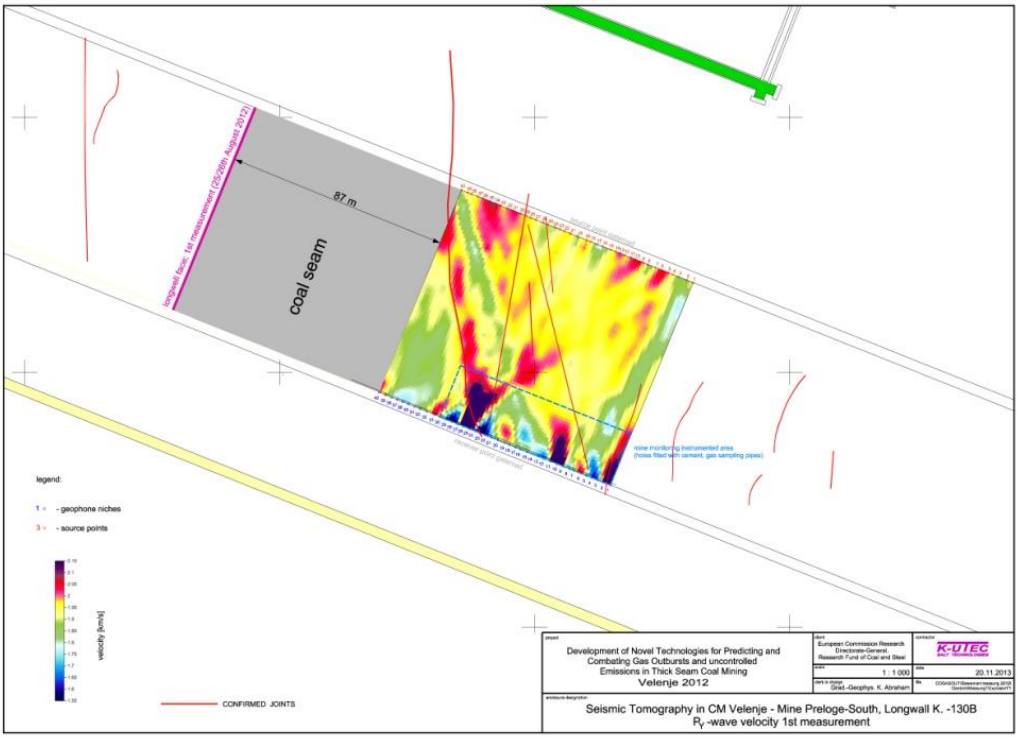


Figure 32: *P_y velocity tomogram, 1st measurement at longwall panel K.-130/B.*

In Figure 32 the Py velocity tomogram of the 1st measurement is displayed. There is an obvious change in seismic velocity due to a fault, which is a stable geological feature at this distance (87 m) to the longwall face. In addition, seismic velocities can reveal unique stress features e.g., pore pressures. Increasing pore pressure can open up cracks and voids in the rock mass, causing a localised decrease in P-wave velocity. Once an increase in pore pressure has opened up the fractures, the remaining high pore pressures can keep the cracks open, retaining the low velocity readings in that zone (Kerr, 2011).

The second tomography measurement was performed when the longwall face had advanced inside the tomography zone. The tomogram reveals typical behaviour of the coal in front of the longwall face i.e., at 1.5 m from the longwall face the stress effect overcomes the fault effect (Figure 33). This stress effect is observed as a large zone of high deformations and low P-wave velocities, which stretches out to 20 m in front of the longwall face.

Figure 34 shows a P_y velocity difference tomogram, calculated as the difference between the 2nd and 1st measurement. A large decrease in P wave velocity is observed as the longwall face advances together with a decrease in velocity of up to 600 m/s at a distance of 2.6 m to the longwall face.

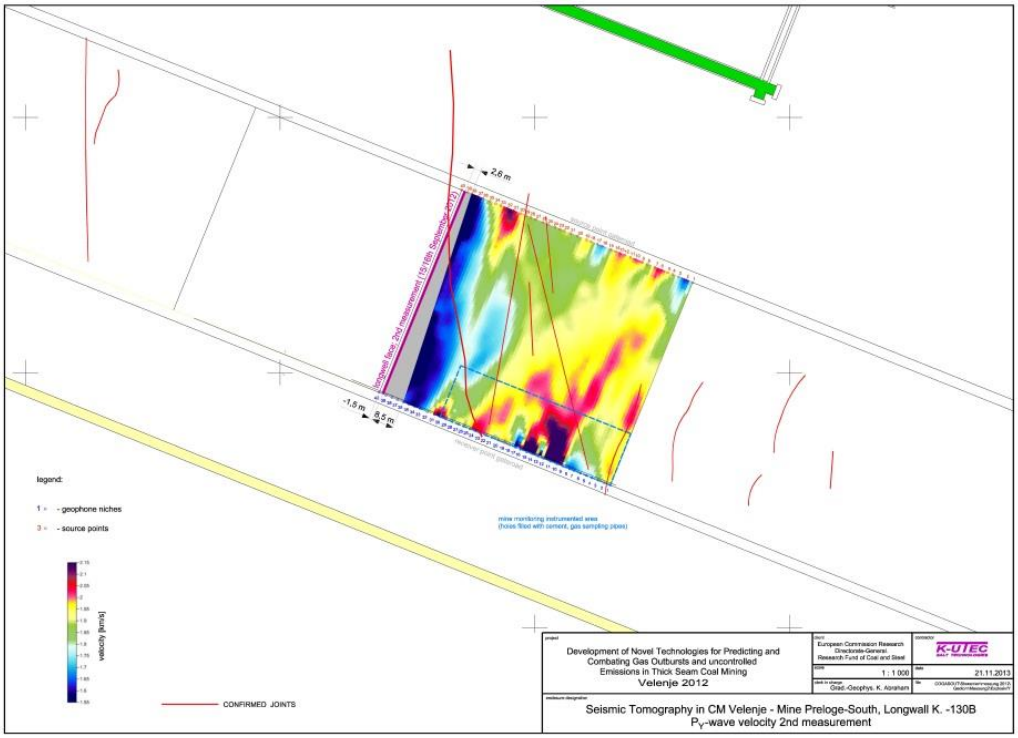


Figure 33: *P_y velocity tomogram, 2nd measurement at longwall panel K.-130/B.*



Figure 34: *P_y velocity tomogram, difference between 2nd and 1st measurement at longwall panel K.-130/B.*

The influence of the fault on the P wave velocity tomogram is interesting. The fault is detected in the P wave velocity tomogram at a distance of 87 m from the longwall face as a high P-wave velocity gradient. This major fault was detected in previously mined longwall panels, revealing seismic tomography to be a good tool for detecting this kind of anomaly. Faults are a major risk factor in outbursts because they represent points of contact

between xylitic and detritic material. If these faults and other contacts can be detected before the longwall face reaches them, then the mine can be properly risk prepared.

4.2.3 S Wave Seismic Tomography Measurements at the Longwall Panel K.-130/B

The S_z velocity difference tomogram of the longwall panel K.-130/B is shown in Figure 35. An increase in the S-wave velocity to 400 m/s was measured as the longwall face advanced. This increase in the increment of the S-wave velocity was observed up to 72 m in front of the longwall face in the southern part and up to 77 m in the northern part of the measurement area. The S-wave velocity increase is influenced by the increasing abutment stress.

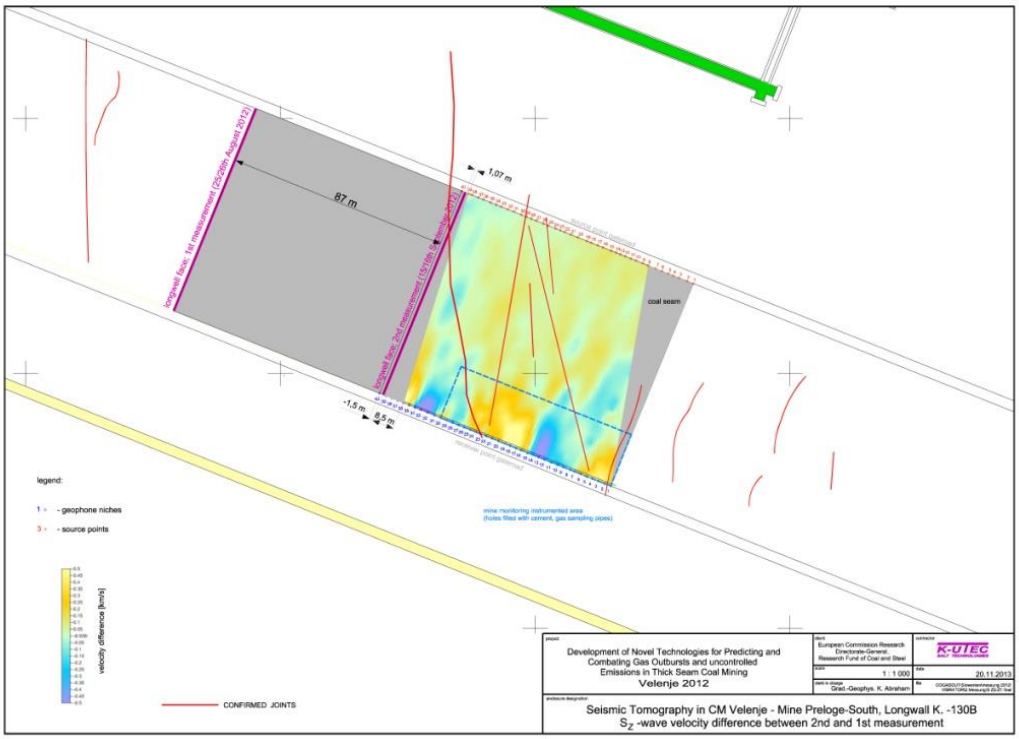


Figure 35: *S_z velocity tomogram, difference between 2nd and 1st measurement at longwall panel K.-130/B.*

There are two exceptions where a decrease in S wave velocity is observed. First, is a decrease of up to 280 m/s that occurs along the fault next to the longwall face and the second is in the south part along the southern section of the 2nd big fault situated at a greater distance from the longwall face. This section is also influenced by the installation of the monitoring equipment. The decrease in the velocity of the S-waves along the faults is caused by a reduction in stress next to the longwall face from the fracturing of the coal and a reduced amount of solid-solid contact.

4.2.4 Conclusions from the Seismic Tomography Measurements

Besides being a risk factor in outbursts, faults and fissures can act as gas reservoir, where under a certain pressure the gas is either fixed in the matrix or free in the pores. When the surroundings of this reservoir remain intact this gas cannot migrate, but when the coal is damaged by the dynamic forces created by the shearer and the crushing of the coal from top coal caving, gas can migrate. Seismic energy is also released when a frictional

instability occurs on pre-existing geological structures, or when new fractures are formed (Urbancic and Trifu, 1997).

Although it is difficult to compare both sets of data from the two seismic tomography campaigns, both reveal a decrease in P-wave velocities as the longwall face approaches. Closer the longwall face is to the measuring area the greater the decrease in velocity. In the seismic tomography campaign at longwall panel K.-130/B the P-wave velocities decreased by up to 600 m/s as the face moved closer to the tomography zone. On the other hand, they decreased by only 250 m/s in the case of longwall panel K.-50/C due to different overburden conditions. Furthermore, the K.-50/C tomography campaign clearly demonstrates that a mainly xylitic coal zone is represented by higher P-wave velocities and can form a high stress barrier ahead of a high gas content detritic zone.

4.3 Coal Seam Gas Pressure Measurements

Coal seam gas pressure monitoring was established to correlate gas pressure behaviour during longwall face advance towards the monitoring point with geotechnical monitoring data such as stress measurements. Coal seam gas pressure measurements using long boreholes began in 2010 at the longwall panel K.-50/C in the Pesje Mine district. Horizontal boreholes were drilled into the longwall panels to a depth of 30 m. Sealing of the boreholes was initially problematic but was improved by changing the inclination of the boreholes from +2° to +10° and the cement filling to a more dense mixture.

A significant amount of CSG pressure monitoring data was collected for the lignite seam at different longwall panel locations. In this thesis, the focus is on CSG pressure measurements and analysis at longwall panels K.-65/F, which is the longwall panel used in modelling and where the gas drainage system was established, and a second longwall panel K.-65/E, where different approach for testing the permeability of the coal seam with CSG pressure borehole was established. The location of the analysed boreholes is shown in Figure 36. Boreholes were drilled into the longwall panel from the gate roads to a length of 30 m, except for boreholes JV E1 and JV E2, which were 40 m in length.

Coal seam gas pressure measurements were performed by manually reading the pressure gauge installed on the boreholes and by using a digital pressure sensor connected to the mines fibre optic system (Figure 37). The fibre optic network system and the mines software provided on-line monitoring of the pressure variations from the individual boreholes. Pressure was measured using digital pressure PEMEX LCFLPDI sensors (*Kirchgaesser, Germany)* with an accuracy of + - 1% of its maximum value. Three different measurement ranges were available for pressure monitoring: 0-10 bar, 0-16 bar and 0-25 bar. The pressure sensors, as with all other equipment used in the mine, were certified as safe for use in mines where methane is present.

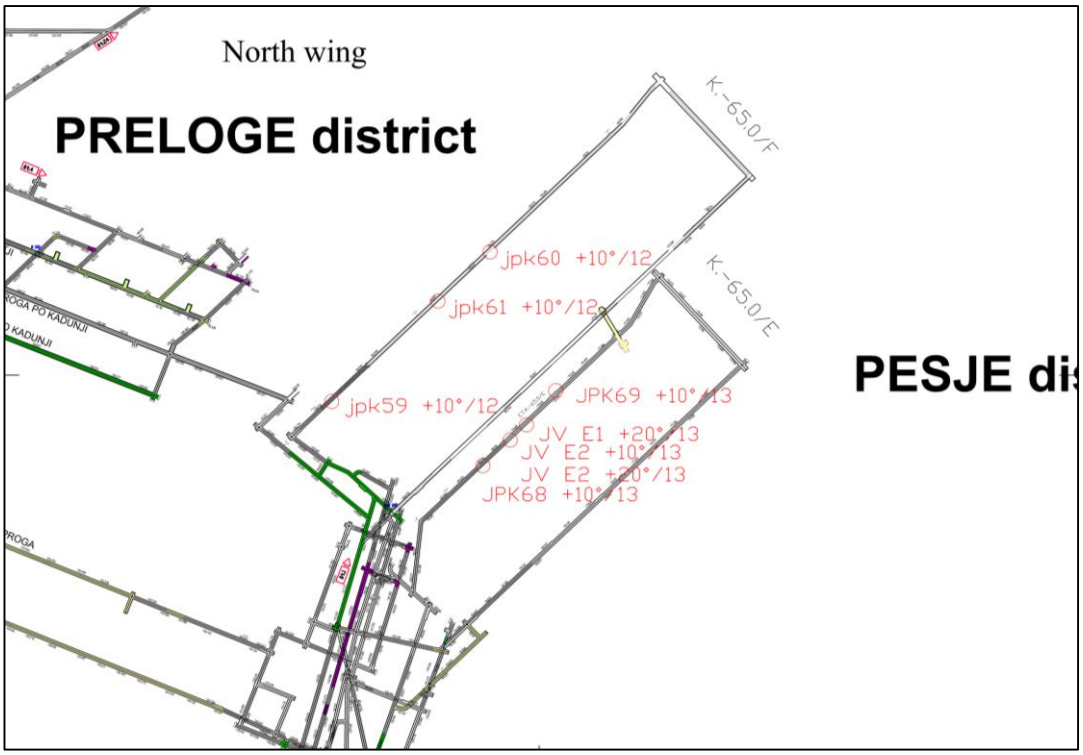


Figure 36: *Location of the CSG pressure boreholes at Mine Pesje.*



Figure 37: *A pressure sensor probe, pressure gauge and temperature probe installed in the CSG pressure borehole in the mine.*

4.3.1 Coal Seam Gas Pressure Data Interpretation

The analysis of the CSG pressure measurements gave very different results for the boreholes in the same longwall panel and for the neighbouring longwall panels. For instance, pressure measurements in panel K.-65/F in boreholes JPK 59 (+10°)/12 (Figure 38), JPK 60 (+10°)/12 (Figure 39) and JPK 61 (+10°)/12 (Figure 40) revealed that the two boreholes (JPK 59 (+10°)/12 and JPK 61 (+10°)/12) could potentially achieve a maximum pressure of up to 2 MPa, but in both cases the pressure actually drops to near zero, without feeling the effects of the advancing longwall face. This drop in gas pressure is a result of a rock burst recorded at a nearby location. The rock burst created new fractures that allowed CSG to escape from the surroundings of the borehole and consequently reduced the CSG pressure. For JPK 59 (+10°)/12 the pressure drop was slower, and for JPK 61 (+10°)/12 the pressure drop was more rapid. On the other hand, the pressure in borehole JPK 60 (+10°)/12 remained very low and not reach the high pressure readings recorded in the other two boreholes

High pressure measurements were recorded at longwall panel K.-65/E in the borehole JPK 69 (+10°)/13 (Figure 41). Therefore, a high CSG pressure of 2 MPa was used as the initial pressure in the flow model which will be discussed in Chapter 6. Figure 41 shows how the CSG pressure changes under the influence of the longwall face advance. At 70 m in front of the borehole, rapid changes in the CSG pressure occur. As it will be discussed later, during this period the CSG composition also changes. Beyond 70 m, the pressure drops to zero due to the coal being deformed around the borehole.

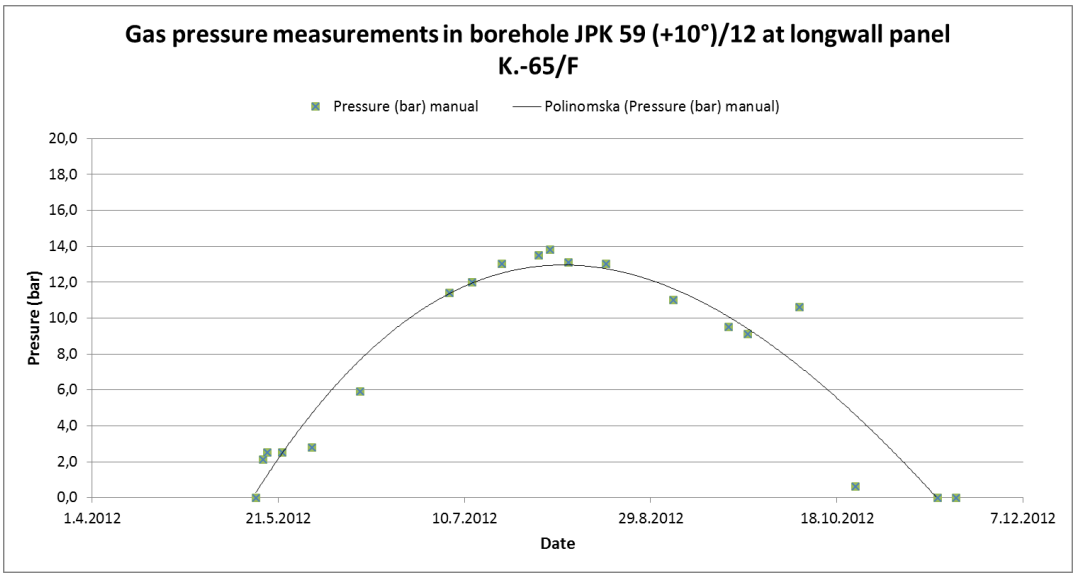


Figure 38: *Gas pressure measurements in borehole JPK 59 +10°/12 at longwall panel K.-65/F.*

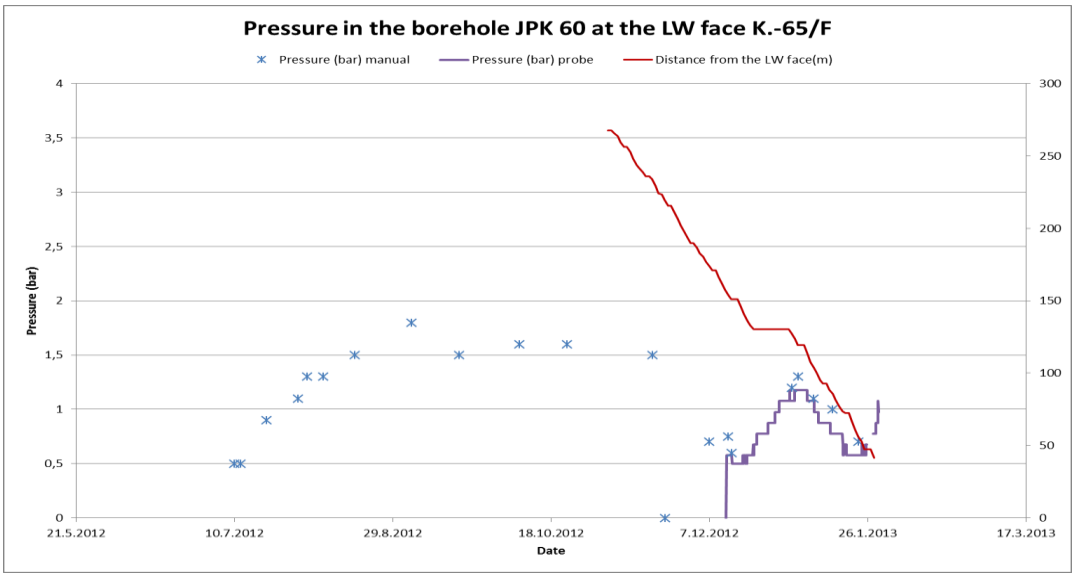


Figure 39: *Gas pressure measurements in borehole JPK 60 +10°/12 at longwall panel K.-65/F.*

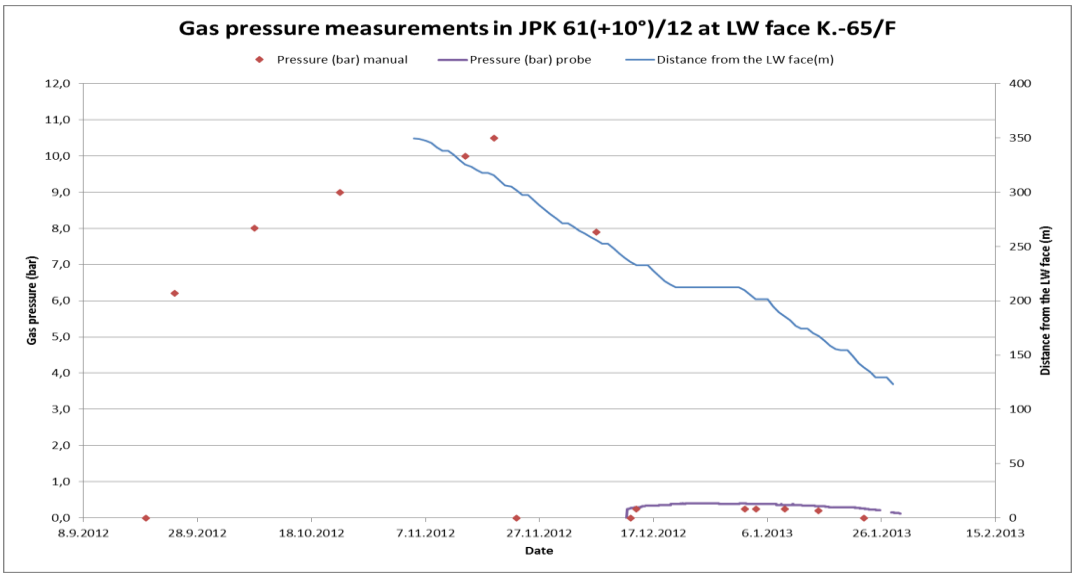


Figure 40: *Gas pressure measurements in borehole JPK 61 +10°/12 at longwall panel K.-65/F.*

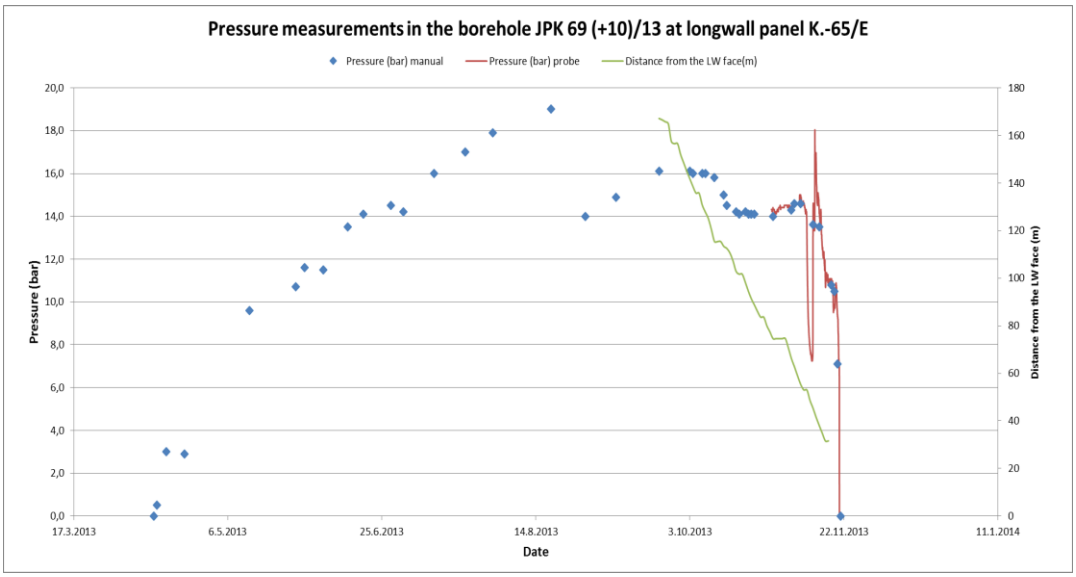


Figure 41: *Pressure measurements in the borehole JPK 69 (+10°)/13 at longwall panel K.-65/E.*

The second drainage trial was meant to be carried out at the longwall panel K.-65/E were the boreholes had been already drilled, but due to a rock burst and the danger of further bursts all drainage activities were halted and the drainage boreholes were used for repeated pressure build-up testing instead. The purpose of the test was to observe time dependent pressure build-up in the borehole. After opening the pressure valve to release the pressure in the borehole, the valve was then closed and the new borehole gas pressure data recorded. The process was repeated as the longwall face advanced towards the boreholes.

In Figure 42, which shows pressure build-up measurements, three different groups are discernible. The first group appears when the distance of the longwall face to the borehole is from 71 m to 55 m. Here pressure builds up at a constant rate without reaching equilibrium. It appears as if the pressure will increase indefinitely although it stops eventually at 1.6 MPa. The second group appears when the longwall face is from 53 to 44 m from the borehole. The pressure build-up is slower than in the first group, reaching a maximum of 1.1 MPa. This lower pressure results from the fractures present in the coal that allows the CSG to migrate to other locations in the seam. The third group appears at a borehole distance of 39 m. The build-up in pressure is rapid but the maximum pressure (0.4 MPa) is much lower than that in the previous measurements. These observations were also seen in boreholes JV E2 (+10°) (Figure 43) and JV E2 (+20°) (Figure 44), which were drilled at the same location but with different inclinations.

Monitoring the pressure at a nearby borehole allowed pressure interference tests to be made between the boreholes. No interference was observed, even though the vertical distance between the filtered parts of the two boreholes is approximately 2.5 m, indicating that the permeability of the coal surrounding the two boreholes is very low. These measurements are also used to calculate coal seam permeability, which increased ~200 fold (from k=0.69 mD to k= 141.2 mD) as the longwall face approached and fractured the coal in the last 5 metres from the boreholes (Durucan et al, 2014).

All of these data are essential for understanding the mechanism of gas pressure formation in the Velenje lignite. Over the years, experiments performed at the Velenje mine have improved drilling and sealing techniques and produced a lot of useful data, which can provide a clearer picture of the chemical and geomechanical mechanisms that occur in the Velenje lignite.

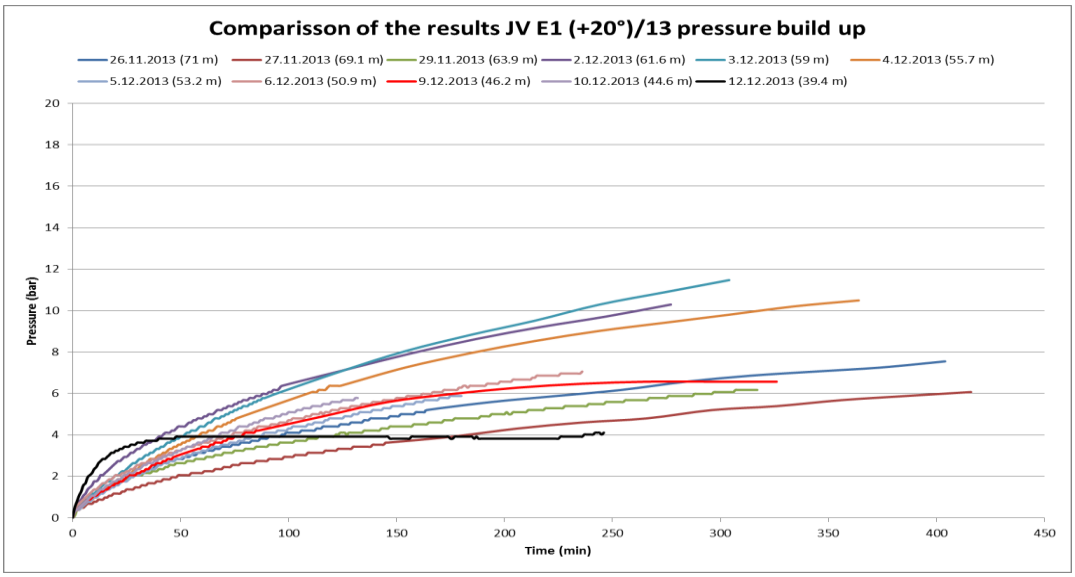


Figure 42: *Comparison of the pressure build up results at borehole JV E1 (+20°)/13.*

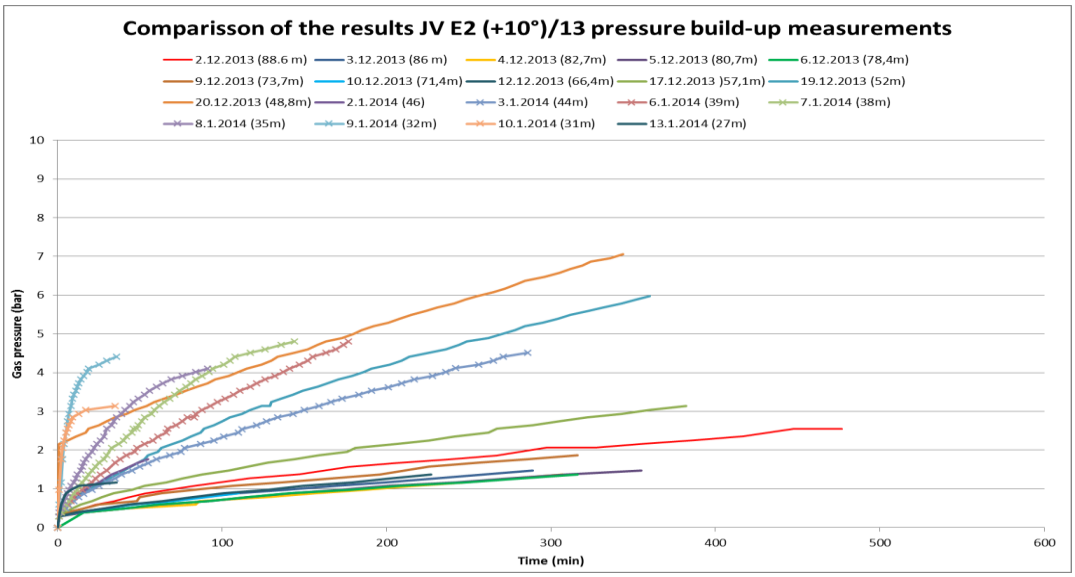


Figure 43: *Comparison of the pressure build up results at borehole JV E2 (+10°)/13.*

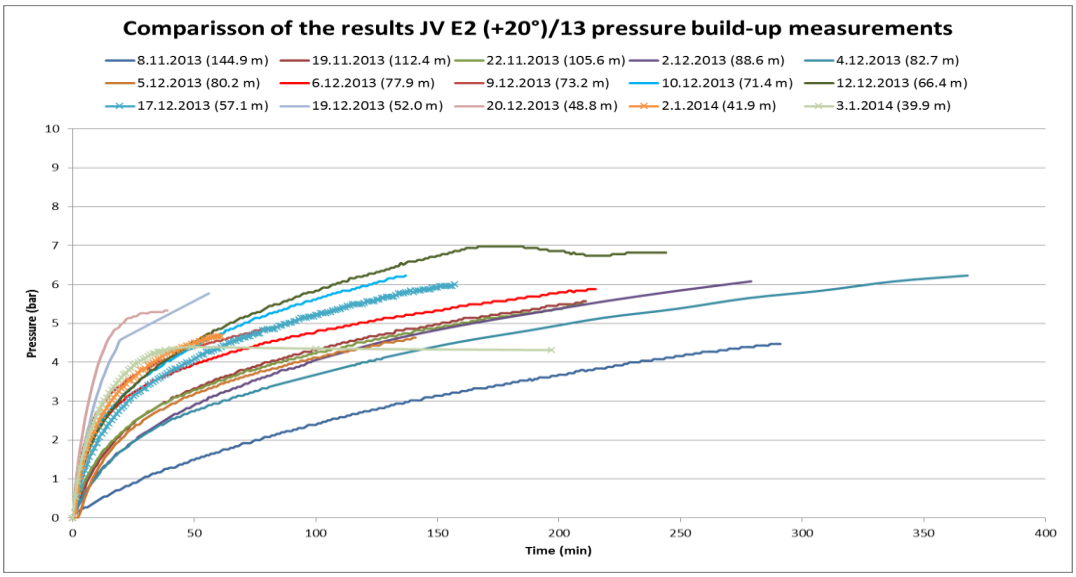


Figure 44: *Comparison of the pressure build up results at borehole JV E2 (+20°)/13.*

4.4 Geochemical Properties of the Coal Seam Gas

Coal seam gas composition and isotopic composition was monitored using gas sampling and monitoring boreholes of various lengths and inclination. Measurements of the SCG composition and its isotopic composition were performed in the Department of Environmental Sciences at the Jožef Stefan Institute, Ljubljana, Slovenia, whereas the measurements of higher hydrocarbons and isotopic composition of deuterium were performed at Istituto Nazionale di Geofisica e Vulcanologia Sezione di Palermo, Italy. More recently, monitoring was performed using 25 m long boreholes (Figure 45). The boreholes were cored using a (Ø=101 mm) drill and steel casings (Ø=85 mm) were inserted to a depth of 20 m. Inside the steel casing was a 25.4 mm (1") diameter Alcaten tube with the last 5 m perforated. Sealant foam was injected to a depth of 20 m to seal the casing. Into this tube was inserted a smaller copper capillary sampling tube (Ø=2 mm) and a back-up copper sampling tube (Ø=6 mm) (Sedlar et al., 2014).

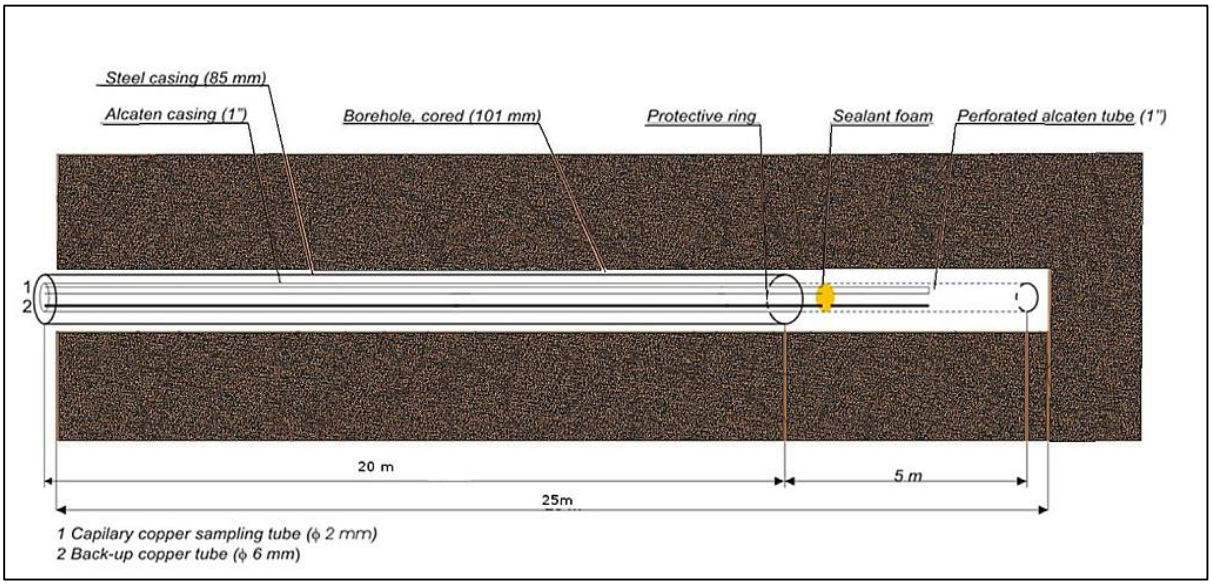


Figure 45: *Figure of the sampling borehole* (Jamnikar, 2015).

Boreholes for coal seam gas sampling were drilled at various locations in the mine ahead of the working faces of five longwall panels (Figure 46). They were located at different depth levels: K.-5/A at level -395 m, K.-50/C at level -445 m, G2/C at level -460 m, K.-130/A at level -536 m and K.-65/F at -462 m in order to trace the coalbed gas distribution in advance of the working face. The number of samples collected was determined in relation to the distance of the longwall face from the borehole. When the longwall face was far away (from 250 m to 90 m), one gas sample per week was collected, two samples were collected between 90 m and 40 m away from the longwall face, and when the longwall face was closer to the borehole (40 m to 0 m) samples were collected daily. “Free” gas includes both the volatiles filling the pores and cracks within the coal structure and partly gas degassed from the coal during drilling and sampling (Kotarba, 2001). The "free gas" migrating from the borehole was collected using a 50 ml plastic syringe and then transferred to a 12 ml glass ampoule, which was flushed with coalbed gas and then filled under pressure. At each location seven samples were collected for different geochemical analyses. The ampoules were then stored at normal atmospheric conditions until analysis. A problem in sampling of coal gases occurred occasionally when the longwall face was advancing toward the location of the borehole where the pressure wave disturbed the coal seam damaging the borehole. In these cases interpreting coalbed gas distribution was not possible.

The concentrations of CH_4, CO_2, nitrogen, oxygen and argon were determined using a custom-made NIER mass spectrometer (Kanduč & Pezdič, 2005). The method of singular decomposition of the matrix was used to allow simultaneous analysis of the gases. The precision of the method was ± 3%. To correct for any possible air contamination of the capillary system and in the evacuated ampoules, sample results were recalculated on an air-free basis. The percentage of oxygen in the sampling ampoules was used to calculate the amount of nitrogen, according to its ratio in air (N_2/O_2= 3.7) and taking into account Dalton's law (Atkins, 1994).

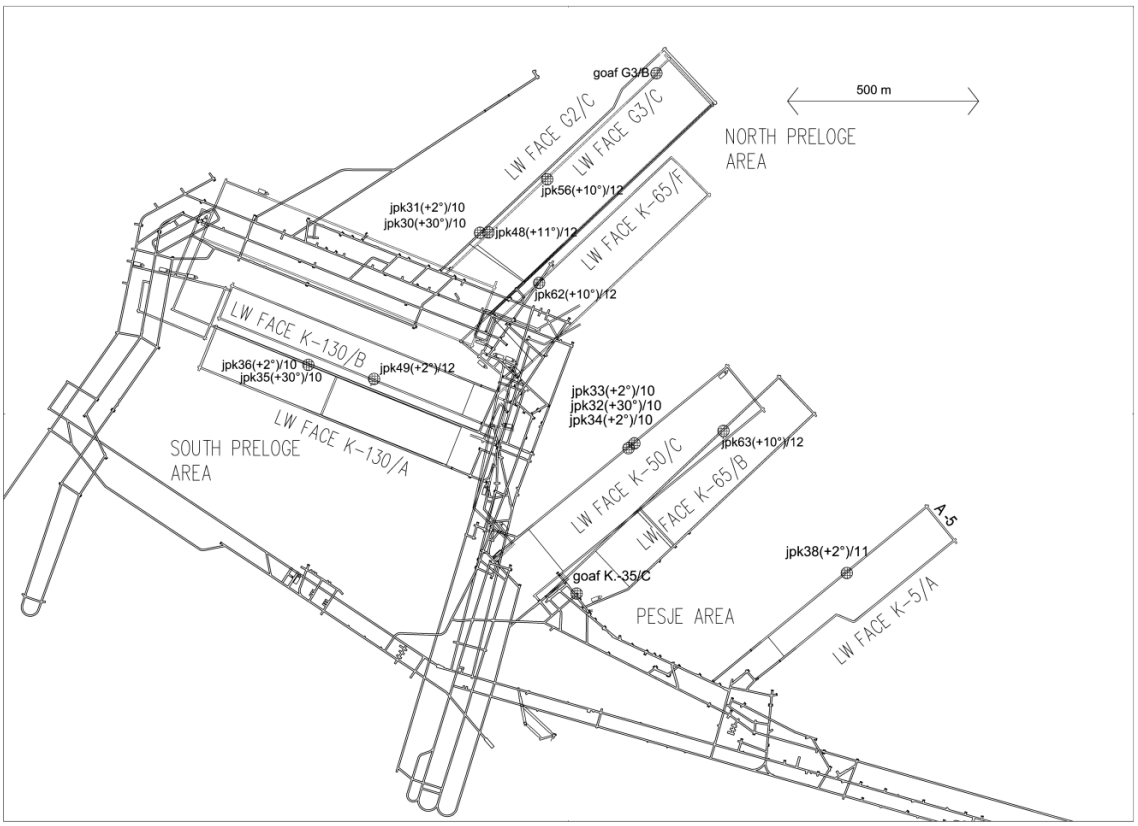


Figure 46: *Location of sampling boreholes in the active parts of the Velenje Coal Mine (Pesje, South Preloge and North Preloge mining districts).*

The stable carbon isotopes of coalbed methane are usually used to identify its genesis (Gouyi et al, 2007). There are three main sources of hydrocarbon gases and CO_2 in sedimentary basins: abiogenic, microbial and thermogenic (Rice, 1993). Thermogenic gases are typically associated with high rank coal, whereas microbial gases are typically associated with low rank coal. Abiogenic sources of gas are typically found in deep subsurfaces (Sherwood Lollar et al., 2006). Primary thermogenic gases have a methane carbon isotope composition higher than -50 ‰ (Golding et al., 2013).

A good review of coalbed methane is given by Moore, (2012). Stable isotopes of CH_4, CO_2 and H_2O have been used in various studies to distinguish the pathways of microbial methane generation i.e. acetate fermentation versus CO_2 reduction (Whiticar et al., 1986; Flores et al., 2008; Bates et al., 2011; Moore, 2012). Because production gases from many CBM and some shale gas fields are relatively dry, the ratio of methane to the sum of ethane and propane (C_1/C_2+C_3)) is widely used to distinguish between microbial and thermogenic gases. Ratios greater than 1000 and less than 100 (wet gases are commonly associated with oil and tend to have ratios of $C_1/(C_2+C_3)<50$) are considered to be characteristic of microbial and thermogenic gas, respectively, when combined with the methane carbon isotope composition (Flores et al., 2008, Osborn and McIntosh, 2010, Smith and Pallaser, 1996, Strapoć et al., 2011). Two pathways have been identified for the generation of biogenic gas: carbon dioxide reduction and methyl-type fermentation (Schoell, 1980; Wolternate et al., 1984; Jenden and Kaplan, 1986; Whiticar et al., 1986).

The isotopic composition of CH_4 and CO_2 ($\delta^{13}C_{CH4}$ and $\delta^{13}C_{CO2}$ in continuation) was determined using a Europa 20-20 continuous flow isotope ratio mass spectrometer (CF-IRMS) with an ANCA-TG preparation module. Gas samples were flushed with a continuous flow of He across two chemical traps (Kanduč et al., 2011). In the first stage, water was removed and CO_2 was analysed directly for its stable isotope content. During the

second stage, all CO_2 was removed in order to analyse the stable isotope composition of CH_4. The CH_4 was then combusted over hot 10% platinum CuO (1000 °C), which converted the CH_4 to CO_2. The CO_2 was analysed for its ^{13}C content. Working standards calibrated to the VPDB (Vienna Pee Dee Belemnite) were used during measurements with a defined value of -3.2 ‰ for CO_2 and -47.5 ‰ for methane (Kanduč et al., 2012). The stable isotope data are presented using the δ notation relative to the VPDB standard and expressed in ‰ (Coplen, 2011). Analytical precision was ± 0.2 ‰ for carbon dioxide and ± 0.6 ‰ for methane.

Determination of the $^2H/H$ ratio of CH_4 was performed using a Thermo Delta XP GC-TC/CF-IRMS coupled to a TRACEGC analyser at the Istituto Nazionale di Geofisica e Vulcanologia Sezione di Palermo in Italy. The gas chromatograph was equipped with an Rt-Q Plot column (30 m x 0.32 mm i.d. Restek) and the oven was held at a constant temperature of 40 °C. The flow rate of the carrier gas (He of 5.6 grade) was held at a constant flux of 0.8 cc min^{-1}. A split/splitless injector with a split ratio from 10:1 to 80:1 was used for sample introduction. Once the CH_4 had separated from the gas mixture, it was quantitatively converted to H_2 by passing the methane through a reactor at 1440 °C. Each sample analysis took about 500 sec. Accuracy and precision was examined by using a standardized gas, which was analysed in the mass spectrometer in the same way as the sample. The accuracy and external precision were better than 0.5 ‰ and 2.5 ‰, respectively.

Whiticar et al. (1986) suggested that variations in carbon isotope fractionation (α) between CO_2 and CH_4 could be utilized to distinguish between CH_4 generated via CO_2 reduction and acetate fermentation as in Equation 9 (Sedlar, et. al, 2014):

$$\alpha^{13}C_{CO2-CH4} = (\delta^{13}C_{CO2} + 1000)/(\delta^{13}C_{CH4} + 1000) \quad (9)$$

4.4.1 Coal Seam Gas Concentration and Stable Isotopic Composition Results

The results for carbon dioxide and methane concentrations and $\delta^{13}C_{CO2}$ and $\delta^{13}C_{CH4}$ from the investigated longwall panels (G2/C-North Preloge mining district, K.-50/C and K. -5/A- Pesje mining district, K.-130/A, South Preloge mining district and K.-65/F, North Preloge mining district) are shown in Tables 2, 3, 4, 5, 6 and 7. The results reveal the heterogeneity of both gas and isotopic composition. Possible contamination with air means the results were recalculated on an air-free basis (Kanduč and Pezdič, 2005). Additionally, the stable hydrogen composition of methane was analysed in 31 gas samples taken at different locations in the mine. The results ranged from -356 ‰ to -248 ‰ (Table 7 and 8).

The approach of the longwall face towards the boreholes affects the stresses and consequently the CSG distribution at the longwall face. During excavation of the lignite secondary fissures are generated due to the rearrangement of the primary stress conditions, which releases CSG stored in the pores of the coalbed reservoir. In previous work, gas concentrations in advance of the longwall face were investigated in the K.-120/B South Preloge mining district, G2/B North Preloge mining district, and K.-50/B Pesje mining district where at 92 m from the working face (rate of advancement of the working face 2.5 m/d) the highest concentration of methane and the lowest concentration of CO_2 were recorded (Kanduč et al., 2011). At 45 m (the rate of advance of the working face around 2 m/d) the next CO_2 maximum was detected, coinciding with a minimum in methane concentration. If the working face advance rate was slow, lower fluctuations in coal seam gases were observed (Kanduč et al., 2011). When the advance rate of the longwall face is slow (less than 2m/day), better opportunities exist for the gradual release of gas under high pressure in the virgin coal. However, at faster rates of advance as is now implemented, less

time is available for the equalisation of gas pressure and mining induced stresses. In the present work coalbed gas concentrations at the North Preloge site (Figure 47) were similar in both boreholes (JPK 30 (+2°)/10 and JPK 31 (+30°)/10). At a distance of 80 m from the longwall face G2/C (advance rate 3.7 m/d) in North Preloge the concentration of CO_2 increases while CH_4 decreases. The CO_2 concentration at the longwall face K.-130/A (Figure 48) was very high, which was expected due to the repeated mining of coal in this area that caused methane to escape from the seam. The location of this longwall face is on the footwall border of the coal seam, approximately 520 m below the surface. Since previous mining activities above this longwall panel accounted for most of the CH_4 migration, only a small amount of methane was found at K.-130/A. Although continuous measurements were performed in the borehole JPK 36(+30°)/10, the majority of the samples were contaminated with air, so that only three measurements could be used (Figure 48).

Table 2: *Methane and carbon dioxide concentrations and their stable carbon isotope composition in coalbed seam gases at G2/C (North Preloge).*

Date	Borehole	Distance from the longwall face (m)	CH_4 (%)	CO_2 (%)	CDMI (%)	$\delta^{13}C_{CO2}$ (‰)	$\delta^{13}C_{CH4}$ (‰)	$\alpha^{13}C_{CO2\text{-}CH4}$ (‰)
2010-08-18	jpk 30/10	341.0	42.2	57.8	57.8	1.8	-31.0	1.0338
2010-08-31	jpk 30/10	307.5	43.9	56.5	56.3	-1.1	-37.2	1.0375
2010-11-24	jpk 30/10	85.4	46.1	53.9	53.9	-6.6	-29.8	1.0239
2010-11-30	jpk 30/10	71.3	42.3	57.7	57.7	0.9	-50.0	1.0536
2010-12-03	jpk 30/10	60.3	46.5	53.5	53.5	0.5	-34.1	1.0358
2010-12-20	jpk 30/10	4.3	47.8	52.2	52.2	1.8	-35.3	1.0385
2010-08-20	jpk 31/10	335.3	45.7	54.3	54.3	-1.7	-45.5	1.0459
2010-08-27	jpk 31/10	316.4	30.7	69.3	69.3	-9.1	-19.8	1.0190
2010-09-22	jpk 31/10	239.7	37.0	63.4	63.4	-3.9	-60.4	1.0601
2010-11-24	jpk 31/10	85.4	46.1	53.9	53.9	-6.6	-29.4	1.0235
2010-11-30	jpk 31/10	71.3	43.3	56.7	56.7	-0.7	-50.3	1.0522
2010-12-03	jpk 31/10	60.3	48.1	51.9	51.9	0.9	-34.2	1.0363
2010-12-08	jpk 31/10	46.8	46.9	53.1	53.1	0.5	-33.6	1.0353
2010-12-20	jpk 31/10	4.3	48.5	51.5	51.5	0.1	-24.9	1.0256

Table 3: *Methane and carbon dioxide concentrations and their stable carbon isotope composition in CSG at K.-50/C (Pesje).*

Date	Borehole	Distance from the longwall face (m)	CH_4 (%)	CO_2 (%)	CDMI (%)	$\delta^{13}C_{CO2}$ (‰)	$\delta^{13}C_{CH4}$ (‰)	$\alpha^{13}C_{CO2\text{-}CH4}$ (‰)
2010-09-14	jpk 32/10	302.6	36.1	63.9	63.9	-4.2	-58.0	1.0571
2010-09-22	jpk 32/10	302.6	26.0	74.0	74.0	-5.3	-56.9	1.0547
2010-11-26	jpk 32/10	285.1	24.3	75.7	75.7	-5.6	-58.9	1.0566
2010-12-07	jpk 32/10	265.5	46.0	54.0	54.0	-5.2	-31.5	1.0272
2011-02-02	jpk 32/10	141.0	29.8	68.1	69.6	-5.2	-46.2	1.0430
2011-02-11	jpk 32/10	117.4	32.8	67.2	67.2	-4.9	-42.8	1.0396
2011-03-03	jpk 32/10	64.5	12.9	87.1	87.1	1.0	-41.1	1.0439
2011-03-11	jpk 32/10	44.5	48.9	51.1	51.2	-3.9	-51.7	1.0504
2011-03-15	jpk 32/10	32.2	43.0	57.0	57.1	-2.2	-51.5	1.0520
2011-03-18	jpk 32/10	22.6	47.1	52.9	52.9	-2.1	-46.6	1.0467
2011-03-21	jpk 32/10	16.0	23.8	76.2	76.3	-5.1	-48.9	1.0461
2011-03-22	jpk 32/10	11.8	27.8	72.2	72.2	-5.0	-46.0	1.0430
2011-03-23	jpk 32/10	10.8	14.6	83.4	85.1	-5.4	-46.0	1.0426
2011-03-24	jpk 32/10	8.0	15.5	84.5	84.6	-5.9	-59.5	1.0570

Table 4: *Methane and carbon dioxide concentrations and their stable carbon isotope composition in CSG at K.-50/C (Pesje) - continued.*

Date	Borehole	Distance from the longwall face (m)	CH_4 (%)	CO_2 (%)	CDMI (%)	$\delta^{13}C_{CO2}$ (‰)	$\delta^{13}C_{CH4}$ (‰)	$\alpha^{13}C_{CO2\text{-}CH4}$ (‰)
2011-03-25	jpk 32/10	6.1	15.2	84.8	84.8	-6.1	-59.6	1.0569
2010-09-10	jpk 33/10	302.6	20.5	79.5	79.5	-6.1	-68.9	1.0674
2010-09-14	jpk 33/10	302.6	25.1	74.9	74.9	-5.2	-59.8	1.0581
2010-10-12	jpk 33/10	302.6	27.6	72.4	72.4	-7.1	-58.2	1.0543
2010-11-26	jpk 33/10	285.1	4.4	95.6	95.6	-4.8	-53.1	1.0510
2011-03-03	jpk 33/10	64.5	37.8	62.2	62.2	-5.3	-66.0	1.0650
2011-03-08	jpk 33/10	50.3	60.9	39.1	39.1	-0.8	-51.7	1.0537
2011-03-11	jpk 33/10	44.5	47.1	52.9	52.9	0.1	-40.0	1.0418
2011-03-15	jpk 33/10	32.2	61.9	38.1	38.1	0.0	-43.2	1.0451
2011-03-18	jpk 33/10	22.6	47.8	52.2	52.2	-1.1	-46.3	1.0474
2011-03-21	jpk 33/10	16.0	49.8	50.2	50.2	-11.0	-45.4	1.0360
2011-03-22	jpk 33/10	11.8	20.3	79.7	79.7	-5.1	-42.5	1.0391
2011-03-23	jpk 33/10	10.8	27.3	69.7	71.9	-4.6	-48.0	1.0456
2011-03-24	jpk 33/10	8.0	24.4	75.6	75.6	-5.4	-48.1	1.0449

Table 5: *Methane and carbon dioxide concentrations and their stable carbon isotope composition in CSG at K.-130/A (South Preloge).*

Date	Borehole	Distance from the longwall face (m)	CH_4 (%)	CO_2 (%)	CDMI (%)	$\delta^{13}C_{CO2}$ (‰)	$\delta^{13}C_{CH4}$ (‰)	$\alpha^{13}C_{CO2\text{-}CH4}$ (‰)
2010-12-08	jpk 35/10	237.9	7.5	92.5	92.5	-8.9	-51.4	1.0448
2011-01-19	jpk 35/10	237.9	17.4	81.0	82.3	5.5	-52.9	1.0617
2011-03-01	jpk 35/10	141.6	4.3	95.7	95.7	2.9	-38.6	1.0432
2011-03-24	jpk 35/10	73.6	7.4	92.6	92.6	1.5	-39.8	1.0430
2011-04-01	jpk 35/10	62.3	13.6	83.7	86.0	1.7	-48.0	1.0522
2011-04-08	jpk 35/10	51.3	19.8	73.5	78.8	2.0	-51.6	1.0565
2011-04-12	jpk 35/10	49.7	14.5	76.7	84.1	2.2	-50.3	1.0553
2011-04-13	jpk 35/10	47.6	16.6	80.4	82.9	1.8	-46.9	1.0511
2011-04-18	jpk 35/10	33.0	18.2	78.2	81.1	2.0	-48.5	1.0531
2011-04-21	jpk 35/10	23.9	30.4	67.1	68.8	-6.1	-37.6	1.0327
2011-04-22	jpk 35/10	21.9	11.3	86.4	88.5	1.3	-57.9	1.0628
2011-04-08	jpk 36/10	51.3	38.7	48.0	55.3	4.3	-38.8	1.0448
2011-04-12	jpk 36/10	49.7	43.2	53.1	55.2	2.8	-46.3	1.0515
2011-04-13	jpk 36/10	47.6	43.3	55.1	56.0	3.4	-34.7	1.0395

Table 6: *Methane and carbon dioxide concentrations and their stable carbon isotope composition in CSG at K.-5A (Pesje).*

Date	Borehole	Distance from the longwall face (m)	CH_4 (%)	CO_2 (%)	CDMI (%)	$\delta^{13}C_{CO2}$ (‰)	$\delta^{13}C_{CH4}$ (‰)	$\alpha^{13}C_{CO2\text{-}CH4}$ (‰)
2011-08-10	jpk 38/11	269.7	21.9	78.0	78.1	-2.4	-67.7	1.0700
2011-08-16	jpk 38/11	269.7	22.9	77.1	77.1	-2.2	-64.5	1.0670
2011-08-23	jpk 38/11	269.7	22.6	77.4	77.4	4.2	-66.7	1.0760
2011-08-31	jpk 38/11	269.7	23.2	76.8	76.8	-2.1	-65.2	1.0680
2011-10-11	jpk 38/11	202.3	25.6	74.4	74.4	-2.0	-65.7	1.0680
2011-10-25	jpk 38/11	165.1	26.0	74.0	74.0	-1.9	-67.0	1.0700
2011-11-16	jpk 38/11	112.6	24.5	75.5	75.5	-1.5	-70.4	1.0740
2011-11-22	jpk 38/11	99.3	24.5	75.5	75.5	-1.9	-65.4	1.0680
2011-11-29	jpk 38/11	80.6	24.9	75.0	75.1	-1.7	-69.0	1.0720
2011-12-01	jpk 38/11	72.7	24.9	75.1	75.1	-1.8	-67.8	1.0710
2011-12-05	jpk 38/11	67.1	23.9	76.1	76.1	-1.6	-68.7	1.0720
2011-12-14	jpk 38/11	42.7	24.0	76.0	76.0	-2.0	-69.4	1.0720
2011-12-20	jpk 38/11	27.9	24.1	75.9	75.9	-1.8	-65.5	1.0680

Table 7: *Methane and carbon dioxide concentrations and their stable carbon isotope composition in CSG at K.-65/F (Pesje).*

Date	Borehole	Distance from the longwall face (m)	CH_4 (%)	CO_2 (%)	CDMI (%)	$\delta^{13}C_{CO2}$ (‰)	$\delta^{13}C_{CH4}$ (‰)	$\delta^{2}H_{CH4}$ (‰)
2013-01-04	jpk 62/12	190.0	42.5	57.5	57.5	-8.0	-48.2	-294.5
2013-01-09	jpk 62/12	174.4	43.3	56.7	56.7	-7.4	-51.6	-296.3
2013-01-15	jpk 62/12	156.2	43.2	56.8	56.8	-7.9	-45.6	-296.4
2013-01-22	jpk 62/12	131.3	44.9	55.1	55.1	-7.2	-50.4	-293.6
2013-01-28	jpk 62/12	121.1	43.3	56.7	56.7	-9.0	-54.3	-298.8
2013-02-06	jpk 62/12	70.9	42.9	57.1	57.1	-7.9	-47.6	-294.9
2013-02-11	jpk 62/12	59.8	53.0	47.0	47.0	-6.5	-52.9	-294.2
2013-02-19	jpk 62/12	34.7	24.5	75.5	75.5	-8.2	-47.8	-292.6
2013-02-20	jpk 62/12	31.2	24.0	76.0	76.0	-8.1	-52.4	-291.4
2013-02-21	jpk 62/12	27.4	19.4	80.6	80.6	-8.1	-50.5	-292.4
2013-02-22	jpk 62/12	25.0	15.9	84.1	84.1	-8.7	-46.3	-293.0
2013-02-23	jpk 62/12	21.4	19.7	80.3	80.3	-8.5	-50.6	-294.0
2013-02-25	jpk 62/12	17.9	19.0	81.0	81.0	-8.3	-50.4	-293.3
2013-02-26	jpk 62/12	14.4	19.8	80.2	80.2	-8.2	-51.3	-295.8
2013-02-27	jpk 62/12	11.1	20.4	79.6	79.6	-8.2	-52.8	-295.8
2013-03-01	jpk 62/12	4.6	17.7	82.3	82.3	-8.4	-47.4	-294.6
2013-03-04	jpk 62/12	1.8	13.6	86.4	86.4	-8.2	-43.4	-298.6

Table 8: *Results of stable carbon and hydrogen isotope composition of methane.*

Date	Borehole	Longwall face	Location	$\delta^{2}H_{CH4}$ (‰)	$\delta^{13}C_{CH4}$ (‰)
2012-02-21	JPK 48+11°	G3/C	North Preloge	-301.4	-46.7
2012-02-28	JPK 48+11°	G3/C	North Preloge	-304.1	-46.5
2012-03-28	JPK 48+11°	G3/C	North Preloge	-334.8	-34.8
2012-04-16	old works	K.-35 C	Pesje	-334.8	
2012-04-17	JPK 52+2°	K.-65/A	Pesje	-248.4	-64.7
2012-04-20	JPK 48+11°	G3/C	North Preloge	-321.9	-31.9
2012-05-16	old works	K.-35 C	Pesje	-348.8	
2012-07-05	JPK 52+2°	K.-65/A	Pesje	-264.4	-49.1
2012-07-17	old works	K.-35 C	Pesje	-336.4	-43.7
2012-08-30	JPK 49+2°	K.-130/B	South Preloge	-358.5	-25.7
2012-09-07	old works	K.-35 C	Pesje	-336.5	-50.4
2012-09-12	JPK 49+2°	K.-130/B	South Preloge	-356.3	
2012-09-16	JPK 49+2°	K.-130/B	South Preloge	-303.5	-52.5
2012-09-18	JPK 49+2°	K.-130/B	South Preloge	-302.4	-41.7

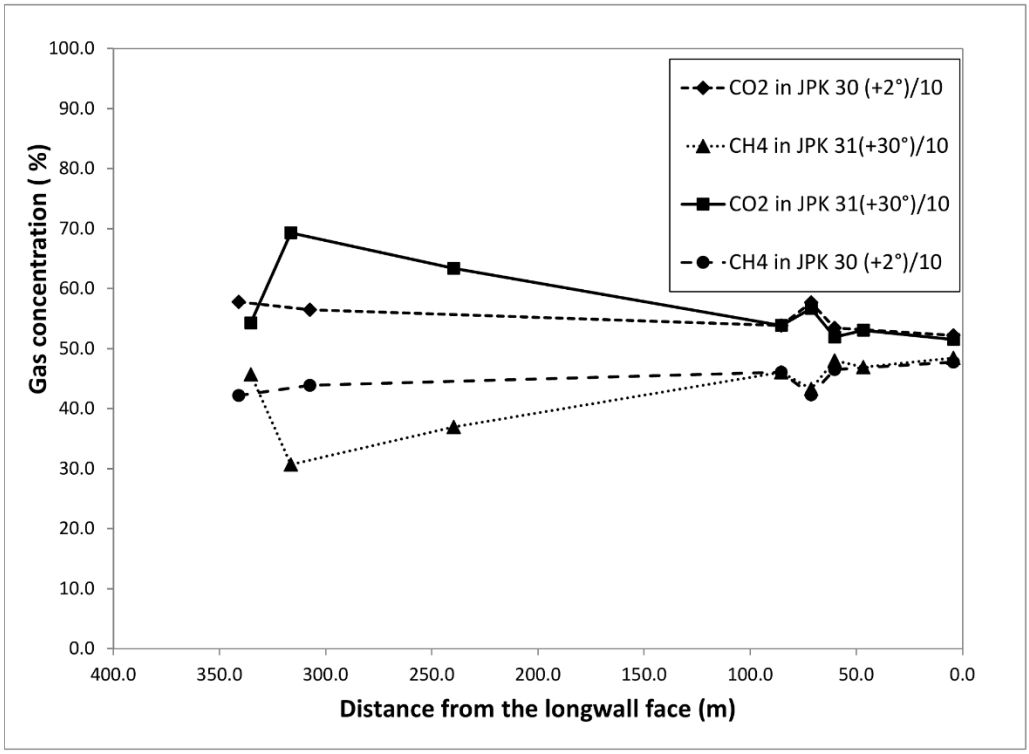


Figure 47: *Distribution of gas concentration as the longwall face advances at longwall G2/C in North Preloge mining district.*

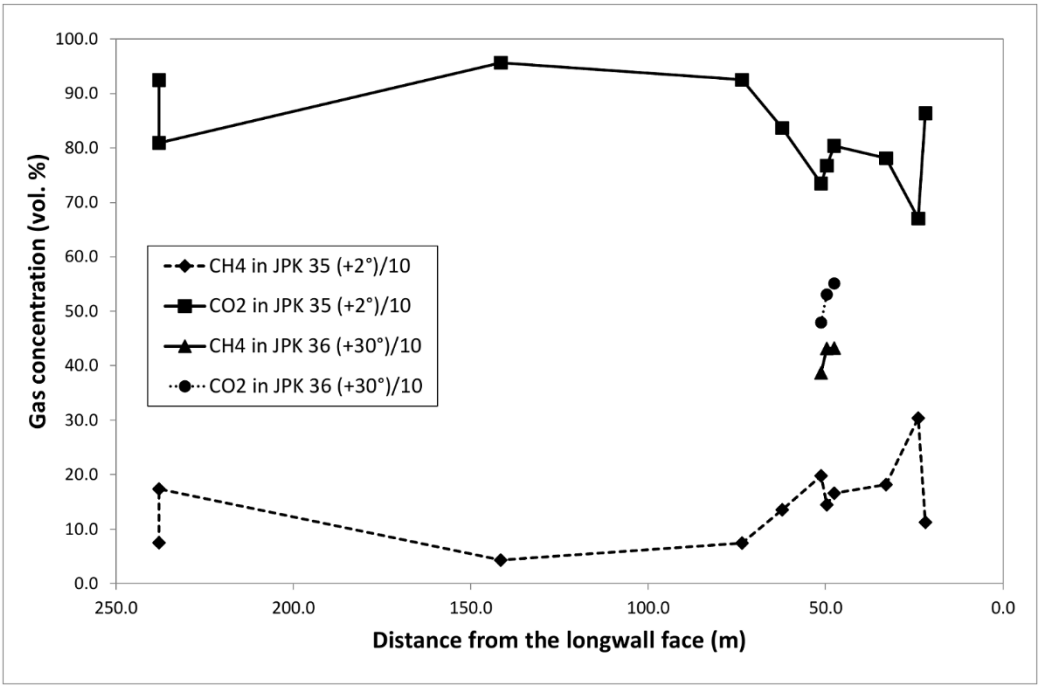


Figure 48: *Distribution of gas concentration as the longwall face advances at longwall K.-130/A in South Preloge mining district.*

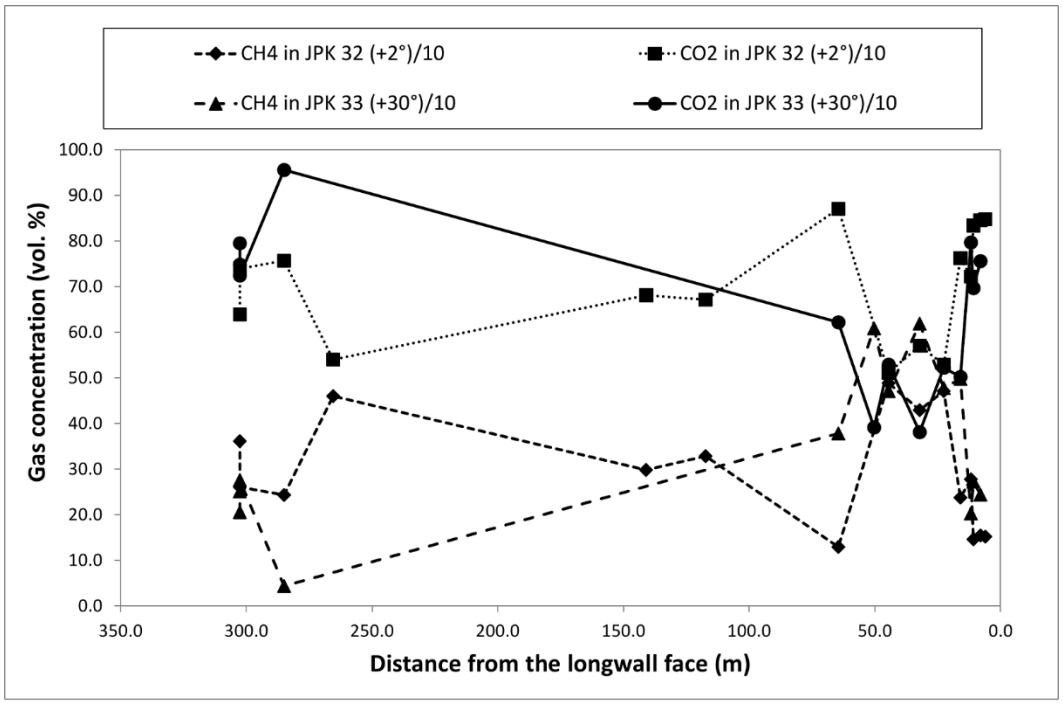


Figure 49: *Distribution of gas concentration as the longwall face advances at longwall K.-50/C in Pesje mining district.*

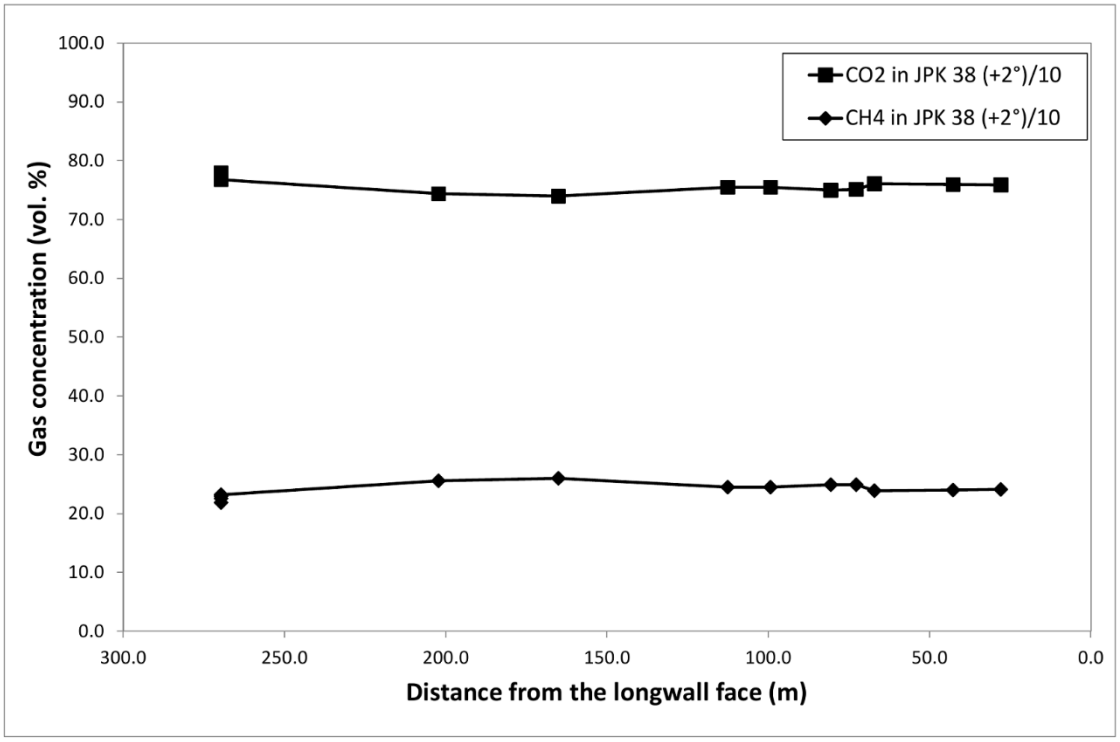


Figure 50: *Distribution of gas concentration as the longwall face advances at longwall K. -5/A in Pesje mining district.*

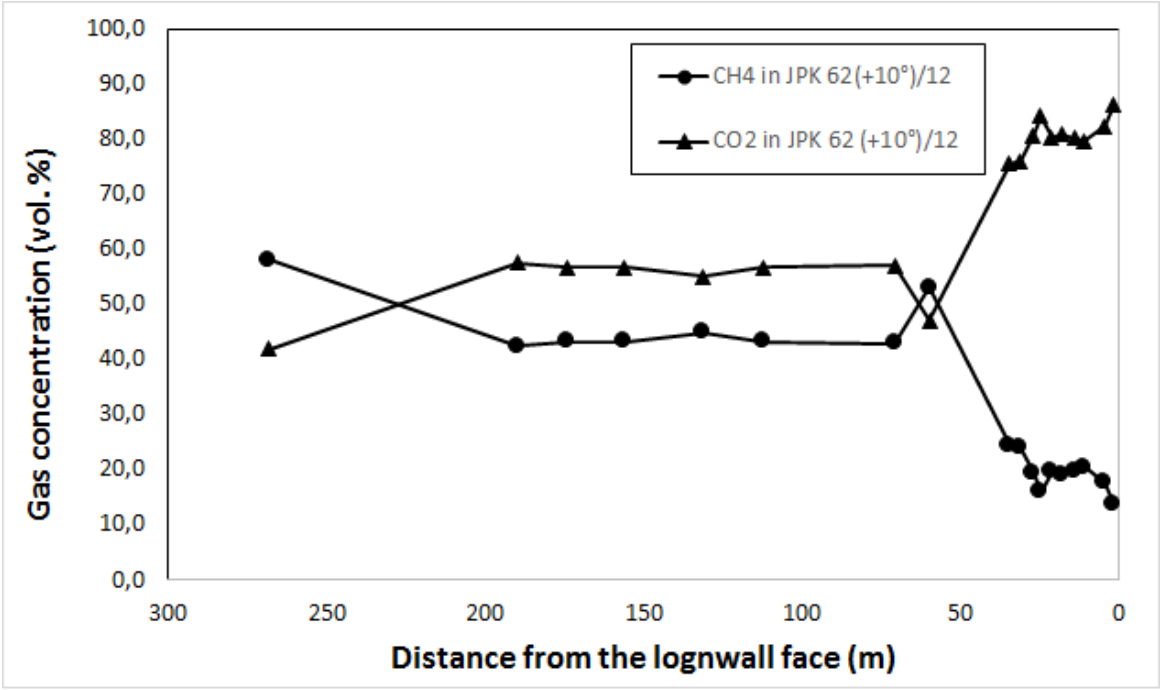


Figure 51: *Distribution of gas concentration as the longwall face advances at longwall K.-65/F in North Preloge mining district.*

De-stressing of the coal pillar due to the release of dynamic stresses occurs at a distance of 100 to 75 m in front of the borehole as the approaching longwall face begins to affects the coal gas content. During excavation, secondary fissures result from the rearrangement of the primary stress conditions, releasing the gas preserved in pores of the coalbed reservoir (Kanduč et al., 2011). At 120 m from the working face vertical stresses increase, while at 120 to 100 m the lignite structure begins to collapse. Methane migrates first due to its smaller molecular size and because it is free within the fractures (Clayton, 1998). Also, in comparison to methane, carbon dioxide is preferentially adsorbed in the coal structure (Mazumder et al., 2006), therefore it can migrate as the stress in the coal structure changes. At 30 to 50 m from the geotechnical measurement points the vertical stresses are so high that the lignite structure collapses (Zavšek, 2004). Finally when the longwall face is in close proximity to the borehole (30 to 50 m), methane migrates from the seam, and stresses reach their maximum values resulting in a release of carbon dioxide. An example of this phenomenon is shown in Figure 49 for the longwall excavation field K.-50/C. The coalbed gas concentrations at the longwall excavation field K. -50/C varied greatly compared with boreholes JPK 32 (+2°)/10 and JPK 33 (+30°)/10, where CO_2 ranged from 51.1 to 87.1 vol. %, and CH_4 from 12.9 to 48.9 vol. % in the case of JPK 32 (+2°)/10, and CO_2 varied from 38.1 to 95.6 vol. %, and CH_4 from 4.4 to 61.9 vol. % in the case of JPK 33 (Figure 49). The boreholes were drilled at the same location in the coal pillar but with different inclinations. Figure 49 shows how methane migrated first in JPK 33 (+30°)/10 because the pressure wave in front of the longwall face reached the zone in the roof around the borehole before the horizontal zone in front of the longwall face at a distance of 50 m. Thus, initial stress conditions in the coal were exceeded causing failure of its structure. Carbon dioxide started to migrate 10 m in front of the face where peak stress values are usually observed in geotechnical monitoring. The rate of advance of the longwall faces at the studied locations varied from 2.1 m/d to 4.2 m/d, and influenced the gas content in the coal seam. When the rate of advancement is high, higher stresses occur in the coal panel and in the surrounding strata, which influences the structure of the coal. New fissures and joints are opened due to longwall face operation. Adsorbed CO_2 under pressure in the coal matrix only migrates

when the structure of the coal is disturbed by the dynamic forces of the advancing coal face.

Gas composition at the longwall panel K.-5/A in Pesje mining district (Figure 50) did not significantly change during monitoring and the CO_2 values remained high. This can be explained by the position of the longwall panel, which was in the bottom part of the seam, where many longwall panels above had been mined. Alternatively, the longwall panel K.-65/F was located under intact overburden and the expectation of a high methane gas concentration was correct (Figure 51). The methane content varied from 13.6 to 58.1 vol. % and the influence of the longwall panel began at 70 m.

To interpret the methane content, Whiticar et al.'s, (1986) $\alpha^{13}C_{CO2\text{-}CH4}$ factor was adopted, and is represented by lines of equal carbon isotope fractionation (αc) between methane and carbon dioxide with values varying from α_c = 1.04 to 1.09 according to Equation 9. Gas samples with $\alpha_{CO2\text{-}CH4}$ values > 1.06 are typically representative of a methanogenic environment dominated by CO_2 reduction, while $\alpha_{CO2\text{-}CH4}$ values < 1.06 are characteristic of acetate fermentation (Whiticar et al., 1986; Whiticar, 1999). Results for both indices (α_c and CDMI), for all the fields investigated, are presented in Tables 2-7. The gas content from different excavation fields of the Velenje coal seam varied in their CDMI index from 38.1 to 95.7 %. In the North Preloge mining area at the longwall panel G2/C, the CDMI index value is around 50 %, and the $\alpha^{13}C_{CO2\text{-}CH4}$ value was mostly below 1.06 (Table 2). At K.-65/F the CDMI index varied from 41.9 % at the beginning to 86.4 % at the end of the sampling period (Table 7). In the Pesje area the CDMI index was higher, ranging from 38.1 to 96.6 % at K.-50/C and from 74.0 to 78.1 % at K.-5/A (on average 67.9 % at K.-50/C and 75.9 % in K.-5/A) than in the North Preloge sites (Tables 3, 4 and 6). The highest long-term concentrations of CO_2 were found at the South Preloge site at the longwall face K.-130/A (located at the deepest level, -536 m) from 56.0 up to 95.7 % (Table 5). Also, microbial CH_4 has a wide range of C and H isotope ratios, varying in $\delta^{13}C_{CH4}$ from -110 ‰ to -50 ‰, and in $\delta^{2}H_{CH4}$ from -400 to -150 ‰ (Whiticar, 1999), which was found in 13 samples from total 28 measured for both isotope ratios (Table 7, 8).

The likely sources of CO_2 in coal depend on its burial and uplift history and may include dissolved CO_2 from the atmosphere and soil gas, microbial degradation of organic substrates, thermal maturation of kerogen, thermal decomposition of carbonates and magmatic/mantle degassing (Dai et al., 1996; Wycherley et al., 1999, Golding et al., 2013).

To determine the origin of the CO_2 in the Velenje Basin, CDMI index versus $\delta^{13}C_{CO2}$ charts were prepared for the four distinct excavation fields (Figures 52, 53, 54, 55 and 56). At all of the four fields the high CDMI index values and $\delta^{13}C_{CO2}$ values between -7 to +5.5 ‰ indicate endogenic CO_2 and microbial CO_2 (a CO_2 reduction process which enriches residual CO_2 with the heavier ^{13}C isotope). Values of $\delta^{13}C_{CO2}$ from -6.6 to 1.8 ‰ in the area of longwall face G2/C in the North Preloge mining district (Figure 52) indicate that the CO_2 originates from thermal decomposition of dolomites and from microbial CO_2 reduction at the bottom of the basin. Figure 53 shows that the origin of CO_2 in the South Preloge mining district (K. -130/A) is endogenic and mixed with microbial CO_2, having values of $\delta^{13}C_{CO2}$ of -8.9 to 5.5 ‰ and CDMI index values up to 95.7 %. In the Pesje mining district it is most likely that CO_2 is of mixed origin, i.e. endogenic with a mixture of microbially reduced CO_2 and CO_2 from acetate fermentation, having values of -11.0‰ (Figure 54 and 55). The similar interpretation of the results can be seen in Figure 56 in the case of CSG measurements at longwall panel K.-65/F, where CO_2 in this area is likely to have mixed origin.

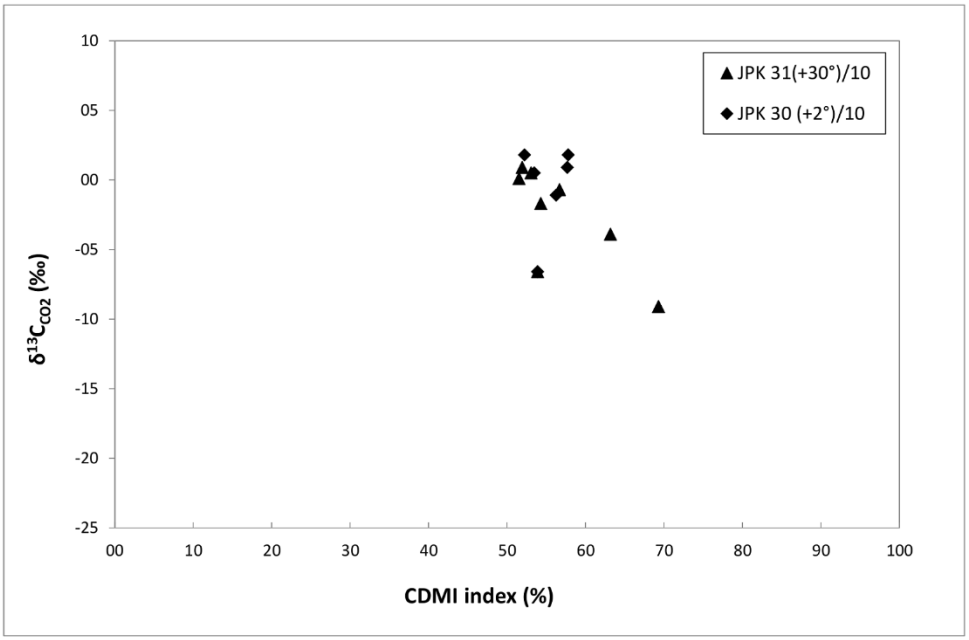


Figure 52: *Interpretation of the origin of CO_2 from the analysed coalbed gas samples from the Velenje Basin using the $\delta^{13}C_{CO2}$ versus CDMI index in the lignite seam ahead of the working face at the longwall face G2/C in the North Preloge mining district.*

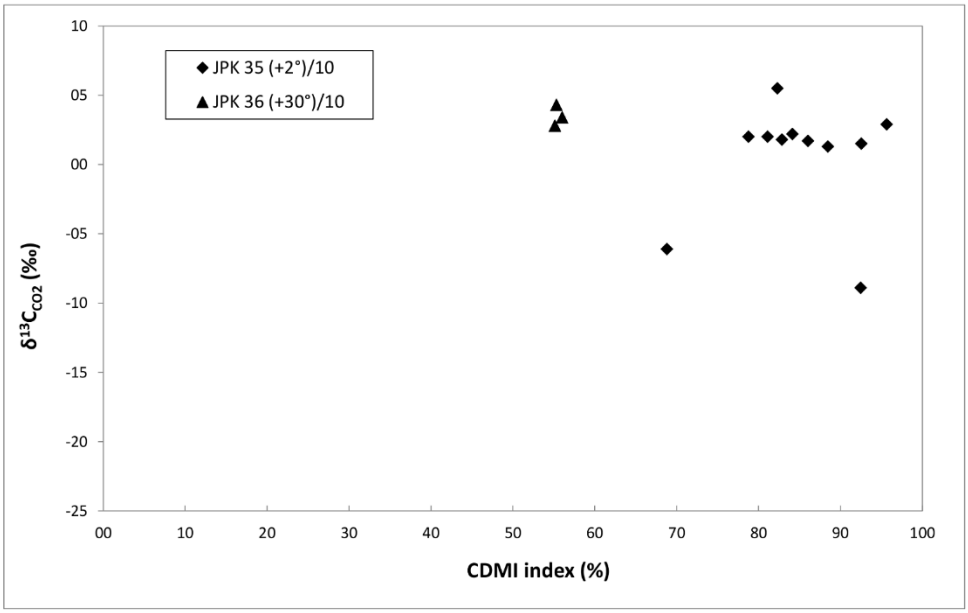


Figure 53: *Interpretation of the origin of CO_2 from the analysed coalbed gas samples from the Velenje Basin using the $\delta^{13}C_{CO2}$ versus CDMI index in the lignite seam ahead of the working face at the longwall face K.-130/A in the South Preloge mining district.*

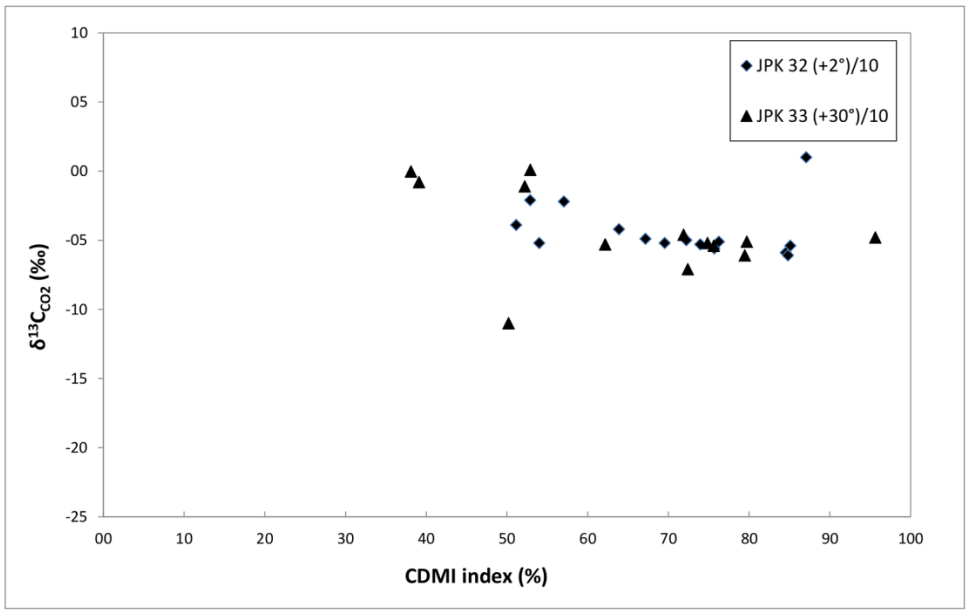


Figure 54: *Interpretation of the origin of CO_2 from the analysed coalbed gas samples from the Velenje Basin using the $\delta^{13}C_{CO2}$ versus CDMI index in the lignite seam ahead of the working face at the longwall face K.-50/C in the Pesje mining district.*

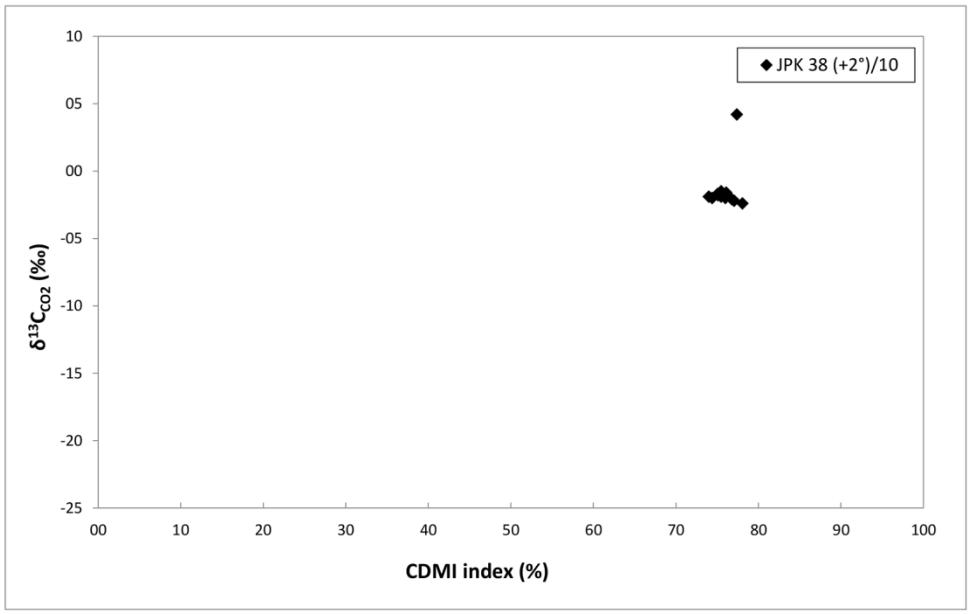


Figure 55: *Interpretation of the origin of CO_2 from the analysed coalbed gas samples from the Velenje Basin using the $\delta^{13}C_{CO2}$ versus CDMI index in the lignite seam ahead of the working face at K.-5/A in the Pesje mining district.*

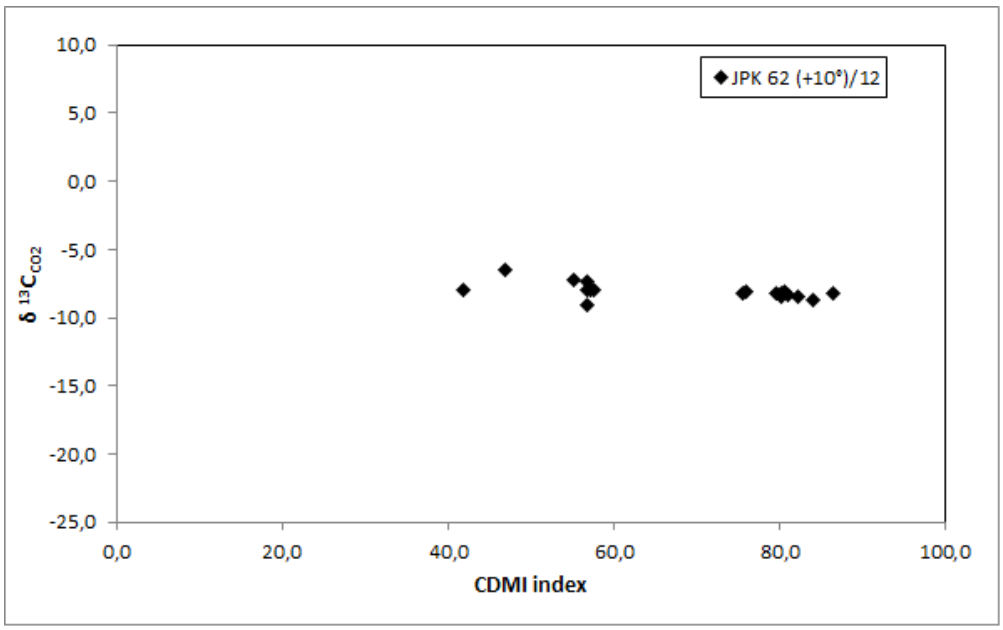


Figure 56: *Interpretation of the origin of CO_2 from the analysed coalbed gas samples from the Velenje Basin using the $\delta^{13}C_{CO2}$ versus CDMI index in the lignite seam ahead of the working face at K.-65/F in the North Preloge mining district.*

In total, 52 samples of methane could be interpreted as being of thermogenic origin from deeper geological formations ($\delta^{13}C_{CH4}$ between -50 ‰ and -20 ‰), which most likely migrated into the coal seam and then mixed with microbial coal gas (Tables 2 - 7).

Thermogenic methane could be generated in the Oligocene marine clays containing high concentrations of organic matter, which were overheated at a depth of over 2000 m, which then migrated through faults and fractures in the lignite strata when the Basin formed (Kanduč et al., 2012). Equally, it could also be a result of secondary processes resulting from mining activities.

4.5 Coal Seam Gas Drainage Trial Test

All research involving the coal seam gas behaviour was made with the purpose of investigating a possible trial of a longwall panel pre-drainage system. The first drainage trial test was established at the longwall panel K.-65/F in the Pesje mine district in 2013 (Figure 57).

4.5.1 Design of the Drainage System

The drainage pilot test was designed according to Slovenian mining regulations. Six boreholes of varying length and/or inclination were installed at the longwall panel K.-65/F. The coordinates, inclination and length of the drainage boreholes are presented in Table 9.

The drainage boreholes were drilled in following sequence (Jamnikar, 2015):

- Drilling for primary casing (∅ = 100 mm, re-drilled with ∅ = 180 mm; to a depth 10 m);
- Insertion of primary casing (∅ = 169 mm steel pipe; length 10 m; flange installed);
- Cementing between the primary casing and surrounding coal;
- Technical column drilling (∅ = 100 mm until the end of the borehole – 30 or 50 m);

- Insertion of the perforated antistatic plastic drainage tube with installed flange;
- Cementing between the primary casing and technical column;
- Borehole connection to the pipeline was via a rubber tube.

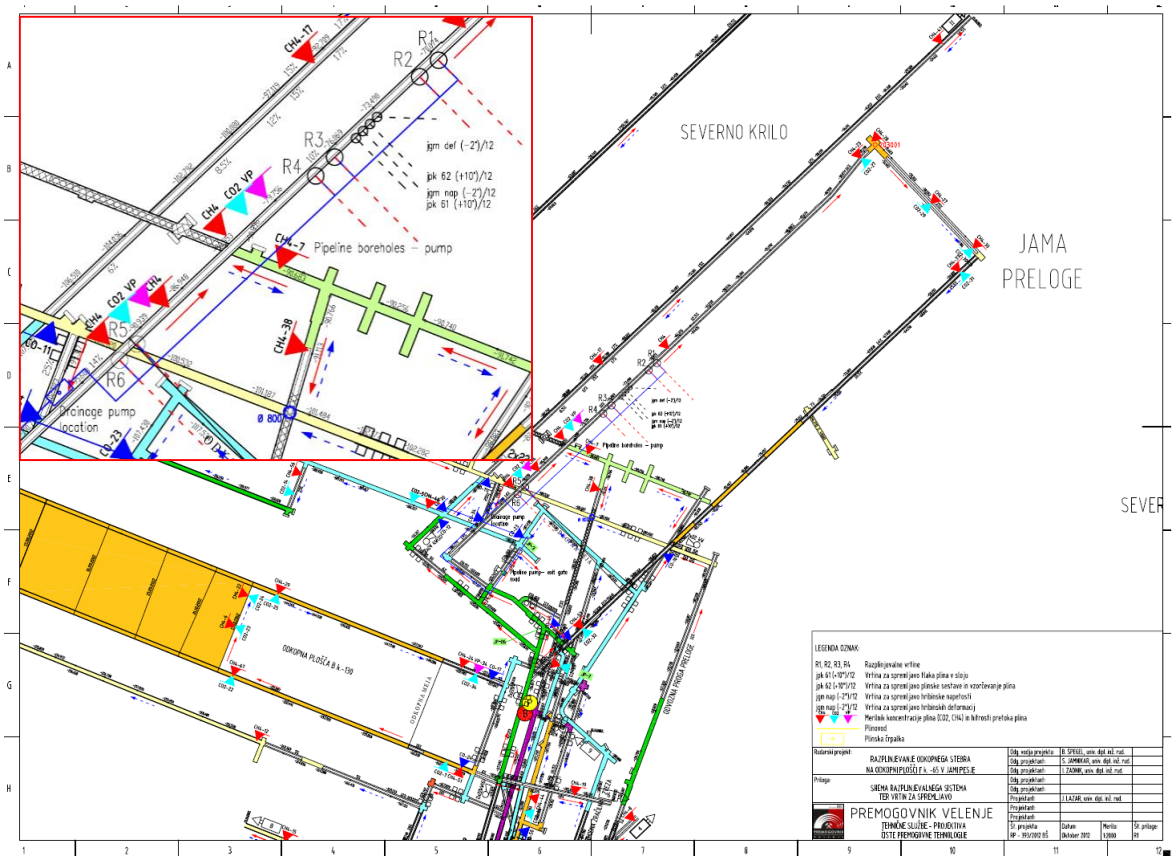


Figure 57: *Trial drainage system location at the longwall panel K.65/F in the Pesje Mine District.*

Table 9: *Drainage borehole parameters.*

Borehole name	Y	X	Z	Inclination (from horizontal)	Length (m)
R1 (+2°)/13	505821.7	137530.5	-72.5	2°	50
R2 (+20°)/13	505799.9	137509.9	-75.0	20°	30
R3 (+2°)/13	505766.0	137478.0	-81.2	2°	50
R4 (-30°)/13	505760.2	137472.6	-83.5	- 30°	30
R5 (+20°)/13	505719.3	137433.9	-90.2	20°	30
R6 (+2°)/13	505712.0	137427.1	-92.0	2°	50

All boreholes were equipped with gas pressure gauges for measuring the pressure inside the borehole (measuring range 0-16 bar) and with pressure sensors for on-line monitoring.

For trial test purposes, a Nash 2BE1 203 vacuum pump was used. The pump only had a certificate for surface industrial gas and petrol drainage use only. Thus all technical documents from for electrical and mechanical part was prepared and compiled together and stored in the certification office as a "Declaration of Safety". The pump was assembled

using a mine certified electric motor and mechanical clutch (Figure 58). Water was used as the working media for the vacuum pump.

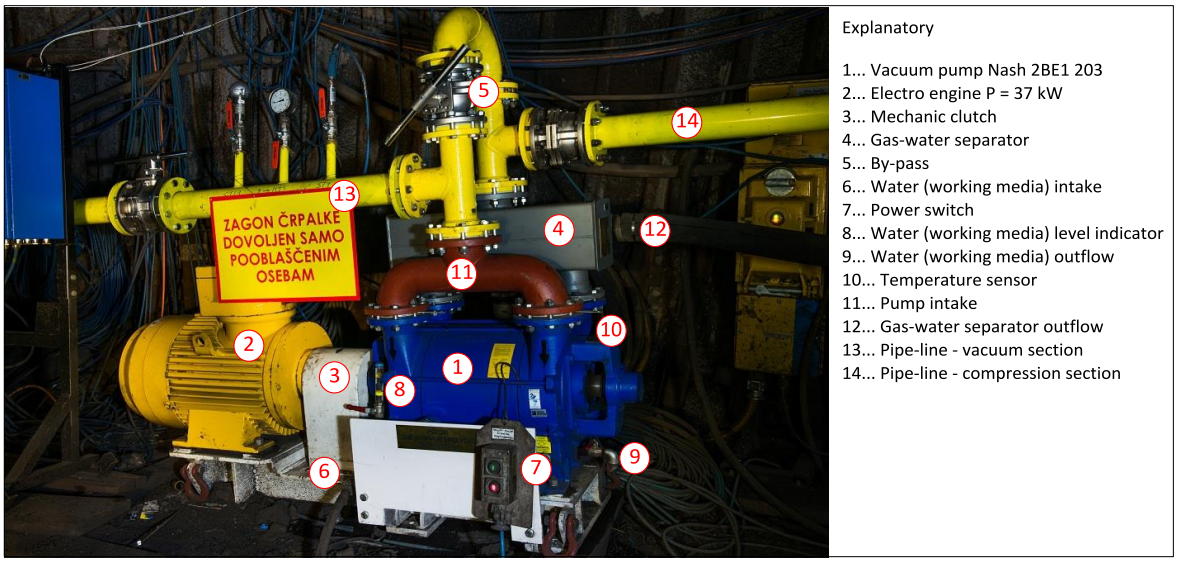


Figure 58: *The Nash 2BE1 203 drainage pump showing all elements* (Jamnikar, 2015).

The CO_2, CH_4, O_2 and CO gas sensors were installed on the pipeline before and after of the drainage pump (Figure 59). The suction pressure in the pipeline was monitored with a pressure sensor and pressure gauge. Temperature was also recorded (Figure 60).



Figure 59: *Drained gas concentration sensors (from left: CO_2 (0 – 100 %), CH_4 (0 – 100 %), CO (0 – 200 ppm)*). (Jamnikar, 2015)



Figure 60: *Drained gas pressure and temperature monitoring (from left: pressure sensor (-1 – 1 bar), pressure gauge (-1 – 5 bar), temperature sensor (0 - 100 ℃)* (Jamnikar, 2015).

4.5.2 Trial Test Procedure

The pilot drainage test was continually monitored. The drainage pump did not have a mine explosive certificate which meant that it was able to work only when the concentration of methane in the gate road was < 0.5 vol. %. It was also necessary to set the drainage pump operation according to the methane potential explosive range. This condition is fulfilled when the methane concentrations in the pipeline is between 4 - 16 vol. % and level of oxygen between 12 - 21.5 vol. %. If the gas composition in the pipeline falls inside these limits, the drainage pump will shut down automatically.

To protect the drainage pump from overheating, a temperature relay safety switch was installed and the limit of the working temperature of the pump was set to 65 °C. The drainage pump had also the required water flow between 50 to 70 l/min. Vacuum pressure was set from -200 to -300 mbar.

During the trial, gas sensors in the exit gate road were measured continuously to monitor the levels of CH_4 and CO_2 in the ventilated air along the whole pipeline, in case the methane concentration exceeded 1.5 vol. % and the CO_2 concentration exceeded 5 vol. %. In addition, the drainage capacity was measured in order that the methane concentration did not exceed 50 l/s i.e. the limit in the return ventilation air.

4.5.3 Summary of the Drainage Analysis

The trial drainage test involved draining gas from the first two boreholes, R1 (50 m, +2°) and R2 (30 m, +20°), with the aim of draining the CSG from the longwall panel and from the top coal area. Unfortunately, the advancing longwall face cut through R1 and R2 so that the boreholes R5 and R6 further along the longwall panel were used as a replacement. The borehole R3 served the same role as R2, and was successfully drilled to a length of 50 m. In total, eleven drainage campaigns were performed using R3 (Table 10).

Initially, the longwall face was 69.4 m away and up to 43.9 m it was not possible to drain gas, since the distance of the longwall face was too far to affect CSG migration. From 43.9 m to 4.5 m CSG drainage was successful. Time periods of the drainage activations varied, from tens of seconds to a maximum of three hours and 38 min.

The results (Table 10) show a drop in the concentration of methane as the longwall advanced towards the borehole. Carbon dioxide is the major gaseous CSG component (from 22 vol. % to 46.39 vol. %) with a CO_2:CH_4 ratio of 2:1. Drainage gas flow rates varied from 141.59 m^3/h to 205.34 m^3/h, with the highest gas flow recorded at a distance

of 22 m from the longwall face.

The borehole R4 was 30 m in length with an inclination of -30° and covered the floor area of the longwall panel. This time, 8 drainage campaigns were conducted using R4 as the distance to the longwall face decreased from 39.7 to 7.9 m. The results show (Table 11) that in R4 unlike in R3, the gas concentration remains constant as the longwall face approaches. In addition, the drainage campaigns were shorter, on average 24 min with the longest lasting 1 hour and 48 min. The maximum total flow was 193.0 m^3/min and the average CH_4 and CO_2 flow rate was 27.6 and 57.0 m^3/h, respectively.

This difference between the drainage capacities of R3 and R4 is related to the different characteristics of the areas being drained. For instance, borehole R4 was drilled into the floor of the coal panel where the geomechanical conditions are different than directly adjacent to the longwall face.

Overall, the gas drainage trials from R5 and R6 gave poor results with all of the campaigns only lasting a few seconds before the drainage pump stopped working. Table 12 presents the data for the only successful drainage test from R5, which was performed at 24 m in front of the longwall face.

The task of the geomechanical model, which fits the drainage location, is to represent the stress behaviour in the longwall panel, in the floor of the panel and in the top coal at different distances from the longwall face. These changes in the stresses in the surrounding coal around the longwall face explains the changes in permeability, i.e., the development of new fractures means that CSG can migrate and as consequence gas drainage is effective.

Table 10: *Drainage results from borehole R3* (Jamnikar, 2015).

Date	Distance (m)	CH_4 (vol. %)	CO_2 (vol. %)	Air (vol. %)	Pressure (bar)	Total flow (m^3/h)	Flow CH_4 (m^3/h)	Flow CO_2 (m^3/h)	Duration
27.2.2013	69.4	35.0	22.0	43.0					
11.3.2013	47.2	37.0	24.0	39.0					
15.3.2013	43.9	37.0	24.0	39.0					
20.3.2013 (1)	31.8	20.7	43.2	36.0	-0.28	186.0	38.5	80.4	0:00:40
20.3.2013 (2)	31.8	17.34	43.8	38.8	-0.29	175.6	30.5	76.9	0:10:50
23.3.2013	31.0	20.0	37.6	42.4	-0.28	188.9	37.0	70.0	0:09:50
25.3.2013	29.0	19.4	44.6	35.9	-0.21	142.4	27.6	63.5	0:40:30
27.3.2013	22.0	19.7	46.4	34.0	-0.20	205.4	40.4	95.2	0:30:40
29.3.2013	20.0	20.2	46.4	33.4	-0.24	181.3	36.6	84.1	0:19:40
2.4.2013	14.0	14.5	44.2	41.3	-0.20	185.2	270	81.9	1:48:50
3.4.2013	12.0	18.8	45.9	35.3	-0.21	193.0	35.2	88.7	0:30:20
5.4.2013	8.0	16.9	44.9	38.2	-0.20	141.6	24.0	63.4	3:38:50
8.4.2013	4.5	2.30	5.8	91.9		50	1.1	2.9	0:03:00

Table 11: *Drainage results from the borehole R4* (Jamnikar 2015).

Date	Distance (m)	CH_4 (vol. %)	CO_2 (vol. %)	Air (vol. %)	Pressure (bar)	Total flow (m^3/h)	Flow CH_4 (m^3/h)	Flow CO_2 (m^3/h)	Duration
20.3.2013	39.7	19.2	42.2	38.6	-0.32	131.4	25.0	55.2	0:11:30
27.3.2013	29.9	20.2	41.7	38.1	-0.23	153.3	30.8	63.8	0:29:40
29.3.2013	27.9	21.9	44.6	33.5	-0.20	149.0	32.7	6.4	0:20:20
2.4.2013(1)	21.9	20.0	37.0	43.0	-0.24	167.8	33.5	62.0	0:16:40
2.4.2013(2)	21.9	17.2	37.0	45.8	-0.19	165.0	28.5	61.0	0:29:40
3.4.2013	19.9	18.6	36.9	44.5	-0.22	173.0	32.3	63.9	0:35:10
5.4.2013	15.9	18.3	37.7	43.9	-0.23	154.6	28.0	58.0	0:27:30
8.4.2013	12.4	20.2	41.4	38.4	-0.17	139.8	28.3	58.0	0:36:10
10.4.2013	7.92	14.8	41.4	43.8	0	60.3	8.9	25.0	0:15:00

Table 12: *Result of gas drainage from borehole R5* (Jamnikar, 2015).

Date	Distance (m)	CH_4 (vol. %)	CO_2 (vol. %)	Air (vol. %)		Pressure (bar)	Total flow (m3/h)	Flow CH_4 (m3/h)	Flow CO_2 (m3/h)	Duration
8.5.2013	24	36.6	22.2	39.2	-0.19	50	19.3	11.1		0:09:50

4.6 Conclusions

The data from different field monitoring campaigns were analysed with the aim of understanding better the geomechanical and geochemical behaviour of the coal and the coal seam gas around the LTCC faces.

Active seismic tomography was used in two different longwall panels (longwall panel K.-50/C and longwall panel K.-130/B) in order to locate the different lithotype structures in the panels, to confirm the presence of faults, and to detect stress abutment zones. Active tomography proved to be very effective in locating potentially dangerous faults in the coal seam. When combined with the knowledge of average gas content of the different lithotypes, the method is a very useful tool for risk assessment for the longwall panel prior to being excavated. This was clearly demonstrated at K.-50/C, where high P-wave velocities were typical for xylitic coal and acted as a gas barrier in front of a high gas content detritic coal zone. In the case of Velenje Coal Mine, this methodology can be implemented to help gas drainage design.

From 2010 onwards, the CSG pressure measurements performed at the Velenje Coal Mine provided a new perspective on CSG distribution, migration and their relationship with the active mining process. Over the years, improvements in the design of pressure monitoring boreholes helped to seal them properly and produce valuable data. Normally, CSG pressure increases with seam depth but, in contrast, the data reveals that the highest CSG pressures existed at the first mining level situated under fresh overburden. High CSG pressure in the upper mining levels also results in high gas content and, therefore, interruption of the production and development work at longwall faces and the gate roads.

The CSG compositional and isotopic data revealed that gas composition changes significantly throughout the seam. New methods of gas sampling, where gas samples are not contaminated with mine air were developed. Also, deuterium isotopic composition measurements were reported for the first, which helps explain the origin of the methane. With more than 80 pressure and gas composition monitoring boreholes drilled in different longwall panels at different depths, the mine now is able to predict the CSG composition very accurately. Within the first mining levels, under fresh overburden it is now known that the methane content is the highest, although on average the CO_2 concentration is still higher.

The most important effects of longwall panel advance and production is the stress abutment created in front of the longwall face, which causes fractures and deformations in the coal. This effect was also observed as an increase in the CSG pressure at the same distance to the face as the stress abutment. Also, the CO_2 and methane composition in the monitoring boreholes followed a similar pattern i.e., as the longwall face approaches to the boreholes, methane migrates within the coal structure and, with the opening of the fracture system, CO_2 is released from the coal structure with some delay.

The pilot drainage system revealed that the inclination and length of the boreholes play an important role in drainage efficiency. These first trials have also shown that longer boreholes (more than 70 m) should be used in the drainage system and cover more than half of the longwall panel width with boreholes drilled from one gate road in order to improve drainage efficiency.

5 Development of Geomechanical Model of Advanced Longwall Face using FLAC^{3D}

5.1 Introduction

FLAC^{3D} is a three-dimensional explicit finite-difference program for engineering mechanics computations, simulating the behaviour of three-dimensional structures built of soil, rock or other materials (Helm, 2011). Mechanical structures modelled in FLAC^{3D} are presented in the form of a mesh or grid with a series of elements or zones. Materials are defined by polyhedral elements within a three-dimensional grid, where the material can yield and flow and the grid can deform and move with the material (Itasca, 2005). In order to setup and run a model in FLAC it is necessary to specify three main components (Helm, 2011):

1. the finite difference grid;
2. constitutive models and material properties;
3. boundary and initial conditions.

Figure 61 shows the distribution of vertical stress around the longwall face. This is one of the examples of stress distribution calculation using FLAC^{3D} in Velenje Coal Mine. The vertical stress reaches zero at the face and at the gate roads (Likar et. al., 2006). In the cross-section A-A the highest vertical stress are observed directly in front of the longwall face.

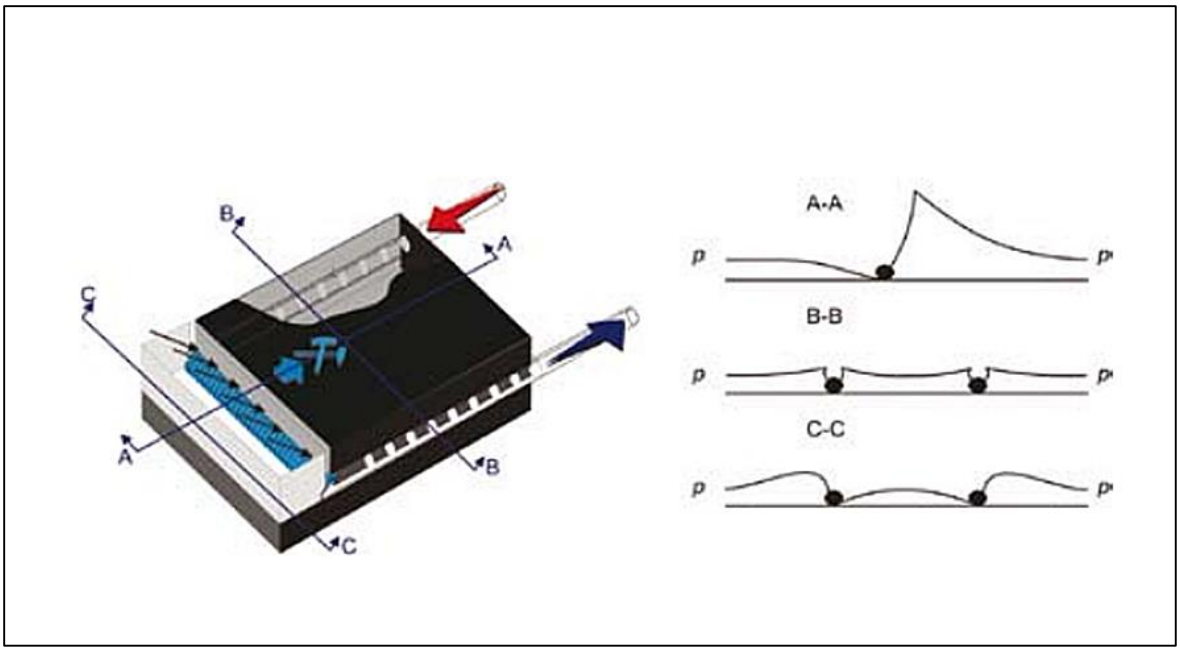


Figure 61: *The distribution of vertical stress around the longwall face* (Likar et. al, 2006).

Geomechanical modelling comprises a number of steps to complete the simulation. The flowchart in Figure 62 shows the basic features of the algorithm and its implementation using rock mass properties derived in the laboratory (Board & Pierce, 2009). Geotechnical data for geomechanical modelling should be taken from a large geotechnical database in

order to have representative data for the coal seam and surrounding strata. Geotechnical data includes:

- **Geology**
  - Lithology of the coal basin;
  - Geometry of the coal basin;
  - Major fault system and shear zones;
- **Geotechnical core logging**
  - Detailed lithology of cores;
  - Percentage of crushed core;
  - Core samples used for laboratory tests;
- **Laboratory testing**
  - Uniaxial and triaxial compressive tests;
  - Tensile strength tests.
- ***In-situ* stress state**.

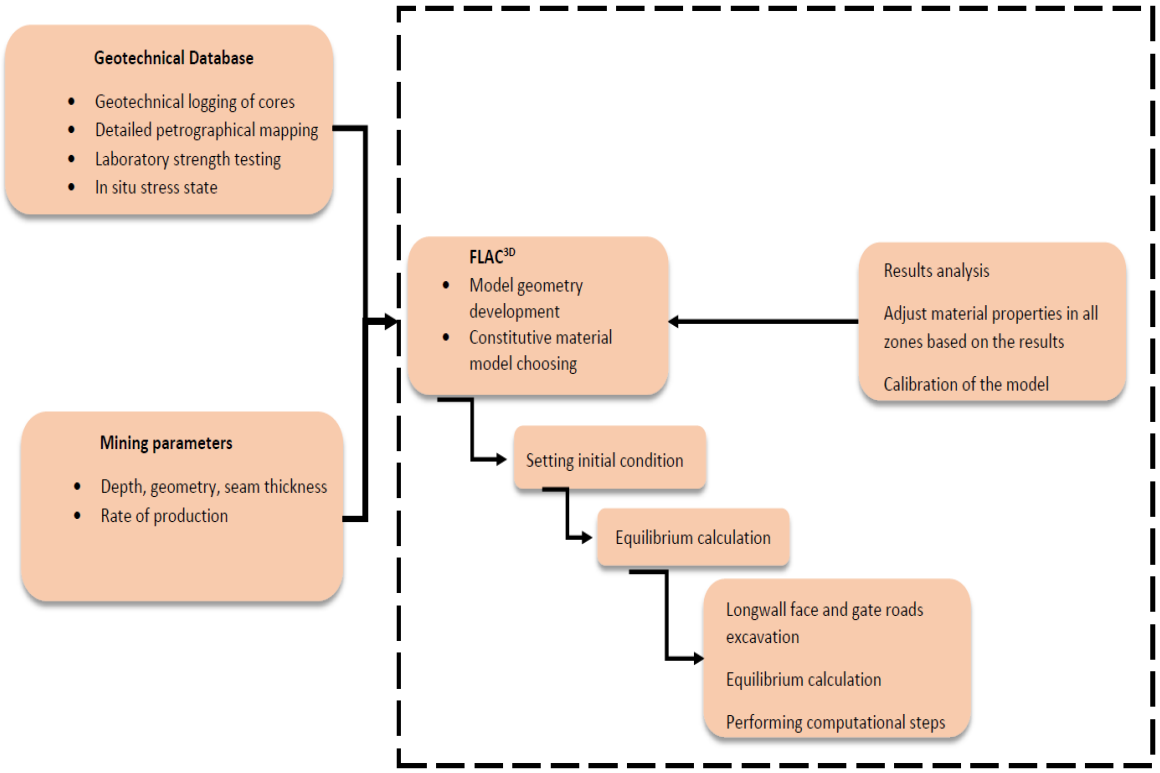


Figure 62: *Flac^{3D} modelling steps flowchart* (modified after Board & Peirce, 2009).

5.2 Grid Generation

Grid generation is used to describe the modelled geometry. During grid generation the properties of different materials is defined using an assigned constitutive model.

5.3 Boundary and Initial Conditions

The boundary conditions consist of imposed boundary tractions and/or velocities (to induce given displacements) (Itasca, 2005). Boundary conditions in the model can be either fixed or dynamic.

5.4 Constitutive Models

In Flac^{3D} there are many basic constitutive models. One of the model groups is the **Null model group** (Itasca, 2005). The second model group is the elastic model group, which is not typically used in mining. The elastic model group includes the elastic isotropic model and the elastic anisotropic model, which is divided in to the orthotropic and transversely isotropic models. The third model group usually used in geotechnology and mining is the plastic model group. These model groups include many different constitutive models. In this chapter all of the plastic models will be briefly presented, after which the most important plastic constitutive models will be described in detail, which includes the following:

- **Drucker-Prager Model**;
  The failure envelope uses a Drucker-Prager criteria with tension cut-off.
- **Mohr-Coulomb Model**;
  The Mohr-Coulomb model is used to represent shear failure in soils and rocks.
- **Ubiquitos-Joint Model**
  The model is a composition of Mohr-Coulomb envelope with tension cut-off.
- **Strain-hardening/softening Model**;
  The strain-hardening/softening model allows a representation of nonlinear material softening and hardening behaviour based on prescribed variations of the Mohr-Coulomb model (Itasca, 2005).
- **Modified Cam-Clay Model**
  This model is an incremental hardening/softening elastoplastic model (Itasca, 2005).
- **Hoek-Brown Model**;
  The Hoek-Brown model is represented as a failure criterion, which characterizes the stress conditions when an intact rock fails.

The failure criterion of plastic flow in FLAC^{3D} is represented by Equation 10:

$$f(\sigma_n) = 0 \tag{10}$$

Where the yield function (*f*) is a known function that specifies the limiting stress combination when plastic flow takes place (Itasca, 2005) and σ_n is referred to generalized stress component from *i=1* to *i=n*.

5.4.1 The Null Model

A null material model is used to represent a material in the model that has been either removed or excavated. The stresses within the null zone are automatically set to zero (Itasca, 2005) by Equation 11:

$$\sigma_{i\,j}^{N} = 0 \tag{11}$$

When modelling backfilling or consolidation, the null models can be replaced with a different material model during later stages in the simulation.

5.4.2 The Mohr-Coulomb Model

To represent the Mohr-Coulomb criterion, a failure envelope is used corresponding to the shear yield function with a tension yield function. The failure criterion consists of normal stresses and shear stresses. The Mohr-Coulomb failure criterion in Flac^{3D} is expressed

(Equation 12) in terms of the principal stresses σ_1, σ_2 and σ_3 (Itasca, 2005), where:

$$\sigma_1 \leq \sigma_2 \leq \sigma_3 \tag{12}$$

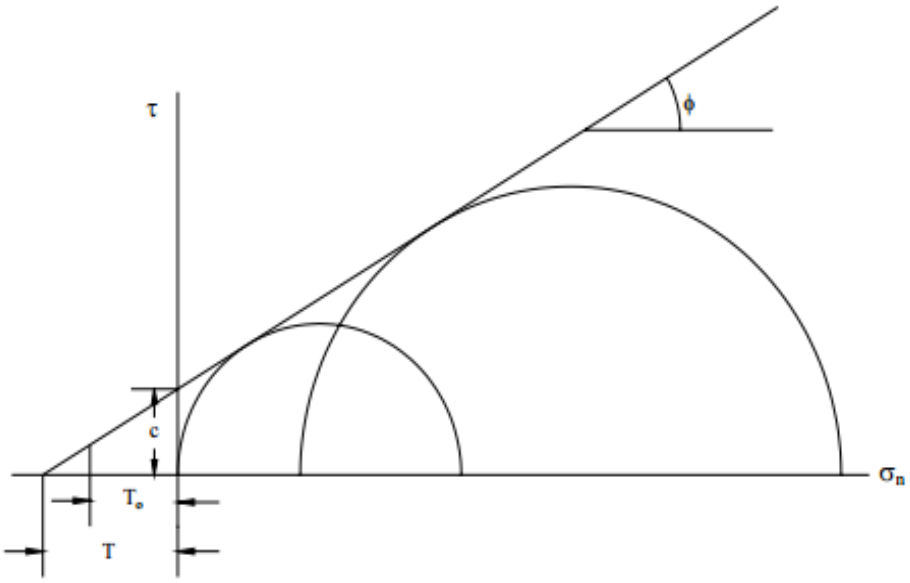


Figure 63: *Mohr-Coulomb Failure Criteria* (Burke, 2003).

Figure 63 represents typical Mohr-Coulomb failure envelopes with principle stresses σ_1, σ_2 and σ_3. In addition to the critical stresses, the angle of internal friction ϕ is also shown. Cohesion is represented by *c* and the tensile strength is labelled *T*. A tensile limit T0 is used when the tensile strength of the material is lower than the strength defined by the failure criterion (Burke, 2003). This parameters σ_1, σ_3 and maximum shear stress can be calculated using the following three equations:

$$\sigma_3 = \frac{\sigma_x+\sigma_y}{2} + \tau_{max} \tag{13}$$

$$\sigma_1 = \frac{\sigma_x+\sigma_y}{2} - \tau_{max} \tag{14}$$

$$\tau_{max} = \sqrt{\tau_{xy}^2 + (\frac{\sigma_y-\sigma_x}{2})^2} \tag{15}$$

5.4.3 The Strain-Hardening/Softening Mohr-Coulomb Model

This model uses the Mohr-Coulomb model as its base. Mohr-Coulomb properties become a function of plastic strain. Some variations do exist between these two models including cohesion, friction, dilation and tensile strength that can either harden or soften after plastic yield commences. In the Mohr-Coulomb model these properties are assumed to be constant (Itasca, 2005). The Strain-Hardening/Softening model allows the properties of cohesion, friction and dilatation to be defined as linear functions.

Flac^{3D} uses hardening and softening behaviours for determining cohesion, friction and dilation in terms of the shear parameter $\Delta\varepsilon^{ps}$ in the form of tables. Each table consists of pairs of values: one for the parameter and one for the corresponding value. These functions can be drawn as in Figure 64, where FLAC uses approximated values as sets of linear segments in place of real variations (Figure 65).

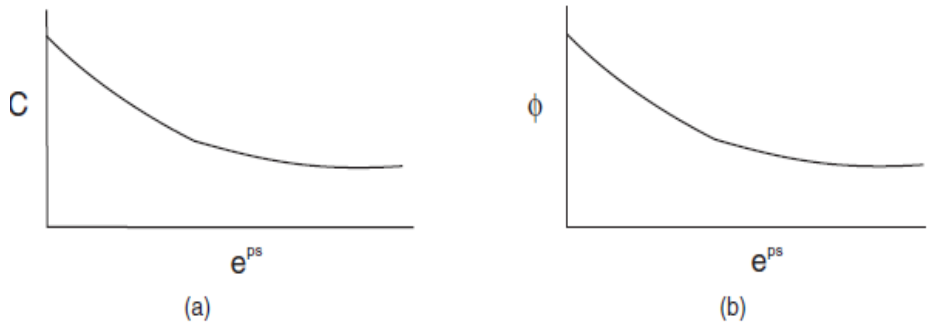


Figure 64: *Variation of cohesion (a) and friction angle (b) with plastic* strain (modified from Itasca, 2005).

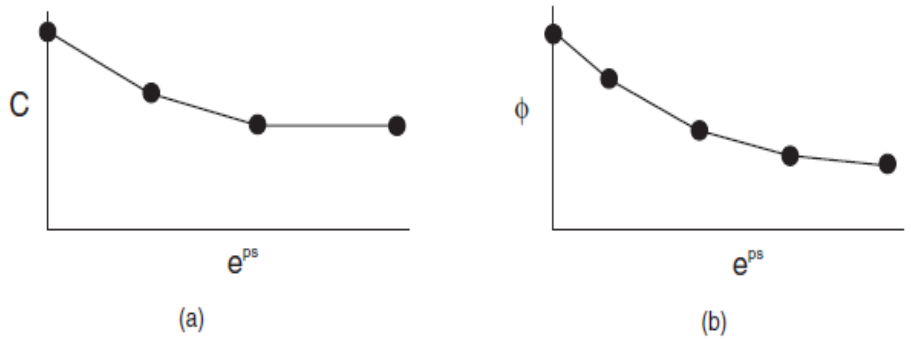


Figure 65: *Approximation by linear segments* (modified by Itasca, 2005).

5.4.4 The Hoek-Brown Model

The Hoek-Brown failure criterion is an empirically derived relationship used to describe a non-linear increase in peak strength of isotropic rock with increasing confining stress (Eberhardt, 2012). Also, it is an empirical relationship that characterizes the stress conditions leading to failure in intact rock and rock masses (Itasca, 2005). One way to assess the mean and range of rock mass strength parameters is the use of the standard Hoek-Brown methodology (Board & Pierce, 2009). Laboratory compressive strength tests give uniaxial compressive strength (UCS). The M_i values and rock mass quality (GSI) are usually hard to determine for coal, therefore these two parameters are just estimations in the model. The generalized non-linear Hoek-Brown criterion for intact rock (Hoek and Brown, 1980) is defined as (Equation 16):

$$\sigma_1 = \sigma_3 + \sigma_{ci}\left\{m_b \frac{\sigma_3}{\sigma_{ci}} + s\right\}^a \tag{16}$$

Where σ_1 and σ_3 are the major and minor effective principal stresses, and σ_{ci}, m_b, s and a are material constants that can be related to the Geological Strength Index (GSI) and rock damage (Hoek et al., 2002). The constant σ_{ci}, is the uniaxial compressive strength of the intact rock material. The parameter m_b is analogous to the frictional strength of the rock and s (Equation 17) represent a factor of how fractured the rock is, and is related to rock mass cohesion (Eberhardt, 2012). The constant m_b is a reduced value of the material constant m_i (Equation 18).

$$s = exp\left[\frac{GSI-100}{9-3D}\right] \tag{17}$$

$$m_b = m_i exp\left[\frac{GSI-100}{28-14D}\right] \tag{18}$$

$$a = \frac{1}{2} + \frac{1}{6}\left[e^{-GSI/15} - e^{-20/3}\right] \quad (19)$$

where m_i is a material constant of the intact rock, *GSI* is the Geological Strength Index, which is estimated from the chart of Marinos et al. (2005), and *D* is a disturbance factor, which depends on how much of the rock is damaged due to blasting. The disturbance factor can vary from 0 for undisturbed in situ rocks to 1 for highly damaged rocks.

5.5 Geomechanical Model of Longwall Panel K.-65/F in the Pesje Mine District

The longwall panel K.-65/F (140 m wide and 471 m in length) was operating entirely under fresh overburden under two regimes of production. For the first 255 m, the coal was extracted (thickness 5 m) at an average advance rate of 4 m/day, while the remaining 216 m of the panel was excavated using cutting and top coal caving (thickness 15 m) at an average advance rate of 2.5 m/day. A cross section of the longwall panel K.-65/F is presented in Figure 66.

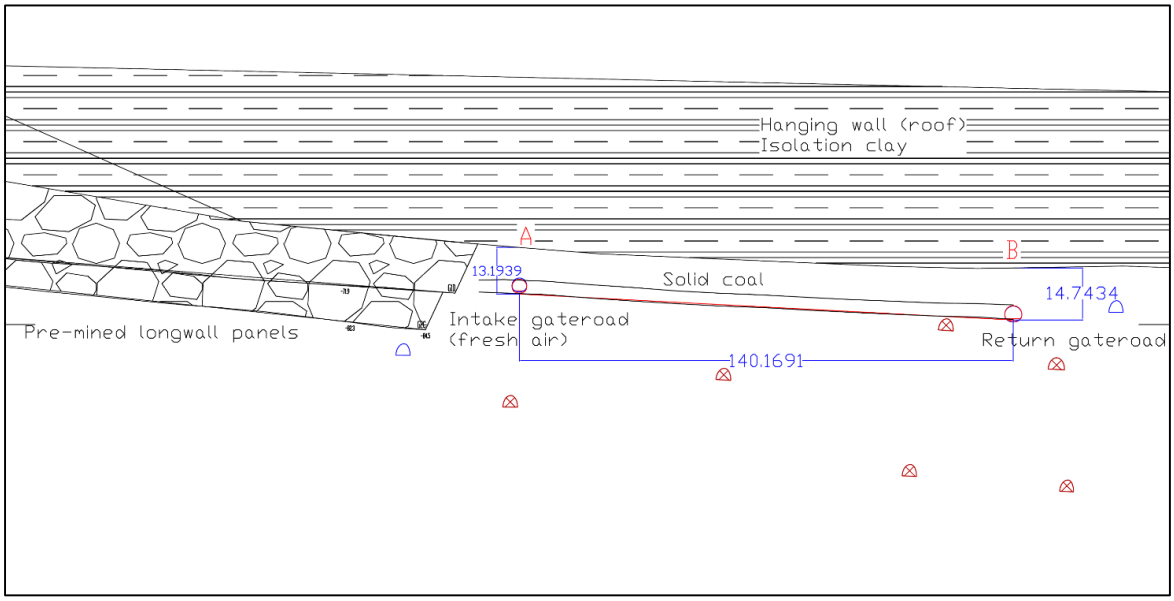


Figure 66: *Cross section of the longwall panel K.-65/F.*

The geomechanical model is constructed as a solid block, which initially did not include any openings. The principle is that the model should first reach equilibrium, after which are placed the gate roads and the longwall panel. Based on the knowledge gained on the different geomechanical and geochemical characteristics of the different lithotypes in the Velenje lignite, the geomechanical and geochemical model are divided into different models with the following characteristics:

- 100 % xylite;
- 100 % fine detrite;
- 50 % xylite and 50 % fine detrite.

A small mesh size was used in all of the models to obtain a more accurate stress distribution results around the longwall panel. Initially, the model was in the form of a solid block, where half of the longwall panel was included with one gate road and half of the longwall face. The face was 70 m wide and the excavated coal panel was 80 m in length. The coal seam was 50 m thick and the model was set in the upper part of the coal seam (first level). Face advance was equivalent to the actual average coal production of 5 m. Two

different types of mining was modelled: mining with only coal cutting using a shearer with a 5 m mining height and top coal caving with 15 m mining height.

All the models have 222,660 zones and 238,742 grid-points and all were computed using the Hoek Brown model. Simplified goaf material properties were used in addition to the crushed and a weakened hanging wall. Geomechanical properties were defined using the RocData program from Rocscience.

After setting the boundary and initial conditions (Figure 67), the model was solved until equilibrium was reached. Afterwards, the gate road and longwall face were included as null elements. All elements in the gate roads and longwall face were 5 m wide and 5 m in height. The model was solved again until equilibrium was achieved once more.

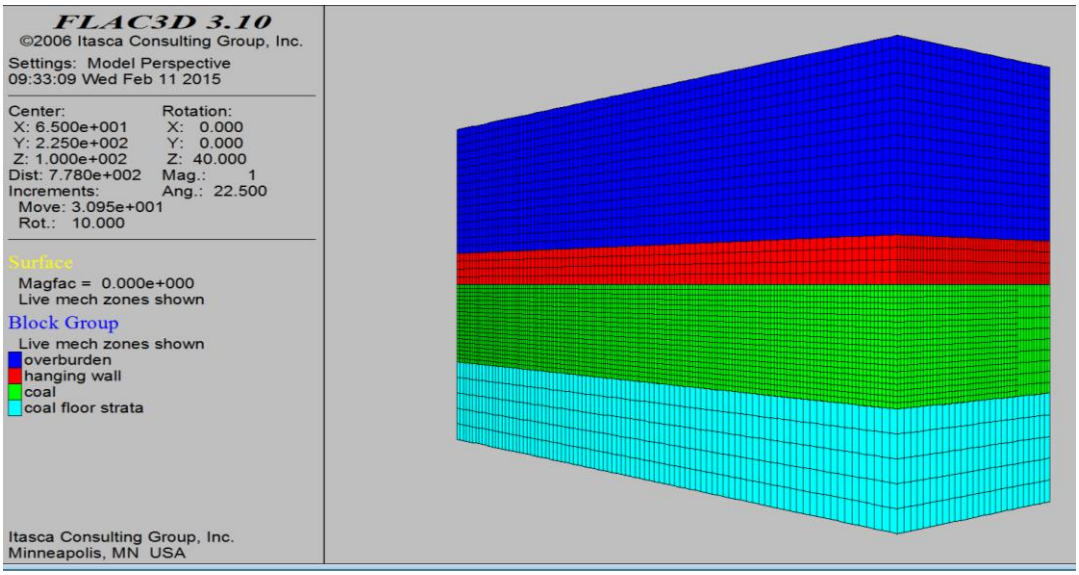


Figure 67: *Geomechanical model with represented block groups.*

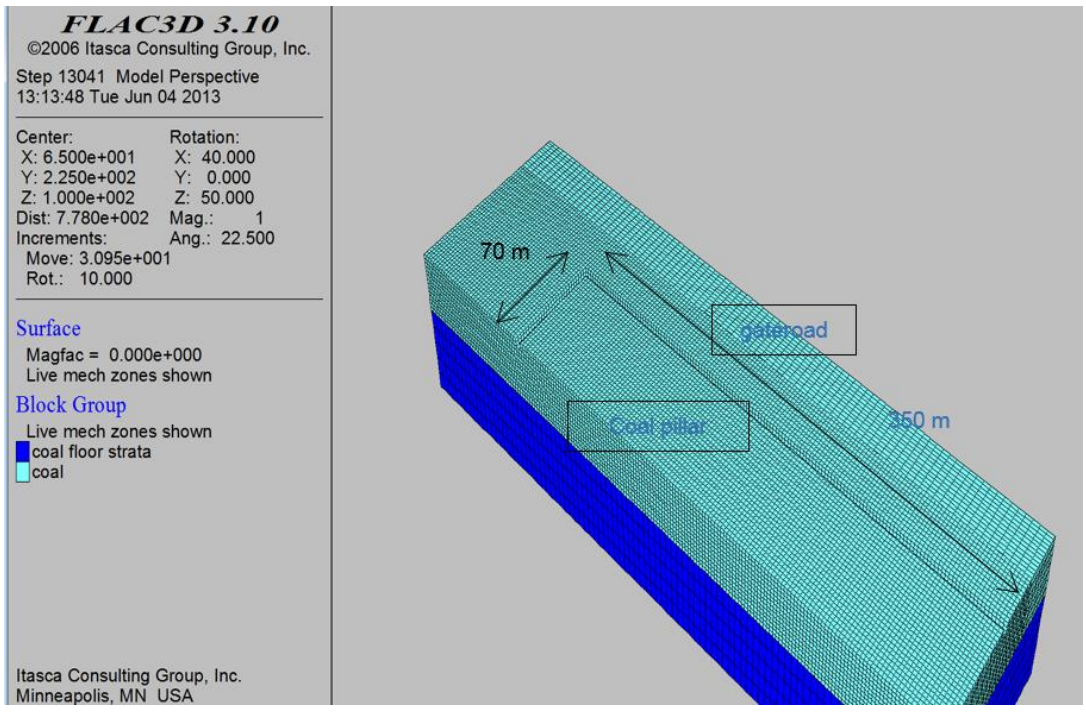


Figure 66: *Schematic representation of the longwall panel K.-65/F model.*

For all three lithotype groups, physical and mechanical parameters were selected

according to laboratory experiments (Tables 13, 14 and 15)**.** These parameters were then used in the RocLab software to determine the Hoek-Brown factors m_b, s and a. The results were calibrated using the theoretic description of the pressure wave at during longwall mining at the Velenje Coal Mine and with previously calculated models from the literature.

Table 13: *Material properties used in a geomechanical model of the longwall panel K. 65/F in the 100 % xylite model.*

Rock type	σ_{ci} (MPa)	GSI	mi	Density (kg/m^3)	Elastic module (MPa)	Friction angle (°)
Overburden	2.5	50	5	2260	570	24.8
Hanging Wall	1.7	70	6	1790	256	31.7
Coal seam	12.6	50	3.57	1240	4800	22.2
Goaf	1.7	5	7	1790	256	12.5
Floor strata	5.9	50	12	1240	750	32.1

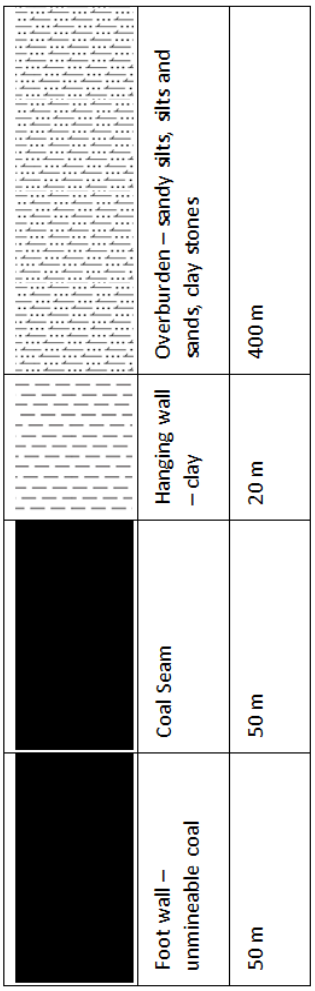


Figure 68: *Geological profile of the model at longwall panel K.-65/F.*

Table 14: *Material properties used in a geomechanical model of the longwall panel K. 65/F in the 100 % fine detrite model.*

Rock type	σ_{ci} (MPa)	GSI	mi	Density (kg/m^3)	Elastic module (MPa)	Friction angle (°)
Overburden	2.5	50	5	2260	570	24.8
Hanging Wall	1.7	70	6	1790	256	31.7
Coal seam	8.5	53	6.16	1240	1100	26.1
Goaf	1.7	5	7	1790	256	12.5
Floor strata	5.9	50	12	1240	750	32.1

Table 15: *Material properties used in a geomechanical model of the longwall panel K. 65/F in the 50 % of xylite and 50 % of fine detrite model.*

Rock type	σ_{ci} (MPa)	GSI	mi	Density (kg/m^3)	Elastic module (MPa)	Friction angle (°)
Overburden	2.5	50	5	2260	570	24.8
Hanging Wall	1.7	70	6	1790	256	31.7
Coal seam	10	50	5.61	1240	700	24.2
Goaf	1.7	5	7	1790	256	12.5
Floor strata	5.9	50	12	1240	750	32.1

5.6 Results and Discussion

From the results of stepwise modelling, using a face advance rate of 5 m/day, stress distributions were calculated for different observation points in the model. Their locations are shown in Figure 69. Different locations in the coal, hanging wall, floor strata were selected so that the pressure wave at different depths according to the position of the longwall face and any difference between horizontal excavation of the coal and longwall top coal caving could be observed. The observation points were 50 m, 150 m and 250 m in front of the longwall face. Using different z-coordinates, data were obtained at observation points in the extracted coal, on the border between coal and the hanging wall and in the hanging wall.

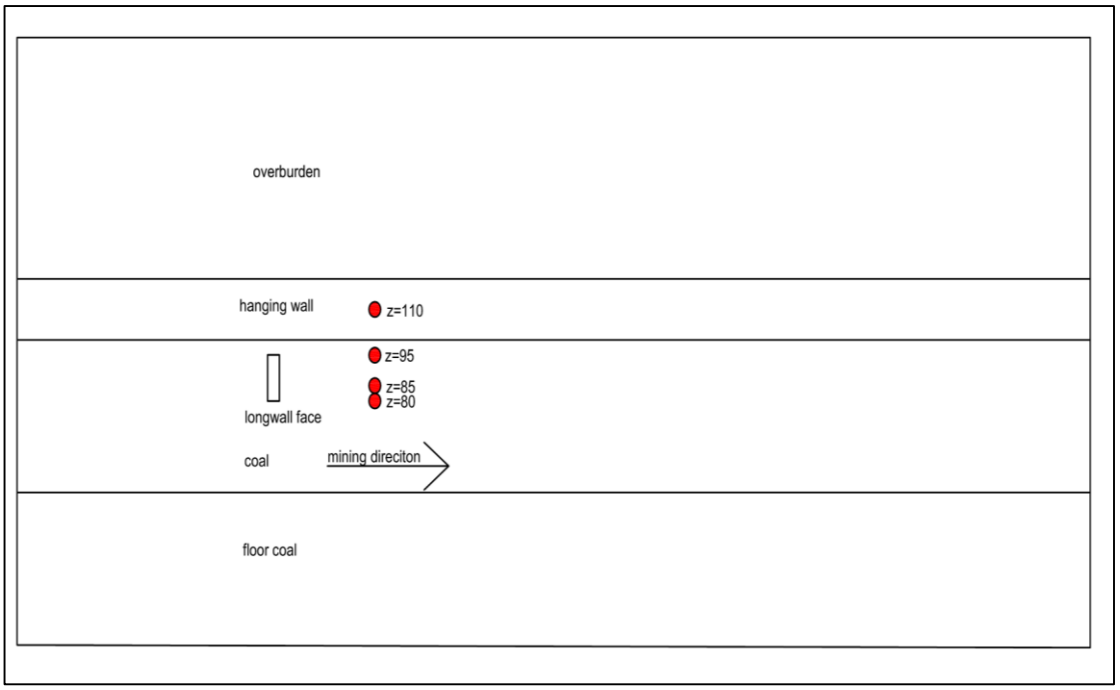


Figure 69: *Schematic illustration of observation points' position in the z-direction.*

Figure 70 reveals how the maximum vertical stresses vary from 21.0 MPa (mixed lithotype) to 23.2 MPa (detrite lithotype) during the horizontal excavation phase. Maximum values occur at 6.7 m, 7.9 m and 6.8 m ahead of the longwall face for detrite, xylite and mixed coal, respectively. A comparison of the data obtained for horizontal excavation and top coal caving mining (Figures 70 and 71) shows an obvious difference between these two mining techniques, top coal caving of up to 15 m has much greater effect on the surrounding strata than coal cutting with longwall shearer only. The maximum vertical stresses in the models using the LTCC method were at 22 m in front of the longwall panel. The maximum vertical stresses were 24 MPa, 26 MPa and 30 MPa in detrite, xylite and mixed lithotype respectively (Figure 71). Jeromel (2010) found that the size and distribution of the vertical stress ahead of the longwall face depends on the following:

- Mining method;
- Advance rate;
- Caving height;
- Geomechanical characteristics of the material;
- Structural characteristics (fractures, faults) and
- Initial stress state.

As expected, the results varied between the different configurations of the caving height and different geomechanical characteristics of each lithotype group. And, because of the heterogeneity of the lignite, different scenarios were modelled. In addition, the amount of CSG in detrite is higher than in the xylite coals.

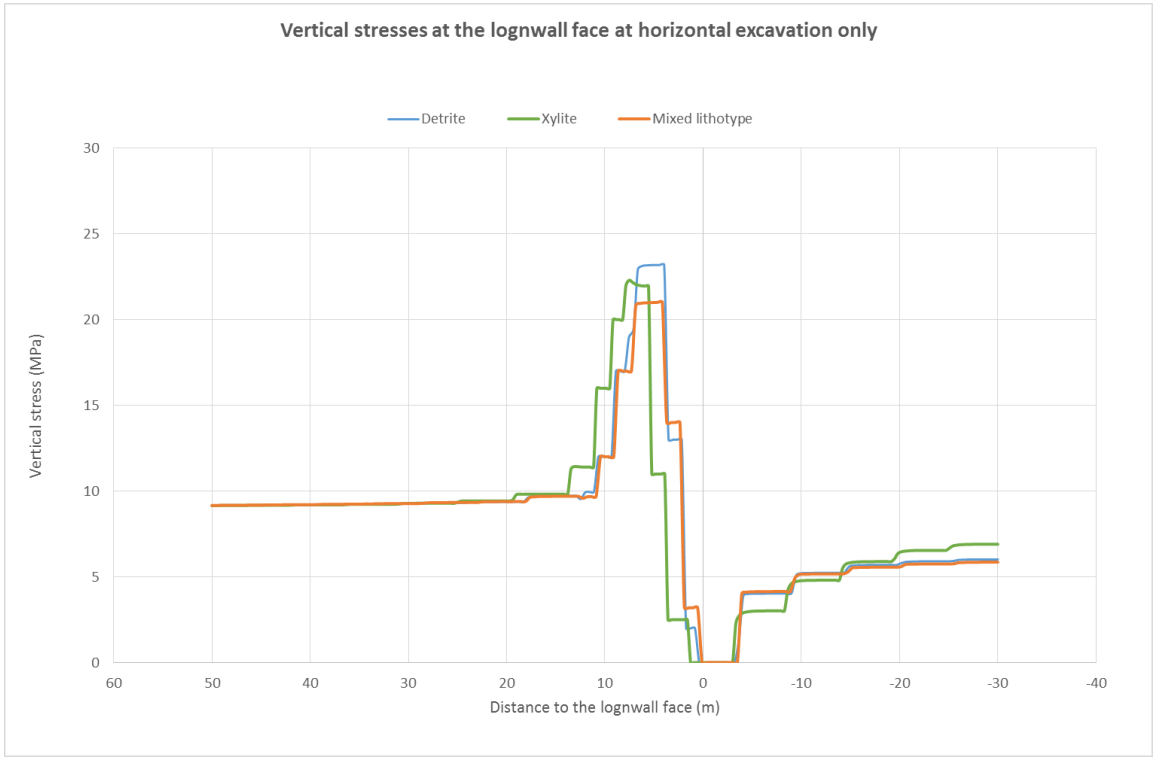


Figure 70: *Vertical stresses at the longwall face during horizontal excavation for different lithotypes.*

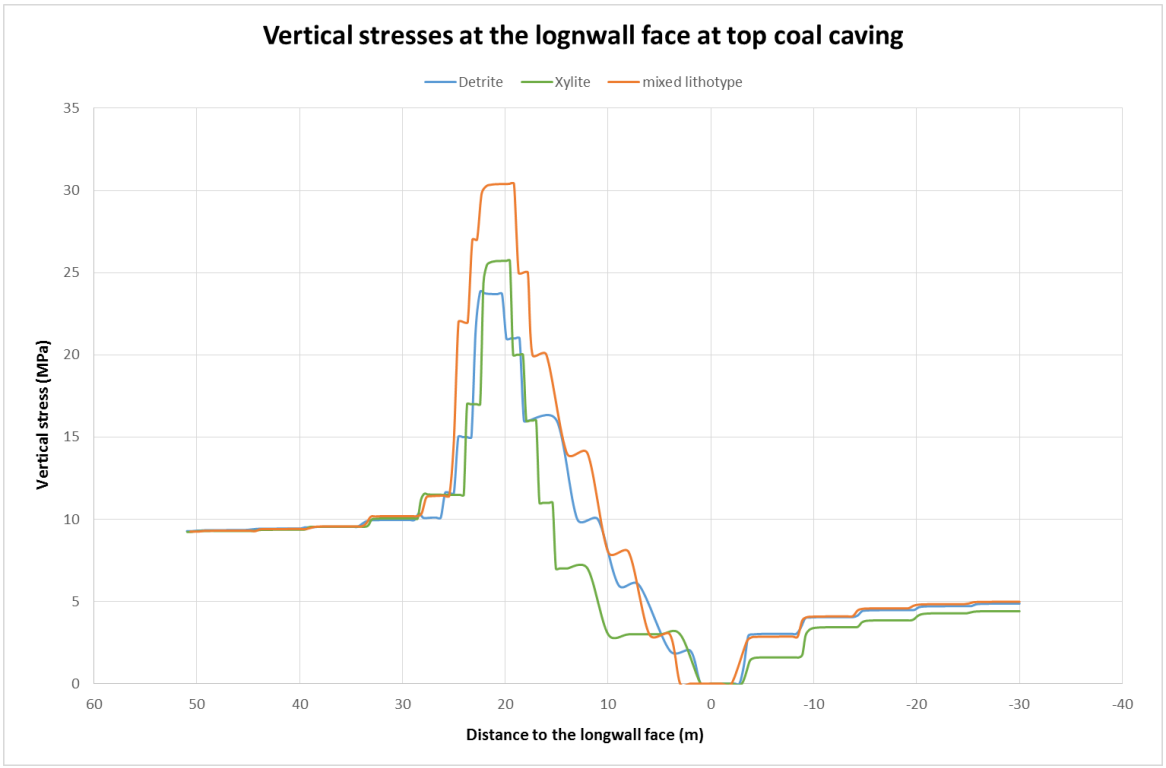


Figure 71: *Vertical stresses at the longwall face during top coal caving for different lithotypes.*

5.7 Conclusions

Before begining gas flow and drainage simulations around the LTCC panels, it was necessary to both model and assess the stress distribution and geomechanical behaviour of the coal seam. This work was carried out using the computational software FLAC^{3D}. First, a 3D model, corresponding to the actual geometry of the longwall panel K.-65/F was developed. Fortunately, FLAC allows the user to design a very detailed geometry, which is helpful in 3D modelling. The downside is that the file size quickly become very large and the computational time of the runs can be very long when using average specification computers. For this reason the model was made symmetrical in order to achieve smaller file sizes.

This study focused mostly on stress abutment distribution analysis in order to obtain the correct input parameters for the coal seam gas flow models. This was achieved by testing and studying the effects of different constitutional models, such as Mohr- Coulomb and Hoek-Brown models. Finally, it was decided to use the Hoek-Brown failure criteria in the remaining geomechanical models, since the main focus of modelling is on gas flow characterisation. Calibration of the model was performed using data obtained previously from geomechanical models and actual in-situ stress measurements.

The revealed that vertical stresses distribution is different when mining only the lower section of the coal at the face compared to that when mining with top coal caving (up to 15 m in height). Also different lithotype groups were found to behave differently in the model, which was one of the main tasks in the research. The maximum vertical stresses vary from 21.0 MPa in case of mixed lithotype to 23.2 MPa in case of the detrite lithotype during the horizontal excavation phase of the coal. Maximum values occur at 6.7 m, 7.9 m and 6.8 m ahead of the longwall face for detrite, xylite and mixed coal respectively.

De-stressing of the coal pillar due to the release of dynamic stresses occurs at a distance of 100 to 75 m in front of the borehole as the approaching longwall face begins to affect the coal gas content. At 30 to 50 m from the geotechnical measurement points the vertical stresses are so high that the lignite structure collapses A comparison of the data obtained for horizontal excavation and top coal caving mining shows an obvious difference between these two mining techniques, top coal caving (up to 15 m) has a much greater effect on the surrounding strata than coal cutting using only a longwall shearer. Still, the geomechanical model showed the maximum vertical stress at a shorter distance to the longwall face. The maximum vertical stresses in the models using the LTCC method were at 22 m in front of the longwall panel. In detrite the maximum vertical stresses were 24 MPa, 26 MPa and 30 MPa in detrite, xylite and mixed lithotype respectively. The difference between the geotechnical measurements taken in the mine and the geomechanical model can be explained by the different location in the mine. It is recorded that the maximum vertical stresses in the mine are 1.5 to 2.5 times of the caving height at the longwall face.

Active tomography measurements revealed the typical behaviour of the coal in front of the longwall face i.e., at 1.5 m from the longwall face the effect of stress is observed as a large zone of high deformations and low P-wave velocities, which stretches out to 20 m in front of the longwall face. A large decrease in the P wave velocity is observed between the 2nd and 1st measurement of the P_y waves as the longwall face advances together with a decrease in velocity of up to 600 m/s at a distance of 2.6 m to the longwall face.

The results show that, for more accurate geomechanical modelling of the longwall top coal mining, the Strain- Hardening/Softening model should be used, rather than the Hoek-Brown constitutive model.

6 Development of a Coal Seam Gas Flow Model

6.1 Model Development in TOUGH2

Nowadays, there are many different types of computational software for modelling fluid flow available on the market. Imperial College, London currently holds a site licence for the software TOUGH2, which provided an excellent opportunity to use this numerical programme in this study. TOUGH2, developed by the Earth Science Division, Lawrence Berkley National Laboratory in the USA is a numerical simulator for non-isothermal flows of multicomponent, multiphase fluids in one, two, and three-dimensional porous and fractured media (Pruess et al., 1999). TOUGH2 code uses different fluid properties or equation-of-state "EOS" modules. It is designed using a modular architecture (Figure 72), in which the main flow and transport module can interface with different fluid property modules (Pruess et al., 1999).

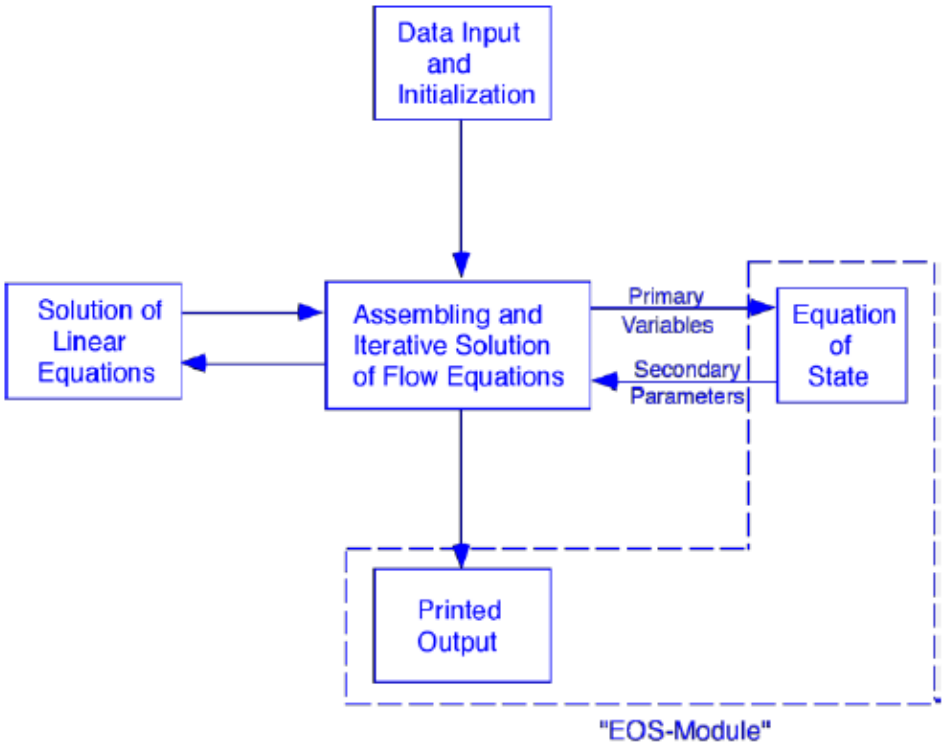


Figure 72: *Modular architecture of TOUGH2 (Pruess, et al., 2012).*

The programme solves mass and energy balance equations that describe fluid and heat flow in general systems (Pruess et al., 1999). Fluid flow is described using Darcy`s law, whereas heat flow is performed by conduction and convection. Typical input parameters include grain density, porosity, permeability, thermal conductivity, specific heat, relative permeability and water retention curves, as well as hydraulic and thermal boundary conditions (Rutqvist, 2011).

TOUGHREACT is one of the TOUGH-family of codes and represents an upgrade of TOUGH2. TOUGHREACT (Xu et al., 1998; Xu et al., 2006; Xu et al., 2011; Xu et al.

2012) is applicable to one-, two-, or three-dimensional geologic domains with physical and chemical heterogeneity and can be applied to a wide range of subsurface conditions. TOUGH2 still forms the base for TOUGHREACT, to which extensions have been added. At the same time, TOUGH2 input files can be used without any modification (Xu et al. 2012). TOUGHREACT has been used to assess nuclear waste disposal, CO_2 geological storage and groundwater contamination and remediation (Xu et al, 2006; Xu et al., 2011).

The major processes for fluid and heat flow are: (1) fluid flow in both liquid and gas phases occurring under pressure, viscous, and gravity forces; (2) interactions between flowing phases are represented by characteristic curves (relative permeability and capillary pressure); (3) heat flow by conduction and convection, and (4) diffusion of water vapour and air (Xu et al. 2012).

The present version of TOUGHREACT provides the following TOUGH2 EOS modules (Xu et al. 2012):

- EOS1 for water, or two waters with typical applications to hydrothermal problems;
- EOS2 for multiphase mixtures of water and CO_2 also with typical applications to hydrothermal problems;
- EOS3 for multiphase mixtures of water and air with typical applications to vadose zone and nuclear waste disposal problems;
- EOS4 has the same capabilities as EOS3 but with vapour pressure lowering effects due to capillary pressure;
- EOS7 for multiphase mixtures of water, brine, and air with density and viscosity effects of salinity as an extension of EOS3;
- EOS9 for single phase water (Richards` equation) with typical applications to ambient temperature and pressure reactive geochemical transport problems, and
- ECO2N for multiphase mixtures of water, CO_2, and NaCl with a typical application being CO_2 geological storage in deep saline aquifers.

TOUGHREACT has simplifying approximations built into the modules but does not take into account hydrodynamic dispersion, deformation of the porous skeleton or fluid and pressure effects influenced by porosity changes. The model also neglects heat effects from chemical reactions and the pressure effect on chemical equilibrium constants.

6.1.1 ECO2N EOS Module

ECO2N is one of the EOS modules of the TOUGH-family of codes (Pruess et al., 1999). ECO2N is a fluid property module for the TOUGH2 simulator that was designed for applications to geologic sequestration of CO_2 in saline aquifers (Pruess, 2005). It can be used for modelling CO_2 injection and for underground CO_2 emission dispersion modelling. The ECO2N module allows either single fluid phase (only aqueous or only gas) or a two fluid phase (both aqueous and gas) modelling, this makes it suitable for modelling CSG migration in the Velenje lignite seam. In this thesis, where the content of CSG is represented by the two major gases: CH_4 and CO_2, CSG migration modelling can be performed only for the carbon dioxide component. Methane can then calculated using the gas balance results from the TOUGH2 models.

When using TOUGH2 the primary variables must be determined and the choice of these variables defines the phase state (single fluid phase or two fluids phase), in which case the primary variables are time-dependent. In the case of a single fluid phase the primary variables are the following:

- P = pressure;

- X_{sm} = salt mass fraction X_s in a two component water-salt system, or solid saturation S_s+10;
- X_3 = CO_2 mass fraction in the aqueous phase, or in the gas phase, in the three-component system water-salt-CO_2;
- T = temperature.

Thermo-physical properties are accurately calculated for gaseous and liquid CO_2, but no distinction is made between gaseous and liquid CO_2 phases in the treatment of flow, and no phase change between liquid and gaseous CO_2 is treated (Pruess, 2005). Assuming local thermodynamic equilibrium, the system's state is defined by the number of balance equations per grid block. In this EOS, the thermo-physical properties include density, viscosity, temperature, pressure and composition. The module ECO2N also has the option to vary permeability but the module is limited since pore pressure must be between 0.1 MPa and 60.0 MPa, and temperature must be between 4°C and 100 °C (Sung et al., 2014).

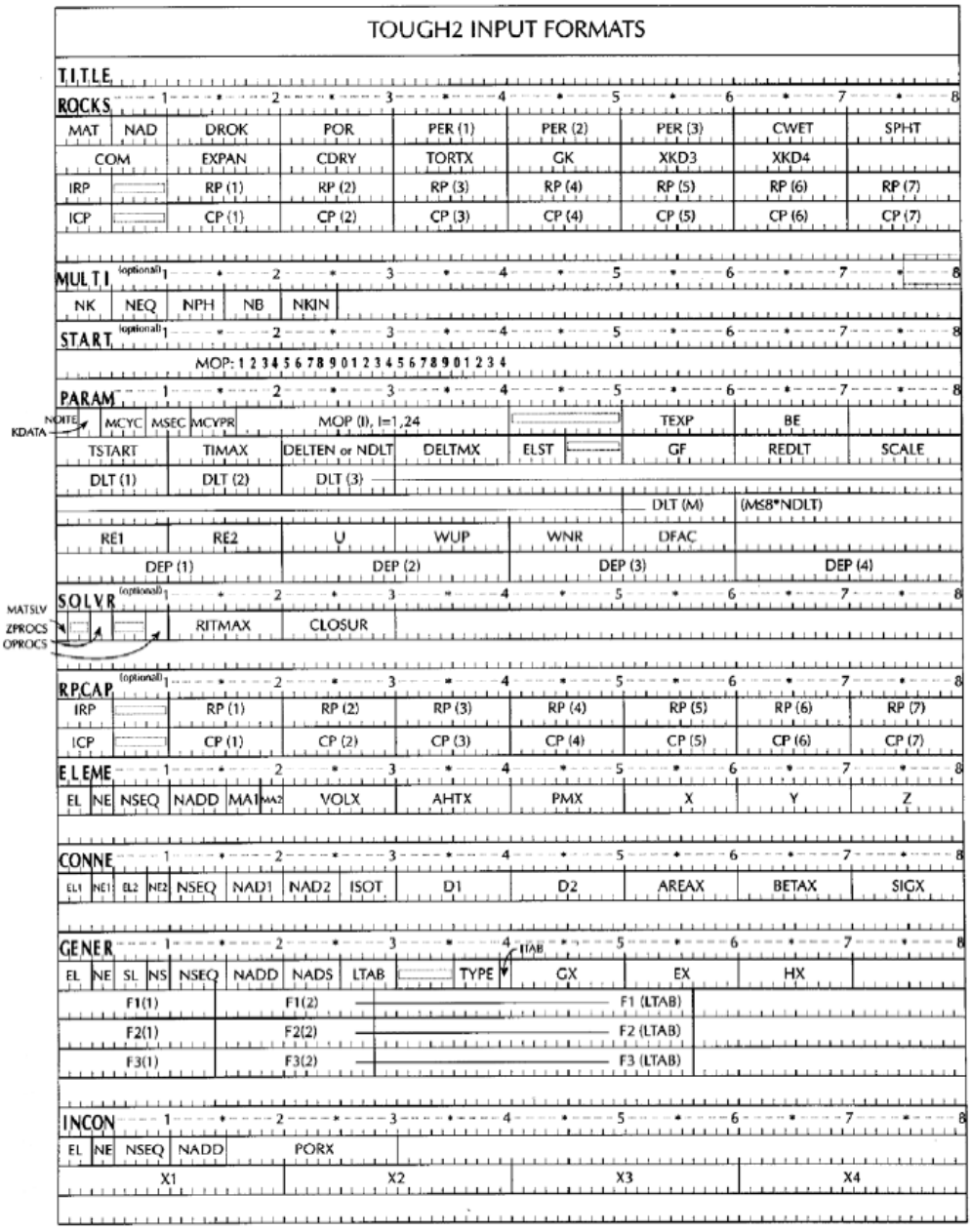


Figure 73: *TOUGH2 input formats* (Pruess et al., 1999).

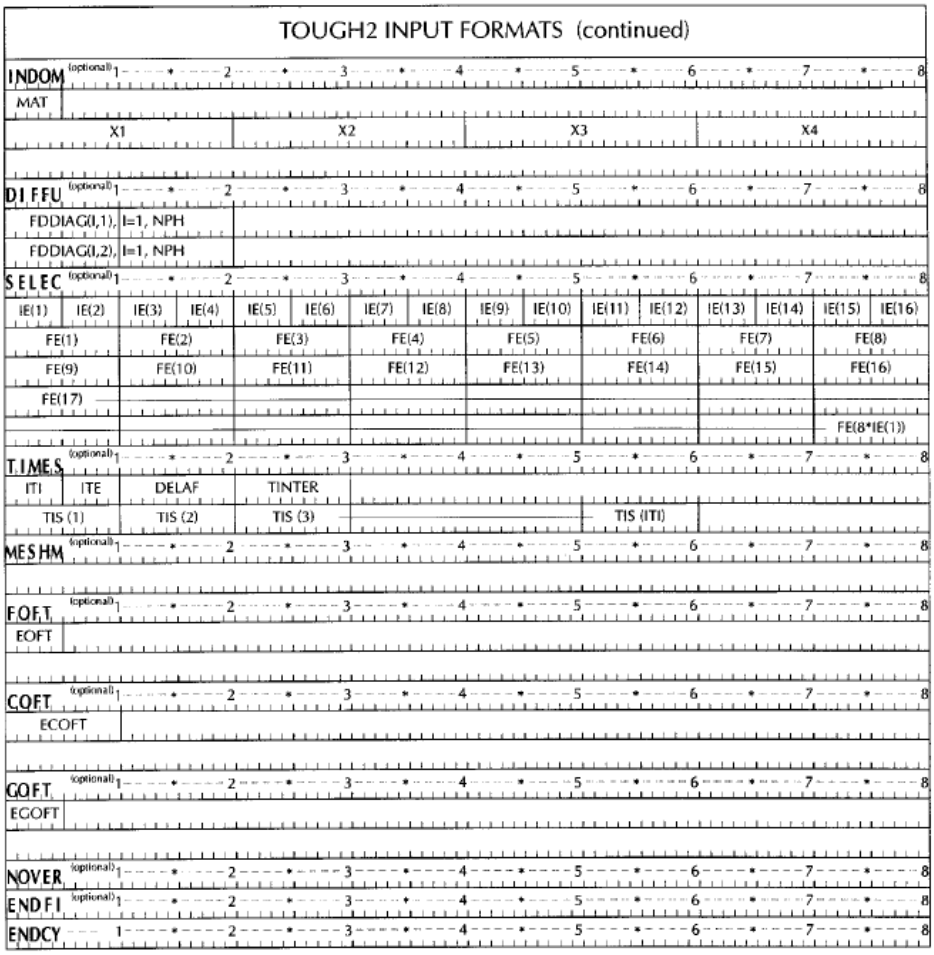


Figure 74: *TOUGH2 input formats (continued)* (Pruess et al., 1999).

6.1.2 Data Collection and Input

Input data in TOUGH2 is by means of either using one or numerous ASCII data files (Pruess, et al., 1999). The organization of the input data is shown in Figures 73 and 74, where all parameters are defined by five-character keywords (Table 16).

Table 16: *TOUGH2 input data blocks* (Pruess et al., 1999).

Keyword	Function
TITLE	One data record (single line) with a title for the simulation problem (first record)
MESHM	Optional; parameters for internal grid generation through MESHMaker
ROCKS	Hydrogeological parameters for various reservoirs domains
MULTI	Optional; specifies number of fluid components and balance equations per grid block
SELEC	Used with certain EOS-modules to supply thermo physical property data
PARAM	Computational parameters; time stepping and convergence parameters
DIFFU	Diffusivities of mass components
FOFT	Optional; specifies grid block for which time series data are desired
COFT	Optional; specifies connections for which time series data are desired
GOFT	Optional; specifies sink/sources for which time series data are desired
RPCAP	Optional; parameters for relative permeability and capillary pressure functions
TIMES	Optional; specification of times for generating printout
ELEME	List of grid blocks (volume elements)
CONNE	List of flow connections between grid blocks
GENER	Optional; list of mass or heat sinks and sources
INDOM	Optional; list of initial conditions for specific reservoir domains
INCON	Optional; list of initial conditions for specific grid blocks
NOVER	Optional; if present, suppresses printout of version numbers and dates of program units executed in aTOUGH2 run
ENDCY	One record to close the TOUGH2 input file and initiate the simulation
ENDFI	Alternative to "ENDCY" for closing a TOUGH2 input file; will cause flow simulation to be skipped; useful if only mesh generation is desired

6.1.3 Boundary and Initial Conditions

After choosing a suitable EOS module, the data block PARAM assigns grid blocks with default thermodynamic conditions. Initial conditions are set when the thermodynamic conditions are written in the PARAM block at the beginning of the simulation, after which TOUGH2 performs a simulation, where these thermodynamic conditions are written to the model in the SAVE file. The SAVE file contains data of initial conditions, which are then copied to the INCON block inside the TOUGH2 model.

TOUGH2 recognises two basic types of boundary conditions. First, are the Dirichlet

conditions that describe thermodynamic conditions, for example pressure and temperature. Second, are the Neumann conditions that describe fluxes of mass or heat crossing the boundary surfaces (Pruess et al., 1999).

For the Dirichlet boundary conditions, large volumes are assigned to the model boundary e.g., $V=10^{50}$ m^3, to make sure that the thermodynamic conditions at the boundaries do not change while the simulation is running. In addition, a small value (i.e., $D=10^{-9}$ m) should be specified for the nodal distance, so that boundary conditions are maintained in close proximity to the surface where they are desired (Pruess et al., 1999).

Using Neumann boundary conditions in TOUGH2 is more complicated in comparison to using Dirichlet boundary conditions. Neumann boundary conditions are time-dependent and can be identified using sink and source rates. When using time-independent Dirichlet boundary conditions, usually in TOUGH2 modelling, simple "active" and "inactive" elements are used. Elements in data block ELEME are taken to be active until the first element entry when either a zero or negative volume is encountered (Pruess, et al., 1999). A negative volume element is referred to as a dummy grid block and all of the elements after the dummy grid block are inactive.

6.1.4 Sinks and Sources

To model gas (or any other fluid or heat) injection ($q>0$) or gas production ($q<0$), TOUGH2 uses sink and sources, which are introduced in the GENER block data. Any of the mass components may be injected in an element at a constant rate, or at time-depended rates prescribed through user-defined tables (Pruess et al., 1999).

6.1.5 Output from TOUGH2 and Visualisation of the Results with TECPLOT360

Once TOUGH2 modelling is complete, the results are saved as a variety of printed outputs. These outputs give the user certain time-stepping information and a total element-by-element report of the modelling execution with all thermodynamic and geochemical results. It is then possible to visualise the TOUGH2 outputs using Tecplot 360, which is a tool for line plotting, 2D and 3D surface plots in a variety of formats, and 3D volumetric visualisation (Tecplot, Inc., 2013). It is also possible to visualize the data in a number of coordinate systems, including 2D, 3D, XY or as a Polar coordinate system. Data can be imported in various formats, which are developed using different executable files from third party programmes. In our case, the most important are Excel, Loader and Tecplot – Format Loader that is coupled to a TOUGH2 executable file, which converts the TOUGH2 output file into a Tecplot readable file. AutoCAD DXF files can also be imported using DXF Loader, but this Loader does not create any zones, only the geometry of the model is inserted in the Tecplot programme. The Excel Loader is useful for basic formats only (Tecplot, Inc., 2013) and the data cannot include any equations, only numbers. The Tecplot Loader uses the standard extension *.dat* for ASCII files and *.plt* for binary files (Tecplot, Inc., 2013), which is useful for importing data. Data in a table format from excel can be plotted as either 2D or 3D plots. Some limitations exist when importing data from a table. For example, each column must be the same length and each cell must contain numeric data (Tecplot, Inc., 2013).

6.2 Gas Flow Model Development under Dynamic Influence of Longwall Face Advance

TOUGH2 enables both geomechanical and geochemical characteristics to be set for the materials used in the models. Therefore for separate geochemical models, different material properties were used, as shown in Tables 17, 18 and 19.

6.2.1 Geometry and Material Properties of the Models

To simulate gas migration around a drainage borehole in the longwall panel K.-65/F, 2D geometries were defined. Models were designed for the different distances of the longwall face (different stress phases caused by the advancing face). Figure 75 shows a schematic of the geometry used in the models. The distance between the longwall face and the borehole changes in steps of 100 m, 60 m, 40 m, 20 m, 10 m and 5 m. The difference between horizontal excavation and top coal caving was also studied.

In all the models, to account for the influence of the longwall face, the permeability and porosity was increased 10 m in front of the longwall panel where the vertical stresses are reduced to zero. The intact pressure state was equal for all of the models and set to 2 MPa, which is equivalent to the maximum pressure measured in the borehole at K.-65/F.

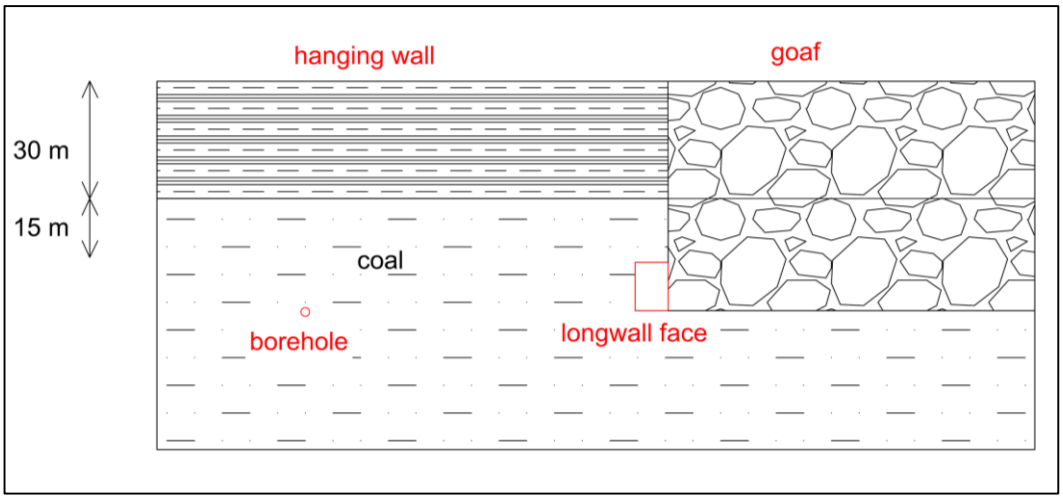


Figure 75: *Schematic geometry used in TOUGH2 flow models in the top coal caving model.*

Material properties were applied differently for each of the lithotypes according to Tables 17, 18 and 19.

Table 17: *Material properties used in the 100% xylite model.*

Material	Density (kg/m^3)	Porosity (%)	Permeability (mD)
Hanging wall	1690	5	0.01
Coal	1240	10	1
Fractured Coal	1240	30	10
Goaf	1690	40	1000

Table 18: *Material properties used in the 100% detrite model.*

Material	Density (kg/m^3)	Porosity (%)	Permeability (mD)
Hanging wall	1690	5	0.01
Coal	1240	20	10
Fractured Coal	1240	30	100
Goaf	1690	40	1000

Table 19: *Material properties used in the 50% xylite and 50% detrite model.*

Material	Density (kg/m^3)	Porosity (%)	Permeability (mD)
Hanging wall	1690	5	0.01
Coal	1240	10	1
Fractured Coal	1240	30	100
Goaf	1690	40	1000

6.3 Results and Discussion

2D flow models were designed to represent a similar grid distribution to that used in the geomechanical model. Boundary conditions meant that large volume elements were used in the models on both sides. After establishing the model's geometry using *Meshmaker*, the next step was to set the initial conditions and run the simulation for 3,000 days. This is necessary for the model to reach equilibrium (Figure 76). At equilibrium the pressure distribution is unified and correlates with depth, and since the CSG pressure measurements in panels exceeds 20 bars (in one case up to 26 bar), the initial pressure was set to either 20 bar (2 MPa).

To represent the K.-65/F drainage model, the longwall panel was located 20 m below the hanging wall with a minimum top coal caving height of 15 m. The distances to the drainage borehole from the longwall face used in the model was 100 m, 60 m, 40 m, 20 m, 10 m, and 5 m. The longwall face is represented as a production area at 1 bar atmospheric pressure (keyword source in TOUGH2), and the borehole is modelled as a production borehole at 300 mbar under pressure (keyword source in TOUGH2). Results of flow modelling are divided into three lithotype groups:

1. 100% xylite;
2. 100% detrite and
3. 50% xylite and 50% detrite (mixed lithotype).

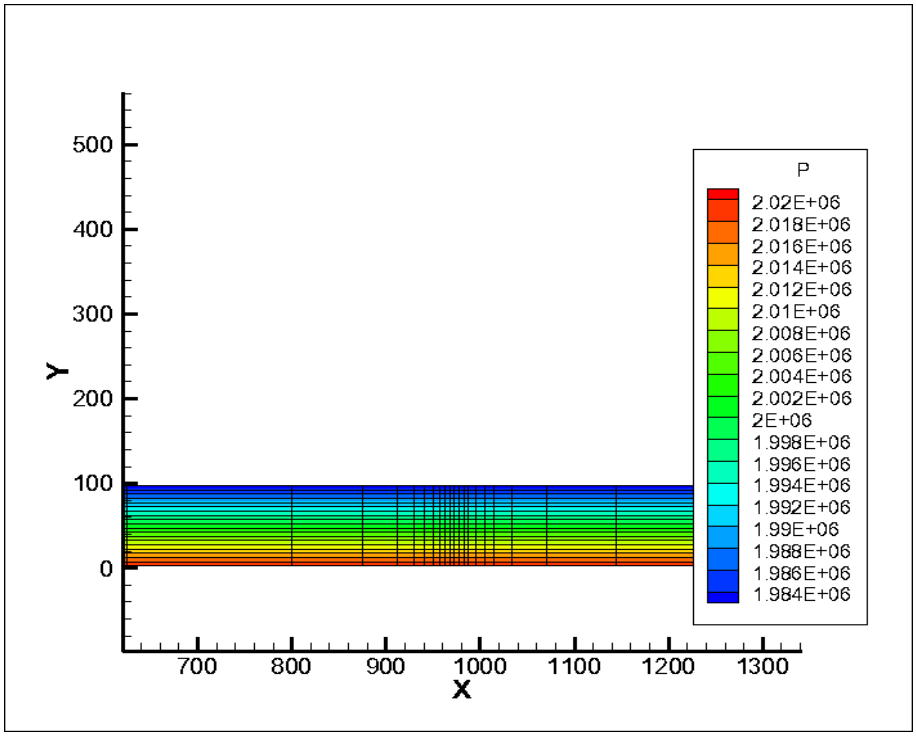


Figure 76: *2D model equilibrium situation.*

6.3.1 100 % Xylite Flow Model

The models show the CO_2 gas flow vectors around the longwall face, whereas around the borehole the gas flow vectors are too small to be visible. The xylite models have a permeability at least one order of magnitude lower in comparison to detrite and the smaller porosity and lower permeability meant the pressure drop in xylite coal is neither as noticeable nor as rapid than for detrite. Also, the hanging wall, which is composed mostly from clay, represents an impermeable stratum that prevents CSG from migrating.

Calibration of the TOUGH2 models was performed with comparison of the results with the actual drainage trial and with *in-situ* gas pressure measurements measured at different longwall panels, especially with gas pressure measurements at the chosen longwall panel K.-65/F.

Drainage trials have shown that only small volumes of CSG were drained from the coal when the longwall face was at a distance of greater than 40 m, similar to that observed in the simulations at 100 m and 60 m in front of the longwall face (Figure 77). This drained gas was only the CSG from the vicinity of the borehole, in an area no larger than 2 m in radius around the borehole i.e., the area of coal disturbed (crushed) during drilling. At

Velenje Coal Mine, laboratory studies of crushed lignite have shown that gas flow increases up to 30-times after the stress state is released (Zavšek, 2004). The amount of gas released depends on the amount of crushed coal. The drilling of boreholes inflicts only a small amount of damage on the surrounding coal compared with the advancing longwall face but despite this, when drilling through pure fine detrite, a significant amount of the CSG can still be released.

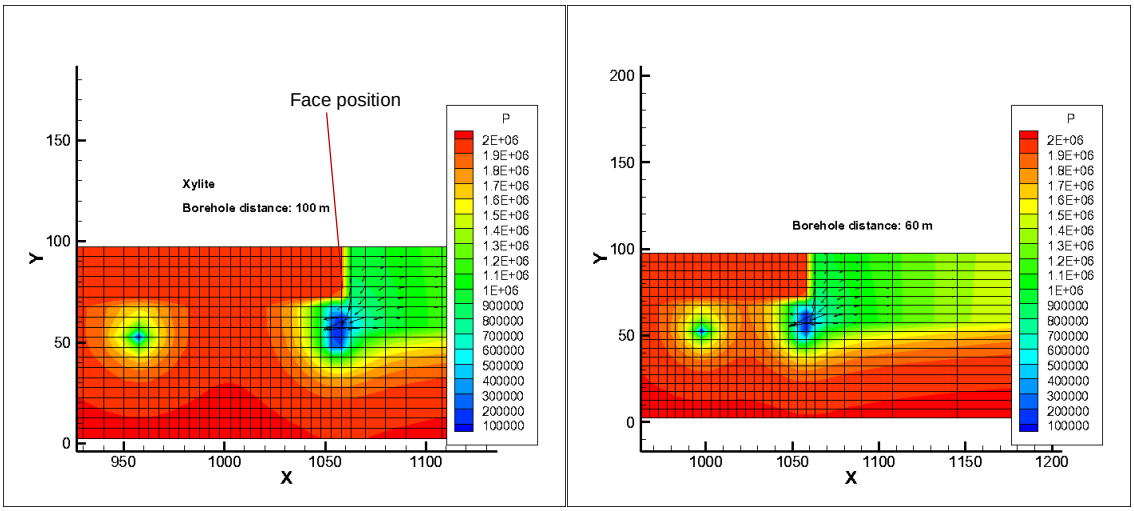


Figure 77: *Left) Simulation results of drainage at 100 m to the longwall face in xylite; Right) Simulation results of drainage at 60 m to the longwall face in xylite.*

When the drainage borehole is 40 m in front of the longwall face (Figure 78: left) the gas flow vectors reach the location of the drainage borehole and higher amounts of CSG can be drained from the coal. At this distance, the coal is heavily fractured and it is these fractures and fissures that allow CSG to flow. At this distance the field drainage trials revealed that a single borehole is capable of producing 38.5 m^3/h of CH_4 and 80.4 m^3/h of CO_2, and the first prolonged period of drainage was possible. Also, between 0-20 m away from the longwall face, seismic tomography revealed a significant decrease in P-wave velocities, which is also a result of the coal being fractured.

Figure 78 right, reveals an increased zone of atmospheric pressure (approx. 0.1 MPa) suggesting a connection between the de-stressed zone in front of the longwall face and the borehole. The direction of the CO_2 gas flow vectors show that a large amount of CSG migrates to the longwall face from the goaf and top coal. The goaf has both a higher porosity and permeability compared with intact coal and the CSG can flow easily from the goaf to the longwall face. Goaf gas mostly consists of CO_2, since the methane would have already escaped from the coal during mining.

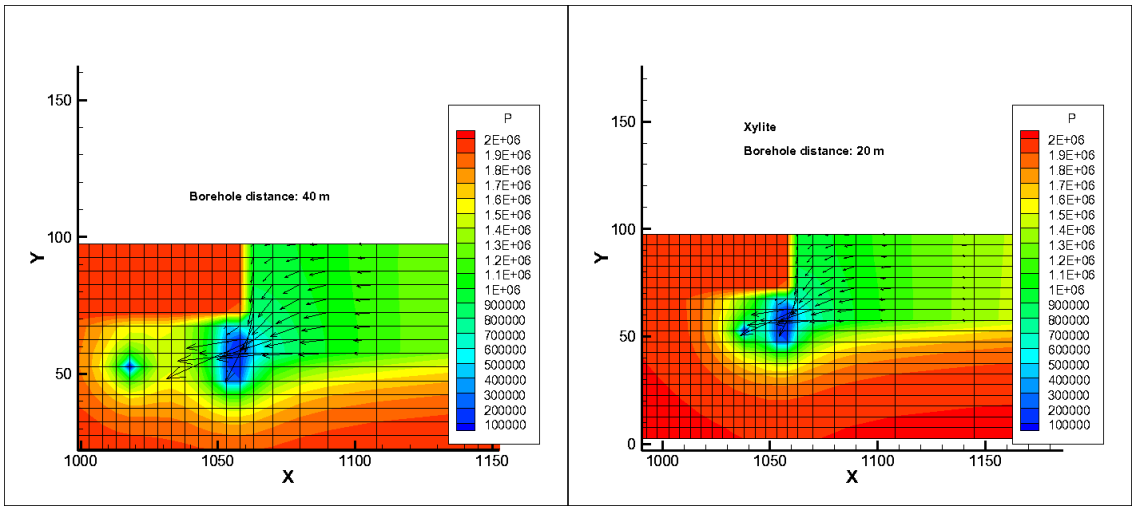


Figure 78: *Left) Simulation results of drainage at 40 m to the longwall face in xylite. Right) Simulation results of drainage at 20 m to the longwall face in xylite.*

When the borehole is 10 m in front of the longwall face (Figure 79, left) gas flow is reduced and the drainage capacity is lower. This is explained by the fracture system becoming dominant that most gas flow is towards the longwall face.

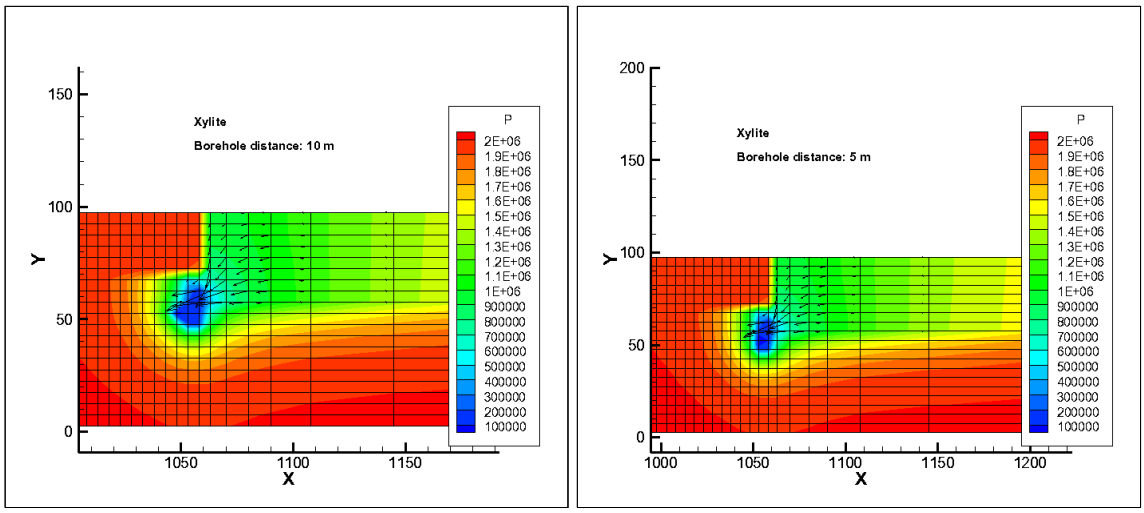


Figure 79: *Left) Simulation results of drainage at 10 m to the longwall face in xylite. Right) Simulation results of drainage at 5 m to the longwall face in xylite*

6.3.2 100 % Detrite Flow Model

Detrite can store higher amounts of CSG than xylite because of its higher specific surface area i.e., 180 m^2/g and 35 m^2/g, respectively (Chapter 3). Modelling of 100% detrite (Figures 80, 81 and 82) reveals a 10 bar (1 MPa) CGS pressure decrease across the whole coal seam, which is due to the fracturing of the coal. Several attempts of measuring CSG pressure in the field were unsuccessful if the lithology of the coal panel around the borehole was detrite. Therefore, when drilled coal cores are logged, it is possible to predict whether or not the pressure in the borehole will be high or low. This pressure decrease is also a result of the high porosity of detrite and, in turn, the higher permeability of the detrite compared to xylite lithotype.

Drainage was most efficient at distances of 40 and 20 m. In Figure 81 gas flow vectors are densest between the longwall face and the borehole. Also, an under pressure of 300

mbar is indicative of a large surface area in the area where gas drainage is most efficient.

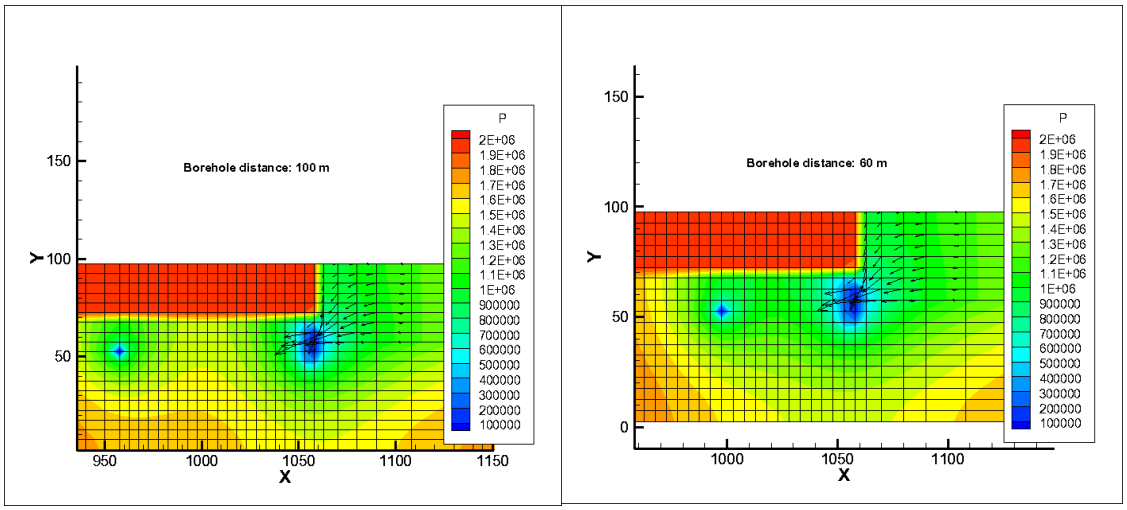


Figure 80: *Left) Simulation results of drainage at 100 m to the longwall face in detrite. Right) Simulation results of drainage at 60 m to the longwall face in detrite.*

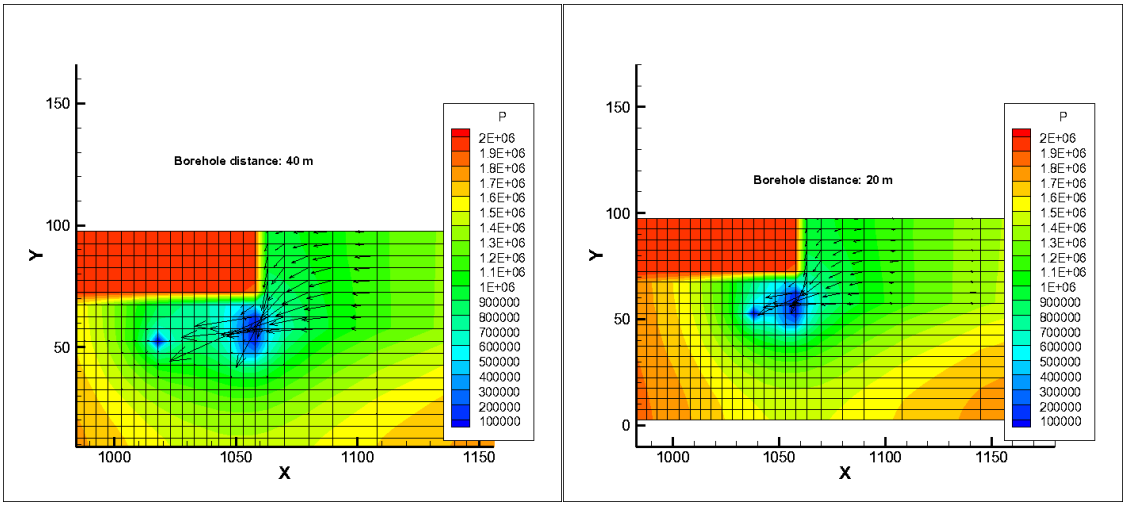


Figure 81: *Left) Simulation results of drainage at 40 m to the longwall face in detrite. Right) Simulation results of drainage at 20 m to the longwall face in detrite.*

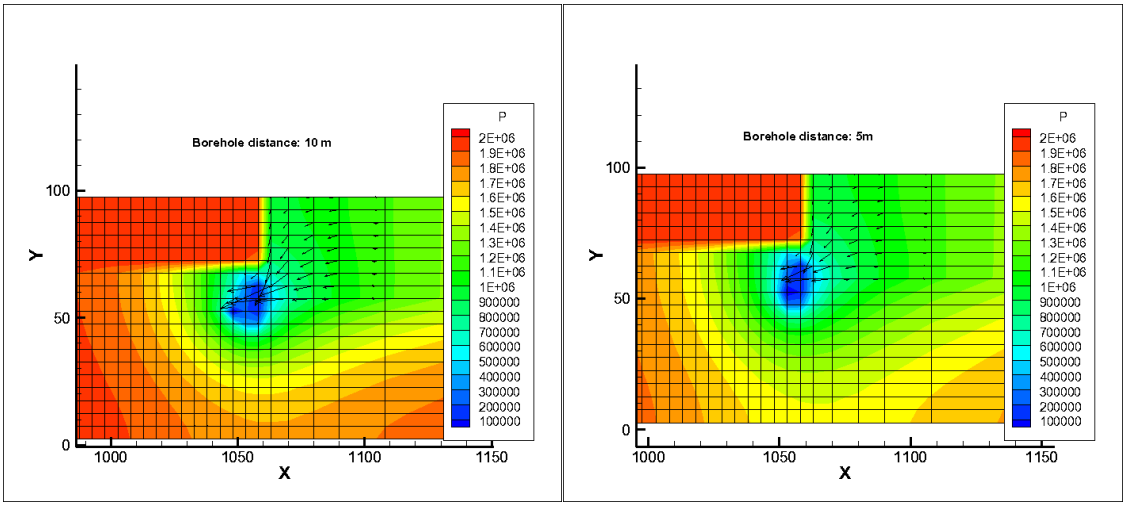


Figure 82: *Left) Simulation results of drainage at 10 m to the longwall face in detrite. Right) Simulation results of drainage at 5 m to the longwall face in detrite.*

6.3.3 50 % Xylite and 50 % Detrite Flow Model

A lithotype composition of 50% xylite and 50 % detrite represents the most common scenario and lignite, which is heterogeneous, is composed of varying ratios of xylite and detrite. Such cases; however, can provide a good insight into what is happening in both lithotypes. Comparison of the data from the drainage trials and flow modelling is best when using mixed lithotype results.

Figures 83, 84, and 85 show the CSG pressure distribution in the mixed lithotype models and together with the CO_2 flow vectors. A barrier, in terms of high gas pressure, exists between the borehole at 100 m from the longwall panel. Small areas of pressure decrease are also seen in Figure 83. The area of fractured coal in front of the longwall face extends to the borehole at a distance of 40 m (Figure 84). The pressure in the coal remains sufficiently high (up to 10 MPa) to allow gas to flow through the fractures and fissures to the borehole. The highest drainage values were observed at 20 m in front of the borehole.

When the borehole is at a distance of <20 m in front of the longwall face, the coal seam gas pressure around both the borehole and the face is reduced to atmospheric pressure, where a connection between the borehole and longwall face exists. The coal is highly fractured, and significant amounts of CSG are desorbed and can be drained from the coal.

Depending on the extent of damage and deformation from the pressure abutment, the CSG can mix with air from the longwall face, exceeding the gas mixture safety limits and causing the drainage pump to shut down. During the pilot drainage tests such a mixture occurred at 4.5 m from the longwall face in the case of drainage from borehole R3 and at 7.9 m in the case of drainage from borehole R4. At shorter distances to the face drainage was no longer possible. Figure 85 shows exactly the high gas flow phase at 10 m. On the other hand, at 5 m the gas flow is significantly reduced due to a drop in pressure around the borehole. The results of the geochemical modelling and the drainage pilot measurements at longwall panel K.-65/F have also confirmed this field and model observations with very similar results.

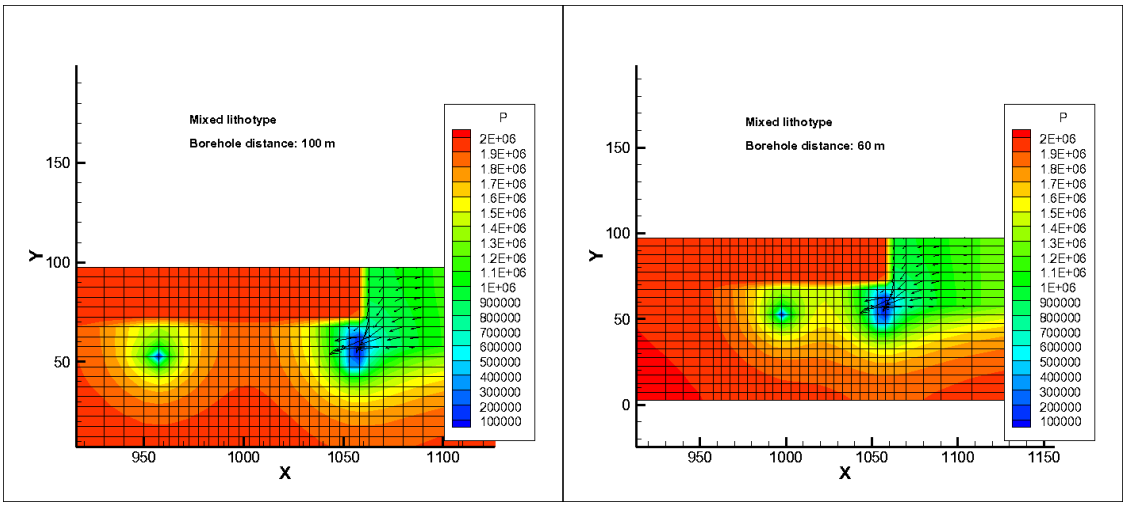


Figure 83: *Simulation results of drainage Left) 100 m in front of the longwall face for a mixed lithotype and Right) 60 m in front of the longwall face for a mixed lithotype.*

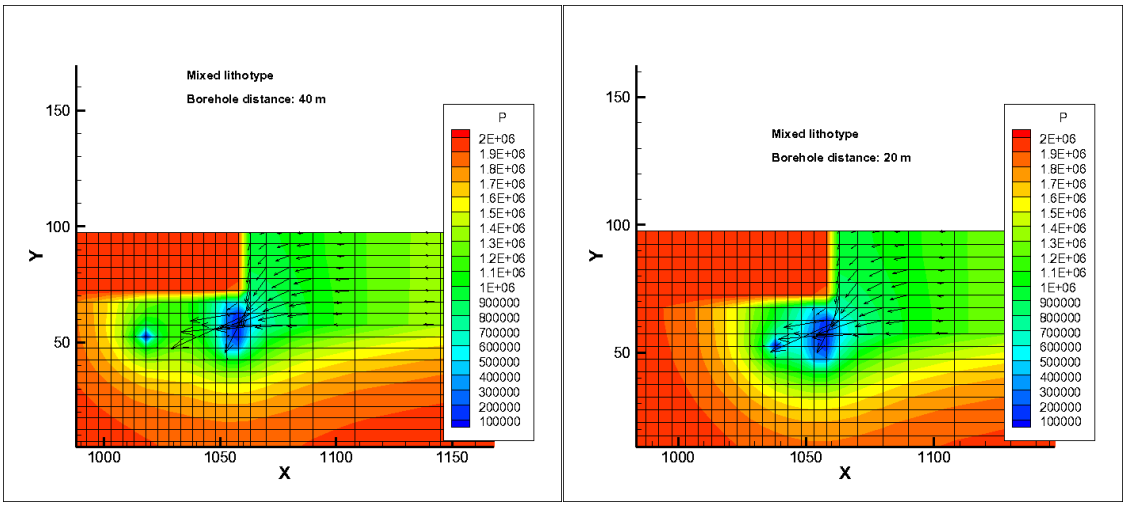


Figure 84: *Left) Simulation results of drainage at 40 m in front of the longwall face for a mixed lithotype. Right) Simulation results of drainage at 20 m in front of the longwall face for a mixed lithotype.*

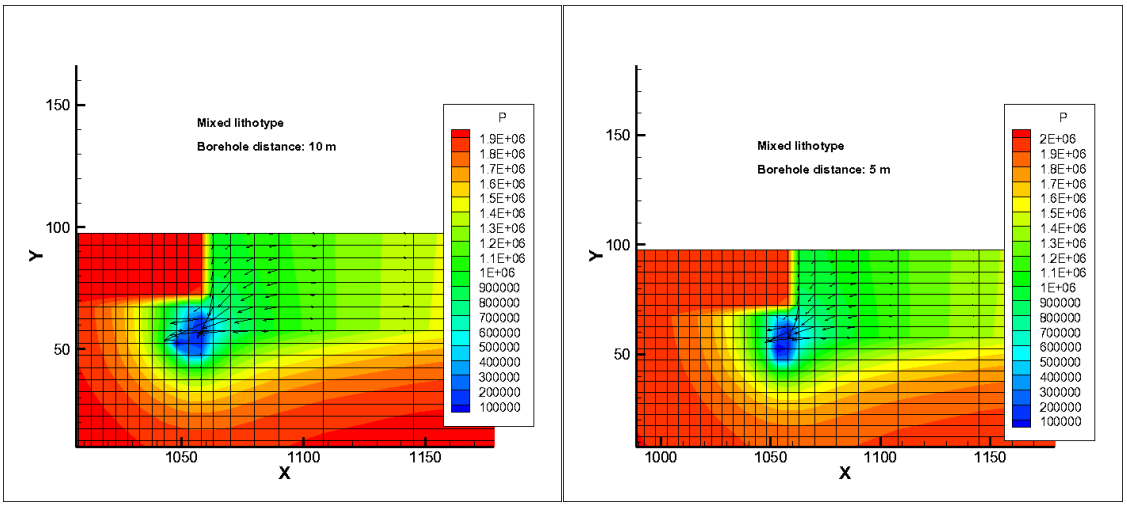


Figure 85*: Left) Simulation results of drainage 10 m in front of the longwall face for a mixed lithotype. Right) Simulation results of drainage at 5 m in front of the longwall face for a mixed lithotype.*

6.4 Conclusions

Coal seam gas flow modelling was performed for the first time in the case of Velenje Coal Mine. The main decision for choosing the software package TOUGHREACT from the TOUGH2 family was because the software was available at Imperial College London.

The structure of the program is very different to the geomechanical model used previously at the Velenje Coal Mine and, therefore, a lot of research time was spent studying the software and designing the model to adequatly represent the gas flow and drainage conditions in the mine.

The coal seam gas flow modelling produced realistic pressure distributions around the drainage boreholes, and gave a close approximation to the real CSG pressure monitoring data collected at the different levels in the mine. As expected and shown by the in-situ monitoring campaigns, different lithotype models confirmed the varying behaviour of the gas pressure distribution and gas flow.

The amount of gas released depends on the amount of crushed coal. When the drainage

borehole is 40 m in front of the longwall face, for all the cases, the gas flow vectors reach the location of the drainage borehole and higher amounts of CSG can be drained from the coal. Modelling of 100% detrite reveals a 10 bar (1 MPa) CGS pressure decrease across the whole coal seam, which is due to the fracturing of the coal, while a barrier, in terms of high gas pressure, exists between the borehole at 100 m from the longwall panel. Although, at 70 m in front of the borehole, rapid changes in the CSG pressure occur, deformations in the coal are not observed. Results showed that the CSG reaches 30 to 40 m before any differences appear in the stress measurements.

When the borehole is at a distance of <20 m in front of the longwall face, the coal seam gas pressure around both the borehole and the face is reduced to atmospheric pressure, where a connection between the borehole and longwall face exists. Here the coal is highly fractured, and significant amounts of CSG are desorbed and can be drained from the coal.

Depending on the extent of damage and deformation from the pressure abutment, the CSG can mix with air from the longwall face, exceeding the gas mixture safety limits and causing the drainage pump to shut down. During the pilot drainage tests such a mixture occurred at 4.5 m from the longwall face in the case of drainage from borehole R3 and at 7.9 m in the case of drainage from borehole R4.

Long term mining activities at the mine will include CSG drainage from the longwall panels, therefore, the development of gas flow models will continue together with analysing different borehole lengths and inclinations, and the spacing between them. For these purposes, a 3D model should be built.

Also, Equations of State (EOS) ECO2N have are limited when modelling only CO_2 composition in the material. For purposes of the Velenje Coal Mine, where gas composition mainly consists from CH_4 and CO_2, it would be better to use a software that can model both major gases. This software should also be capable of modelling stress changes in the coal seam, and not only the porosity and permeability. Nevertheless, TOUGHREACT provided very good results in 2D models.

7 Conclusions

Coal seam gas (CSG) emission in coal mines can create unsafe working conditions and CSG outbursts are responsible for many mining accidents leading to injury and death. High CSG emissions also cause economic losses due to production stoppages and increase the costs of mine ventilation. Mining at the Velenje Coal Mine is made difficult, not just because of the depth of the seam (500 m) but also due to the high CSG emissions. The Lignite seam is heterogeneous and is comprised of different lithologies, where these porosities and fracture systems act as gas reservoir and where the gas stored in the coal creates the ever-present risk of coal and gas outbursts. When mining activity disturbs one of these areas of high-pressure and mechanical strength, conditions for a gas outburst can develop.

At Velenje Coal Mine the CSG is predominately CO_2 and CH_4 at a ratio of 2:1, where a high proportion of the carbon dioxide is adsorbed in the coal structure and methane is free in the fractures. Outbursts involving CO_2 are typically more violent, more difficult to control and more dangerous because of the greater sorption capacity of coal for CO_2. Usually, outbursts occur in high rank coals, but in the Velenje lignite, which is a low rank coal, outbursts also occur, representing a real danger to miners.

Velenje lignite is characterized by different lithotype groups: fine detrite, xylite and gelite. Fine detrital lignite is most prone to outbursts when it is trapped in pockets within xylite rich lignite. The most critical zones are the contacts between the two lithotypes, arising from the differences in permeability, porosity, gas content and mechanical strength.

There exists the potential for capturing the CSG before it can be released into the working areas and various gas drainage systems are already in place in mines around the world. While Velenje lignite is a low permeability coal, new drainage technologies are currently being developed. All the *in-situ* activities at Velenje Coal Mine, such as CSG composition monitoring, gas pressure measurements, and gas migration research, have been performed in order to understand the physical and chemical behaviour of CSG in the lignite. These activities were necessary in order to design and install the first pilot-scale gas drainage system. As a result, six drainage boreholes were drilled at the longwall panel K.-65/F in 2013.

Active seismic tomography was conducted at two 100 m sections of two longwall panels: K.-50/C and K.-130/B. P-waves and S-waves were measured and the resultant tomograms confirmed the presence of known faults in the coal seam and the accumulation of stress in the xylite lithotype, and the influence of the advancing longwall face on the stress and potential gas pressure peaks in the coal.

Coal seam gas pressure monitoring was used to determine gas pressure under the dynamic influence of the longwall face. Measurements were performed in boreholes drilled into longwall panels at different positions. The results revealed that the gas pressure changes not just in the borehole but also through the whole seam. It was found that the location of borehole is crucial to whether high or low gas pressure is expected. Gas pressure is high (up to 2.5 MPa) under fresh overburden and low pressure is found in the previously over-mined panels. High gas pressure is connected with high gas volumes: therefore, gas drainage is most efficient in the first levels in the coal mine. Monitoring of gas pressure showed a peak in pressure when the longwall face was at approximately 10 m to the

borehole, where the longwall face stress abutment peak closed the fractures and fissures in the coal seam.

Coal seam gas samples from different boreholes drilled in the longwall panel were collected for geochemical monitoring. The concentration and the molecular and stable carbon isotope composition of methane and carbon dioxide, and the stable hydrogen isotope composition of methane in CSG were investigated in order to obtain a better understanding of its origin and behaviour ahead of the working face. The isotopic composition of methane confirmed the different origins of the CSG. The stable carbon isotope composition of methane and carbon dioxide indicate that methane was generated via acetate fermentation and the reduction of CO_2 ($\delta^{13}C_{CH4}$ from -70.4 to -50.0‰), which was confirmed by the $\alpha^{13}C_{CO2\text{-}CH4}$ fractionation factor. The higher values of $\delta^{13}C_{CH4}$ also indicate that thermogenic methane ($\delta^{13}C_{CH4}$ values from -50.0 to -18.8‰) migrated from deeper layers in the basin. The presence of thermogenic methane can also be explained by secondary processes, such as migration due to excavation and microbial oxidation of methane, causing enrichment of residual methane with the ^{13}C isotope. The $\delta^{13}C_{CH4}$ and $\delta^{2}H_{CH4}$ values in the Velenje Basin indicate a microbial and mixed origin of the CSG due to the migration process in a dynamic system with active lignite excavation.

The first drainage trial was established at the longwall panel K.-65/F in the Pesje mine district in 2013 and the results from the drainage test were compared with gas flow numerical modelling. Boreholes were drilled into the longwall panel with different inclinations and lengths. A reduction in the concentration of methane is observed as the longwall face advances towards the drainage borehole. The ratio between CO_2:CH_4 was 2:1. Drainage gas flow rates were variable while the highest gas flow was recorded at a distance of 22 m from the longwall face. The results showed that in drainage borehole R4, unlike in R3, the gas concentration remained constant as the longwall face approached. In addition, the periods of gas drainage on average lasted 24 min with the longest lasting 108 min. Maximum total flow was 193.0 m^3/min and the average CH_4 and CO_2 flow was 27.6 m^3/h and 57.0 m^3/h, respectively.

State-of-the-art computer numerical modelling was also performed using measured *in-situ* data, to construct a gas flow model for the mine, simulating the gas migration and drainage from the coal seam. Geomechanical modelling was performed using $FLAC^{3D}$ software for different lithotypes: 100% xylite, 100% fine detrite and a 50% of xylite and 50% of fine detrite mixed lithotype. Maximum vertical stresses vary depending on lithotype and were highest for the detrite lithotype (23 MPa) during horizontal excavation. The distance to the longwall face where these maximum values occurred varied from 6.7 m for detrite to 7.9 m for xylite and 6.8 m for mixed lithotype coal. Top coal caving models produced maximum vertical stresses at 22 m in front of the longwall panel. The maximum vertical stresses were 24 MPa in detrite, 26 MPa in xylite and 30 MPa in mixed lithotype, respectively.

Gas flow modelling was also performed using TOUGHREACT version of TOUGH2 software with ECO2N equation-of-state (EOS). In the xylite models, permeability was ten times lower that determined for the fine detrite models. The result was that the pressure drop around the borehole in the coal was not as noticeable and rapid as in fine detrite models. In all the gas flow models a similar pattern was observed i.e., the most efficient gas drainage occurs when the borehole is between 40 m and 20 m to the longwall face - a fact confirmed by the pilot-scale drainage studies.

In the fine detrite gas flow models, the gas pressure is reduced overall by 10 bar. This derives from highly fractured nature of detrite compared to the xylite, which is known to act as a barrier to gas flow in the lignite. Permeability is higher, allowing gas pressure to flow easily in the coal although fine detrite can store more CSG than the xylite lithotype.

Gas flow through a 50 % xylite and 50 % detrite composition reflected most accurately the real lignite composition. The area of fractured coal in front of the longwall face reaches the drainage borehole at a distance of 40 m. When the borehole was < 20 m to the longwall face, the pressure dropped to almost the atmospheric pressure, but gas still flowed. Closer to the longwall face (5 m) gas flow reduced and drainage was no longer possible, a fact also verified by the pilot-scale drainage studies.

Future work regarding drainage tests and numerical modelling should involve the following:

- using an increased number of drainage boreholes at one longwall panel;
- the use of longer drainage boreholes (up to 100 m or half of the longwall panel width);
- constructing complex 3D gas flow models with all the drainage boreholes located in the longwall panel.

8 References

Adeboye, O.O. (2011). *Effects of coal composition and fabric on porosity, sorption capacity and gas flow properties in Western Canada sedimentary basin coals.* (Master of Science degree.) Retrieved from: https://circle.ubc.ca/bitstream/id/107997/ubc_2011_spring_adeboye_oyeleye.pdf

Atkins, P.W. (1994). *Physical Chemistry, 5th edition*. W.H. Freeman, 1031 p.

Aul, G.N., & Ray, R. (1991). Optimizing methane drainage system to reduce mine ventilation requirements. *Proceedings 5th US Mine Ventilation Symposium, Morgantown, WV.*

Bates, B.L., McIntosh, J.C., Lohse, K.A., & Brooks, P.D. (2011). Influence of groundwater flow paths, residence times and nutrients on the extent of microbial methanogenesis in coal beds: Powder River Basin, USA. *Chemical Geology 284, 45-61.*

Beamish, B.B. (1984). Overseas visit to West Germany. Technical Report. CCP-009-84. Collinsville Coal Co. Pty, Collinsville, 38 pp.

Beamish, B.B. & Crosdale, P.J. (1998). Instantaneous outburst in underground coal mines: An overview and association with coal type. *International Journal of Coal Geology*, 35, 27-55.

Black, D.J. (2011). *Factors affecting the drainage of gas from coal and methods to improve drainage effectiveness.* (Doctoral dissertation). Retrieved from: http://ro.uow.edu.au/cgi/viewcontent.cgi?article=4339&context=theses

Blažič, A., Dervarič, E., Mayer, J., Lenart, M., Lah, R., Jeromel, G., Likar, J., Čadež, J. (2007). Analize sprememb napetosti in deformacij v prostoru v vplivnem območju napredovanja širokočelnega odkopavanja premoga (in Slovene). *Zbornik Strokovnega posvetovanja rudarjev in geotehnologov ob 40. Skoku čez kožo, Ljubljana.* 30-37.

Board, M., & Pierce, M.E. (2009). A review of recent experience in modelling of caving. *Proceedings of the International Workshop in Numerical Modelling for Underground Mine Excavation Design, NIOSH, Pittsburgh, 19-28.*

Brezigar, A., Ogorelec, B., Rijavec, L., & Mioč, P. (1987). Geologic setting of the Pre-Pliocene basement of the Velenje depression and its surroundings. *Geologija 30, 31-65 (in Slovene).*

Burke, L.M. (2003). *Numerical Modelling for Increased Understanding of the Behaviour and Performance of Coal Mine Stoppings*. (Master of Science degree.) Retrieved from: http://scholar.lib.vt.edu/theses/available/etd-05132003-150725/unrestricted/thesis_final2.pdf

Ceglarska-Stefańska, G., Zarębska, K., & Wolsczak, J. (2008). Sorption of pure components and mixtures CO_2 and CH_4 on hard coals. *Gospodarska Surowcami Mineralnymi, 24.*

Cervik, J. (1969). Behaviour of coal-gas reservoirs. Bureau of Mines Methane Control Program, Technical Progress Report – 10, U.S. Department of the Interior. Retrieved from: http://www.cdc.gov/niosh/mining/userfiles/works/pdfs/tpr10.pdf

Clayton, J.L. (1998). Geochemistry of coalbed gas – A review. *International Journal of Coal Geology 35, 159-173.*

CMG (2003). *Users Guide STARS*. Computer Modelling Group Ltd., Calgary, Canada.

Connell, L.D. (2009). Coupled flow and geomechanical processes during gas production from coal seams. *International Journal of Coal Geology 79, 18-28.*

Dai, J.X., Song, Y., Dai, C.S., & Wand, D.R. (1996). Geochemistry and accumulations of carbon dioxide gases in China. *American Association of Petroleum Geologists Bulletin 80, 1615-1626.*

Dunmore, R. (1975). A theory of emission of a mixture of methane and ethane from coal. *International Mine Ventilation Congress, Johannesburg, 7 p.*

Durucan, S. (1981). *An investigation into stress-permeability relationship of coal and flow patterns around working longwall faces.* (Doctoral dissertation).

Durucan, S., & Edwards, J.S. (1986). The effects of stress and fracturing on permeability of coal. *Mining Science and Technology, 3, 205-216.*

Durucan, S., Daltaban, T.S., Shi, J.Q., & Foley, L. (1993). Permeability characterisation for modelling methane flow in coal seams. *Proceedings of the 1993 International Coalbed Methane Symposium, Tuscaloosa, Alabama.*

Durucan, S., Korre, A., Shi, J.Q., Syed, A., Brenkley, D., Jozefowicz, R., …, Paulik, S. (2011). *Development of Novel Technologies for Predicting and Combating Gas Outbursts and Uncontrolled Emissions in Thick Seam Coal Mining*, Annual report, CoGasOUT, RFCR-CT-2010-00002. London.

Durucan, S., Korre, A., Shi, J.Q., Syed, A., Brenkley, D., Jozefowicz, R., …, Paulik, S. (2012). *Development of Novel Technologies for Predicting and Combating Gas Outbursts and Uncontrolled Emissions in Thick Seam Coal Mining*, Mid-term technical implementation report, CoGasOUT, RFCR-CT-2010-00002. London.

Durucan, S., Korre, A., Shi, J.Q., Syed, A, Si, G., Jamnikar, S.,…, Zavšek, S. (2014). *Greenhouse Gas Recovery from Coal Mines and Coalbeds for Conversion to Energy*, Deliverable N. 4.2, Report on numerical modelling results at Velenje. ENERGY.2010.5&6.2-1, London.

Eberhardt, E. (2012). The Hoek-Brown Failure Criterion. *Rock Mechanics and Rock Engineering, 45, 981-988.*

Ediz, I.G. (1991). *An application of numerical methods to the prediction of strata methane flow in longwall mining.* (Doctoral dissertation). Retrieved from: http://eprints.nottingham.ac.uk/12412/1/335202.pdf

Esterle, J.S., Williams, R.J., Sliwa, R., & Malone, M. (2006). Variability in gas reservoir parameters that impact on emission estimations for Australian black coals. *Final Report ACARP Project C13071, Brisbane, 36 pp.*

Esterhuinzen, G.S., & Karacan, C.O. (2005). Development of Numerical Models to Investigate Permeability Changes and Gas Emissions around Longwall Mining Panel. Retrieved from: http://www.cdc.gov/niosh/mining/UserFiles/works/pdfs/donmt.pdf

Faiz, M.M., Saghafi A., Barclay S.A., Stalker L., Sherwood, NR, & Whitford, DJ. (2007). Evaluating geological sequestration of CO_2 in bituminous coals. The Southern Sydney Basin, Australia as a natural analogue. *International Journal of Greenhouse Gas Control, 1, 223-235.*

Flores, R.M., Rice, C.A., Stricker, G.D., Warden, A., & Ellis, M.S. (2008). Methanogenic pathways of coalbed gas in the Powder River basin, United States: the geological factor. *International Journal of Coal Geology, 76, 52-75.*

Friedel, M.J., Scott, D.F., & Williams, T.J. (1997). Temporal imaging of mine-induced stress change using seismic tomography. *Engineering Geology, 46, 131-141.*

Furniss, M.D. (2009). *Quantitative comparison of seismic velocity tomography with seismic activity around a deep coal longwall panel.* (Masters of Science). Retrieved

from: http://scholar.lib.vt.edu/theses/available/etd-05122009-134212/unrestricted/Quantitative_Comparison_of_Seismic_Velocity_Tomography_with_Seismic_Activity_around_a_Deep_Coal_Longwall_Panel.pdf

Harpalani, S., & McPherson, M.J. (1986). Retention and release of methane in underground coal workings. *International Journal of Mining and Geological Engineering, Vol. 4, No. 3, 217-233.*

Gentzis, T., Deisman, N., & Chalaturnyk, R.J. (2007). Geomechanical properties and permeability of coals from the Foothills and Mountain regions of western Canada. *International Journal of Coal Geology, 69, 153-164.*

Gilfillan, S.M.V., Lollar, B.S., Holland, G., Blagburn, D., Stevens, S., Schoell, M., … Ballantine, C. J. (2009). Solubility trapping in formation water as dominant CO_2 sink in natural gas fields. *Nature, 458, 614-618.*

Glazer, S.N., & Lurka, A. (2007). Application of Passive Seismic Tomography to Cave Mining Operations Based On Experience at Palabora Mining Company, South Africa. *The Southern African Institute of Mining and Metallurgy 1st International Symposium on Block and Sub-Level Caving Cave Mining, Johannesburg, 369-388.*

Golding, S.D., Boreham, C.J., & Esterle, J.S. (2013). Stable isotope geochemistry of coal bed and shale gas and related production waters: A review. *International Journal of Coal Geology, 120, 24-40.*

Gou, X., Du, Z., & Li, S. (2003). Computer Modelling and Simulation of Coalbed Methane Reservoir. *SPE Eastern Regional/AAPG Eastern Section Joint Meeting in Pittsburgh, Pennsylvania.*

Guoyi, H., Jin, L., Chenghua, M., Zhisheng, L. Zgang, M. & Qiang, Z. (2007), Characteristics and Implications of the Carbon Isotope Fractionation of Desorbed Coalbed Methane in Qinshui Coalbed Methane Field, China. *Earth Science Frontiers 14 (6), 267- 272.*

Hanson, D.R., Vandergrift, T.L., DeMarco, M.J., & Hanna, K. (2002). Advanced techniques in site characterization and mining hazard detection for the underground coal industry. *International Journal of Coal Geology,50, Issues 1-4, 275 - 301.*

Helm, P.R. (2011). *Analysis of the Stability of Shallow Abandoned Colliery Workings.* (Doctoral dissertation) Retrieved from: https://theses.ncl.ac.uk/dspace/bitstream/10443/1378/1/Helm11.pdf

Hemza, P. Sivek, M., & Jirásek, J. (2009). Factors influencing the methane content of coal beds if the Czech part of the Upper Silesian Coal Basin, Czech Republic. *International Journal of Coal Geology, 79, 23-39.*

Hendriks, C. & de Jager, D. (2001). Economic Evaluation of Sectoral Emission Reduction Objectives for Climate Change: Economic Evaluation of Methane Emission Reduction in the Extraction, Transport and Distribution of Fossil Fuels in the EU. Bottom-up Analysis. Final Report. Retrieved from: http://ec.europa.eu/environment/enveco/climate_change/pdf/fossilfuel.pdf

Hoek, E., & Brown, E.T., (1980). *Underground excavations in rock.* The Institution of Mining and Metallurgy, London.

Hoek, E., Carranza-Torres, E.C., & Corkum, B. (2002). Hoek-Brown failure riterion – 2002 Edition. *Proceedings of NARMS-TAC 2002, 5th North American Rock Mechanics Symposium and 17th Tunneling Association of Canada Conference, Toronto, Canada, July 2002, Vol. 1, 267-271.*

Hu, G., Li, J., Ma, C., Li, Z., Zhang, M., & Zhou, Q. (2007). Characteristics and Implications of the Carbon Isotope Fractionation of Desorbed Coalbed Methane in Qinshui Coalbed Methane Field, China. *Earth Science Frontiers 14 (6), 267-272.*

IEA Statistics: CO_2 emissions from fuel combustion; Highlights, 2013 Edition. Retrieved from: http://www.iea.org/publications/freepublications/publication/co2emissionsfromfuelcombustionhighlights2013.pdf

Itasca (2005). Flac3D: Fast Lagrangian Analysis of Continua in 3 Dimensions, User Manual.

Jedrysek, M.O. (1995). Carbon isotope evidence for diurnal variations in methanogenesis in freshwater lake sediments. *Geochimica et Cosmochimica Acta 59, 557-561.*

Jamnikar, S. (2015 in preparation). *An investigation into the flow of gases around longwall top coal caving faces and gas drainage trials at Velenje Coal Mine.* (Doctoral dissertation)

Jeromel, G. (2010). *Constitutive model of multiple hanging wall caving in underground coal mining.* (Doctoral dissertation)

Jeromel, G., Medved, M., & Likar, J. (2010). An analysis of the geomechanical processes in coal mining using the Velenje Mining Method. *Acta Geotechnical Slovenica*, 1, 2010.

Kanduč, T., & Pezdič, J. (2005). Origin and distribution of coalbed gases from the Velenje Basin, Slovenia. *Geochemical Journal 39, 397-409.*

Kanduč, T., Žula, J., & Zavšek, S. (2011). Tracing coalbed gas dynamics and origin of gases in advancement of the working faces at mining areas Preloge and Pesje, Velenje Basin. *RMZ – Materials and Geoenvironment 58, 273-288.*

Kanduč T., Markič M., Zavšek S., & McIntosh J. (2012). Carbon cycling in the Pliocene Velenje Coal Basin, Slovenia, inferred from stable carbon isotopes. *International Journal of Coal Geology 89, 70-83.*

Kanduč T., Grassa F., McIntosh J., Stibilj V., Ulrich-Supovec M., & Jamnikar S. (2014). A geochemical and stable isotope investigation of groundwater/surface-water interactions from the Velenje Basin, Slovenia. *Hydrogeological Journal*. Doi: 10.1007/s10040-014-1103-7.

Kanduč, T., Grassa, F, Sedlar, J., Zavšek, S. (2015). Geochemical and isotopic characterization of coalbed gases in active excavation fields at Preloge and Pesje (Velenje Basin) mining areas. *RMZ – Materials and Geoenvironment, 62, 21 – 35.*

Karacan, C.Ö., W.P. Diamond, & S.J. Schatzel (2007a). Numerical analysis of the influence of in-seam horizontal methane drainage boreholes on longwall face emission rates. *International Journal of Coal Geology 72(1), 15-32.*

Karacan, C.Ö., Esterhuizen, G.S., Schatzel, S.J., & Diamond, W.P. (2007b). Reservoir simulation-based modelling for characterizing longwall methane emissions and gob gas vent hole production, *International Journal of Coal Geology, 71(2-3), 225-245.*

Karacan, C.Ö. (2008). Modelling and prediction of ventilation methane emissions of U.S. longwall mines using supervised artificial neural networks. *International Journal of Coal Geology 73(3-4), 371-387.*

Karimi, K. (2005). Coal Bed Methane Reservoir Simulation Studies. (Masters of Science). Retrieved from: http://www.unsworks.unsw.edu.au/primo_library/libweb/action/dlDisplay.do?vid=UNSWORKS&docId=unsworks_765

Keen, T.F. (1977). *The simulation of methane flow in carboniferous strata.* (Doctoral dissertation).

Kerr, J. (2011). *Applications of Double-Difference Tomography for a Deep Hard Rock Mine*. (Master's degree).

Kidybinski, A., & Babcock, C.O. (1973.) Stress distribution and rock fracture zones in the roof of longwall face in a coal mine. *Rock Mechanics and Rock Engineering, 4, 1-19.*

Kim, A. G., & Douglas, L. J. (1973). Gases desorbed from five coals of low gas content. *US Bur Mines Rep Invest, 7768.*

Kočar F., Veselič, M., Ribičič, M., Mramor, J. (1989) Safety criteria of coal excavation under aquifer layers in Velenje Coal Mine. *Mining and metallurgy quarterly: periodical for geology, mining and metallurgy, 36, Vol. 2, 421-438.*

Kormendi, A., Bodoy, L., Hermann, L., Dianisda, L., & Kalman, T. (1986). Seismic measurements for safety in mines. *Geophysical Prospecting, 34, 1022-1037.*

Kotarba M.J., & Rice D.D. (2001). Composition and origin of coalbed gases in the Lower Silesian Basin, north western Poland. *Applied Geochemistry, 16, 895-910.*

Kotarba, M.J. (2001). Composition and origin of coalbed gases in the upper Silesian and Lublin basins, Poland. *Organic geochemistry, 163-180.*

Koutsabeloulis, N.C., & Hope, S.A. (1998). *Coupled stress/fluid/thermal multi—phase reservoir simulation studies incorporating rock mechanics.* SPE/ISRM EUROCK-98 Symposium, Norway, 449-454.

Lama, R.D., & Bodziony, J. (1998). Management of outburst in underground coal mines. *International Journal of Coal Geology 35, 83-115.*

Lama, R.D., & Saghafi, A. (2002). Overview of Gas Outbursts and Unusual Emissions. *Underground Coal Operators´ Conference, University of Wollongong, the Australasian Institute of Mining and Metallurgy, 74-88.*

Li, W., Cheng Y.P., Wang L., Zhou H.X., Wang H.F, & Wang L.G. (2013). Evaluating the security of geological coalbed sequestration of supercritical CO_2 reservoirs: The Haishiwan coalfield, China as a natural analogue, *International Journal of Greenhouse Gas Control 13, 102-111.*

Likar, J., Dervarič, E., Medved, M., Čadež, J., & Jeromel, G. (2006). Some methods of analysing caving processes in sublevel coal mining. *RMZ – Materials and Geoenvironment, Vol. 53, No. 2, 203-220.*

Liu, H., Cheng, Y., Chen, H., Kong, S., & Zhai, Q. (2011). Numerical Simulation of the De-stressed Deformation of Mining Coal Strata at Different Pore Pressures, *11th Underground Coal Operators` Conference, University of Wollongong & the Australasian Institute of Mining and Metallurgy, 361-368.*

Loschetter, A., Smai, F., Sy, S., Burnol, A., Leynet, A., … & Thoraval, A. (2012). Simulation of CO2 storage in coal seams: coupling of TOUGH2 with the solver for mechanics CODE ASTER. *TOUGH Symposium – Lawrence Berkley National Laboratory, Berkley, California, September 17-19, 2012.* Retrieved from: http://www.code-aster.org/V2/spip.php?article686

Lunarzewki, L.W. (2001). Gas Drainage Practices. *Coal Operators´ Geotechnology Colloquium, University of Wollongong & the Australasian Institute of Mining and Metallurgy, 34-44.*

Malolepszy, Z. (2003). Man-made, low-temperature geothermal reservoirs in abandoned workings of underground mines on example of Nowa Ruda coal mine, Poland. *International Geothermal Conference, Reykjavik, 2003, 23-29.*

Markič, M., & Sachsenhofer, R.F. (1997). Petrographic composition and depositional environments of the Pliocene Velenje lignite seam (Slovenia). *International Journal of Coal Geology, 33, 229-254.*

Markič, M. (2009). *Petrology and genesis of Velenje Lignite.* (Doctoral dissertation).

McCants, C.Y., Spafford, S., & Stevens, S.H. (2001). Five-spot production pilot on tight spacing: rapid evaluation of a coalbed methane block in the Upper Silesian Coal Basin, Poland. *The 2001 International Coalbed Methane Symposium, University of Alabama, Tuscaloosa, 193-204.*

McKee, C.R., Blumb, A.C., & Koening, R.A. (1988). Stress-dependent permeability and porosity of coal and other geologic formations. *Society Petroleum Engineering Formation Evaluation 3 (1), 81-91.*

McPherson, M.J. (1975). The occurrence of methane in mine workings. *Journal of the Mine Ventilation Society of South Africa, Vol. 28, No. 8, 118-128.*

Medved, M., & Golob L. (2013). Sustainable development of Velenje mining method and its global use. *5th Jubilee Balkan Mining Congress, 18th-21st September 2013, Ohrid.*

Moore T.A. (2012). Coalbed methane: A review. *International Journal of Coal Geology 101, 36-81.*

Nelson, C. R. (2000). Effects of Geologic Variables on Cleat Porosity Trends in Coalbed Gas Reservoirs. *SPE 59787, 2000 SPE/CERI gas technology symposium proceedings. Society of Petroleum Engineers. 651-655.*

Noack, K. (1998). Control of gas emissions in underground coal mines, *International Journal of Coal Geology, 35(1-4), 57-82.*

O'Shaughnessy, S.M. (1980). *The computer simulation of methane flow through strata adjacent to a working longwall coalface.* (Doctoral dissertation).

Owili-Eger, A.S.C., & Ramani, R.V. (1974). Mathematical modelling of methane flow in mines. *Proceedings of the 12th International Symposium on the Application of Computing and Mathematics in Mining Industry, Colorado School of Mines, Vol.2, Section G, 1974, 218-229.*

Ozbay, U., & Rozgonyi, T.G. (2003). Numerical modelling of stress and deformations encountered in deep longwall coal mines using strain softening failure criterion. *International Conference on safety and environmental aspects of mining. University of Miskolc Series A. Mining, Vol. 63, 123-135.*

Paterson, M.S., & Wong, T-F. (1978). *Experimental rock deformation - The brittle field.* Berlin: Springer.

Pruess, K., Oldenburg, C., & Moridis, G. (1999). TOUGH2 User`s Guide, Version 2.0. Earth Sciences Division, Lawrence Berkley National Laboratory, University of California, Berkley.

Pruess, K. (2005). ECO2N: A TOUGH2 Fluid Property Module for Mixtures of Water, NaCl, and CO2. Earth Sciences Division, Lawrence Berkley National Laboratory, University of California, Berkley.

Ren, T., & Edwards, J. (2000). Three-dimensional computational fluid dynamics modelling of methane flow through permeable strata around a longwall face. *Mining Technology 109 (1), 41-48.*

Rice, D.D. (1993). Composition and origins of coalbed gas. *Law, B.E., Rice, D.D. (Eds.), Hydrocarbons from Coal, AAPF Studies in Geology #38, Tulsa, OK, 159-184.*

Rowe, D. & Muehlenbachs, A. (1999). Low-temperature thermal generation of hydrocarbon gases in shallow shales. *Nature 398, 61-63.*

Rutqvist, J., Wu, Y.S., Tsang, C.F., & Bodvarsson, G. (2002). A modelling approach for analysis of coupled multiphase fluid flow, heat transfer, and deformation in fractured porous rock. *International Journal of Rock Mechanics & Mining Sciences. 39, 429-442.*

Rutqvist, J. (2011). Status of the Tough-Flac simulator and recent applications related to coupled fluid flow and crustal deformations. *Computers & Geosciences, Vol. 37, 6, 739-750.*

Salamon, M.D.G. (1991). Deformation of stratified rock masses: A laminated model. *International Journal of Rock Mechanics and Mining Sciences, 91, 9-25.*

Scott, A.R., Kaiser, W.R., & Ayers Jr, W.D. (1994). Thermogenic and secondary biogenic gases, San Juan Basin, Colorado and New Mexico – implication for coalbed gas

production. *American Association of Petroleum Geologists Bulletin, 78, 1186-1209.*

Sedlar, J., Kanduč, T., Jamnikar, S., Grassa, F., & Zavšek, S. (2014). Distribution, composition and origin of coalbed gases in excavation fields from the Preloge and Pesje mining areas, Velenje Basin, Slovenia. *International Journal of Coal Geology, 131, 363 – 377.*

Seidle, J.P., Jeansonne, D.J., & Erickson, D.J. (1992). Application of matchstick geometry to stress dependent permeability in coals. *SPE 24361. SPE Rocky Mountain Regional Meeting. Casper, Wyoming, 18 – 21 May.*

Seher, A. (1995). *The history of Coal Mine Velenje* (in Slovene). Vol. 1. Velenje: Velenje Coal Mine. 526 p.

Scott, S., Anderson, B., Crosdale, P.J., Dingwall, J., & Leblang, G. (2007). Coal petrology and coal seam gas contents of the Walloon Subgroup – Surat Basin, Queensland, Australia. International Journal of Coal Geology, 70, 209-222.

Sharma, P.D. (2008). *Coal-bed Methane (CBM) drainage from Underground Coal Mines – Safer and eco-friendly option of green energy.* Retrieved from: http://saferenvironment.wordpress.com/2008/10/15/coal-bed-methane-cbm-drainage-from-underground-coal-mines-%E2%80%93-safer-and-eco-friendly-option-of-green-energy/

Sherwood Lollar, B., Lacrampe-Couloume, G., Slater, G. F., Ward, J., Moser, D. P., Gihring, … Onstott, T. C. (2006). Unravelling abiogenic and biogenic sources of methane in the Earth`s deep subsurface. *Chemical Geology, 226, 328-339.*

Shi, J.Q., & Durucan, S. (2003). A Bidisperse Pore Diffusion Model for Methane Displacement Desorption in Coal by CO_2 Injection. *Fuel, 82, 1219-1229.*

Shi, J.Q., & Durucan, S. (2004). Drawdown induced changes in permeability of coalbeds: a new interpretation of the reservoir response to primary recovery. *Transport in Porous Media 56, 1-16.*

Si, G., Jamnikar, S., Sedlar, J., Shi, J.Q., Durucan, S., ... & Zavšek, S. (2015). Monitoring and modelling of gas dynamics in multi-level longwall top coal caving of ultra-thick coal seams. Part I., Borehole measurements and a conceptual model for gas emission zones. *International Journal of Coal Geology, 144/145, 98 – 110.*

Si, G., Shi, J.Q., Durucan, S., Korre, A., Sedlar, J., ... & Zavšek, S. (2015). Monitoring and modelling of gas dynamics in multi-level longwall top coal caving of ultra-thick coal seams. Part II., Numerical modelling. *International Journal of Coal Geology, 144/145, 58 – 70.*

Sing, M.M, & Kendorski, F.S. (1981). Strata disturbance prediction for mining beneath surface water and waste impoundments. *Proceedings 1st Conference on Ground Control in Mining, 76- 89.*

Smith, J.W., & Gould, K.W. (1980). An isotopic study of the role of carbon dioxide in outbursts in coal mines. *Geochemical Journal, 14, 27 – 32.*

Smith, J.W., & Pallasser, R.J. (1996). Microbial origin of Australian coalbed methane. *AAPG Bull. 80, 891-897.*

Strąpoć, D., Mastalerz, M., Schimmelmann, A., Drobniak, A., & Hedges, S. (2008). Variability of geomechanical properties in a microbially dominated coalbed gas system from the eastern margin of the Illinois Basin, USA. *International Journal of Coal Geology 76, 98-110.*

Sung, R.T., Li, M.H., Dong, J.J., Lin, A.T.S., Hsu, S.K., …, &Yang, C.N. (2014). Numerical assessment of CO_2 geological sequestration in sloping and layered heterogeneous formations: A case study from Taiwan. *International Journal of Greenhouse Gas Control, 20, 168-179.*

Syed, S.A. (2011). *Permeability and Injectivity Enhancement of the Near Wellbore Region for CO_2 Enhanced Coalbed Methane Recovery and CO_2 storage.* (Doctoral dissertation).

Tecplot, Inc. (2013). Tecplot 360 User's Manual.

Thill, R.E., 1973. Methods for Monitoring Failure in Rock. University Park 14th Symposium on Rock Mechanics,

Thoksoz, M.N., Cheng, C.H., & Timur, A. (1976). Velocity of seismic Waves in porous rocks. *Geophysics Society of Exploration Geophysicists, V. 41, No.4, 621-645.*

Wang, K., & Xue, S. (2008). Gas Drainage Practices and Challenges in Coal Mines of China. *Coal Operators` Conference, University of Wollongong & the Australasian Institute of Mining and Metallurgy, 178-185.*

Walsh, R., Calder, N., & Avis, J. (2012). A simple implementation of 1D hydromechanical coupling in TOUGH2. *Proceedings, TOUGH Symposium 2012.*

Weniger, P., Francú, J., Kroos, B.M., Búzek, F., Hemza, P., & Littke, R. (2012). Geochemical and stable isotopic composition of coal-related gases from the SW Upper Silesian Coal Basin, Czech Republic. *Organic Geochemistry, 53, 153-165.*

Westman, E.C., Heasley, K.A., Swanson, P.L., & Paterson, S. (2001). A correlation between seismic tomography, seismic events and support pressure. *Proceedings 38th Rock Mechanics Symposium, Washington DS, July 7-10, 319-326.*

Westman, E.C., Luxbacher, K.D., & Swanson, P.L. (2008). Local Earthquake Tomography for Imaging Mining-Induced Changes Within the Overburden above a Longwall Mine. Retrieved from: http://www.cdc.gov/niosh/mining/userfiles/works/pdfs/letfi.pdf

Whittaker, B.N. (1974). An appraisal of strata control practice. *Transaction if the Institution of Mining and Metallurgy, 134 (166), 9-24.*

Whiticar, M.J., Faber E., & Schoell M. (1986). Biogenic methane formation in marine and fresh water environment, CO_2 reduction vs. acetate fermentation-isotopic evidence. *Geochimica et Cosmochimica Acta, 50, 693-709.*

Whiticar, M.J. (1999). Carbon and hydrogen isotope systematics of bacterial formation and oxidation of methane. *Chemical Geology 161, 291-314.*

Whittles, D.N., Lowndes, I.S., Kingman, S.W., Yates, C., & Jobling, S. (2006). Influence of geotechnical factors on gas flow experienced in a UK longwall coal mine panel. *International Journal of Rock Mechanics & Mining Sciences, 43, 369-387.*

Williams, R.J., & Weissman, J.J. (1995) .Gas emission and outburst assessment in mixed CO_2 and CH_4 environments, *ACIRL Underground Mining Seminar Brisbane, Paper.*

Wycherley, H., Fleet, A., & Shaw, H. (1999). Some observations on the origins of large volumes of carbon dioxide accumulation in sedimentary basins. *Marine and Petroleum Geology 16. 489 – 494.*

Xu, T., & Pruess, K. (1998). *Coupled modelling of non-isothermal multiphase flow, solute transport and reactive chemistry in porous and fractured media: 1. Model development and validation.* Lawrence Berkeley National Laboratory Report LBNL-42050, Berkeley, California, 38 pp.

Xu, T., Sonnenthal, E. L., Spycher, N., & Pruess, K. (2006). TOUGHREACT - A simulation program for non-isothermal multiphase reactive geochemical transport in variably saturated geologic media: Applications to geothermal injectivity and CO_2 geological sequestration, *Computer & Geoscience, Vol. 32/2, 145-165*

Xu, T., Spycher N., Sonnenthal E., Zhang G., Zheng L., & Pruess, K. (2011). TOUGHREACT Version 2.0: A simulator for subsurface reactive transport under non-isothermal multiphase flow conditions, *Computers & Geosciences, 37, 763-774.*

Xu, T., Spycher, N., Sonnenthal, E., Zheng, L., & Pruess, K. (2012). TOUGHREACT User`s Guide: A Simulation Program for Non-isothermal Multiphase Reactive Transport

in Variably Saturated Geologic Media, Version 2.0.

Xue, Z. (2005). Effects of coal matrix swelling on seismic wave monitoring of CO_2 in coal seams. *Coal and Safety, 26, 11-18.*

Yatsili, N.E., & Unver, B. (2005). 3-D numerical modelling of stresses around a longwall panel with top coal caving. *The Journal of the South African Institute of Mining and Metallurgy, 105, 287-300.*

Yi, J., Akkutlu, I., Karacan, C., & Clarkson, C. (2009). Gas sorption and transport in coals: A poroelastic medium approach. *International Journal of Coal Geology, 77, 137-144.*

Yu, G, Vozoff, K, & Durney, D. (1993). The influence of confining pressure and water saturation on dynamic elastic properties of some Permian coals, *Geophysics, 58, No. 1, 30-38*

United Nations Economic Commission for Europe Methane to Markets Partnership (2010). Best Practice Guidance for Effective Methane Drainage and Use in Coal Mines. ECE Energy Series No.31, New York and Geneva. Retrieved from: http://www.unece.org/fileadmin/DAM/energy/se/pdfs/cmm/pub/BestPractGuide_MethDrain_es31.pdf

Vakili, A., Albrecht, J., & Gibson, W. (2010). Mine-scale numerical modelling of longwall operations. *10th Underground Coal Operators´ Conference, University of Wollongong & the Australasian Institute of Mining and Metallurgy, 115-124.*

Vutukuri, V.S., & Lama, R.D. (1986). *Environmental Engineering in Mines.* Cambridge: Cambridge University Press, 504 p.

Zavšek, S. (2004). *Model for research of structural and petrographical changes of the Velenje lignite depending on various stress states and presence of gases.* (Doctoral dissertation)

Zavšek, S., Richter, T., Pippig, U., Weller, A., Nordsiek, S., …, & Lorenz, K. (2008) Results of the international PROINNO-EUREKA project VELGASPREVENT-EDITORIAL. *International workshop on Mine (Green-House) gases CO_2, CH_4, Mine Safety, Prevention, Managing and Utilization, Velenje, 91-99.*

Zavšek, S., Dimaki, A. V., Dmitriev, A. I., Shilko, E., V., Pezdič, J., & Psakie, S. G. (2013). Hybrid Cellular Automata Method. Application to Research on Mechanical Response of Contrast Media. *Physical Mesomechanics, 16, No. 1, 42-51.*

Zipf, Jr., R.K. (2006). Numerical modelling procedures for practical coal mine design. Retrieved from: http://www.cdc.gov/niosh/mining/userfiles/works/pdfs/nmpfp.pdf

Zheng, Z., Khodaverdian, M., & McLennan, J.D. (1991). Static and dynamic testing of coal specimens. *SCA Conference Paper, No. 9120.*

Appendix

Appendix 1: List of publication related to the dissertation

Sedlar, J., Kanduč, T., Jamnikar, S., Grassa, F., & Zavšek, S. (2014). Distribution, composition and origin of coalbed gases in excavation fields from the Preloge and Pesje mining areas, Velenje Basin, Slovenia. *International Journal of Coal Geology, 131, 363 – 377.*

Si, G., Durucan, S., Jamnikar, S., Sedlar, J., Abraham, K., ...Lurka, A. (2015). Seismic monitoring and analysis of excessive gas emissions in heterogeneous coal seams. *International Journal of Coal Geology, DOI, 10.1016/j.coal.2015.06.016.*

Si, G., Jamnikar, S., Sedlar, J., Shi, J.Q., Durucan, S., ... & Zavšek, S. (2015). Monitoring and modelling of gas dynamics in multi-level longwall top coal caving of ultra-thick coal seams. Part I., Borehole measurements and a conceptual model for gas emission zones. *International Journal of Coal Geology, 144/145, 98 – 110.*

Si, G., Shi, J.Q., Durucan, S., Korre, A., Sedlar, J., ... & Zavšek, S. (2015). Monitoring and modelling of gas dynamics in multi-level longwall top coal caving of ultra-thick coal seams. Part II., Numerical modelling. *International Journal of Coal Geology, 144/145, 58 – 70.*

Kanduč, T., Grassa, F, Sedlar, J., Zavšek, S. (2015). Geochemical and isotopic characterization of coalbed gases in active excavation fields at Preloge and Pesje (Velenje Basin) mining areas. *RMZ – Materials and geoenvironment, 62, 21 – 35.*